



University
of Glasgow

Lee, Louisa Chi Yin (2016) *Investigation of mesenchymal stem cell response to bioactive nanotopography*. PhD thesis.

<http://theses.gla.ac.uk/7180/>

Copyright and moral rights for this thesis are retained by the author

A copy can be downloaded for personal non-commercial research or study

This thesis cannot be reproduced or quoted extensively from without first obtaining permission in writing from the Author

The content must not be changed in any way or sold commercially in any format or medium without the formal permission of the Author

When referring to this work, full bibliographic details including the author, title, awarding institution and date of the thesis must be given

Investigation of Mesenchymal Stem Cell Response to Bioactive Nanotopography

Louisa Chi Yin Lee

(BSc Hons, MRes)



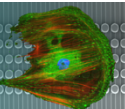
University
of Glasgow

**Submitted in fulfilment of requirements for the degree of
Doctor of Philosophy (PhD)**

**Centre for Cell Engineering
Institute of Molecular, Cell and Systems Biology
College of Medical, Veterinary and Life Sciences
University of Glasgow
Glasgow, G12 8QQ**

October 2015

Centre for
Cell Engineering



Abstract

Mesenchymal stem cells (MSC) are multipotent stem cells that have much potential for application in regenerative medicine, with their ability to self-renew and to undergo differentiation into several lineages, including those that comprise fat, bone, and cartilage. Studies on MSCs have mainly focused on exploiting their capacity to differentiate, rather than self-renewal, yet understanding of the latter process is pivotal for the expansion of these cells to sufficient numbers for use in future clinical treatments.

Aspects of MSC behaviour can be induced by culture on nanopatterned substrates, known as nanotopography. Use of established nanopit features, in arrangements known to maintain MSC multipotency over long periods in culture (SQ), in addition to an osteogenic promoting arrangement (NSQ), were used as a tool to study self-renewal in MSCs, and begin to elucidate some of the potential mechanisms underlying the effects of the nanotopographies on stem cell fate.

This study utilised patient-specific primary MSCs derived from bone marrow, which were optimised in terms of initial seeding density, to make efficient use of our nanotopographies. Once the fundamental details pertaining to optimal conditions for use of the substrates and cells were established, exploration of changes in metabolism, cell cycle and gene expression were carried out. Results indicated that MSCs on SQ contained more unsaturated metabolites, and that cell cycle may be altered, which warranted further investigation. Further study identified some differences in cell cycle regulatory proteins when compared to NSQ and flat controls. Further inferences were achieved by analysis of transcript abundances and differential expression, supporting the hypothesis of a heterogeneous population existing on NSQ, and activation of pathways linked to differentiation, consistent with previous work. A greater percentage of MSCs on SQ were shown to be in the early G0/G1 stages of the cell cycle in comparison to those on flat, suggesting that cell cycle is altered and further establishes a link between self-renewal and cell cycle regulation.

Nanotopography was assessed for a novel application, namely the potential of SQ to reprogram differentiating MSCs. Nanotopography was used to induce and

reverse the onset of osteogenic differentiation, and evaluated in conjunction with the addition of an epigenetic modifier, valproic acid. Results did not indicate that nanotopographical cues were able to reprogram MSCs. However, promising indications that stem cell marker STRO-1 levels increased, is consistent with SQ being a surface that maintains 'stemness' and multipotency of MSCs with culture *in vitro*.

Table of Contents

Abstract	ii
List of Tables	vii
List of Figures	viii
Presentations	xi
Publications	xi
Acknowledgement	xii
Author’s Declaration	xiii
Abbreviations	xiv
1 General Introduction	1
1.1 Tissue engineering and regenerative medicine	2
1.2 The extracellular matrix	4
1.3 The evolution of biomaterials for tissue engineering	4
1.4 Stem cells	8
1.4.1 Mesenchymal stem cells	10
1.4.2 The role of the niche in regulation of stem cells.....	14
1.5 Topography: from micro to nano	19
1.5.1 Directing MSC phenotype with nanotopography.....	22
1.6 Control of MSC growth	24
1.6.1 Mechanotransduction	25
1.6.2 Integrins	26
1.6.3 Cell-extracellular matrix adhesions	28
1.7 The cytoskeleton	32
1.7.1 The role of the cytoskeleton in mechanotransduction and cell sensing	34
1.8 The cell cycle and its potential role in stem cell self-renewal	36
1.9 Thesis aims	39
2 Chapter 2	41
2.1 Materials and reagents	42
2.1.1 Cell culture reagents	42
2.1.2 Induction media reagents	42
2.1.3 Immunostaining reagents	43
2.1.4 Western blotting reagents	43
2.1.5 Cell staining reagents	44
2.1.6 In-cell western reagents	44
2.1.7 Scanning electron microscopy reagents.....	44
2.1.8 Primary antibodies	45
2.1.9 Metabolomics sample preparation	45
2.1.10 Collagen gel reagents	45
2.2 Solutions for cell culture	46
2.3 Methods	47
2.3.1 Primary cell culture	47

2.3.2	Substrate fabrication and preparation.....	51
2.3.3	Material Characterisation	53
2.3.4	Cell seeding	54
2.3.5	MSC Characterisation.....	55
2.4	Microscopy and imaging.....	59
2.4.1	Brightfield microscopy	59
2.4.2	Fluorescence Microscopy.....	59
2.4.3	CellProfiler Image Analysis.....	60
2.4.4	Synchronisation and release of MSCs for analysis of cell cycle.....	60
2.4.5	Preparation of samples for flow cytometry	60
2.4.6	Quantitative in-cell western and detection	61
2.4.7	Filopodial inhibition.....	62
2.4.8	Next generation sequencing	62
2.4.9	Western blotting	64
2.5	Metabolomics	65
2.5.1	Sample preparation.....	65
2.5.2	Liquid chromatography mass spectrometry	65
2.5.3	Data analysis	66
2.6	Preliminary collagen gel study	66
2.6.1	Collagen gel preparation	66
2.6.2	Cell viability assay.....	67
2.7	Statistical Analysis	67
3	Chapter 3.....	68
3.1	Introduction	69
3.2	Results.....	72
3.2.1	Reproducibility of polycarbonate substrates	72
3.2.2	Plasma cleaning of nanotopographical substrates.....	74
3.2.3	Effect of nanotopography on phenotype of MSCs cultured on PCL.....	82
3.2.4	Characterisation of CD271 ⁺ MSCs	83
3.2.5	Optimising seeding density for nanotopography efficiency.....	86
3.2.6	MSC proliferation on nanotopography	100
3.2.7	Metabolomic profile of CD271 ⁺ MSCs.....	102
3.3	Discussion.....	124
3.3.1	Characterisation of substrates	124
3.3.2	Initial seeding density affects response to nanotopography	125
3.3.3	Metabolism of CD271 ⁺ MSCs on nanotopography.....	127
4	Chapter 4.....	130
4.1	Introduction	131
4.2	Results.....	134
4.2.1	Assessing seeding density for STRO-1+ MSCs	134
4.2.2	Synchronisation and release of MSCs for analysis of cell cycle.....	135
4.2.3	Cell cycle screening on nanotopographies.....	136
4.2.4	Analysis of cell cycle stages on SQ using flow cytometry.....	139
4.2.5	Observing filopodial spread on nanotopography.....	142
4.2.6	Chemical inhibition of filopodia development.....	147
4.2.7	Assessment of filopodia inhibition on CDK6 protein expression	149

4.2.8	Identifying signalling networks using Next-Generation Sequencing.....	150
4.3	Discussion.....	164
4.3.1	Interpretation of cell cycle protein levels analysed by ICW	164
4.3.2	Changes in cell signalling networks and cell cycle regulation	166
4.3.3	Link between filopodia and cell cycle regulation was not established	167
4.3.4	Proposed models of self-renewal on SQ in relation to cell cycle	168
5	Chapter 5.....	170
5.1	Introduction	171
5.2	Results.....	173
5.2.1	Investigating nanotopography for reprogramming	173
5.3	Discussion.....	184
6	Chapter 6.....	187
6.1	General discussion.....	188
6.1.1	Utilising nanotopographies as a tool for study of MSCs	189
6.1.2	Metabolomic changes in self-renewing and differentiating MSCs.....	190
6.1.3	Influence of nanotopography on cell cycle and gene expression of MSCs	191
6.1.4	Topography for MSC reprogramming	194
6.2	Thesis conclusion.....	195
6.3	Recommendations for future work.....	196
6.3.1	Nanotopography for the culture of MSCs in vitro.....	196
6.3.2	Three-dimensional MSC environments.....	197
6.3.3	MSCs as supporting cells for regenerative medicine	200
6.3.4	Nanotopography as a platform to investigate adhesion and tension.....	201
	List of references	202

List of Tables

Table 1-1: MSC and differentiation cell surface markers used in the study.....	14
Table 2-1: Reagent volumes for the preparation of collagen gels.....	66
Table 3-1: Quantification of detailed XPS spectra corresponding to air plasma treated polycarbonate.....	78
Table 3-2: Quantification of detailed XPS spectra corresponding to oxygen plasma treated polycarbonate.....	78
Table 5-1: Summary of statistical significance calculated for initial assessment of STRO-1.....	176
Table 5-2: Summary of statistical significance calculated for further assessments of STRO-1 (Patient 2).....	178
Table 5-3: Summary of statistical significance calculated for further assessments of STRO-1 (Patient 3).....	178
Table 5-4: Summary of statistical significance calculated for ALCAM (Patient 2).....	180
Table 5-5: Summary of statistical significance calculated for ALCAM (Patient 3).....	180
Table 5-6: Summary of statistical significance calculated for OPN (Patient 2).....	183
Table 5-7: Summary of statistical significance calculated for OCN (Patient 3).....	183

List of Figures

<i>Figure 1-1: The evolution of biomaterials across three generations.....</i>	<i>6</i>
<i>Figure 1-2: Generation and differentiation of iPSCs.</i>	<i>10</i>
<i>Figure 1-3: Mesenchymal stem cell multipotency/differentiation in vitro.....</i>	<i>12</i>
<i>Figure 1-4: MSCs selected using MACs techniques and a stem cell marker-specific antibody</i>	<i>13</i>
<i>Figure 1-5: Regulatory components of stem cell function in the niche.</i>	<i>16</i>
<i>Figure 1-6: Hypothetical model depicting stem cell polarity and orientation of the mitotic spindle by the niche</i>	<i>18</i>
<i>Figure 1-7: Topography to induce cell response</i>	<i>21</i>
<i>Figure 1-8: Focal adhesions observed at cell periphery.</i>	<i>29</i>
<i>Figure 1-9: Schematic of cytoskeletal filament assembly.</i>	<i>34</i>
<i>Figure 1-10: Schematic of the cell cycle</i>	<i>38</i>
<i>Figure 2-1: Location of the mononuclear cell fraction.</i>	<i>48</i>
<i>Figure 2-2: Outline of magnetic separation procedure for selection of CD271-positive MSCs from human bone marrow.....</i>	<i>49</i>
<i>Figure 2-3: Cell seeding device</i>	<i>55</i>
<i>Figure 2-4: Application of a grid for quantification of samples stained using IRdye fluorescent secondary antibodies.</i>	<i>62</i>
<i>Figure 3-1: Reproducibility of the nanopatterns across batch manufacture</i>	<i>73</i>
<i>Figure 3-2: Measured and calculated theoretical water contact angles for polycarbonate flat and nanopatterned surfaces.</i>	<i>74</i>
<i>Figure 3-3: XPS analysis of air plasma treated polycarbonate.....</i>	<i>76</i>
<i>Figure 3-4: XPS analysis of oxygen plasma treated polycarbonate.</i>	<i>77</i>
<i>Figure 3-5: SEM images of flat and nanopatterned surfaces following air plasma treatment.....</i>	<i>79</i>
<i>Figure 3-6: Effect of air plasma treatment on nanotopography surfaces assessed by AFM imaging.</i>	<i>80</i>
<i>Figure 3-7: Plasma treated nanotopography pit depth measurements derived from AFM images.....</i>	<i>81</i>
<i>Figure 3-8: Osteogenesis promoting and stem cell maintaining phenotypes induced by nanopit nanotopography on PCL.</i>	<i>82</i>
<i>Figure 3-9: Selected MSCs using a CD271 magnetic separation kit stain positive for CD271..</i>	<i>83</i>
<i>Figure 3-10: The CD271⁺ MSC population stain positively for stem cell markers STRO-1, CD63, and niche marker nestin.</i>	<i>84</i>
<i>Figure 3-11: Chemically induced osteogenic and adipogenic differentiation of CD271⁺ MSCs.</i>	<i>85</i>
<i>Figure 3-12: Comparison of conventional seeding and seeding with a device.....</i>	<i>86</i>
<i>Figure 3-13: Initial assessment of cell spread and coverage when seeding at different densities using a seeding device.</i>	<i>87</i>
<i>Figure 3-14: CD271⁺ MSCs cultured at different densities exhibit unique cell growth patterns.....</i>	<i>93</i>
<i>Figure 3-15: Growth and spread of CD271⁺ MSCs on flat and nanopatterned substrates after 28 days culture.</i>	<i>94</i>
<i>Figure 3-16: Effect of seeding density on protein expression in MSCs seeded on nanotopography.</i>	<i>95</i>
<i>Figure 3-17: Quantified protein expression levels by densitometry.</i>	<i>96</i>

Figure 3-18: Effect of seeding density on protein expression in CD271 ⁺ MSCs, assessed by image analysis.	99
Figure 3-19: BrdU incorporation in CD271 ⁺ MSCs.	100
Figure 3-20: Assessment of MSC growth on nanotopographies over time.	101
Figure 3-21: Overview of detected and significant metabolites in MSCs on SQ in comparison to flat after 7 days of culture.	104
Figure 3-22: Grouped total metabolite fold changes for MSCs cultured on nanotopographies.	105
Figure 3-23: Nucleotide metabolite profiles on SQ and NSQ after 7 days of culture.	106
Figure 3-24: Amino acid metabolite profile on SQ and NSQ after 7 days of culture.	107
Figure 3-25: Lipid related metabolite profile on SQ and NSQ after 7 days of culture.	108
Figure 3-26: Carbohydrate metabolite profiles on SQ and NSQ after 7 day culture.	109
Figure 3-27: Secondary metabolites, vitamins and cofactors (and other remaining smaller groups) profile on SQ and NSQ after 7 days culture.	110
Figure 3-28: Profile of unclassified metabolites on SQ and NSQ after 7 days culture.	111
Figure 3-29: Biosynthesis of amino acids KEGG map with elevated NSQ metabolites. ...	113
Figure 3-30: Up-regulations and down-regulations in metabolic pathways in MSCs on SQ after 7 days.	114
Figure 3-31: Up-regulations and down-regulations in metabolic pathways on NSQ after 7 days culture.	115
Figure 3-32: Ingenuity pathway highlighting direct and indirect associations for amino acid metabolites in MSCs cultured on SQ nanotopographies.	116
Figure 3-33: Krebs cycle/tricarboxylic acid (TCA) cycle in MSCs on SQ.	117
Figure 3-34: Ingenuity pathway highlighting direct and indirect associations for amino acid metabolites in MSCs cultured on NSQ nanotopographies.	118
Figure 3-35: Outline of metabolite profile of MSCs after two weeks culture.	119
Figure 3-36: Total metabolic intensity fold changes in MSCs cultured on nanotopographies within pathway groups after two weeks.	120
Figure 3-37: Metabolites in MSCs on SQ show an increased number of upregulated metabolites with unsaturated structures.	123
Figure 4-1: Western blotting at a seeding density of 1000 cells/cm ² was adequate for use of nanotopographies with STRO-1 ⁺ MSCs.	134
Figure 4-2: Validation of synchronisation procedure using flow cytometry.	136
Figure 4-3: Testing GAPDH levels in MSCs cultured on different surfaces.	137
Figure 4-4: Levels of cell cycle proteins assessed in synchronised MSCs on nanotopography	138
Figure 4-5: Elevated CDK6 protein levels observed on SQ.	139
Figure 4-6: Elevated percentage of G0/G1 MSCs observed on SQ (patient 1).	140
Figure 4-7: Higher percentage of G0/G1 MSCs observed on SQ (patient 2).	141
Figure 4-8: Filopodia observed in MSCs following synchronisation.	143
Figure 4-9: Distribution of filopodia after 1 hour release into the cell cycle.	144
Figure 4-10: Distribution of filopodia after 4 hours release into the cell cycle.	145
Figure 4-11: Distribution of filopodia after 24 hours release into the cell cycle.	146
Figure 4-12: Chemical inhibition of filopodia in MSCs.	148
Figure 4-13: Effect of 20 μM cdc42 inhibitor on filopodial spread on nanotopography. ..	149
Figure 4-14: CDK6 is not affected in MSCs subjected to cdc42 inhibition.	150
Figure 4-15: Downstream effects analysis of differentially expressed genes in synchronised MSCs cultured on nanotopography.	152
Figure 4-16: Up-regulations and down-regulations of signalling processes in synchronised MSCs cultured on SQ nanotopography.	153

<i>Figure 4-17: Up-regulations and down-regulations in signalling processes in synchronised MSCs cultured on NSQ nanotopography.....</i>	<i>154</i>
<i>Figure 4-18: Downstream effects analysis of differentially expressed genes in MSCs released into cell cycle for 24 hours on nanotopography..</i>	<i>155</i>
<i>Figure 4-19: Up-regulations and down-regulations within signalling pathways in MSCs post-release into the cell cycle, cultured on SQ nanotopography..</i>	<i>157</i>
<i>Figure 4-20: Up-regulations and down-regulations within signalling pathways in MSCs post-release into the cell cycle, cultured on NSQ nanotopography (part 1)..</i>	<i>158</i>
<i>Figure 4-21: Up-regulations and down-regulations within signalling pathways in MSCs post-release into the cell cycle, cultured on NSQ nanotopography (part 2)..</i>	<i>159</i>
<i>Figure 4-22: ERK/MAPK signalling pathway on SQ nanotopography following release of MSCs into the cell cycle after synchronisation.</i>	<i>161</i>
<i>Figure 4-23: Cyclins and cell cycle regulation pathways on SQ nanotopography after release of MSCs into the cell cycle.</i>	<i>162</i>
<i>Figure 4-24: Stress-activated protein kinases (SAPK)/Jun amino-terminal kinases (JNK) signalling pathway on NSQ nanotopography following release of MSCs into the cell cycle.</i>	<i>163</i>
<i>Figure 5-1: CD63 protein levels before and after reprogramming on SQ nanotopography.</i>	<i>173</i>
<i>Figure 5-2: ALCAM levels before and after reprogramming on SQ nanotopography.</i>	<i>174</i>
<i>Figure 5-3: STRO-1 protein levels in differentiating MSCs reseeded on SQ to assess reprogramming potential..</i>	<i>175</i>
<i>Figure 5-4: Further assessment of STRO-1 protein levels in differentiating MSCs reseeded on SQ.....</i>	<i>177</i>
<i>Figure 5-5: ALCAM protein levels following reseeded of NSQ-induced MSCs on SQ and flat substrates..</i>	<i>179</i>
<i>Figure 5-6: OCN protein levels following reseeded of NSQ-induced MSCs on SQ and flat substrates.</i>	<i>182</i>
<i>Figure 6-1: Application of a collagen gel increases nestin expression.</i>	<i>198</i>
<i>Figure 6-2: Live/dead staining of MSCs and HSCs in the nanotopography-collagen gel system..</i>	<i>199</i>

Presentations

2013 Glasgow Orthopaedic Research Initiative (GLORI) meeting.

“Nanotopographical control of mesenchymal stem cells.” Glasgow, UK (Poster presentation)

2013 Tissue and Cell Engineering Society (TCES). “Nanotopographical direction of adult mesenchymal stem cell growth and differentiation.” Cardiff, UK (Poster presentation)

2014 Tissue Engineering and Regenerative Medicine International Society (TERMIS). “Investigating self-renewal of mesenchymal stem cells on nanotopography.” Genoa, Italy (Poster presentation)

2014 TCES. “Investigating self-renewal of mesenchymal stem cells on nanotopography.” Newcastle, UK (Poster presentation)

2014 European Society for Biomaterials (ESB). “Mesenchymal stem cell self-renewal on nanotopography.” Liverpool, UK (Rapidfire oral presentation and poster presentation)

2014 European Materials Research Society (EMRS). “Influence of nanotopography on mesenchymal stem cell multipotency, cell cycle and growth.” Warsaw, Poland (Oral presentation)

2014 GLORI meeting. “Investigating growth and cell cycle changes in MSCs cultured on nanotopography.” Glasgow, UK (Oral presentation)

Publications

Dalby MJ, Macintyre A, Roberts JN, Yang J, Lee LC, Tsimbouri PM, McNamara LE. (2012) Influence of local ligand density on formation of focal adhesions on nano- and micro-nanostructured surfaces. *Nanomedicine (Lond)*. 7(1):20.

Dalby MJ, Lee LC, Yang J, MacIntyre, A, McCully M. (2013) Endothelial co-culture with mesenchymal stem cells on nanotopography to direct osteogenesis. *Nanomedicine (Lond)*. 8(11):1743-4

Acknowledgement

I would like to thank my supervisors, Professor Matthew Dalby, Professor Nikolaj Gadegaard, Dr Stephen Yarwood and orthopaedic surgeon RM Dominic Meek, for their roles in the project: to Matt, for his initial encouragement for me to undertake a PhD in his group and guidance over the past years, to Nikolaj and the engineers for the supply of materials, to Stephen for his technical advice and lastly to Dominic for provision of bone marrow.

I am very grateful to all of the people who had a part in this project, from XPS, flow cytometry to SEM, there were a lot of techniques involved that required the help of others, so thanks to Rasmus, Margaret, Maria, Anwer, to name but a few. Sorry if I've missed anyone here, I'm sure you'll be mentioned in the thesis elsewhere! All the help given was much appreciated.

I must also thank those in the Centre for Cell Engineering who supported me, especially when things were not going to plan. To Laura and Monica for their kind words and Jingli for helpful discussion. It always meant a lot to see you all take the time to look out for me.

Thanks to my constant office buddies, Niall and Emily, for all your positivity, the (often food-related!) chat and laughs over the years. Thanks also go to Ya Hua and Doaa for all the fun times we had, our Italy trip, trying out many of the restaurants in Glasgow, and catching up on lots of TV series to keep us going. Thanks to friends, Elaine, Diana, Eirini, Krishna, Suzanne, Sindy and Fiona for all their advice, visits (and tolerance of my stressing) during my PhD years. I couldn't have done it without you.

Lastly, the biggest thank you must go to my family for their continuous support. To mum and dad, who have always strived to give me the opportunities they never had. I hope that I have managed to show just a little of the determination that you both have displayed over many years. Thank you for always believing in me and encouraging me to do my best; when I stumble and fall, I will always try to overcome.

Author's Declaration

I hereby declare that the research reported within this thesis is my own work, unless otherwise stated, and that at the time of submission is not being considered elsewhere for any other academic qualification.

Louisa Lee

1st October 2015

Abbreviations

List of abbreviations

µm	Micrometre
nm	Nanometer
µl	Microlitre
ml	Millilitre
αMEM	Alpha minimal essential media
AFM	Atomic force microscopy
ALCAM	Activated leukocyte cell adhesion molecule
ANOVA	Analysis of variance
a.u.	Arbitrary units
BrdU	5-bromo-2'-deoxyuridine
BSA	Bovine serum albumin
CD271/p75NTR	Low-affinity nerve growth factor receptor/p75 neurotrophin receptor
Cdc2	Cell division cycle 2
Cdc42i	Cdc42 inhibitor
DAPI	4'-6-Diamidino-2-Phenylindole
DMEM	Dulbecco's Modified Eagle's Medium
E2F-1	E2F transcription factor 1
ECM	Extracellular matrix
EDTA	Ethylenediaminetetraacetic acid
ERK	Extracellular signal-related kinase
FBS	Foetal bovine serum
FITC	Fluorescein isothiocyanate
G0	Quiescent phase
G1	Gap phase 1
G2	Gap phase 2
GAPDH	Glyceraldehyde 3-phosphate dehydrogenase
HCl	Hydrochloric acid
HEPES	4-(2-Hydroxyethyl)piperazine-1-ethanesulfonic acid
HSC	Haematopoietic stem cell
ICW	In-cell western
IgG	Immunoglobulin G
iPSC	Induced pluripotent stem cell
IRDye	Infrared dye
JNK	c-Jun N terminal kinase
M phase	Mitosis
MACS	Magnetic activated cell sorting
MSC	Mesenchymal stem cell
NaCl	Sodium chloride
NGS	Next-generation sequencing
NSQ	"Near square" nanotopography with a square lattice arrangement of nanopits ± 50nm displacement
OCN	Osteocalcin
OGM	Osteogenic media
OPN	Osteopontin
PBS	Phosphate buffered saline

PBST	Phosphate buffered saline with Tween-20
PC	Polycarbonate
PCL	Polycaprolactone
PMMA	Polymethylmethacrylate
p-myosin	Phosphorylated myosin
p-value	Probability value
PVDF	Polyvinylidene fluoride
Rb	Retinoblastoma tumour suppressor
RNA	Ribonucleic acid
ROCK	Rho-associated kinase
S phase	Synthesis phase
SDS	Sodium dodecyl sulphate
SEM	Scanning electron microscopy
STRO-1	Stromal cell surface protein
SQ	Nanotopography with a square lattice arrangement of nanopits
Tris	Tris(hydroxymethyl)aminomethane
WCA	Water contact angle
w/v	Weight per volume
v/v	Volume per volume
XPS	X-ray photoelectron spectroscopy

Chapter 1

General Introduction

1 General Introduction

1.1 Tissue engineering and regenerative medicine

The concept of tissue engineering developed from an idea to create new tissue with the aim of repairing failing or damaged tissue and restoring its associated function (Langer and Vacanti, 1993). Materials have been used to make templates or scaffolds to cultivate cells for eventual tissue formation (Langer and Tirrell, 2004). Several promising studies identified aspects of the tested materials that were sufficient to induce changes in cell behaviour, including differentiation, growth and proliferation (Engler *et al.*, 2006, Dalby *et al.*, 2007, McMurray *et al.*, 2011, Lee *et al.*, 2014a). Tissue engineering commonly applies the strategy of mimicking a cell's natural environment, often bringing together cells, scaffolds and biochemical factors (Langer and Vacanti, 1993, Shah *et al.*, 2014, Zhang *et al.*, 2014). With a trend towards a largely aging population, such research is becoming increasingly important, leading to the evolution of the field of regenerative medicine (Haseltine, 2003). Regenerative medicine incorporates tissue engineering with the additional aim of advancing research on the induction of self-repair (regeneration) of tissues and organs, presenting some truly revolutionary approaches in the treatment of disease (Salgado *et al.*, 2013).

Examples of particularly well-publicised and promising preliminary work for potential future clinical treatments range from the implant of vascular grafts (Dahl *et al.*, 2011) to the transplantation of a tissue-engineered trachea (Macchiarini *et al.*, 2008). The derivation and subsequent development of tissue engineering constructs has now become commonly utilised to overcome issues with organ replacement, particularly during the last decade. Expansion of cells from the patient themselves, and generating autologous tissues, may reduce the likelihood of rejection (Boehler *et al.*, 2011).

The basis of these types of clinical therapy are studies illustrating that cells in the body require supporting mechanical structures for their establishment and orientation, as well as instructional cues that influence their behaviour (Melchels

et al., 2010, Gee *et al.*, 2012, Evans and Gentleman, 2014). Normally these would be obtained from the extracellular matrix (ECM), which is produced and secreted by the cells themselves. However, the structural aspect of the ECM can be provided artificially by building a substrate from materials such as a polymer or using natural materials (Ma *et al.*, 2001, Chastain *et al.*, 2006, Geckil *et al.*, 2010). Such substrates are commonly referred to as ‘biomaterials’, designed to mimic the native composition and arrangement of the ECM, attempting to recapitulate the microenvironment as closely as possible (Navarro *et al.*, 2008, Damanik *et al.*, 2014). Subsequent supplementation of cells and additional growth factors to the material construct or ‘scaffold’ can then lead to support of other cell types and successful formation of tissues for use in medical applications (Cenni *et al.*, 2011, Chen *et al.*, 2014a).

Stem cells will likely underpin regenerative medicine, with biomaterials also being recognised as useful tools. The former are important, due largely to the unique ability of stem cells to self-renew and their versatility in differentiating into many cell types (potentially complex tissues) (Yao *et al.*, 2006, Abdallah and Kassem, 2007, Wilson *et al.*, 2008, Sarugaser *et al.*, 2009, Blin *et al.*, 2010). Stem cells are complemented by the potential of next-generation biomaterials in directing stimulation of stem cells without the need for chemical intervention (Dalby *et al.*, 2007, McMurray *et al.*, 2011). The combination of advantages offered by both biomaterials and stem cells could lead to a workable platform in the treatment of degenerative diseases, such as future implants for bone conditions such as osteoarthritis (Sjöström *et al.*, 2009, Sjöström *et al.*, 2013), and vascular grafts to overcome cardiovascular complications (Matsumura *et al.*, 2003, Zhao, 2013), which are affecting increasing numbers of people in modern society. Tissue engineering now encompasses both *in vitro* (Friedenstein *et al.*, 1987, Ma *et al.*, 2001) and *in situ* (Ko *et al.*, 2013, Andreas *et al.*, 2014) strategies that allow even greater potential for regenerative medicine.

Individual aspects that comprise the foundations for tissue engineering and regenerative medicine will be discussed in further detail in the following sections.

1.2 The extracellular matrix

The extracellular space between cells in tissues is known as the extracellular matrix (ECM). The ECM contains a vast network of glycoproteins, polysaccharides, proteoglycans and macromolecules, and their spatial arrangement gives rise to the distinct physical attributes of numerous tissues of the body (Mouw *et al.*, 2014). Some examples of ECM proteins include fibronectin, vitronectin, collagen and laminin (Frantz *et al.*, 2010). These are important scaffolding proteins necessary for cell-matrix adhesion and structural organisation (Woods *et al.*, 1986, Steele *et al.*, 1992, Heino, 2007, Frantz *et al.*, 2010, Marthiens *et al.*, 2010).

The ECM does not merely offer structural support and stability within a tissue or scaffolding for cell anchorage; changes in ECM composition have influence on migration, proliferation, morphology and other aspects of cellular function and behaviour (Bhadriraju and Hansen, 2002, Barker, 2011, Charras and Sahai, 2014, Nakamura *et al.*, 2014). A decrease in effective anchorage of cell adhesion related molecules in the ECM is associated with diseases such as osteoporosis (Perinpanayagam *et al.*, 2001), cancer (Mason *et al.*) and asthma (Vanderslice *et al.*, 2004). This outlines the importance of regulation, reorganisation and remodelling of the constituents of the ECM to maintain a state of homeostasis within tissues in response to external pressures from their microenvironment. Moreover, these findings underline the fact that the ECM must be highly adaptable at any given point in time, so that it may respond as cells are undergoing changes themselves.

In the context of this thesis, the term ECM will be used as reference to the extracellular environment, inclusive of the substrate biomaterial utilised in this study, rather than solely the macromolecules secreted by other cells.

1.3 The evolution of biomaterials for tissue engineering

Interaction of cells with the ECM has been well established as being important in influencing subsequent cell development and behaviour (Lukashev and Werb, 1998). Extending this knowledge towards investigating the interaction of cells

and tissues with the surfaces of synthesized substrates forms the basis of biomaterials research. This research is critical as medical implants and devices require an understanding of the properties of cells and tissues in order to provide a safe and feasible means of treatment in the body (Uludağ, 2014). Over time, the definition of the term 'biomaterial' has undergone changes to encompass the increasing number of materials, chemistries and multi-component systems that are now being studied (Williams, 2009). A biomaterial can be considered as an engineered substance that can be used in isolation or in conjunction with other substances, to regulate entities and thereby processes of living systems for medical purposes (Williams, 2009).

A wide range of biomaterials can be selected to produce a scaffold or substrate, dependent on the property deemed most important for a specific aim or function. In general terms, the classically used materials fall into the broad categories of metals (Dolder *et al.*, 2003, Wall *et al.*, 2009, McNamara *et al.*, 2011), ceramics (Saikia *et al.*, 2008, Lin *et al.*, 2009), and synthetic or naturally derived single or blended polymers (Di Martino *et al.*, 2005, He *et al.*, 2005), which all present their own advantages and disadvantages. As there is often not an ideal 'gold standard material' that can meet all the requirements, distinct properties and complexities of native tissue, a compromise of these factors must be decided upon. The evolution in the design of biomaterials appears to have progressed across three distinct stages, or 'generations' up to the turn of the century, as outlined by Hench and Polak (Hench and Polak, 2002) (*Figure 1-1*).

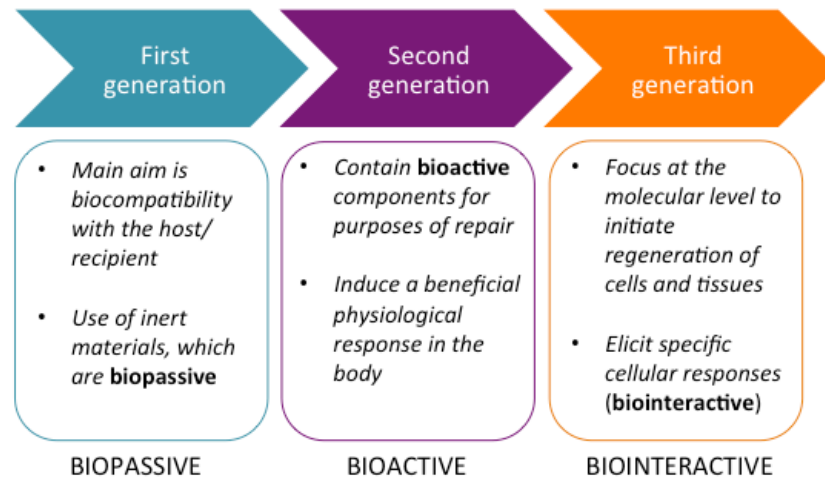


Figure 1-1: The evolution of biomaterials across three generations. Flow diagram depicting the changing focus and trends of biomaterial design. The history of biomaterials design can generally be divided into three categories commonly referred to as ‘generations’. The three generations can be summarized using three basic terms: *biopassive*, *bioactive*, and *biointeractive*, respectively (Hench and Polak, 2002, Navarro *et al.*, 2008).

The design focus of the earliest biomedical materials was to emulate native mechanical properties such as that of bone, which then shifted to achieve biological ‘inertness’, and reduction in the likelihood of an immune response from the host (Hench, 1980, Navarro *et al.*, 2008); example materials include metals and ceramics. This was particularly important in surgical prostheses and the rule still holds true to date. Nevertheless, use of nearly inert materials in isolation did not prove an ideal solution, as insufficient adhesion and cellular interaction with these types of implants meant that often a thin fibrous area of tissue developed in the region between the implant and the native tissue (Hench, 1980, Anderson *et al.*, 2008). In contrast, use of materials that induced greater immune reaction also typically resulted in the formation of a fibrous capsule around such materials, (observed to be of increased thickness due partly to inflammation), which, in turn, would apply a degree of stress to surrounding tissues (Anderson *et al.*, 2008). Moreover, the lack of blood supply would mean that white blood cells would not be available to fight off any developing infection (Hench, 1980). It was therefore understood that biocompatibility alone was not enough to elicit the desired responses of tissue repair in the body (Williams, 2008).

Second-generation biomaterials developed the concept of localized bioactivity, in that the substrate itself could generate a physiological response from the

tissue surrounding it (Navarro *et al.*, 2008). Bioactive glasses and bioactive ceramics such as hydroxyapatite were reported as being able to facilitate formation of bone (Reilly *et al.*, 2007). There was additionally an increasing emphasis on biodegradability, such that a scaffold would be gradually removed over time (Nair and Laurencin, 2007). Polymers approved by the Food and Drug Administration (FDA) for use in the body, such as polyglycolic acid (PGA), which is bioresorbable, poly(lactic-co-glycolic acid) (PLGA) and polycaprolactone (PCL) which are biodegradable polymers, were utilised as they were regarded as being both biocompatible and removable in the long-term (Gunatillake and Adhikari, 2003). Once the scaffold or construct biomaterial is resorbed, this would leave the cells that were seeded within the scaffold to interact with those located in the surrounding environment, eventually aspiring to incorporate a blood system and nerves from the recipient. However, it was increasingly recognised that specific cell-material interactions must take place to give rise to the most benefits for the patient (McBeath *et al.*, 2004, Chen *et al.*, 2014b).

This led to the development of ‘third generation’ biomaterials, which progressed towards surfaces that would involve bioactive components for the support and regeneration of tissue (Hench and Polak, 2002). They aimed to induce changes at a molecular level, inhibiting or activating cellular activities or inducing expression of specific genes to aid the regeneration process. To this end, biomaterials must mimic a cell’s natural environment at a molecular level (Lutolf *et al.*, 2009). One strategy has been to incorporate features emulating the ECM onto the material surface, often at a micro- or nanoscale range (topography) (Arnold *et al.*, 2004, Bettinger *et al.*, 2009, Albuschies and Vogel, 2013). Advances have already been made with examples of biomaterials having influence on a range of cellular processes such as cell migration (Cavalcanti-Adam *et al.*, 2007), proliferation (Ali *et al.*, 2014) and differentiation (Dalby *et al.*, 2007, Teo *et al.*, 2013). Cellular responses have been reported for a range of cell types including fibroblasts (Loesberg *et al.*, 2007), osteoblasts (Lamers *et al.*, 2010), endothelial cells (Dreier *et al.*, 2013), neuronal cells (Micholt *et al.*, 2013) and stem cells (Chen *et al.*, 2012). Stem cells present an exciting prospect in regenerative medicine as they can differentiate into many cell types. With regards to the control of stem cells with biomaterials, the next challenge herein lies in determining how to elicit beneficial stem cell self-renewal or guide

differentiation to a particular cell lineage (Hench and Polak, 2002). Strategies employed include the use of different topographies over several scales (Wilkinson *et al.*, 2002), varying chemistries (Lutolf *et al.*, 2009) and elastic modulus (Engler *et al.*, 2006). All of these studies are linked in their attempt at provision of a tailored method of stimulation to gain a specific functional cellular response. The next step would be to generate complex tissues such as bone tissue, which are distinguished by their unique physical, chemical and structural topographical features (Stevens and George, 2005), and to develop systems in three-dimensions (Baker and Chen, 2012) to allow for incorporation of aspects of geometric positioning.

1.4 Stem cells

Stem cells are defined by the possession of two distinctive properties: that of self-renewal in an undifferentiated state, and a potential to differentiate into a range of specialized cell lineages, known as potency (Blanpain *et al.*, 2004). There are several degrees of potency, namely unipotency (differentiation into a single cell type) pluripotency (the ability to differentiate into all three germ layers; endoderm, mesoderm or ectoderm) multipotency (able to differentiate into a number of cell types) or totipotency (can form all cell types) (Kolios and Moodley, 2013).

Embryonic stem cells (ESCs) are pluripotent and are derived from the inner cell mass of a blastocyst from an embryo (Nichols and Smith, 2012), which makes human ESCs difficult to obtain due to a number of ethical factors pertaining to the donation of *in vitro* fertilized eggs for research (Wert and Mummery, 2003). ESCs were initially cultured with a 'feeder layer' of mouse (Thomson *et al.*, 1998, Reubinoff *et al.*, 2000) or human derived (non-dividing) fibroblasts (Amit *et al.*, 2003) to supply nutrients to the ESCs, however, use of foreign cells from another species and the risk of virus transmission would prevent ESC treatments from being successfully transferred to the clinic. With the advent of new technologies, xeno and feeder-free culturing methods are being investigated (Jang *et al.*, 2013).

An alternative source of stem cells can be extracted from adult tissue such as bone marrow, adipose and brain tissue (Friedenstein *et al.*, 1987, Meirelles *et al.*, 2006, Bunnell *et al.*, 2008). These cells are referred to as somatic stem cells or adult stem cells, and those derived from bone marrow, are commonly termed mesenchymal stem cells (MSCs) (Abdallah and Kassem, 2007). MSCs also possess the capacity to self-renew, though they possess a limited differentiation capacity in comparison to ESCs (Blau *et al.*, 2001). MSCs exhibit multipotency which means that they can differentiate into a small number of lineages (Pittenger *et al.*, 1999). The discovery and history of MSCs will be expanded upon in the following section.

Induced pluripotent stem cells (iPSCs) are derived from successful reprogramming of somatic cells to once again ascribe them ESC-like properties. The initial discoveries were attributed to Yamanaka and collaborators, who reported reprogramming of mouse cells (Takahashi and Yamanaka, 2006), followed by reprogramming of human cells shortly thereafter (Takahashi *et al.*, 2007). Intriguingly, the retroviral delivery of the same four transcription factors (Oct3/4, Sox2, Klf4, and c-Myc) to both mouse and human fibroblasts resulted in the generation of iPSC cells (Takahashi and Yamanaka, 2006, Takahashi *et al.*, 2007). The generation of human iPSCs was thought to be a groundbreaking discovery as it opened up the potential for large quantities of autologous patient stem cells to be created for regenerative medicine (*Figure 1-2*). However, a caveat to creating these cells is that there is no screening method to ensure that complete nuclear reprogramming has taken place. Partially reprogrammed iPSCs will not exhibit all the desired ESC-like characteristics, and aberrations in reprogramming may impair differentiation potential and pose a higher risk of teratoma formation (Yamanaka, 2009). Indeed, a study by Okita *et al.* reported that expression of *c-myc* could be reactivated and cause formation of tumours (Okita *et al.*, 2007) with additionally safety concerns due to the uncontrolled and random nature of integration of DNA into the host genome (Takahashi *et al.*, 2007).

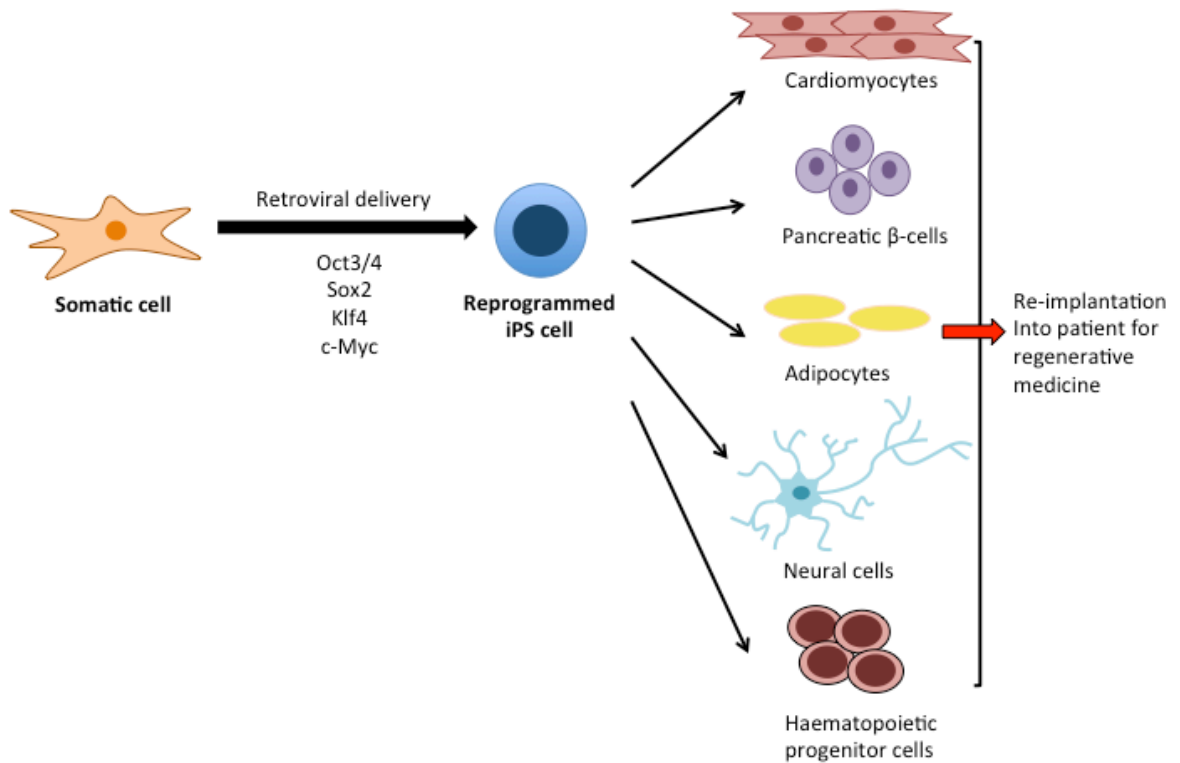


Figure 1-2: Generation and differentiation of iPSCs. Delivery of four factors using retroviruses can reprogram a somatic cell taken from a patient, such as a fibroblast cell, and generate an induced pluripotent stem cell. These can then be differentiated into a number of cell types, and re-implanted into the patient for the purposes of regenerative medicine. Adapted from Yamanaka, 2009.

1.4.1 Mesenchymal stem cells

In 1970, Friedenstein and colleagues described cells from the bone marrow, which included a small population that were adherent, similar to fibroblasts in morphology, and exhibited clonal growth. These were shown to be progenitor cells, with the ability to differentiate into osteoblasts (Friedenstein *et al.*, 1970). At the time, Friedenstein called them ‘colony forming units’, and these were, in fact, stem cells. Caplan eventually assigned the term ‘mesenchymal stem cells’ to the subpopulation in bone marrow that exhibited an ability to differentiate into cartilage and bone (Caplan, 1991).

Amongst the mixture of MSCs isolated from bone marrow are osteoprogenitors, chondrogenic progenitors and adipocyte progenitors (Muraglia *et al.*, 2000) that can be viewed as partially defined in terms of their stem cell fate. MSCs are multipotential, and have been reported to differentiate into a number of cell

types including adipocytes, osteoblasts, chondrocytes, myoblasts, and fibroblasts; cells comprising fat, bone, cartilage, muscle and skin respectively (Figure 1-3)(Pittenger *et al.*, 1999, Barry *et al.*, 2001, Gang *et al.*, 2004). Aside from these widely accepted cell types, some studies controversially report cases of trans-differentiation across tissue types, for example into neuronal cells, hepatocytes and endothelial cells, though these are mostly considered rare events and that trans-differentiation would be more achievable through reprogramming (Orlic, 2003, Song and Tuan, 2004, Jopling *et al.*, 2011). MSCs, along with other stem cell types, therefore offer great therapeutic potential for use in future clinical therapies, which is dependent on furthering our understanding of the regulation of self-renewal and lineage commitment. This will allow MSCs to be expanded and directed as necessary to meet the needs of particular patients. It is likely that MSCs will first be exploited for trophic effects related to immune and inflammatory modulation properties, to assist with transplant survival (Caplan and Dennis, 2006, Wu *et al.*, 2011, Yoo *et al.*, 2013). Expanded MSCs would offer immune protection for the initial stages of transplant and then dwindle over time (Wu *et al.*, 2011).

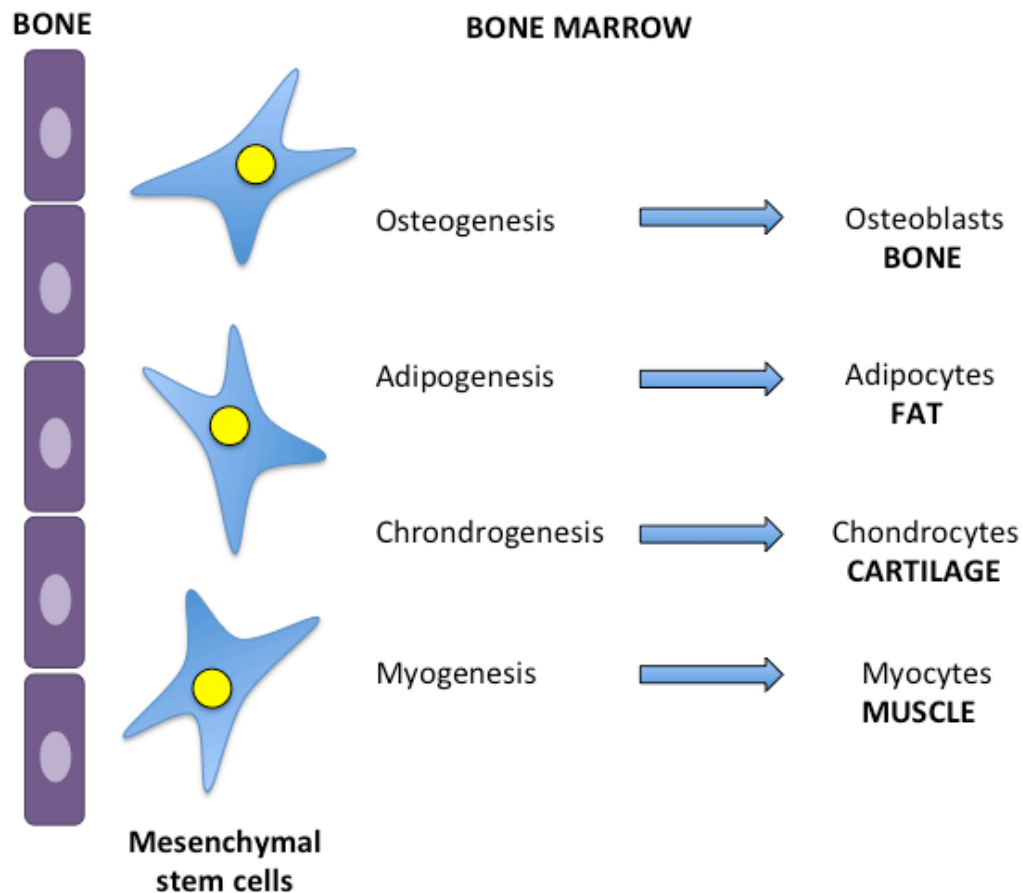


Figure 1-3: Mesenchymal stem cell multipotency/differentiation in vitro. Bone marrow-derived mesenchymal stem cells can differentiate into multiple lineages, including cells comprising that of bone, fat, cartilage, muscle, and into stromal cells. Adapted from Frenette *et al.* 2013 (Frenette *et al.*, 2013).

Current methods to isolate MSCs remain largely based on detection of the presence or absence of certain cell surface markers (Baddoo *et al.*, 2003). A number of MSC-specific markers have been identified which can be exploited in the selection of particular MSC subpopulations from human tissue samples (Jones *et al.*, 2002, Boxall and Jones, 2012, Gothard *et al.*, 2014). These can be cell adhesion molecules or surface antigens for example. No universal marker has been identified that can be used in isolation for all MSCs, however, one of the most highly published and widely known is the STRO-1 antigen (Simmons and Torok-Storb, 1991). Recently, CD271 (low-affinity nerve growth factor receptor, also known as p75 neurotrophic receptor) has emerged as a strong marker for isolating MSCs from human bone marrow aspirate (Bühning *et al.*, 2007, Jones *et al.*, 2010) (Figure 1-4). STRO-1 and CD271 have been reported to be highly

expressed in bone marrow-derived MSCs, and absent in fibroblasts, supporting their use as markers for selection (Jones *et al.*, 2002).

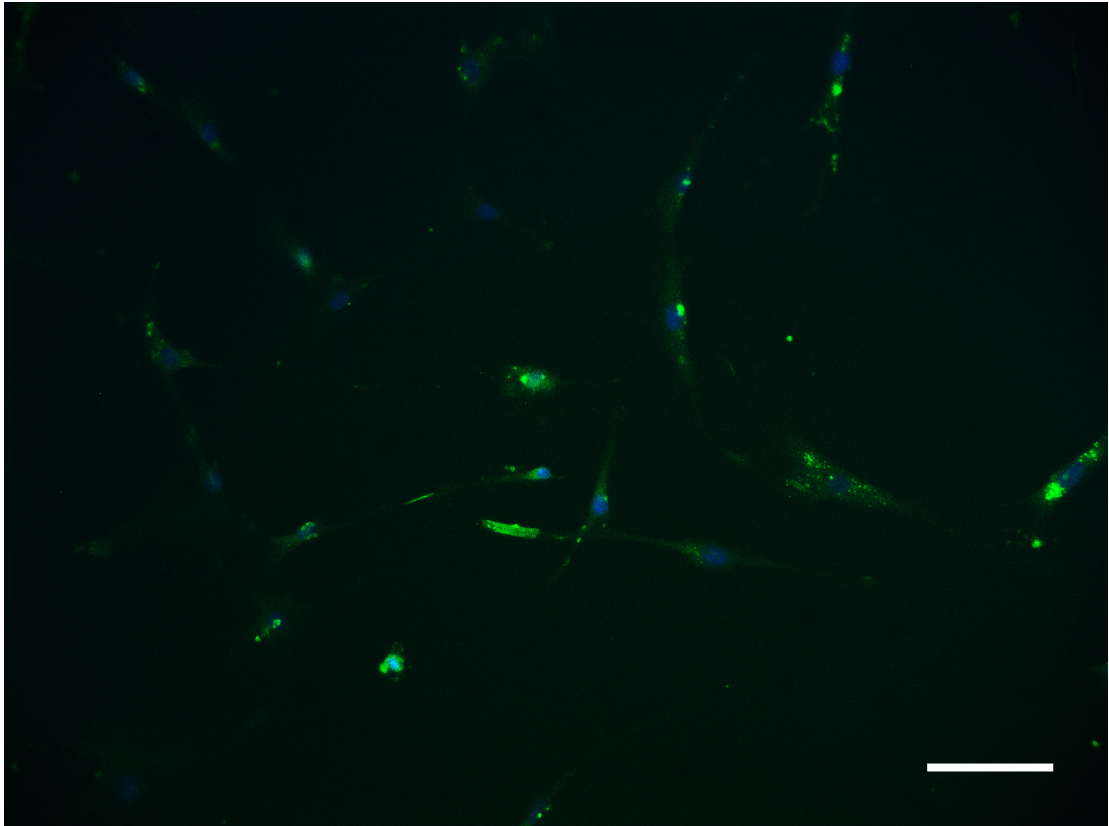


Figure 1-4: MSCs selected using MACs techniques and a stem cell marker-specific antibody. MSCs stained for marker CD271 (green) and nuclei (blue) after selection. Scale bar: 100 μ m

With the use of markers, a higher purity population of multipotent MSCs may be isolated from the mixture of adherent bone marrow cells. These markers can also be exploited for characterisation purposes, quantifying their expression levels with and without treatments in order to show stem or differentiation status (Qian *et al.*, 2012). STRO-1 and CD271 can therefore be used as indicators of ‘stemness’. This surface profile at the gene or protein level can be compared to markers associated with differentiated states, such as those related to osteogenesis, for example osteopontin and osteocalcin (Kulterer *et al.*, 2007). ALCAM (CD166) is another marker used as an indicator of stem cell state (McMurray *et al.*, 2011), however, it is believed to define a population of MSCs that are beginning to commit to differentiation.

A summary of the markers used in this study is shown in *Table 1-1*.

Name	Description	Marker type
CD271/p75NTR	Surface antigen	MSC marker
STRO-1	Surface antigen	MSC marker
CD166/ALCAM	Surface antigen	MSC and early progenitor marker
Osteocalcin (OCN)	Bone mineralisation	Osteogenic marker
Osteopontin (OPN)	Bone mineralisation	Osteogenic marker
CD63	Surface antigen	MSC marker
Nestin	Intermediate filament protein	Bone marrow niche marker

Table 1-1: MSC and differentiation cell surface markers used in the study.

Bone marrow-derived MSCs offer the advantage of being relatively easily sourced from patients undergoing routine (orthopaedic) knee/hip arthroplasty (Al-Nbaheen *et al.*, 2013, Gothard *et al.*, 2014). Isolated cells can be further expanded *in vitro* and have formed the basis of many studies into their potential use in regenerative medicine. Although MSCs can now be derived from alternative sources such as dental pulp, olfactory mucosa and adipose tissue (Bunnell *et al.*, 2008, Tomé *et al.*, 2009, Johnstone *et al.*, 2011, Pisciotta *et al.*, 2015), historically, much work has been carried out on bone marrow-derived MSCs, and thus the latter source is used throughout this thesis. The abbreviation MSCs will be used from herein to refer to bone marrow-derived mesenchymal stem cells.

1.4.2 The role of the niche in regulation of stem cells

MSC division must be subjected to strict regulation in order to maintain adequate pools of non-differentiated cells and to provide the required committed progenitor cell types to surrounding tissues when necessary as a response to injury (Ehninger and Trumpp, 2011). The supporting microenvironments of stem cells in the body are often referred to as a 'niche'; Schofield proposed the concept in 1978 which has been widely accepted as the method by which different types of stem cells are maintained and regulated (Schofield, 1978). The niche incorporates the progeny stem cells, supporting

cells and structures that immediately surround the stem cell populations that reside there (*Figure 1-5*). Stem cells within the niche are exposed to growth factors, have interactions with cells within the same localized vicinity, as well as with their extracellular environment in the formation of cell contacts, all of which have influence on eventual stem cell fate (Kerever *et al.*, 2007). Thus the environments in which MSC populations reside contain components that provide instructional cues in directing stem cell differentiation or maintenance of phenotype, and that additionally serve to regulate the processes of cell growth and survival.

Aside from eliciting specific cell growth and differentiation behaviours, many stem cells in their niche enter a state of quiescence that prevents their progression through the cell cycle (Kunisaki *et al.*, 2013). When required, stem cells will integrate into tissues via the production of progeny or ‘transit amplifying’ cells (Hsu *et al.*, 2014). For example, in response to injury or disease, homing of these cells will occur, followed by terminal differentiation into the required cell type (Rustad and Gurtner, 2012, Eseonu and De Bari, 2015). However, despite the extensive research on stem cells, which spans many years, mammalian stem cell niches are poorly understood, and the precise location of the stem cell niches are often widely debated (Meirelles *et al.*, 2006, Ehninger and Trumpp, 2011, Lander *et al.*, 2012). Although, MSCs can be found in several different sites in the body, these do not necessarily constitute a niche unless there is evidence that the environment contributes both anatomically and functionally to preserve the stem cells that reside there.

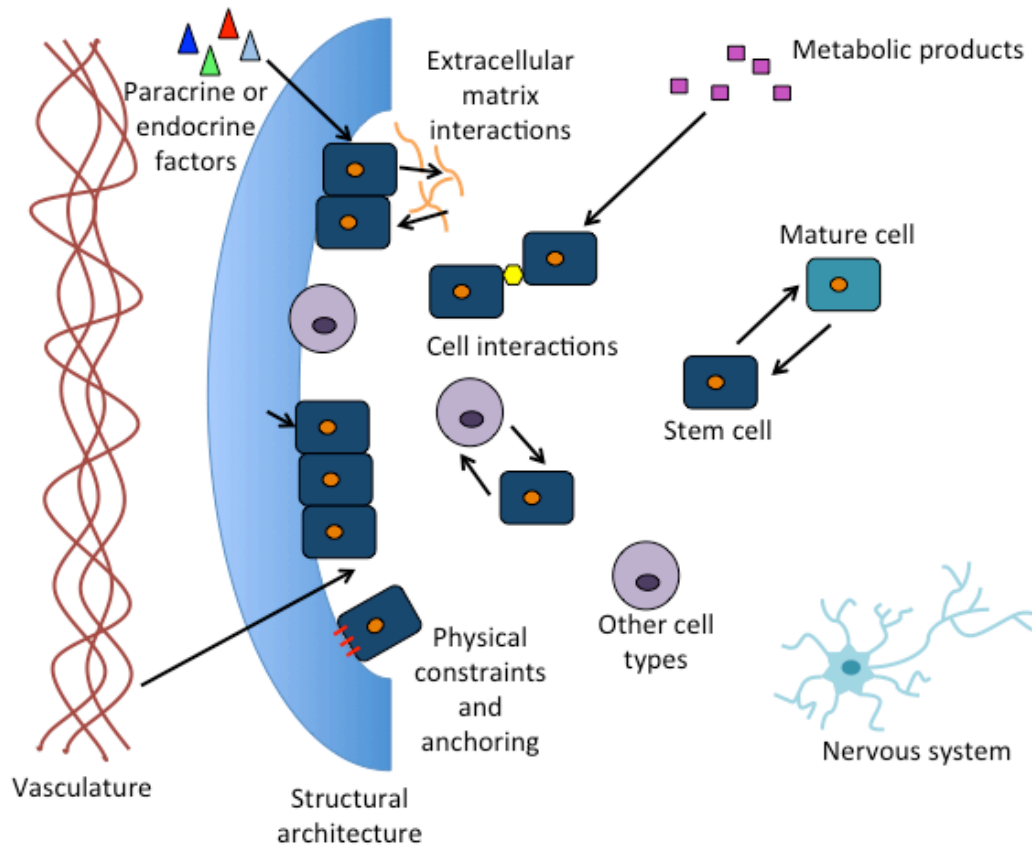


Figure 1-5: Regulatory components of stem cell function in the niche. Elements of the stem cell niche based on factors defined in experimental studies include, factors from the vasculature network, paracrine (localised)/endocrine (distant) signalling, physical interactions with the niche architecture and extracellular matrix, cell interactions between other cells inhabiting the niche (could be other stem cells, mature or committed stem cells, or different cell types), metabolic products, and input from the neural network. Image adapted from Scadden, 2006 (Scadden, 2006).

Our knowledge of stem cell niches is thus far limited to several types, including that of the germline stem cell niche in *Drosophila melanogaster*, the neural stem cell niches in the brain, the epidermal stem cell niche in the hair follicle and HSCs in the bone marrow niche (Song *et al.*, 2002, Doetsch, 2003, Blanpain *et al.*, 2004, Mendez-Ferrer *et al.*, 2010). In recent years, more evidence pertaining to the bone marrow niche has come to light, clarifying some of the implicated components and describing a number of residing cell types, each commanding functionalities to maintain homeostasis within the microenvironment. It has been suggested that a self-renewing population of MSCs in the bone marrow, characterised by their positive nestin expression, act as supporting cells of HSCs (Mendez-Ferrer *et al.*, 2010). When the number of nestin⁺ MSCs was decreased, this had a detrimental impact on the ability of HSCs

to 'home' towards the MSCs, and instead they migrated towards the spleen (Mendez-Ferrer *et al.*, 2010). Evidence points to MSCs being located in the endosteum and on the sinusoidal vessels (as part of the perivascular niche) perforating the marrow (Ehninger and Trumpp, 2011). Their placement within the niche brings them into close proximity to interact with neighbouring cells and to support and regulate other stem cells, such as in their interaction with HSCs (Ehninger and Trumpp, 2011).

The understanding that the multitude of localised physical, chemical and cellular components in a cell's microenvironment all have influence on cell behaviour, have both inspired and influenced research and design concepts in tissue engineering (Burdick and Vunjak-Novakovic, 2008, Ma, 2008). Scientists have attempted to replicate characteristic properties of stem cell niches in order to study stem cell behaviour in an environment that more closely resembles that which is observed *in vivo* (Ko and Cho, 2013, Mano, 2015). This can sometimes pose a challenge, as biological niches can be very complex, and require 3D geometric positioning of multiple cell types and molecules (Saleh *et al.*, 2012), which is difficult to recapitulate *in vitro*. An example of such a study is the spatial positioning of MSCs and endothelial cells to investigate their migration relative to each other using tunable hydrogel shapes (Eng *et al.*, 2013). Nevertheless, creating culture systems that resemble physical attributes of a cell's native environment appears to be of benefit to preserving the self-renewal capacity of stem cells: an example being muscle stem cells which were cultured on a softer hydrogel instead of tissue culture plastic, recapitulating the characteristic physiological tissue rigidity, were successfully propagated in an undifferentiated state and subsequently regenerated muscle following transplantation (Gilbert *et al.*, 2010).

Hypotheses have been proposed that suggest the niche has a role in orientation of both the cell and spindle that define whether stem cell division will be symmetric or asymmetric (Quyn *et al.*, 2010, Yadlapalli and Yamashita, 2012). Symmetric division can either result in two daughter stem cells (self-renewal) or two differentiated cells (lineage commitment), whilst a stem cell dividing asymmetrically will produce a daughter stem cell and a differentiated cell (Morrison and Kimble, 2006). Details about how this 'decision process' of

division takes place remains unclear. This may involve spatial positioning of differentiation or stem cell retention factors such that the daughter cell will either be committed to overcome its 'stemness' state, or used to maintain the stem cell pool. In a hypothetical model proposed by Fuchs *et al.* (Figure 1-6), the polarity of a stem cell will be determined by its interaction with neighbouring stem cells within the niche as well as its contact with the basal surface (such as the basal lamina)(Fuchs *et al.*, 2004). These two determinants will in turn affect the distribution of internal cell fate determinant molecules, and alter mitotic spindle orientation into an arrangement favourable for asymmetric renewal (determinants at the apical region) or symmetric renewal (determinants located at the lateral region) (Fuchs *et al.*, 2004).

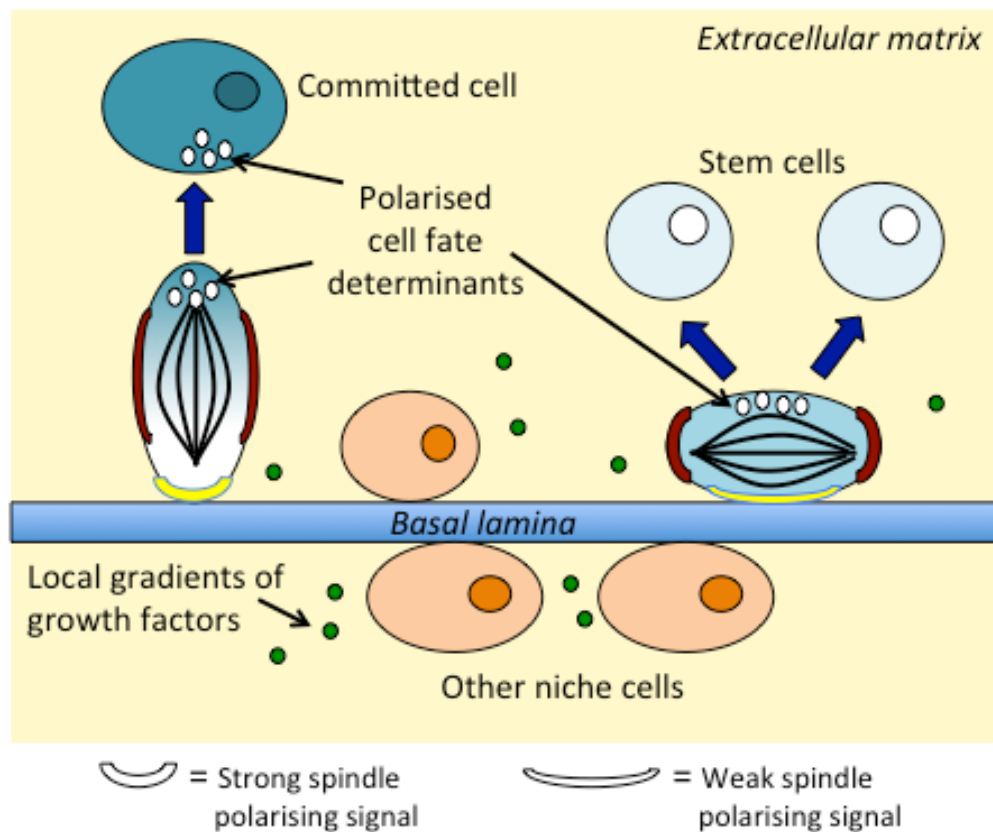


Figure 1-6: Hypothetical model depicting stem cell polarity and orientation of the mitotic spindle by the niche. This model proposes that stem cell polarity and arrangement of the mitotic spindle and intrinsic cell fate molecules are determined by entities found in the niche environment, including adhesion to the surface architecture (in this case, the basal lamina), interaction with neighbouring cells and exposure to growth factors. These in turn provide the cell with polarising signals of differing strengths, so that a decision can be made to undergo symmetric or asymmetric self-renewal. Adapted from Fuchs *et al.*, 2004 (Fuchs *et al.*, 2004).

1.5 Topography: from micro to nano

Introducing patterned features (topography) to the surface of a biomaterial is a simple way to integrate physical stimulating cues to a base substance. The earliest study of cell response to physical cues was in 1914 when Harrison observed that frog embryonic cells showed a response when grown on strands of spider silk (Harrison, 1914). It appeared that the mechanical stiffness of the fibres was the key factor that allowed the cells to extend and spread in a unidirectional manner (Harrison, 1914). Following his initial discovery, other cell types (such as fibroblasts, osteoblasts, and neuronal cells) were have been shown to be affected by topographical features such as grooves, which had visible effects on cell morphology and behaviour (Hsu *et al.*, 2007, Biggs *et al.*, 2008, Biggs *et al.*, 2009b, Brydone *et al.*, 2011). Early pioneering work described observations such as these as exhibition of ‘contact guidance’, defined as alignment with substrate features (Weiss, 1945). Curtis and Varde attributed these cellular changes to a reaction to aspects of the topographical features themselves (Curtis and Varde, 1964). The idea here being that cells must be sensitive to their microenvironment due to the size of physical features being of the same scale as the cell. This means that interaction between proteins and structural features can feasibly occur.

Early research identified that cells respond to patterning at a micro-level with the use of photolithographic techniques employed in the microelectronics industry in the construction of simple topographies. The foremost topographical substrates made use of features such as steps (Clark *et al.*, 1987), ridges, fibres and grooves (Clark *et al.*, 1990), the majority of which were of micron scale due to limitations in fabrication technologies at the time. A microtopography consisting of a series of heightened steps impeded cell movement across the features and thereby cell alignment (contact guidance) (Clark *et al.*, 1987), and in a continuing study, increasing depth of parallel grooves caused increase in the degree of cell alignment (Clark *et al.*, 1990). Research findings largely agreed with Dunn and Heath’s hypothesis, and demonstrated that the shape of substrate features would physically restrict microfilaments, requiring the cell to alter its morphology to accommodate the substrate. In Dunn and Heath’s original study, fibroblasts were observed to develop shorter protrusions at the cell edges if the curvature of the substrate had a steeper angle, which contributed to the

changes in overall cell morphology (Dunn and Heath, 1976). These observations formed the foundations of our understanding of the effects of topography on cell function, and led to exploration into the use of biomaterials to recapitulate this natural phenomenon in cell regulation.

Furthermore, the influence of geometry of substrates was exhibited with fibroblasts seeded on regular arrays of pits of microscale diameters and spacing (Berry *et al.*, 2004). The cells appeared to move into the pits or respond to the grooves. The largest diameter of pit tested allowed the cells to enter or exit the pits and form large focal adhesions, whereas the smallest diameter of pit appeared to promote motility and allow cells to form smaller focal adhesions (Berry *et al.*, 2004). A common theme of these prior studies is an indication that the underlying effect of topographies is dependent in the resultant ability of a cell to form outreaching protrusions, leading to the development of focal contacts and adhesions on the substratum.

As tools and techniques in the electronics and semiconductor industries began to become more advanced and refined, scientists have exploited these technologies to further reduce topography feature sizes from the microscale to the nanoscale level (Gadegaard *et al.*, 2006, Bettinger *et al.*, 2009) (*Figure 1-7*). Advantages arise in the regularity conferred by use of electron beam lithography, used to ‘write’ the pattern shapes onto a master silicon wafer. Production of features with precise positioning and size can be achieved (Altissimo, 2010). It is important to maintain this degree of uniformity as it has previously been shown that cells respond differently if the spacing of nanotopographical features varies (Dalby *et al.*, 2007, Gadegaard *et al.*, 2008, McMurray *et al.*, 2011). The silicon wafers with the master pattern can then be sputter coated with nickel and further electroplated with nickel. The metallic ‘shim’ can then be removed from the silicon master to provide a negative of the pattern in a hard material. This shim can then be used for embossing and injection moulding of thermoplastics down to 5 nm fidelity (Gadegaard *et al.*, 2003).

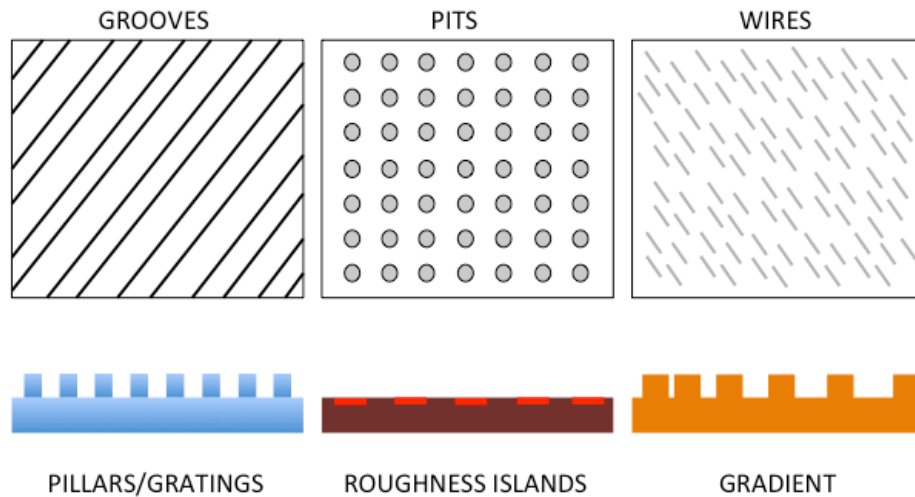


Figure 1-7: Topography to induce cell response. Schematic diagram depicting examples of topographies utilised in studies reported in the literature. These include grooves, pits, wires, pillars or gratings, 'islands' of altered roughness surrounded by smooth regions, and variations in distribution of the aforementioned features, such as gradients.

These smaller nanoscale features can now be produced at the same scale as cell receptors (for example the human fibronectin receptor is approximately 8 nm in diameter)(Nermut *et al.*, 1988), to allow for interactions between intrinsic protein and molecular components and nanotopography (Dalby *et al.*, 2014). Consistent with the possibility that nanotopographies possess the capability to regulate cellular processes through activation of membrane receptors and signalling pathways, many cell types indeed show specific responses to particular nanoscale fabrications that fall within a size range (Gallagher *et al.*, 2002, Curtis *et al.*, 2004, McNamara *et al.*, 2011). Through replication of characteristics of the ECM, alterations at the nanoscale level should allow for changes at greater magnitudes, affecting cellular processes, thereby having a wider influence over the entire cell.

Direction of stem cell behaviour with nanotopography has shown a degree of promise. Proliferation and differentiation of neural stem cells was affected following culture on polyethersulfone fibre meshes in comparison to standard tissue culture plastic (Christopherson *et al.*, 2009). A trend for decreasing proliferation rates with increasing mesh fibre diameters was noted, and different diameters were seen to allow cells to differentiate preferably to glial or to neuronal lineages (Christopherson *et al.*, 2009). Chen *et al.* demonstrated that human ESCs could undergo self-renewal over long periods on vitronectin-

coated smooth glass (exhibiting lots of filopodial protrusions), whereas vitronectin-coated nanorough glass surfaces (with a low degree filopodial extensions) induced spontaneous differentiation (Chen *et al.*, 2012). Response of MSCs to nanotopography has also garnered significant attention; studies have reported the direction of MSCs to undergo differentiation (Dalby *et al.*, 2006b) and self-renewal (McMurray *et al.*, 2011). Examples whereby nanotopographical induction of osteogenic differentiation in MSCs was achieved include culture on titanium substrates patterned with nanopillars (McNamara *et al.*, 2011), and using disordered nanopit poly(methyl methacrylate) substrates (Dalby *et al.*, 2007). Although some success has been reached with regards to promoting MSC differentiation, it is the continuation of the self-renewal process that presents the greater challenge.

1.5.1 Directing MSC phenotype with nanotopography

MSC differentiation to a particular lineage can be achieved with the use of differentiation media containing a cocktail of soluble chemical factors, however, the use of nanotopography confers a distinct advantage. Physical cues on the substrate can direct MSC behaviour without having to control the release of any soluble factors or molecules. Previous work had shown that nanotopography alone was effective in promoting MSC differentiation to an osteoblastic lineage (Dalby *et al.*, 2007) and in maintaining a stem cell self-renewing state (McMurray *et al.*, 2011). In these cases, the nanopit features on each surface were identical, with only the degree of disorder being changed between them; thus it appears that distribution of the nanotopographical features is of importance to the eventual behaviour of the cells. A highly ordered square lattice arrangement (SQ) of nanoscale pits (120 nm diameter, 100 nm depth and 300 nm centre-centre spacing) was shown to promote self-renewal of MSCs (McMurray *et al.*, 2011). However, a slightly disordered 'near square' arrangement (NSQ, similar to SQ, but with a random, up to ± 50 nm offset in the X and Y position of the pit from the centre position) having geometry similar to collagen X (Kwan *et al.*, 1991), swayed MSCs in favour of osteogenesis (Dalby *et al.*, 2007). As mentioned in the previous section, it has been demonstrated that nanotopography can promote osteogenic differentiation of MSCs (Zouani *et al.*, 2012), with further studies showing enhanced induction of chondrogenesis (on polycaprolactone

fibres, though cultured in the presence of transforming growth factor beta 1; TGF- β 1)(Wise *et al.*, 2008), neural differentiation (Yim *et al.*, 2007), and myogenesis (Teo *et al.*, 2013).

It has been observed that grooved nanotopography caused alignment of MSCs with decreased expression of integrin subunits, suggesting that nanotopography is a principal factor that affects the distribution and clustering of focal adhesions (Yim *et al.*, 2010). Moreover, previous work on nanopitted surfaces has indicated that the number and size of focal adhesions vary between MSCs cultured on nanotopographical substrates compared to planar controls (Biggs *et al.*, 2009a). McMurray *et al.* further highlighted that a Rho-associated kinase (ROCK) is important in creating the high degree of intracellular tension (conferred by the ECM) that favours MSC differentiation to osteoblasts and the low tension state that drives differentiation to an adipocyte lineage, with tensile force also likely to have a part in the maintenance of MSC multipotency (McMurray *et al.*, 2011). Therefore, the transmission of physical forces from the ECM to the nucleus by means of the cytoskeleton (direct mechanotransduction) is one mechanism that may explain how a cell adapts expression of genes in response to topographical cues (Alenghat and Ingber, 2002). In turn, this notion correlates with the 'tensegrity' (tensional integrity) theory, which assumes that a continuous state of tension exists, generated by microfilaments and intermediate filaments, which is resisted by microtubules (Ingber, 1993). Any mechanical stress on the cell could therefore result in deformation of the nucleus and rearrangement of chromosomes to evoke changes in gene expression (Dalby, 2005).

The scale of nanofeatures confers an exciting ability to manipulate the spatial arrangement of integrin clustering and focal adhesion formation, with larger focal adhesions being detected in MSCs cultured on the disordered NSQ nanotopography that stimulated differentiation to osteoblasts (Dalby *et al.*, 2007). The process of indirect mechanotransduction, involving integrin receptors and focal adhesions in the activation of intracellular signalling cascades and chemical messengers could be another mechanism at work (Dalby, 2005). Interestingly, nanotopographies appear to enhance the sensitivity of MSCs to mechanical signals, effectively increasing the degree of mechanotransduction

(Salvi *et al.*, 2010), likely to be caused by certain regions of the surface being conducive to promoting or impeding cell attachment (Cavalcanti-Adam *et al.*, 2008). Focal adhesion kinase (FAK) is associated with the cytoplasmic tails of integrins, ideally placed for signal transduction upon activation by the integrins themselves. It has been shown that FAK and signalling mediator c-Src can activate extracellular signal-related kinase ERK2 (Schlaepfer *et al.*, 1998), which is involved in proliferation. Inactivation or downregulation of cascades such as the extracellular signal-related kinase (ERK) and p38-mitogen activated protein kinase (MAPK) pathways leads to a decrease in transcription factors such as Runt related transcription factor (Runx2) which are crucial for osteogenesis (Artigas *et al.*, 2014), and may offer a potential explanation as to how the aforementioned SQ nanotopography maintains MSC self-renewal (McMurray *et al.*, 2011).

These themes of adhesion, cytoskeleton and mechanotransduction will be explored in more detail in subsequent sections.

1.6 Control of MSC growth

Several studies report that MSCs undergo spontaneous differentiation when cultured over time on standard tissue culture plastic-ware (Naruse *et al.*, 2004). Long periods of culture and passaging *in vitro* cause MSCs to become senescent (Cheng, 2011), which restricts the window at which they can be effectively used for clinical applications. To date, limited work has been carried out on MSC self-renewal because it has been difficult to control this process until now, and much of the existing literature on self-renewal is based on studies that have been carried out on pluripotent stem cells. However, the precise mechanisms implicated in self-renewal remain largely unknown, however, some possible regulators have been suggested from results of related studies. Though mouse ESCs could be continuously expanded in culture by provision of leukaemia inhibitory factor (LIF), which induces STAT3 signalling (Williams *et al.*, 1988), contradictory results report LIF having little effect on human ESCs (Thomson *et al.*, 1998, Dahéron *et al.*, 2004), showing that there must be differences in mechanisms between ESCs between different species.

MicroRNAs (non-coding RNAs) and transcription factors influence ESC self-renewal and differentiation. MicroRNAs suppress or reinforce cellular processes, therefore can enhance or impede self-renewal (Melton and Blelloch, 2010). Melton et al. proposed that ESC cell cycle regulating (ESCC) miRNAs and the let-7 miRNA family have opposing effects on each other, with the ESCC miRNAs acting to prevent the suppressive action of let-7 on self-renewal (Melton *et al.*, 2010). Balance of transcription factors is also pivotal to preservation of self-renewal. The presence of transcription factor Nanog was associated with maintenance of ESC state whilst depletion increased endoderm differentiation (Mitsui *et al.*, 2003). The self-renewal aspects of Nanog were attributed to an ability to repress differentiation-promoting genes, such as *gata4* and *gata6* (Mitsui et al., 2003).

Regulation and coordination of the cell cycle is likely to be implicated in stem cell self-renewal, and has been explored in ESCs and HSCs (Orford and Scadden, 2008). Cell cycle will be discussed in further detail in section 1.8. Finally, self-renewal can be promoted by culture on synthetic substrates. Deng *et al.* cultured human iPSCs on a synthetic substrate tethered with peptide ‘brushes’, which allowed for long-term self-renewal and expansion of the cells up to ten serial passages. This was evidenced by maintenance of characteristic morphology and pluripotency markers, and observations of cell adherence and proliferation, suggesting that physical cues have a role (Deng *et al.*, 2013).

1.6.1 Mechanotransduction

Physical cues and mechanical stimuli from the ECM or surface of a substrate are converted to biochemical signals through the process of mechanotransduction. The key initiation point of mechanotransduction is located at the interface between the cell and ECM. This is where integrins and protein receptors are found, which means that they are ideally placed for cell sensing of their environment, to form focal adhesions (FAs) to assist adhesion, and to transduce external signals into the cell.

These biochemical signals in turn lead to alterations in gene expression and cell signalling pathways, that can result in functional changes as an adaptive response to the initial stimulus. Mechanical stimuli may consist of external

forces conferred on the cell such as tension or fluid shear stress, or internal forces arising from intracellular adjustments of cellular stiffness in response to alterations in stiffness of the ECM (Dahl *et al.*, 2008). Mechanotransduction can be either direct or indirect, depending on how the signal is relayed to the nucleus (McNamara *et al.*, 2010). Signal propagation through direct mechanotransduction is achieved through force-induced adjustments in cytoskeletal conformation and cellular morphology that in turn, cause deformations in the nucleus and redistribution of chromatin or conformation changes in DNA (Dahl *et al.*, 2008, Wang *et al.*, 2009).

Indirect mechanotransduction is achieved through activation of signalling pathways to transfer information to the nucleus, primarily the extracellular-signal-regulated kinase/mitogen-activated protein kinase (ERK/MAPK) signalling cascade, induced at the level of focal adhesions and integrins (Dalby *et al.*, 2014). The ERK/MAPK pathway has been implicated in proliferation and differentiation, and is therefore of particular interest with regards to understanding the regulation of stem cells (Li *et al.*, 2007, Gharibi *et al.*, 2012, Michailovici *et al.*, 2014). Studies on the interaction between cells and biomaterial substrates have additionally indicated that focal adhesion kinase (FAK) and integrin-linked kinase (ILK) have roles in mechanotransduction (Sun *et al.*, 2012).

Integrins and focal adhesions, the adhesion components that work together in tandem to initiate the process of mechanotransduction will be discussed in the following sections.

1.6.2 Integrins

Integrins are a large family of cell surface, heterodimeric transmembrane receptors, involved in cellular adhesion and bidirectional signalling between the ECM and from within the cell itself. This allows a direct association between the intracellular and extracellular environments to be established. Integrins can simultaneously bind proteins in the extracellular matrix such as fibronectin, vitronectin, collagen and laminin, whilst the inner cytoplasmic domain connects

to the actin cytoskeleton (Selhuber-Unkel *et al.*, 2010) via linker proteins including α -actinin, paxillin, talin and vinculin (Zamir and Geiger, 2001). They are composed of alpha (α) and beta (β) subunits. There are 18 α and 8 β subunits thus far known to exist in mammalian cells, which combine and assemble into 24 different integrins, each with a distinct functionality and binding specificity to particular extracellular proteins (Hynes, 2002, Humphries *et al.*, 2006). This means that varied responses can be induced from each type of integrin (Zaidel-Bar *et al.*, 2007). Each (heterodimer) subunit spans the membrane once, and possesses a large extracellular 'head' domain (>1600 amino acids), and two shorter cytoplasmic 'tail' domains (20-50 residues) (Hynes, 2002). The crystal structure of integrin $\alpha_v\beta_3$ 'at rest' and its structure when bound to a ligand, revealed a 'bent' inactive conformation when no ligand was bound (Xiong *et al.*, 2001, Xiong *et al.*, 2002). Upon ligand binding, the structure exhibits an extended and open conformation to allow interaction between the integrin and focal adhesion proteins. Thus the open form exhibits high affinity for the ligand, whereas the closed form has low affinity for the ligand (Shimaoka *et al.*, 2001). In general, integrins recognise ligand motifs, which can be exploited to facilitate ligand binding, such as the widely recognised arginine, glycine, aspartic acid (RGD) peptide sequence (Humphries *et al.*, 2006).

Ligand binding to the extracellular domain establishes a direct link from the ECM to the nucleus via the cytoskeleton and associated proteins, allowing for integrin-mediated signalling to take place (Hynes, 2002). 'Inside-out' signalling describes the intracellular regulation of binding activity in the extracellular domains of the receptor (Calderwood, 2004). 'Outside-in' signalling refers to binding of ligands in the ECM which produces signals that are subsequently transferred into the cell via focal adhesions and the cytoskeleton (Hynes, 2002). Integrins have pivotal roles in mediating interactions from cell-to-cell, in addition to those between the cell and extracellular environment, making them essential to maintenance of cellular integrity (Raducanu *et al.*, 2009, Watson *et al.*, 2010). Furthermore, contraction of the cytoskeleton pulls clusters of integrins together (integrin gathering) to assemble growing adhesions; this means that larger adhesions form in response to a higher degree of tension in the cytoskeleton (Dalby *et al.*, 2014).

Integrins appear to be a crucial element of cell response to nanotopography (Teo *et al.*, 2013). For osteogenic commitment from MSCs, high degrees of adhesion and resultant increase in intracellular tension have been shown to be critical (McBeath *et al.*, 2004, Kilian *et al.*, 2010). Indeed, on the osteogenic, NSQ, nanotopography, adhesion size was noted to be much larger on the planar controls (Biggs *et al.*, 2007b).

1.6.3 Cell-extracellular matrix adhesions

Adhesions between the cell and the extracellular matrix assist anchoring of the cell in addition to acting as bridging sites between the actin cytoskeleton and the ECM for integrin-mediated signal transduction (Alenghat and Ingber, 2002). Furthermore, adhesions are important in the processes of migration and spreading (Aplin and Juliano, 1999, Ballestrem *et al.*, 2001). Different types of cell adhesions are characterized by their size, location and constituent components. The smallest are focal complexes (of approximately 1 μm diameter), which are located primarily around the cell periphery, near the lamellipodia at the leading edge of the cell (Nobes and Hall, 1995, Galbraith *et al.*, 2002). Focal contacts or focal adhesions are larger and can be found within the cell in addition to the periphery, typically measuring 1-5 μm in length (Zamir and Geiger, 2001, Biggs and Dalby, 2010)(*Figure 1-8*). Fibrillar or supermature adhesions compose the largest size of adhesions (>5 μm) and extend from focal adhesions in the central region of the cell (Wozniak *et al.*, 2004).

During initial adherence of a cell to a surface, membrane protrusions are stabilised as integrins bind to the ECM and begin to cluster together (Wozniak *et al.*, 2004). The integrin receptors involved will be largely dictated by the constituents of the ECM as integrins demonstrate specificity for particular ligand motifs.

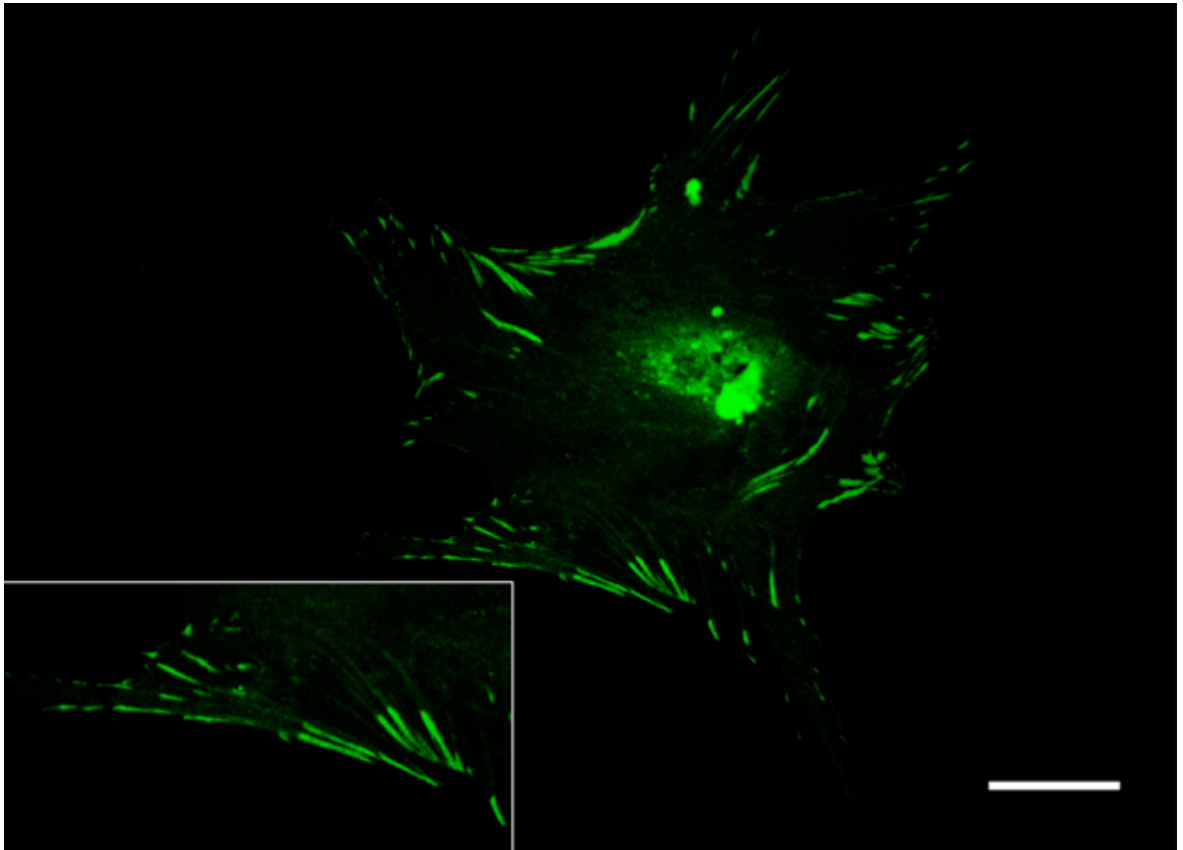


Figure 1-8: Focal adhesions observed at cell periphery. Immunofluorescent staining for vinculin indicates the presence of small projections (focal adhesions) located at the edges of cells. Scale bar (relates to larger image): 50 μm . Boxed area shows an enlarged view of a section of the cell edge. Lee, unpublished data.

One of the main ECM adhesion proteins, fibronectin, leads to the development of focal adhesions containing integrin $\alpha_v\beta_1$ (Zhang *et al.*, 1993), while vitronectin in the ECM will drive formation of focal adhesions containing integrin $\alpha_v\beta_3$ (Horton, 1997). Consequently, the smallest adhesions, focal complexes are formed, and mature into focal adhesions in response to subsequent changes in intracellular tension (Bershadsky *et al.*, 1985, Rivelin *et al.*, 2001). Due to the fact that focal adhesions are formed as a result of protein clustering, they comprise an assembly of proteins, of which focal adhesion kinase (FAK) and adaptor proteins α -actinin, paxillin, talin, tensin and vinculin are usually present, as well as Src tyrosine kinases (Calalb *et al.*, 1995, Miyamoto *et al.*, 1995, Chen and Lo, 2003, Lawson *et al.*, 2012). Larger mature adhesions can be distinguished by the additional recruitment of zyxin (Zaidel-Bar *et al.*, 2004). In particular, vinculin is an important adaptor protein that translocates to focal adhesions and is involved in regulating cell adhesion and force transduction (Humphries *et al.*, 2007). Depletion of vinculin is detrimental to adhesion and motility as vinculin is

thought to link actin filaments to integrins, together with α -actinin and talin (Coll *et al.*, 1995).

Members of the ras-related GTPase family (Rho, Rac and cdc42) are pivotal to the formation of stress fibres, focal adhesions, lamellipodia and filopodia (Ridley and Hall, 1992, Ridley *et al.*, 1992, Nobes and Hall, 1995). Focal adhesion formation is dependent on myosin II contractility, activated by Rho-associated kinase (known as Rho-kinase or ROCK), a downstream target of Rho GTPase (Riveline *et al.*, 2001). When localized tension was applied to GFP tagged-vinculin-containing focal complexes, they developed into focal adhesions within the vicinity of the applied stress, with Rho inhibition suppressing this observed effect (Riveline *et al.*, 2001). Rho and Rac proteins are additionally established as having actions downstream from surface receptors, being involved in diverse signalling pathways (Schwartz, 2004). A hierarchical relationship exists between cdc42, Rac and Rho, where activation of cdc42 leads to activation of Rac, which stimulates Rho (Nobes and Hall, 1995). Following activation of Rho, actin polymerisation is initiated, resulting in the development of stress fibres (Ridley and Hall, 1992, Nobes and Hall, 1995, Chrzanowska-Wodnicka and Burridge, 1996). In turn, stress fibres are attached to the plasma membrane by way of the aforementioned focal contacts (Naumanen *et al.*, 2008).

The spatial distribution of ligands and subsequent gathering of integrin receptors is pivotal to focal adhesion formation. A distance of 58-73 nm between ligands was proposed by Arnold *et al.* as being optimal for successful receptor accumulation (Arnold *et al.*, 2004). Distance between integrin ligands (local ligand density), and whether the required ligand distribution is spread throughout the surface or confined to localised regions (global ligand density), has been investigated for integrin $\alpha_v\beta_3$ (Deeg *et al.*, 2011). It was demonstrated that the local density was the more dominant factor in influencing formation of focal adhesions (Deeg *et al.*, 2011). Focal adhesions can alternatively form through adhesion bridging, whereby structural proteins vinculin and zyxin can stretch to span patches of vitronectin or fibronectin to form a focal adhesion bridge with another adhesion (Malmström *et al.*, 2011). As integrins did not undergo adhesion bridging, this suggests that an excess of adhesion is not required for focal adhesion formation. Furthermore, the concept of bridging can

be applied to nanopatterned substrates, where it is likely there will be regions of a surface that will encourage larger adhesions in addition to areas where it will be difficult for adhesions to develop.

FAK is a tyrosine kinase and a crucial downstream constituent of integrin-mediated signalling, that has been shown to be important for cell migration (Wang *et al.*, 2001) and in promoting adhesion maturation. FAK is activated by auto-phosphorylation of tyrosine residues following clustering of integrins. Tyrosine-397 (Tyr397) is the most documented activation site, with other phosphorylation sites being identified as tyrosine-407, -576 (Tyr576), -577 (Tyr577), -861 and -925 (Ciccimaro *et al.*, 2006). Tyrosine phosphorylation appears to only occur following recruitment of vinculin, paxillin and FAK to the focal adhesions themselves (Kirchner *et al.*, 2003). Following phosphorylation at Tyr397, Src is able to bind to FAK via the Src-homology 2 (SH2) domain, facilitating phosphorylation at Tyr576 and Tyr577. FAK can subsequently interact with phosphatidylinositol kinase (PI3K) to achieve cell adhesion (Chen *et al.*, 1996) and migration (Reiske *et al.*, 1999).

The notion of focal adhesions acting as mechanosensors, and integrins as process regulators, provides a mechanism as to how cells respond to changes in substrate mechanical stiffness and tension (Cavalcanti-Adam *et al.*, 2008, Selhuber-Unkel *et al.*, 2010, Prager-Khoutorsky *et al.*, 2011). Cell spreading is limited on a soft collagen gel in comparison to a stiff gel or glass substrate (Engler *et al.*, 2004). Stress fibres are typically observed to be well ordered throughout the cell together with the presence of defined focal adhesions on the rigid substrates (Engler *et al.*, 2004). Interestingly, stem cell differentiation can be directed through culture in gels of differing elasticities, with differentiation to an osteogenic phenotype being observed with stiffer gels, and differentiation to myogenic and neuronal lineages being observed with softer gels (Engler *et al.*, 2006). This may be due to the substrates allowing focal adhesions of sufficient size and stability to be formed; for example, osteoblasts typically possess many supermature adhesions (Biggs *et al.*, 2008).

Furthermore, cell morphology has been indicated as affecting MSC differentiation, as constraining MSCs within geometric features that increase

actomyosin contractility favoured osteogenic differentiation (Kilian *et al.*, 2010). Prominent F-actin stress fibres were found at the edges of cells cultured on the differentiation-promoting star-shaped micropattern, with concomitant concentration of vinculin, and thereby focal adhesions, at the points of the shape (Kilian *et al.*, 2010). Moreover, ERK signalling cascades can be activated following maturation and elongation of focal adhesions, which may influence proliferation and differentiation (Fincham *et al.*, 2000, Biggs *et al.*, 2009b). Thus, there is evidence that focal adhesion signalling can affect eventual stem cell fate (Kilian *et al.*, 2010, Gautrot *et al.*, 2014). However, as the assembly and turnover of focal adhesions is complex and dynamic (Ballestrem *et al.*, 2001), all the details pertaining to the mechanisms of these processes are difficult to ascertain. A further insight into the complexity of focal adhesions can be observed with the plethora of known interacting proteins and components that comprise the focal adhesion assembly, connecting integrins to the actin microfilament network (collated from published experimental data), which currently stands at 156 associated components with 690 modifying interactions (Zaidel-Bar *et al.*, 2007).

Whilst adhesion requirements for osteogenesis are becoming well known, for self-renewal this is less explored. Assessment of focal adhesions on the SQ and NSQ nanotopographies after three days culture revealed that a greater number of longer adhesions and higher levels of phospho-myosin were detected on the differentiating NSQ surface in comparison to SQ (Tsimbouri *et al.*, 2012, Tsimbouri *et al.*, 2014). Furthermore, pharmacological inhibition of ERK1/2 caused a drop in stem cell marker gene expression (Tsimbouri *et al.*, 2012). Together, this indicates that differences in adhesion and tension profile of MSCs are associated with differentiating and self-renewing phenotypes. Changes in adhesion and downstream signalling will impact on ERK cascades and suggests potential control of cell growth in a way that could mediate self-renewal.

1.7 The cytoskeleton

Protein filaments and molecular motor proteins mesh together in a network to form the cytoskeleton in eukaryotic cells (Pollard, 2003). The cytoskeleton carries out an array of fundamental and diverse functions, assisting the cell in

retaining its rigidity and shape when faced with mechanical stresses (Luna and Hitt, 1992), being involved in cell motility and migration (Pollard, 2003), and reorganising the cell to undergo morphological adaptations (Sims *et al.*, 1992). Furthermore, the cytoskeleton facilitates transport and positioning of organelles and small molecules, utilising motor proteins, kinesin, dynein and myosin (Hirokawa *et al.*, 2009). The three major constituents that are involved in shaping the cell architecture are cytoskeletal protein filaments; actin filaments (microfilaments), intermediate filaments and microtubules (Fuchs and Weber, 1994)(*Figure 1-9*). Dynamic assembly and disassembly of these components takes place within the cytoskeleton, corresponding to fluctuations in the requirements of the cell (Vadlamudi *et al.*, 2002, Iwasa and Mullins, 2007).

Actin filaments (F-actin) are made from monomeric units of globular G-actin (Oda *et al.*, 2009). Assembled actin bundles are described as microfilaments, and actin filaments can join with motor proteins to form the actin cytoskeleton (Bremer and Aebi, 1992, Dos Remedios *et al.*, 2003). Intermediate filaments are assembled from several types of proteins, and therefore vary in their subunit composition (Fuchs and Weber, 1994). They are structurally stable, and provide support to tubulin in conjunction with microtubules (Fletcher and Mullins, 2010). Some intermediate filaments are specific to certain cell types, and others, such as vimentin, are found in all cells (Cooper, 1985).

Microtubules are hollow tube-like filaments formed from basic units of polymerised α and β tubulin heterodimers (Kadavath *et al.*, 2015). These are the largest of the three types of filaments in the cytoskeleton, having a diameter of 25 nm (Murphy *et al.*, 2001, Mikhaylova *et al.*, 2015).

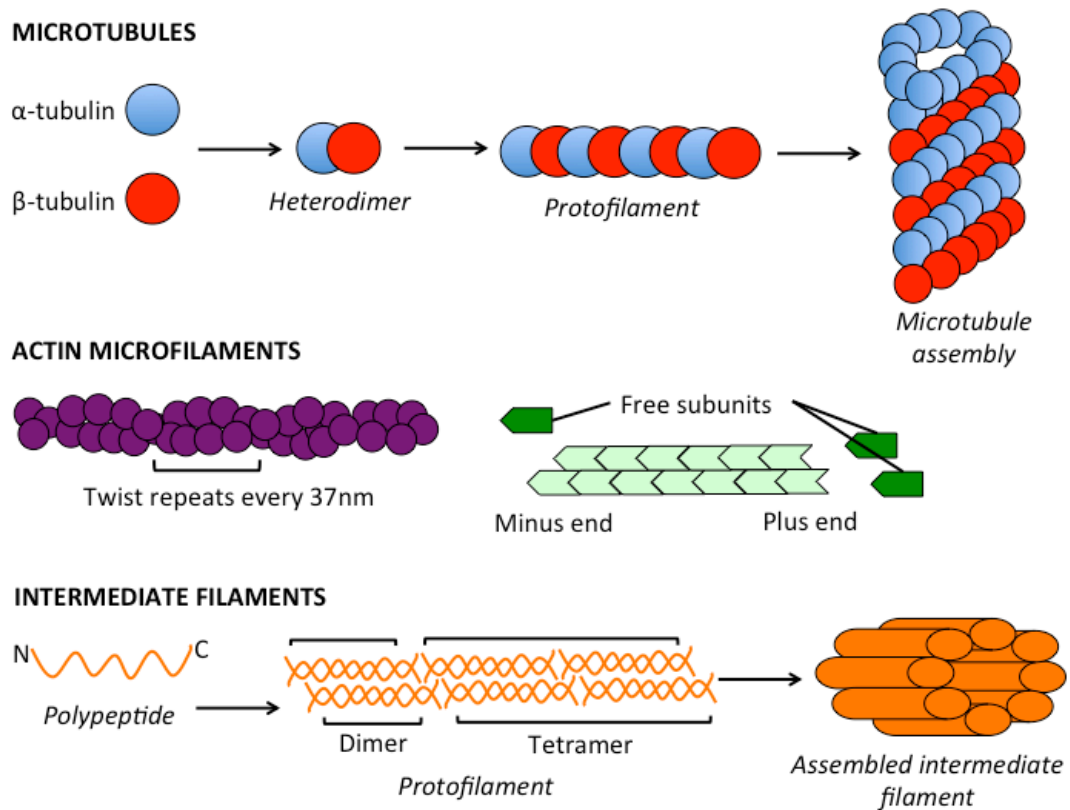


Figure 1-9: Schematic of cytoskeletal filament assembly. Diagram depicting the basic assembly and structure of microtubules, (F-actin) microfilaments, and intermediate filaments. Microtubules are assembled from α and β tubulin subunits, that form dimers, then assemble into protofilaments. Protofilaments gather together to form a microtubule that resembles a hollow tube-like structure. Actin microfilaments are helical structures comprised of subunits, with each repeating twist occurring every 37 nm. One end of the microfilament is termed the minus end, which is slow growing, and the other end is termed the plus end, which is fast growing. Intermediate filaments consist of many polypeptides gathered together as protofilaments, with eight protofilaments further assembling into a long filament by twisting together like a rope. Adapted from Fletcher and Mullins (Fletcher and Mullins, 2010).

1.7.1 The role of the cytoskeleton in mechanotransduction and cell sensing

The dynamic nature of the cytoskeleton indicates the degree of responsiveness it must have to changes in the cell microenvironment. Firstly, cells must probe the physical and chemical composition of its surroundings to adapt accordingly to extracellular conditions (Albrecht-Buehler, 1979). Cells utilise numerous projected extensions, called lamellipodia, to explore the space and surface at which it inhabits (Albrecht-Buehler, 1976). Filopodia, are smaller actin-rich finger-like projections that have been implicated in ‘sensing’ of the microenvironment (Albuschies and Vogel, 2013). These structures are formed when actin polymerization is directed against cell membrane, generating force

(DeMali and Burridge, 2003). Actin filaments can also produce contractile forces, through formation of contraction bundles in conjunction with myosin II filaments, α -actinin and tropomyosin (Weber and Groeschel-Stewart, 1974, Lazarides, 1976). The energy derived from adenosine triphosphate (ATP) drives the motor domains of myosin II along the actin filament, generating contraction of the actin-myosin (actomyosin) bundle (Thoresen *et al.*, 2011). Collections of actomyosin bundles in non-muscle cells are termed stress fibres (Chrzanowska-Wodnicka and Burridge, 1996). Stress fibres tend to be less in number and thinner in structure in highly motile cells, whilst conversely, they are more numerous and larger in cells that do not migrate readily (Hotulainen and Lappalainen, 2006). Additionally, the formation of stress fibres appears to be more apparent on rigid substrates in comparison to soft surfaces (Prager-Khoutorsky *et al.*, 2011).

The cytoskeleton is also known to have a role in mechanotransduction (Alenghat and Ingber, 2002). Any applied forces or mechanical stresses will be transferred to the cytoskeletal architecture, and many cell types have been shown to be mechanosensitive, ranging from osteoblasts to smooth muscle (Tang *et al.*, 1999, Nomura and Takano-Yamamoto, 2000). The cytoskeleton itself can generate forces and relay them to adhesion sites. This coupling of the cytoskeleton with focal adhesions is central to the process of mechanotransduction as growth of focal adhesions can be induced by tension, demonstrated by the application of external forces (Pelham and Wang, 1997, Riveline *et al.*, 2001). Changes in tension will additionally alter the distribution of the cytoskeleton and therefore impact on associated proteins. One identified mechanism that results from this is the exposure of protein binding sites in response to increased tension. An increase in binding could bring key proteins together and lead to activation of downstream signalling cascades (del Rio *et al.*, 2009). Tension affects the conformation of fibronectin, and when released, promotes unfolding of the protein, which in turn exposes hidden binding sites (Baneyx *et al.*, 2002). Alternatively, the arrangement of proteins will change if the cytoskeletal organization has been affected (Kubler *et al.*, 1991), meaning that the interaction proximity of binding partners may become more favourable. These observations indicate that numerous mechanisms are likely to be occurring to facilitate mechanotransduction via the actin cytoskeleton.

If nanotopography can be used to increase the lifespan of MSCs, whilst preserving their differentiation potential, this would be of great benefit to the future of MSC treatments. This may be achievable by use of appropriately arranged mechanical cues to create an intermediate degree of intracellular tension, one that could be said to maintain a stem cell phenotype, and to allow sufficient interaction with integrins to trigger desired downstream pathways via the cytoskeleton.

1.8 The cell cycle and its potential role in stem cell self-renewal

The cell cycle consists of a series of highly regulated phases resulting in cell division and production of two daughter cells. There are two growth phases, termed Gap 1 (G1) and Gap 2 (G2), a synthesis phase (S) and a mitotic phase (M). Cells that are not actively cycling (quiescent) exit G1 and are described as being in resting state, termed the G0 phase (Orford and Scadden, 2008, Cheung and Rando, 2013)(*Figure 1-10*).

The classic model of the cell cycle describes cyclin-dependent kinases (CDKs), having regulatory roles during specific phases (Malumbres and Barbacid, 2005). During early G1, D-type cyclins (D1, D2, and D3) bind to their respective cyclin-dependent kinases (CDK4 and CDK6) forming complexes (Sherr and Roberts, 1999). The resultant cyclin D-CDK complexes then initiate phosphorylation of retinoblastoma protein (Rb), thereby removing its repressive action on the E2F family of transcription factors (Matsumoto and Nakayama, 2013). These transcription factors become free to induce expression of cyclins E and A and other genes required to progress into S phase (Sherr and Roberts, 1999). The classical model has been challenged with the advent of knockout experiments with mice (Satyanarayana and Kaldis, 2009). These studies revealed that progression through the cell cycle was still possible without all of the CDKs being functional, due to compensatory mechanisms between cyclins and CDKs (Satyanarayana and Kaldis, 2009). For example, the ablation of CDK2 function was compensated for, by CDK1 and CDK4 (Barrière *et al.*, 2007). Intriguingly, it has since been shown that the master regulator of the mammalian cell cycle is

CDK1, which can solely guide the cycle to completion, working in isolation from the other CDKs (Santamaria *et al.*, 2007).

The cell cycle is considered to be a prominent factor in the self-renewal of stem cells. Supporting evidence includes observations that bone marrow haematopoietic stem cells (HSCs) maintain their cell population and preserve their self-renewal capabilities by continuously switching between a state of quiescence and self-renewal, entering and exiting the cell cycle (Cheshier *et al.*, 1999, Wilson *et al.*, 2008). The activities of CDKs are controlled by CDK inhibitors (Sherr and Roberts, 1999) and recent studies have suggested that inhibitor p57KIP2 (p57) has a role in both quiescence and self-renewal of HSCs (Tesio and Trumpp, 2011). Collectively, this evidence supports a theory that prevention of entry into G1 will preserve the self-renewal characteristic of stem cells.

In trying to decipher MSC self-renewal, the G1 phase of the cycle is of particular interest. This is due to the fact that G1 is mitogen-dependent for progression to S phase (Matsushime *et al.*, 1994). The G1/S checkpoint divides G1 into early and late phases. Once the cell passes this checkpoint and enters the late G1 phase, any external stimuli will no longer have any effects, and the cell is committed to progression through the cell cycle (Tesio and Trumpp, 2011). Mouse embryonic stem cells have a shortened G1 phase, allowing them to progress through the cycle and proliferate quickly. This is due to sustained activation of the cyclin E-CDK2 complex, which deactivates the R checkpoint that separates early and late stages of G1 (Orford and Scadden, 2008). Induced pluripotent stem cells have also been reported to have a shortened G1 phase and faster proliferation rate (Ghule *et al.*, 2011). As MSCs will garner instructional cues from the surface topography, this external stimulus may have strong effects during G1, in parallel with observations that G1 is important in HSCs and ESCs.

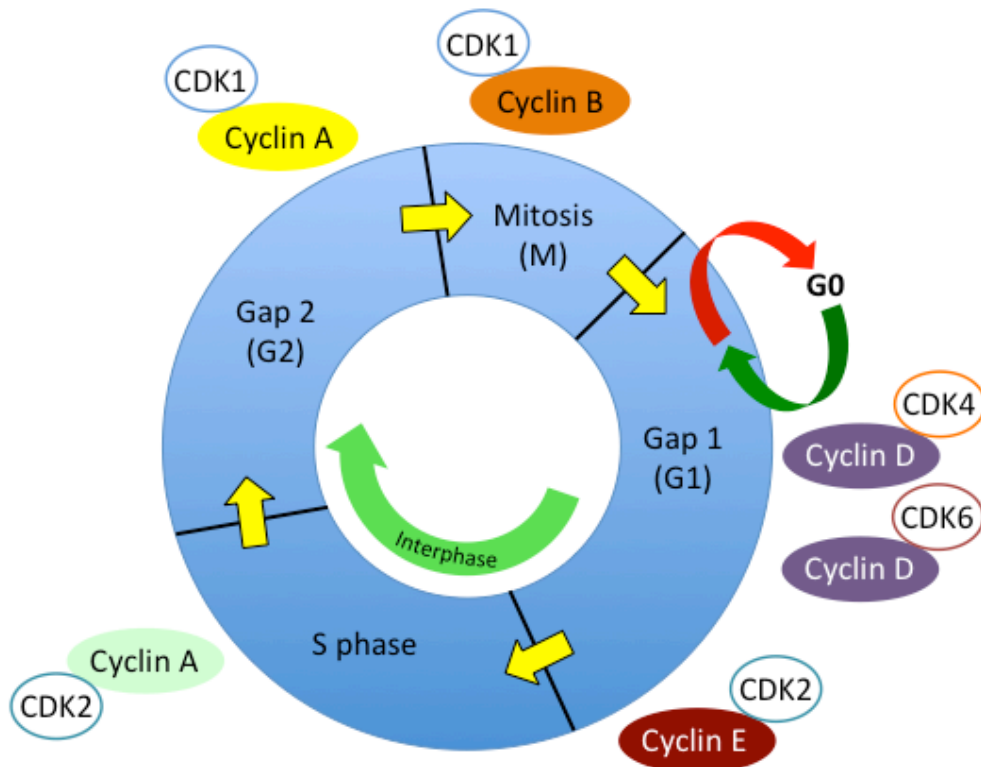


Figure 1-10: Schematic of the cell cycle. The cell cycle comprises four stages, Gap1 (G1), Synthesis (S) phase, Gap 2 (G2) and mitosis (M). Cells not actively cycling are in a resting state, termed G0. G1, S and G2 constitute interphase. The cell cycle is regulated by cyclins and their associated CDKs during particular phases. Adapted from Vermeulen *et al.*, 2003 (Vermeulen *et al.*, 2003).

Integrin-related signalling could lead to changes in activation of ERK1/2, and studies have shown that ERK is critical for S-phase progression. Specifically, the presence of ERK2 protein maintains expression of cyclin-D1 during G1 (Cárcamo-Orive *et al.*, 2008). ERK also appears to have a role in down-regulating genes that are associated with suppression of S-phase entry, with down-regulation occurring when ERK is continuously activated (Yamamoto *et al.*, 2006). Additionally, a link has been identified between the cell cycle and integrin-mediated signalling, in that members of the Rho-family GTPases which regulate changes in the actin cytoskeleton and activate ROCK, are also implicated in continuous ERK activation (Welsh *et al.*, 2001). Previous work showed that ERK1/2 was downregulated in MSCs on SQ nanotopography (Biggs *et al.*, 2009b). However, the precise mechanisms underlying MSC self-renewal remain unclear. A model for stem cell self-renewal was suggested by Li and Clevers, (Li and Clevers, 2010) which consisted of populations of both quiescent and active state stem cells in contrast with the previous idea that an individual stem cell would

be able to support the whole tissue. For example, HSCs are directed to enter or exit into a quiescent state by their niche, in order to preserve a store of HSCs (Wilson *et al.*, 2008).

There is a link between cell shape, cytoskeletal tension and cell cycle progression, which could be at work in the niche and when cells are cultured on biomaterial substrates. More rounded and less well spread cells appear to be impeded in their progression past G1 into S phase (Huang *et al.*, 1998). Moreover, fibroblasts that were unable to form stable attachments exhibited a downregulation of cyclin D1 and increase in expression of CDK inhibitors (Fringer and Grinnell, 2001).

1.9 Thesis aims

There is great potential for implementing the use of MSCs together with specific phenotype-inducing biomaterials for future medical applications. Furthermore, nanotopography has emerged as an important modulator of MSC processes in recent years. However, the caveats to wide-scale use of MSCs in regenerative medicine to-date are (i) limitations due to the low number of native cells, and (ii) a requirement for a method of effective expansion that maintains long-term symmetrical self-renewal.

This work builds on the initial research into the SQ nanotopography, which showed much promise for providing long-term self-renewing physical instructional cues for bone marrow-derived MSCs. McMurray and colleagues demonstrated the ability of SQ nanotopography to maintain STRO-1 selected skeletal stem cells over a period of 8 weeks whilst retaining multipotency. Conversely, standard culture plastics do not allow MSC populations to be maintained, resulting in rapid differentiation of the cells reminiscent of a fibroblast-like phenotype. Having identified the nanocues that elicit stem cell self-renewal in addition to stimulating osteogenic differentiation, it is now possible to begin detailing the mechanistic processes that allow direction of the cells into particular phenotypes.

This work attempts to clarify MSC self-renewal induced on nanotopography. The NSQ surface will be used as a control for comparison, as a differentiating surface.

The main aims of this study are:

- To optimise culture and seeding conditions for best use of the SQ polycarbonate nanotopography, in order to maximise self-renewal of primary MSCs without the addition of chemical factors, and to investigate differences in the metabolism of cells cultured on different nanotopographies.
- To assess levels of different cell cycle-related proteins and gene expression in synchronised MSCs cultured on SQ as they progress through the cycle, and look for wider networks and pathways through analysis of sequencing data.
- To explore the potential application of SQ nanotopography for MSC reprogramming, using a wholly nanotopography-based system for investigation.

Chapter 2

Materials and Methods

2 Chapter 2

2.1 Materials and reagents

2.1.1 Cell culture reagents

Name	Supplier
Dulbecco's Modified Eagles Medium	Sigma-Aldrich
Foetal bovine serum	Sigma-Aldrich
Minimum Essential Medium Non-Essential Amino Acids	Gibco by Life Technologies
L-Glutamine 200mM (100x stock)	Gibco by Life Technologies
Fungizone® Amphotericin B (250µg/ml)	Gibco by Life Technologies
Sodium Pyruvate (100mM)	Sigma Life Science
Penicillin-Streptomycin (10mg/ml stock)	Sigma-Aldrich
1xTrypLE™ Select cell dissociation solution	Gibco by Life Technologies
Trypsin 10x solution	Sigma-Aldrich
Versene*	Made in house
Hepes Saline*	Made in house
Phosphate buffered saline	Sigma-Aldrich
Sodium chloride	VWR Chemicals
Potassium chloride	VWR Chemicals
Glucose	Fisher Scientific
HEPES	Fisher Scientific
Ethylenediaminetetraacetic acid (EDTA)	Sigma-Aldrich
Phenol Red indicator solution (0.5%)	Sigma-Aldrich
Ficoll-Paque PREMIUM density gradient media	GE Healthcare Life Sciences
EasySep™ Human CD271 Selection Kit	Stemcell Technologies
Dimethyl sulfoxide (DMSO)	Fisher Scientific UK
Cdc42/Rac1 GTPase Inhibitor, ML141	Calbiochem, Merck Millipore

2.1.2 Induction media reagents

Name	Supplier
Insulin	Sigma-Aldrich
Isobutylmethylxanthine (IBMX)	Sigma-Aldrich
Dexamethasone	Sigma-Aldrich
Ascorbate-2-phosphate	Sigma-Aldrich
Indomethacin	Sigma-Aldrich

2.1.3 Immunostaining reagents

Name	Supplier
Formaldehyde (38%)	Fisher Scientific UK
Sucrose	Fisher Scientific UK
Sodium Chloride	VWR Chemicals
4-(2-hydroxyethyl)-1-piperazine-ethanesulphonic acid (HEPES)	Fisher Scientific UK
Triton X-100	Sigma-Aldrich
Magnesium chloride hexahydrate	Sigma-Aldrich
Bovine serum albumin	Sigma-Aldrich
Phosphate buffered saline	Sigma-Aldrich
Tween 20	Sigma-Aldrich
Rhodamine Phalloidin	Molecular Probes, Life Technologies
Horse Biotinylated anti-rabbit IgG	Vector Laboratories
Horse Biotinylated anti-mouse IgG	Vector Laboratories
Fluorescein streptavidin	Vector Laboratories
Texas Red streptavidin	Vector Laboratories
Vectashield Mounting Medium with DAPI	Vector Laboratories

2.1.4 Western blotting reagents

Name	Supplier
Sodium dodecyl sulphate	Sigma-Aldrich
Sodium deoxycholate	Sigma-Aldrich
Phosphatase inhibitor cocktail	Roche
Protease inhibitor cocktail	Roche
Bradford's reagent	Bio-Rad
Polyvinylidene difluoride (PVDF) membrane	Immobilon P, Millipore
ECL solutions	Thermo Scientific, Pierce
HRP linked anti-rabbit IgG	Sigma-Aldrich
HRP linked anti-mouse IgG	Sigma-Aldrich
4-12% NuPAGE bis-tris acrylamide gels	Novex; Life Technologies
NuPAGE 20x running buffer	Novex; Life Technologies
NuPAGE 20x transfer buffer	Novex; Life Technologies
Methanol	Fisher Scientific UK
Dried skimmed milk powder	Marvel
Medical X-ray film	Kodak

2.1.5 Cell staining reagents

Name	Supplier
Coomassie Blue G250	Sigma-Aldrich
Acetic acid	Fisher Scientific
Methanol	Fisher Scientific
Oil Red O	Sigma-Aldrich
Triethyl phosphate	Sigma-Aldrich
Mayer Haematoxylin solution	Sigma-Aldrich
ImmunoHistoMount	Sigma-Aldrich
Silver nitrate	Sigma-Aldrich
Sodium thiosulphate	BDH Biosciences
Nuclear Fast Red	Sigma-Aldrich
Anti-BrdU kit	GE Healthcare
LIVE/DEAD [®] Viability/Cytotoxicity kit	Invitrogen

2.1.6 In-cell western reagents

Name	Supplier
Odyssey Blocking Buffer	LI-COR
IRDye conjugated goat anti-mouse secondary antibody	LI-COR
IRDye conjugated goat anti-rabbit secondary antibody	LI-COR
CellTag 700 Stain	LI-COR
Tween 20	Sigma-Aldrich
Phosphate buffered saline	Sigma-Aldrich

2.1.7 Scanning electron microscopy reagents

Name	Supplier
Glutaraldehyde	Sigma-Aldrich
Sodium cacodylate	Agar Scientific
Osmium tetroxide	OxKem
Uranyl acetate	Sigma-Aldrich
Hexamethyldisilazane	Fluka Analytical
Double-sided conductive carbon tape	Agar Scientific

2.1.8 Primary antibodies

Name	Supplier
Anti-CD271 antibody	Abcam, UK/Cell Signaling Technology, USA
Anti-CD63 antibody	Santa Cruz, USA
Anti-STRO-1 antibody	Santa Cruz, USA
Anti-ALCAM antibody	Epitomics/Abcam, UK
Anti-Osteocalcin antibody	Santa Cruz, USA
Anti-Osteopontin antibody	Santa Cruz, USA
Anti-Bromodeoxyuridine (BrdU) antibody	GE Healthcare, UK
Anti-CDK6 antibody	Cell Signaling Technology, USA
Anti-E2F-1 antibody	Cell Signaling Technology, USA
Anti-Phosphorylated ERK antibody	Cell Signaling Technology, USA
Anti-Total ERK1/2 antibody	Cell Signaling Technology, USA
Anti-Cyclin D1 antibody	Cell Signaling Technology, USA
Anti-Phosphorylated Rb antibody	Cell Signaling Technology, USA
Anti-Total Rb antibody	Cell Signaling Technology, USA
Anti-Cdc25 antibody	Cell Signaling Technology, USA
Anti-p27kip antibody	Cell Signaling Technology, USA
Anti-GAPDH antibody	Abcam, UK/Millipore, Germany

2.1.9 Metabolomics sample preparation

Name	Supplier
Acetonitrile	Sigma-Aldrich, UK
Chloroform	Sigma-Aldrich, UK
Formic acid	Sigma-Aldrich, UK
Methanol	Fisher Scientific, UK

2.1.10 Collagen gel reagents

Name	Supplier
Rat tail collagen solution	First Link, UK
10X MEM	First Link, UK
FBS	Sigma Aldrich, UK
0.1M sodium hydroxide	Sigma Aldrich, UK

2.2 Solutions for cell culture

HEPES-saline solution

HEPES-saline was used to wash cells prior to detachment with trypsin/versene. 150 mM NaCl, 5 mM KCl, 5 mM glucose, 10 mM HEPES, 0.5% (v/v) phenol red solution. The pH was adjusted to 7.5. Solutions were autoclaved prior to use to ensure sterility for use in cell culture.

Trypsin-versene solution

Trypsin/versene was used to assist detachment of cells from substrates. 150 mM NaCl, 5 mM KCl, 5 mM glucose, 10 mM HEPES, 1 mM EDTA, 0.5% (v/v) phenol red indicator solution, adjusted to pH 7.5 and autoclaved prior to use to ensure sterility for cell culture. Trypsin stock (10x) was added as appropriate to produce a final working solution for detachment of cells.

2.3 Methods

2.3.1 Primary cell culture

All primary cells were maintained in a complete media consisting of a base of Dulbecco's Modified Eagles Medium (DMEM) supplemented with 10% foetal bovine serum (FBS), 10% antibiotic-antimycotic-glutamine mix (1% penicillin-streptomycin, 0.8 mM L-glutamine, 5% (v/v) Fungizone[®] amphotericin B) and 1% non-essential amino acids. Media changes were carried out twice weekly. All cells were kept in a humidified incubator at 37 °C with an atmosphere of 5% CO₂. Passaging of cells, and detachment for the purposes of selection and expansion, was achieved by washing cells with sterile PBS and incubating with TrypLE[™] Select (a mild detachment reagent) at 37 °C for 5 minutes.

2.3.1.1 Extraction of osteoprogenitors from bone marrow

Human mesenchymal stem cells were derived upon purification of bone marrow obtained from patients undergoing routine orthopaedic (hip/knee replacement) surgery at the Southern General hospital, Glasgow. Bone marrow aspirate was transferred into sterile transport media (0.6g EDTA, 5% (v/v) antibiotic-antimycotic-glutamine mix in 200ml PBS, pH 7.2) and stored at 4 °C upon arrival. After removal of visible blood clots, bone fragments and fat, processing of the marrow sample commenced with initial washes with complete media containing 10% FBS (as outlined in section 1.3.1 'primary cell culture'). This involved centrifugation of the aspirate at 345g for 10 minutes to pellet all cells and resuspending the resulting pellet with fresh media, with these steps being repeated twice. The cleaned cell suspension was layered carefully onto Ficoll-Paque[™] PREMIUM (GE Healthcare) density gradient media and subjected to a period of 45 minutes centrifugation at 445g to remove blood cells and isolate the mononuclear cell fraction.

The interface between the clear Ficoll-Paque[™] and the red coloured DMEM complete media defines the region where mononuclear cells can be found (*Figure 2-1*).

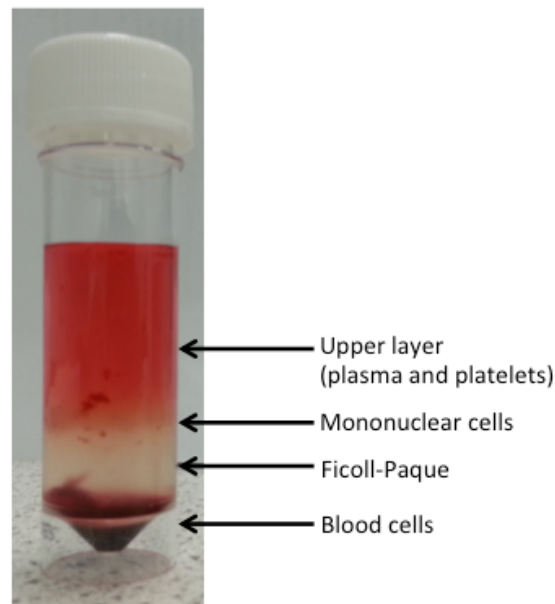


Figure 2-1: Location of the mononuclear cell fraction. Bone marrow aspirate after overlaying onto Ficoll-Paque™ media and centrifugation shows a yellowish coloured fraction located at the central interface. This fraction contains MSCs. Blood cells are pelleted at the bottom of the tube following centrifugation. Photograph acquired with a Samsung Galaxy Note II camera.

The mononuclear cell fraction was extracted into a new tube and washed in DMEM complete media three times after successive centrifugation at 345g and resuspension of the cell pellet in fresh DMEM complete media. The resulting cells were transferred into culture flasks and the adherent population (hereby referred to as ‘adherent bone marrow-derived cells’) were then cultured to as near to 70-80% confluency for several weeks prior to further selection.

2.3.1.2 Magnetic activated cell sorting for CD271⁺ mesenchymal stem cells

Magnetic-activated cell sorting (MACS) was carried out on the adherent bone marrow-derived cells using a CD271 positive selection kit (STEMCELL technologies). This additional step was implemented to isolate a CD271⁺ subpopulation, and thereby increase the purity and heterogeneity of the cells used in the study (Figure 2-2).

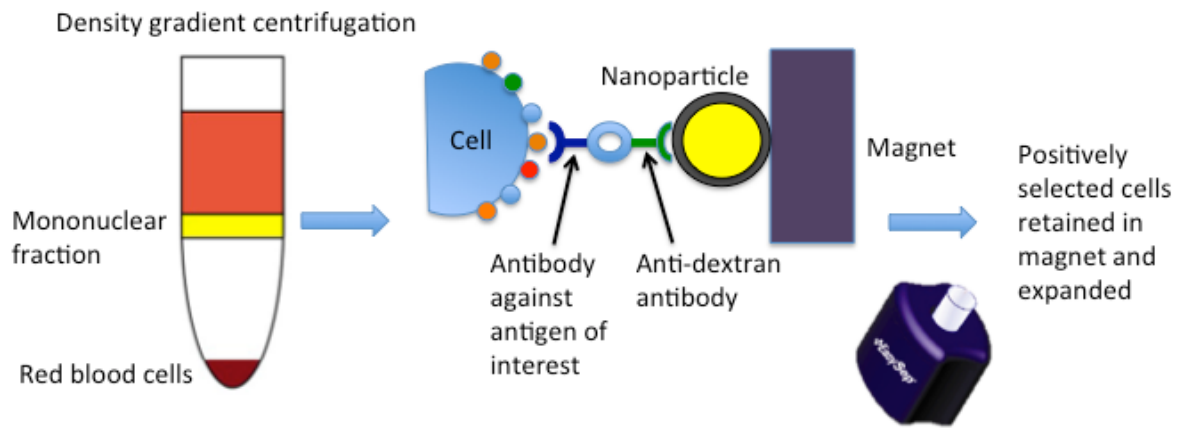


Figure 2-2: Outline of magnetic separation procedure for selection of CD271-positive MSCs from human bone marrow. Human bone marrow aspirate (cleaned for fat particles and blood clots) is overlaid onto Ficoll-Paque density gradient media and centrifuged to pellet the red blood cells and to define the mononuclear cell fraction. The MACs procedure involves the addition and incubation of CD271 antibody and magnetic nanoparticles, which allows a complex to be made between cells expressing the CD271 surface antigen and the nanoparticles. Once the tube containing the cells, antibody and nanoparticles is placed into a strong magnet, any positively labelled cells should be retained inside the tube when the setup is inverted. Adapted from the EasySep[®] protocol for human CD271 positive selection kit version 1.0.1.

Adherent bone marrow-derived cells were detached using TrypLE[™] Select cell dissociation reagent prior to carrying out magnetic sorting. Cells were washed with sterile PBS and incubated with the dissociation reagent for 5 minutes at 37°C. Upon agitation, the cells were observed to detach from the surface of the flasks and a volume of complete media was added to stop the action of the enzyme.

The cell suspension was sedimented by centrifugation at 345g for 5 minutes, and after removal of the supernatant, the cell pellet was resuspended in 500 µl of recommended medium (2% FBS in PBS) as per the manufacturers guidelines, and subsequently transferred to a sterile round-bottomed tube. All incubations were carried out at room temperature unless stated otherwise. 12.5 µL of Fc blocking solution was added and mixed by pipetting, followed by 25 µl of CD271 positive selection cocktail. The solution was incubated with the antibody for 15 minutes, followed by addition of 25 µl of nanoparticles for a further 15 minutes incubation. The volume of solution was made up to 2.5 ml with recommended medium and mixed by pipetting up and down before each tube was placed inside a magnet for 5 minutes. This allowed sufficient time for the positively marked cells to be retarded against the magnetic walls. Each magnet was then inverted

in turn, with any unlabelled cells being decanted from the tube. This washing step was repeated a further two times for a total of three inversions of the magnet. 400 µl of complete media was added to the resultant positively labelled cells, and mixed to obtain an even suspension. These cells were smeared across the bottom of cell culture flasks, and left to attach for approximately 1 hour at 37°C and 5% CO₂. After confirming cell attachment by light microscopy, the cells were flooded with a larger volume of complete media. These positively-labelled cells are forthwith referred to as 'CD271⁺ MSCs' in this thesis.

2.3.1.3 MACs selection of STRO-1⁺ MSCs

Selection of MSCs positive for the STRO-1 antigen (provided by Professor Richard Oreffo, University of Southampton) was carried out by Ms Julia Wells, from bone marrow tissue that would normally be discarded following routine total hip replacement surgery. Aspirate from trabecular bone marrow was centrifuged at 250g for 4 minutes at 4°C to pellet the cells within. The pellet was resuspended in minimum essential medium Eagle with alpha modification containing L-glutamine and nucleosides (alpha-MEM) and passed through a 70 µm pore mesh. Red blood cells were removed using lymphoprep gradient solution in combination with centrifugation. Cells in the buffy coat fraction were resuspended in 10 ml of HEPES saline containing 5% (v/v) FBS, 5% (v/v) human serum, and 1% (w/v) BSA. This was followed by incubation with STRO-1 antibody in hybridoma supernatant (Dr Beresford, University of Bath) and washing steps with MACs buffer. Human anti-IgM magnetic microbeads (Miltenyi Biotec) were added for a period of incubation, with bound cells positively labelled for STRO-1 being held in the magnetic column. These cells (STRO-1⁺ MSCs) were eluted and transferred to culture flasks for expansion and transported to the laboratory after reaching 80% confluency. Upon arrival, these cells were maintained as outlined for primary cell culture (section 1.3.1).

2.3.2 Substrate fabrication and preparation

Substrates were kindly produced by members of the Gadegaard group (department of biomedical engineering, University of Glasgow). The following subsections briefly outline the main steps in substrate production.

2.3.2.1 Electron Beam Lithography

Master substrates for each nanopattern were fabricated using electron beam lithography (Gadegaard *et al.*, 2003). The square-lattice arranged (SQ) nanopattern consisted of an ordered array of 120 nm diameter pits with 100 nm depth and 300 nm centre-centre spacing, and the disordered near-square (NSQ) nanopattern consisted of the same features as SQ, with an additional element of controlled disorder (± 50 nm), maintaining an average 300 nm centre-centre spacing. Interchangeable nickel inlays for the injection moulder were fabricated from patterned resists (silicon), and a thin layer of Ni-V (50 nm) was sputter-coated onto the patterned structures, prior to electroplating. The resultant nickel shims were cleaned with chloroform in an ultrasound bath for 15 minutes. Any silicon residue was removed by wet etching in 25% KOH at 80 °C for 1 hour, washed in ROH₂O and subjected to a final air-drying step. This process was outsourced.

2.3.2.2 Fabrication of polycarbonate substrates by injection moulding

Nanopatterned substrates were produced in large numbers by injection moulding with an Engel Victory 28 hydraulic injection moulder and Makrolon[®] OD2015 polycarbonate. Polycarbonate was added to the machine after inserting the required inlay. The first melt temperature was 280 °C and applied through the nozzle which the beads of polycarbonate pass through. The polymer was then cooled to around 80 °C. A clamping force of 250 kN assisted imprinting and transfer of the pattern from the inlay to one face of the substrate. The final surface area of each manufactured substrate measured 24 mm x 24 mm.

2.3.2.3 Hot embossing/Replication of nanotopographies on polycaprolactone

Imprints of the SQ and NSQ nanopatterns were transferred onto polycaprolactone (PCL) by hot-embossing using a fabricated nickel shim. Hot-

embossing of flat regions of the shim were used to generate un-patterned control surfaces. The shim was placed onto a hot plate set at 80 °C to melt the methanol-washed PCL beads (PCL has a melting temperature of 60 °C). The beads were positioned onto the desired areas of the shim and pressure was applied to a glass slide placed carefully over the melted polymer to imprint the pattern onto the material. After cooling, the patterned PCL disk could be carefully lifted off, subjected to plasma cleaning and sterilisation and then transferred into cell culture plates ready for seeding.

2.3.2.4 Plasma Cleaning

A 30 second air plasma treatment at the highest setting (30W power and a total pressure of 0.27mbar) of the plasma cleaner (Harrick Plasma, USA) was applied to all PCL substrates and 20 second air plasma treatment at the highest setting was applied to all polycarbonate substrates for surface cleaning and to assist with cell attachment and overcome the slight hydrophobicity of these polymers. Substrates were covered in 70% ethanol solution overnight to sterilise prior to seeding.

Oxygen plasma cleaning for X-ray photoelectron spectroscopy was performed by PhD student Daniel Morrison (University of Glasgow) using an oxygen barrel asher (Gala Instruments Plasmarep 5 asher) with oxygen gas at 0.2 mbar total pressure, 32W power (the nearest equivalent setting to the air plasma treatment) in a clean room environment.

2.3.3 Material Characterisation

2.3.3.1 Atomic Force Microscopy

Images of plasma treated surfaces were acquired using atomic force microscopy (AFM) in AC mode on a NanoWizard 3 atomic force microscope using NCH Silicon cantilevers (NanoWorld) with assistance from Dr Alex Winkel (JPK).

2.3.3.2 X-ray Photoelectron Spectroscopy

X-ray photoelectron spectroscopy (XPS) is a technique that provides quantitative information about the surface of materials. Samples were plasma treated for the required times and cleaned by immersion in 70% ethanol overnight, and dried before proceeding with XPS. Processing and analysis was performed by Dr Rasmus Pedersen (University of Glasgow) using a SAGE 100 XPS system (Specs Surface Nano Analysis GmbH, Germany) with spatial resolution of approximately 6 mm. The base pressure in the analysis chamber was approximately 2×10^{-7} mbar, and the x-ray source was $\text{AlK}\alpha$ -operated at an anode voltage of 9.5 kV and 140 W power. The pass energy for the hemispherical analyser was 50 eV for initial survey scans, and 15 eV for final high resolution scans. Spectra were recorded at a 90° take-off angle and subsequently analysed using casaXPS processing software. Identification of atomic composition was determined by integration of peak areas using a standard Shirley background.

2.3.3.3 Scanning electron microscopy

Images of substrates and MSCs growing on the surfaces at high magnification was achieved using scanning electron microscopy (SEM). After the required culture periods, cells on the samples were fixed with 1.5% glutaraldehyde buffered in 0.1M sodium cacodylate for 1 hr at 4°C . Cells were post-fixed in 1% osmium tetroxide in 0.1M sodium cacodylate buffer, and stained with uranyl acetate. Dehydration was achieved with the following alcohol series (30%, 50%, 70%, 90%, absolute ethanol, and dried absolute ethanol). Following this, hexamethyldisilazane was used in a final dehydration step. Upon removal of the solution, samples were placed inside a dessicator overnight to dry out. Following this, they were attached to aluminium stubs with double-sided conductive

carbon tape and sputter coated with gold-palladium to a thickness of 15-20 nm (Polaron SC515 SEM coater). Sputter coating and image acquisition were performed with kind assistance from Margaret Mullin and Peter Chung (University of Glasgow) using either a JEOL JSM 6400 scanning electron microscope with Olympus Scandium software or Sigma Variable Pressure analytical scanning electron microscope (Carl Zeiss) with Oxford Microanalysis software at an accelerating voltage of 10kV.

2.3.3.4 Water Contact Angle Measurement

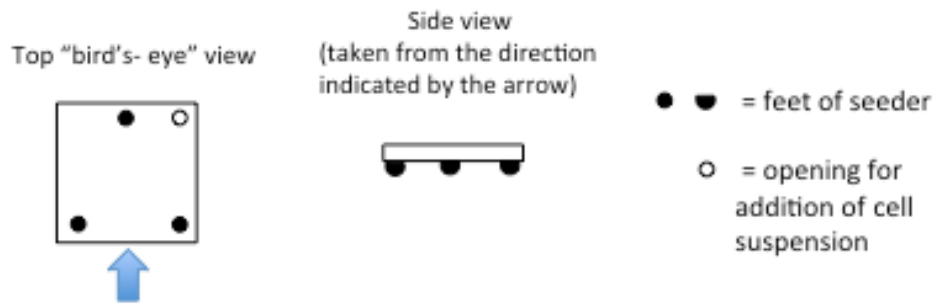
Multiple water contact angle (WCA) measurements at three random regions of each substrate were taken at room temperature using a sessile drop technique and a KSC CAM 100 contact angle goniometer (KSV instruments, USA). A droplet of water was suspended from the point of a needle with attached syringe (clamped in position so that the droplet was in range of the camera). A trigger point was set so that when the droplet was transferred to the surface of the substrate, measurement of angles would take place 2 seconds afterwards, giving time for the droplet to settle. Measurements for the same surface type were subsequently averaged to obtain the final values.

2.3.4 Cell seeding

Substrates left sterilising overnight were washed to remove traces of ethanol and particulates prior to seeding: twice in sterile PBS, and once in media. These were transferred into wells of 6 well plates. All MSCs were seeded using polycarbonate cell seeding devices (designed by Dr Mathis Riehle, and fabricated by Dr Paul Reynolds, University of Glasgow). This device was patented (application number PCT/GB2013/052776, publication number WO2014064449 A1; inventors: Paul Reynolds, Mathis Riehle, Nikolaj Gadegaard).

Sterilised seeding devices were placed carefully onto the top of each 24 mm x 24 mm square nanotopography (2 mm thickness), and 500 μ l of cell suspension was carefully pipetted through a circular opening located in the corner of each seeder (*Figure 2-3*). The entire setup was placed into the incubator for 1-2 hours to allow initial cell attachments to form, before addition of more media to each well and subsequent removal of the device.

(a)



(b)

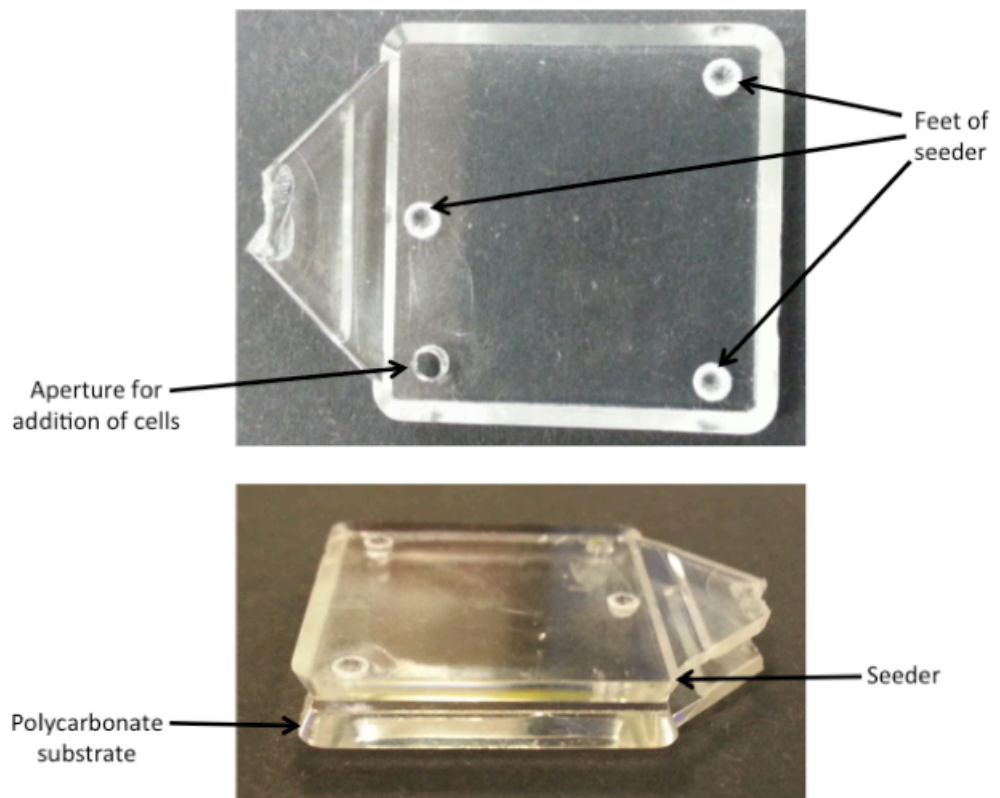


Figure 2-3: Cell seeding device. (a) Schematic diagram of the device. The seeding device consists of a 22mm x 22mm square piece of polycarbonate with 3 'feet' on the underside (denoted as black half/full circles) and an inlet for pipetting the cell suspension located in the corner (denoted by an unfilled circle). (b) Photographic images. Taken with a Samsung Galaxy Note II camera.

2.3.5 MSC Characterisation

2.3.5.1 Driving differentiation using chemical induction media

Chemical induction of MSCs to undergo adipogenic or osteogenic differentiation was achieved using DMEM media supplemented with a number of inducing agents.

CD271⁺ MSCs were seeded at a density of 1000 cells/cm² onto 13mm glass coverslips and cultured for a period of 6 weeks. Samples were cultured in either adipogenic induction media alternated with maintenance media to achieve adipogenesis or osteogenic induction media for osteogenesis.

In the case of MSCs induced to undergo adipogenesis, the adipogenic induction media was added to the cells first, then replaced with maintenance media at the next media change, with repeated switching between the two media types maintained throughout the culture time.

Adipogenic induction media consisted of DMEM basal media containing 10% (v/v) FBS, 1% antibiotic-antimycotic-glutamine mix, insulin (1.7 nM), indomethacin (200 µM), and isobutylmethylxanthine (500 µM).

Adipogenic maintenance media consisted of DMEM basal media containing 10% (v/v) FBS, 1% antibiotic-antimycotic-glutamine mix, and insulin (1.7 nM)

Osteogenic induction media consisted of DMEM basal media containing 10% (v/v) FBS, 1% antibiotic-antimycotic-glutamine mix, dexamethasone (1 nM) and ascorbate-2-phosphate (350 µM).

Media was changed on cells twice weekly throughout the duration the experiment.

2.3.5.2 Fixing cells for staining

After removal of media, samples were washed with PBS and fixed (in duplicate/triplicate for each type of topography per experiment) in buffered 4% formaldehyde: 2% sucrose solution at 37°C for 15 minutes. Fixative was then removed and enough PBS was added to cover the cells. Samples were stored at 4°C until ready to proceed with various staining protocols.

2.3.5.3 Oil Red O staining

Oil Red O solution (10 mg/ml) in 60% (v/v) triethyl phosphate (aqueous; aq) was used to confirm adipogenesis in MSC cultures supplemented with adipogenic media. Cells were fixed as outlined in 1.3.5.2, and then rinsed with 60% (v/v)

triethyl phosphate (aq). A volume of Oil Red O solution was added (sufficient to cover the cells) and left at room temperature for 10 minutes to allow staining of lipid deposits to occur. After this time, the solution was removed and cells were washed again in 60% (v/v) triethyl phosphate (aq) to remove excess staining solution. Filtered Mayer Haematoxylin solution was added to the cells for 2 minutes at room temperature, and rinsed off with tepid tap water. Coverslips were mounted onto glass slides using ImmunoHistoMount mounting medium.

2.3.5.4 Von Kossa staining

Von Kossa stain demonstrates the presence of calcium phosphate and calcium carbonate, indicators of progress in osteogenesis. A 5% (v/v) silver nitrate was prepared (aq) and added in sufficient volumes to cover the samples. All samples were exposed to UV light for 30 minutes, and then the solution was replaced with 5% (v/v) sodium thiosulphate (aq) for a further 10 minutes incubation. Samples were washed using a slow stream of tepid tap water for 5 minutes, and then rinsed in distilled water. These were counterstained with nuclear fast red prior to mounting onto glass slides using ImmunoHistoMount mounting medium.

2.3.5.5 Nuclear Fast Red Staining

Nuclear counterstaining with Nuclear Fast Red was performed for the samples subjected to Von Kossa staining. A 0.1% (v/v) Nuclear Fast Red solution was prepared containing 1.5 mM aluminium sulphate (aq). The solution was boiled for 10 minutes with continuous stirring, cooled and filtered prior to use. Samples were incubated with the staining solution for 4 minutes, and then rinsed well with distilled water and briefly in 70% (v/v) ethanol.

2.3.5.6 Coomassie Staining

After removal of the culture media, MSCs were fixed in 4% (v/v) paraformaldehyde: 2% (w/v) sucrose fixative at 37°C for 15 minutes. These were then stained with filtered 0.5% (w/v) Coomassie blue stain (Coomassie blue G250, prepared in 50% (w/v) methanol and 10% (v/v) glacial acetic acid) for 10 minutes at room temperature. Excess staining solution was then removed, and samples were washed three times successively with distilled water. Brightfield

images were acquired using a Zeiss Axiovert 25 inverted transmitted light microscope with a 5x A-plan objective (Zeiss). Full size scans of the substrates were also obtained using an Epson scanner at 800 dpi resolution in 24 bit colour.

2.3.5.7 Immunostaining

Cells were fixed as outlined in section 1.3.5.2. For immunostaining, cells were permeabilised with permeabilisation buffer (0.1% (w/v) sucrose, 50 mM NaCl, 3 mM MgCl₂.6H₂O, 20 mM HEPES, 0.5% (v/v) Triton X-100 in H₂O and adjusted to pH 7.2) and blocked in 1% (w/v) BSA in PBS for 15 minutes at 37°C. Anti-ALCAM antibody (1:150) or anti-STRO-1/OCN/OPN antibodies (1:50 dilution) were added and incubated with the cells at 37°C for 1 hr. After washing three times with 0.5% (v/v) Tween-20 in PBS (PBST), the samples were incubated with biotin-conjugated anti-rabbit/mouse secondary antibody for 1 hr at 37°C. Samples were washed again three times with PBST, and further incubated with fluorescein isothiocyanate (FITC) conjugated streptavidin (diluted 1:50 in 1% BSA) for 30 minutes at 4°C. A final three washes were carried out before samples were mounted onto glass coverslips using mounting medium containing 4', 6-diamidino-2-phenylindole (DAPI).

2.3.5.8 BrdU labelling

1mM BrdU in complete DMEM media was added to cells for the final 6 hours of the required culture time, and incubated at 37°C and 5% CO₂ as for normal cell culture. Following this, MSCs were washed with PBS, fixed, permeabilised and blocked as outlined in 1.3.5.7 for immunostaining. Anti-BrdU antibody was diluted 1:100 in DNase I solution and incubated with the cells for 2.5 hrs at 37°C. After washing with PBST, samples were incubated for 1 hr at 37°C with anti-mouse secondary antibody conjugated to texas red diluted 1:50 in blocking solution. Following further washes with PBST, the samples were mounted using mounting medium containing DAPI.

2.4 Microscopy and imaging

Images of the cells were acquired using brightfield, fluorescence or confocal microscopy. The specific details pertaining to each of these will be discussed in the following subsections. An indicator of scale was either obtained through the imaging software itself (confocal) or through acquiring an image of a 1mm graticule under the appropriate magnification lens (brightfield and fluorescence). This was then converted into pixels using Image J software (Abramoff *et al.*, 2004, Schneider *et al.*, 2012).

2.4.1 Brightfield microscopy

Stained or unstained cells were observed using a Zeiss Axiovert 25 light microscope. Images were acquired using QCapture software. Other specific details are outlined in figure legends and relevant sections as appropriate.

2.4.2 Fluorescence Microscopy

Immunostained specimens were imaged using either an inverted microscope (Axiovert 200M; Carl Zeiss, Germany) linked to a CCD camera (QImaging) or an upright microscope (Olympus BX51) with motorised stage capabilities (Prior) linked to a QCapture camera. Both of these microscopes operated using Image Pro software (the Olympus uses ImageProPlus) (Media Cybernetics, UK). The motorised stage was utilised for the samples subjected to BrdU staining. This involved setting a scan pattern so that the stage moved horizontally across the substrate, down one step, then horizontally in the reverse direction, repeated continually until a preset number of images had been obtained. Acquired greyscale images corresponding to the different filters were converted to RGB colour format using Adobe Photoshop imaging software. Composite images were generated by overlaying the coloured greyscale images (red, green or blue depending on the fluorescence emission of the fluorophores used in the staining process).

2.4.3 CellProfiler Image Analysis

Grey-scale images corresponding to cell nuclei, cell cytoskeleton and a protein of interest were inspected using CellProfiler open source cell image analysis software (version 2.1.0). CellProfiler software allowed for the quantification of proteins of interest in cells following immunostaining and microscopy. Pipelines were designed to define the location of cells by first identifying the nuclei from the images corresponding to DAPI-staining. Briefly, this was achieved through defining threshold strategies alongside filtering criteria such as size and intensity rules which would be applied to the relevant images. The area covered by each cell was then extrapolated from the locations of the nuclei to the edges, which were designated using images corresponding to cytoskeletal staining of F-actin. After correct segmentation parameters were implemented, measurements pertaining to the cell area and protein of interest were made for a number of cells detected across 20 images per substrate. Exposure times during image acquisition were maintained at a constant for the protein of interest, to allow valid comparisons to be made between samples.

2.4.4 Synchronisation and release of MSCs for analysis of cell cycle

STRO-1⁺ MSCs were seeded on substrates at a density of 1000 cells/cm² and allowed to attach and establish for a period of 48 hours. The cells were washed in serum free media and then incubated for a further 48 hours in 0.1% FBS (low serum) media (Jaejin *et al.*, 2012) to induce cell cycle arrest and thereby synchronise the cells.

After this period in low serum media, MSCs were released back into the cycle by replacement of this media with serum containing maintenance media (10% FBS) for the required durations for each experiment.

2.4.5 Preparation of samples for flow cytometry

STRO-1⁺ MSCs were seeded on substrates at a density of 1000 cells/cm² and synchronised as described in section 1.4.4. The media was changed to maintenance media containing 10% FBS for 24 hours following synchronisation. Cells were washed with sterile PBS, trypsinised, and pooled (according to

substrate type/culture condition). Cells were pelleted by centrifugation at 345g and the supernatant was removed. Cells were washed twice, each time resuspending the pellet in PBS and then centrifuging as described in the previous step. Fixing was achieved by adding 3 ml of cold ethanol (molecular grade; Sigma-Aldrich) drop-wise whilst vortexing to minimize clumping, and left at 4°C for 1 hour. Samples were then sent to the University of Southampton, where cells were washed and propidium iodide staining solution (3.8 mM sodium citrate, 40 µg/ml propidium iodide in PBS) was added to the pellets together with RNase A (10 µg/ml RNase A in PBS) for 3 hours at 4°C (protected from light). Flow cytometry was carried out on a Guava® easyCyte flow cytometer (Merck Millipore), with subsequent analysis performed using FlowJo data analysis software.

2.4.6 Quantitative in-cell western and detection

MSCs cultured on all surfaces were fixed in 4% paraformaldehyde and briefly permeabilised in the appropriate buffer as outlined previously for immunostaining. Surfaces were then transferred to new plates so that there would be no signal from cells that had not adhered to the samples during the culture period. Samples were then blocked in Odyssey blocking buffer for 1.5 hours at room temperature. Primary antibodies (protein of interest and GAPDH as a normalisation protein) were diluted in the same blocking buffer and applied to the samples for 3 hours at room temperature. Washes were carried out using 0.1% Tween in PBS washing solution. Liquid was added and aspirated carefully as not to dislodge any cells. A total of 3 washes were performed each time. IRDye secondary antibodies (red and green; 680 and 800 respectively) were diluted to 1:800 in blocking buffer and incubated with the samples for 1 hour at room temperature, protected from light. After further washing and removal of as much residual washing solution as possible, measurement of intensity from labelled proteins was achieved using the Odyssey Sa imaging system (LI-COR) which has a plate reading format. After performing dual scanning at both wavelengths, a grid was applied to the resulting scan in order to quantify the intensity solely from a square region corresponding to the seeded portion of the substrates (*Figure 2-4*).

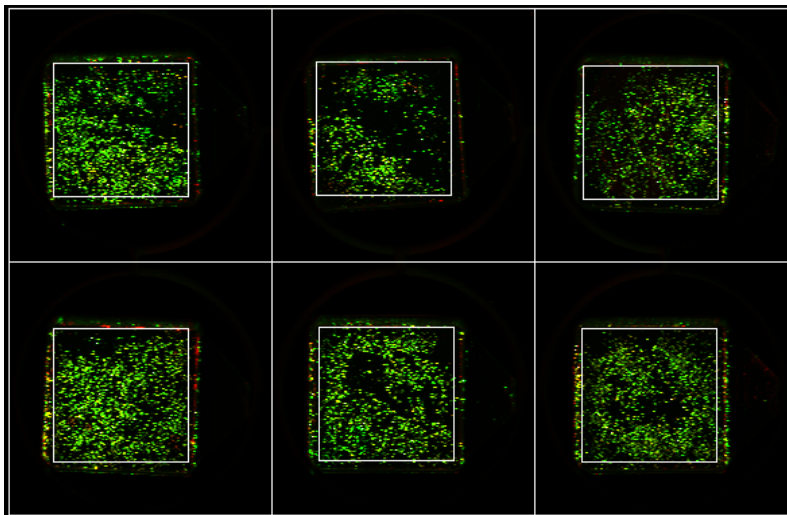


Figure 2-4: Application of a grid for quantification of samples stained using IRdye fluorescent secondary antibodies. After scanning, a grid was applied to the resultant image. The integrated intensity within the white boxes at two wavelengths corresponding to the red and green channels was measured in each experiment.

2.4.7 Filopodial inhibition

Inhibition of filopodia was attempted using a chemical inhibitor of cdc42. Complete media containing the inhibitor was made fresh prior to beginning the experiment. Initial testing of inhibition was assessed with MSCs seeded onto glass coverslips, with different concentrations of inhibitor in media being added to the cells 1 hour post-seeding. Cells were then fixed and stained for F-actin using rhodamine phalloidin as outlined for immunostaining. Coverslips were transferred onto glass slides for ease of handling and visualisation. Fluorescence images were taken using a Zeiss Exciter confocal microscope. For the proceeding nanotopography filopodia studies, cdc42 inhibitor was added at the determined optimal concentration with the complete media after synchronisation of the cells. These were then fixed for visualisation by SEM. Images were acquired with kind assistance from Mrs Margaret Mullin (SEM facility, University of Glasgow).

2.4.8 Next generation sequencing

Synchronised and 24 hour released MSCs were trypsinised from the surfaces, pooled accordingly and washed with PBS. The cell pellets were subsequently

frozen on dry ice and transferred to -80°C storage until ready to proceed with RNA extraction. This was performed using the RNeasy extraction kit procured from QIAGEN following the manufacturer's instructions.

Briefly, the cell pellets were dislodged by flicking the tubes and disrupted in buffer RLT. Then 70% ethanol was added, and the lysate was transferred to a spin column. The remainder of the procedure was followed as per outlined in the instructions provided with the kit. The RNA was eluted from the columns after addition of 10 μl of RNase-free water. RNA quality and concentration of samples were then determined using a Nanodrop ND1000 spectrophotometer (Thermo Scientific) using water as a blank. Absorbance readings at 260 nm (A_{260}) were used for quantification with the A_{260}/A_{280} ratio being noted as an assessment of purity. Samples were stored at -80°C until ready to proceed with the next steps.

Extracted RNA samples were processed and analysed by Mrs Jing Wang and Ms Julie Galbraith (Polyomics facility, University of Glasgow). 136 ng of total RNA per sample were processed using a TruSeq[®] stranded mRNA low throughput kit according to the manufacturer's protocol (Illumina). Conversion of the mRNA within the total RNA was required to generate a library of template molecules for sequencing. The steps carried out included poly A selection for purification of poly A-containing mRNA followed by fragmentation, first and second strand cDNA synthesis, sample cleanup, adenylation of 3' ends, ligation and cleaning of adapters, PCR amplification (98°C for 30 seconds followed by 15 cycles of: 98°C for 10 seconds, 60°C for 30 seconds, 72°C for 30 seconds, then 72°C for 5 minutes, hold at 4°C) and cleanup. All cleanup steps were performed using AMPure XP beads (Beckman Coulter). This was followed with sequencing by adding 3.2 pM libraries (Illumina NextSeq 500 sequencer). The raw data was pre-processed by bioinformatician Manikhandan Mudaliar (Polyomics facility, University of Glasgow), using the BaseSpace[®] next-generation sequencing cloud computing environment (Illumina) (Anders and Huber, 2010, Dobin *et al.*, 2013).

Generated logfold change values and adjusted p values were then uploaded and analysed using the (QIAGEN) Ingenuity[®] Pathway Analysis (IPA) online software application (www.ingenuity.com) and the data assessed for up- or downregulation of canonical pathways and networks.

2.4.9 Western blotting

MSCs on the substrates were harvested by detaching the cells from each surface with 1x trypsin/versene working solution followed by use of a cell scraper. After 5 minutes incubation at 37°C, the cells could be seen to begin detaching under a light microscope. After scraping, cells from several of the same type of substrates were pooled together in order to gather enough protein for subsequent analysis. Cells were lysed in RIPA buffer (150 mM NaCl, 50 mM Tris-HCl, 1% Triton-X 100, 1% sodium deoxycholate, 1% sodium dodecyl sulphate, adjusted to pH 7.5) supplemented with protease and phosphatase inhibitor cocktails. The lysates were transferred into tubes and subjected to end-over-end mixing at 4°C before removal of any cell debris by centrifugation at 10,000g and transfer of the supernatant into new tubes. The amount of extracted protein obtained in each sample was measured by performance of a Bradford's assay and comparison with a range of BSA standards (Bradford, 1976). Readings were measured using a spectrophotometer (Molecular Devices Spectra Max Plus) for absorbance at 595 nm or with an automated plate reader at 595 nm (Anthos Labtec 2010 with ADAP version 1.6 software).

Samples were equalised for protein and 2x Laemlli loading buffer containing beta-mercaptoethanol (4% SDS, 10% 2-mercaptoethanol, 20% glycerol, 0.004% bromophenol blue, 0.125M Tris HCl, pH 6.8) was added to each (Laemlli, 1970). The lysates were resolved at 200V constant voltage using pre-cast 4-12% gradient NuPAGE bis-tris polyacrylamide gels and accompanying gel system (Novex) and subsequently transferred onto a PVDF membrane according to the manufacturer's instructions. Antibodies were added to the membrane at the appropriate dilutions in 1% non-fat milk powder overnight at 4°C. Levels of GAPDH, alpha-tubulin or total protein when looking at phosphorylation, were used as loading controls. HRP-conjugated secondary antibodies were diluted at 1:5000, and incubated on the membrane for 1hr with shaking. After washing the membrane with PBST, detection was achieved using enhanced chemiluminescence methods. Western blot bands were quantified by densitometry, with the use of image J (Abramoff *et al.*, 2004, Schneider *et al.*, 2012).

2.5 Metabolomics

2.5.1 Sample preparation

MSCs cultured on surfaces had media removed, and were washed in cold PBS prior to carrying out the extraction procedure. Metabolites were extracted using a cold methanol-chloroform solution (1:3:1 ratio of chloroform: methanol: water). To achieve this, each substrate was inverted on top of the extraction solvent, and sealed with parafilm within culture plates to minimise evaporation. The same steps were performed for a series of 'blanks', which consisted of placing the solvent onto substrates that had not been seeded with cells throughout the culture period. All of the samples were vigorously agitated on a rotary shaker for 1 hour at 4 °C.

The resulting solutions were transferred to tubes, centrifuged for 3 minutes 13000g to remove cell debris, then kept at -80 °C until ready to proceed with liquid chromatography mass spectrometry. A pooled aliquot of all samples within the batch was made and used for quality control purposes as requested by the metabolomics facility at Glasgow Polyomics (University of Glasgow).

2.5.2 Liquid chromatography mass spectrometry

These steps were performed by staff at the metabolomics facility of Glasgow Polyomics (University of Glasgow), headed by Dr Karl Burgess, with assistance from Dr Lesley-Anne Turner.

Liquid chromatography mass spectrometry was employed as a technique to isolate each metabolite from the mixture of metabolites within each sample, and for the detection of each separated metabolite according to their mass (UltiMate 3000 RSLC with a 20 mm x 2.1 mm ZIC-pHILIC guard column coupled to a 150 mm x 4.6 mm ZIC-pHILIC analytical column running at 300 µl/min, coupled to an Orbitrap Q-Exactive (Thermo Fisher). Each detected metabolite generates a spectrum of peak intensity against retention time.

Known 'standard' samples were analysed together with each batch of samples, which consist of known metabolites. The retention times of these were used to assist identification of sample metabolites.

2.5.3 Data analysis

Raw mass spectrometry data was first processed using XCMS for peak picking (Tautenhahn *et al.*, 2012). An IDEOM/MzMatch Excel interface (Scheltema *et al.*, 2011, Creek *et al.*, 2012) was used for the purposes of converting all the raw data files, chromatographic peak selection and subsequent measurement of peak intensities, in order to filter, post-process and finally investigate the putative identities of the separated metabolites. The KEGG database was referenced for inference of metabolomics pathways.

2.6 Preliminary collagen gel study

2.6.1 Collagen gel preparation

All reagents used to make the gels were at 4°C prior to commencing the protocol.

Reagent	Volume (ml) for 1x mix
Rat tail collagen solution	2.5
0.1M sodium hydroxide	1.0
10X MEM	0.5
FBS	0.5
Complete media	0.5

Table 2-1: Reagent volumes for the preparation of collagen gels. The values could be scaled up accordingly to produce enough gel mixture for several plates.

FBS, 10x MEM and complete media were added to a universal tube and kept on ice. In another tube, 0.1M sodium hydroxide was added directly to the collagen solution and inverted several times to mix. This solution was then poured into the first tube containing media and FBS. This resulted in a yellow solution. Additional 0.1M sodium hydroxide was added gradually until a colour change to pink was observed, indicating neutralisation of the collagen. The pH of the final solution was checked using a pH probe to ensure that the range was between 7.0-7.5.

The final mixture was divided between wells of 6 well plates as required (2ml per well), on top of seeded nanotopographies and incubated at 37°C for at least 30 minutes to form a gel. The volumes outlined in table 1 were scaled up as necessary for additional samples.

2.6.2 Cell viability assay

The viability of the cells was assessed by carrying out live/dead staining. Complete media containing calcein acetoxymethyl ester (calcein AM) and ethidium homodimer (1 μ l of each into 1 ml of media, with volumes scaled up as required) were added to the cells and incubated for 1 hr at 37°C. After incubation, media was removed and three successive washes with media were carried out. Imaging was then performed using a Zeiss Axiovert 200M inverted fluorescence microscope. Non-fluorescent calcein AM permeates cells, whereby the acetoxymethyl group is hydrolysed by intracellular esterases, leaving calcein, which emits a green signal. In contrast, the ethidium homodimer binds to nucleic acids resulting in emission of red fluorescence. Thus, any red fluorescent signal must be due to damage to the cell membrane, and assigned as a dead cell.

2.7 Statistical Analysis

Suitable statistical tests were performed using Microsoft Excel (t-tests for comparisons between two groups) or Graphpad Prism 6 software (multiple comparison tests to analyse data from three groups or more). Statistical significance was noted when the p value was less than 5% confidence (0.05). Standard error was calculated using Microsoft Excel.

Chapter 3

Characterisation of Mesenchymal Stem cells and Nanotopography Optimisation

3 Chapter 3

3.1 Introduction

MSCs are subject to a plethora of instructional physical and biochemical cues within niche microenvironments in the body, which exert a level of control on the state of the stem cells and regulate their differentiation. As mentioned in chapter 1, in order to successfully promote these cells to undergo either self-renewal or differentiation on biomaterials for regenerative medicine, we must successfully mimic an aspect of these cues and transfer these to the interacting surfaces.

In this study, polycarbonate substrates with nanoscale pits were utilised with the distribution of the nanotopographical features being of importance in influencing antagonistic effects on stem cell fate. The fabrication method for these topographies was developed by Gadegaard *et al.* (Gadegaard *et al.*, 2003), with the nanotopographies being named square (SQ) - describing a square lattice arrangement of ordered pits - and near square (NSQ), whereby an element of disorder was introduced (± 50 nm) giving a degree of offset from an absolutely square arrangement of pits. Culture of MSCs on the NSQ nanotopography was conducive for MSC differentiation into bone (Dalby *et al.*, 2007) whilst it was more recently shown that the SQ surface maintained MSC phenotype (McMurray *et al.*, 2011). These established SQ and NSQ nanopatterns allow for investigation into the basis of self-renewal and differentiation at the molecular level, without the use of additional chemical factors.

One important aspect of experimental design and setup that must be considered is the quantity of materials used. Researchers must continually devise strategies to minimise any wastage of biological and substrate materials, as the former can be difficult to acquire (particularly in the case of stem cells) and the latter can be costly. In addition, the seeding density of cells on a surface can have a considerable impact on the phenotype of cells, and thus should be controlled for reproducibility. Cell density can affect cell morphology and stem cell differentiation. For example, a previous study noted that lower seeding densities directed stem cells towards an osteogenic phenotype, whereas higher seeding densities drove adipogenic differentiation (McBeath *et al.*, 2004). Increasing

efficiency of seeding, and maximising data yield from the substrates available can be addressed through the technique employed.

Conventional cell seeding onto scaffolds and substrates typically adopt the static seeding method, one that is hampered by the disadvantages of low seeding efficiencies and non-uniform distribution of cells across surfaces. This involves adding a suspension of cells contained within a small volume directly to the substrate or scaffold held within a culture dish (Shahin and Doran, 2011). Other seeding methods include the semi-static cell suspension technique, whereby the added cell suspension is manually shaken at periodic intervals in the attempt to improve the distribution of cells (Dolder *et al.*, 2003) and other more elaborate methods involve dynamic seeding in bioreactors and use of vacuum systems. It could be argued that the better methodology must be one that incorporates the simplicity and high reproducibility of static cell seeding, together with the increased seeding efficiency of micromass culture, with the uniform cell distribution that is associated with dynamic seeding. In this work, a cell seeding device (patented by Mathis Riehle, Paul Reynolds and Nikolaj Gadegaard, University of Glasgow) was utilised to counter the outlined limitations related to currently available seeding techniques. Each seeder can be easily placed on top of substrates and a suspension added through an inlet incorporated into the design.

Continuous promotion of symmetrical MSC self-renewal is desirable due to the importance in amassing large numbers of cells for downstream applications as native numbers are low (Caplan, 2007). Expanded cells could later be induced to differentiate into the required cell type. As cells are the building blocks of tissues, which in turn are components of organs, these fundamental components are the greatest limiting step to regenerative medicine. It is important to remember that in addition to efficient cell propagation, stem cell phenotype must be retained in tandem. This has proved a particular difficulty with *in vitro* culture, with spontaneous differentiation increasing over time (Bosnakovski *et al.*, 2004, Streckfuss-Bömeke *et al.*, 2013). In order to indicate the state that a stem cell has reached in terms of differentiation, numerous studies make use of phenotypic marker proteins. Using osteogenic differentiation as an example, osteoprogenitor cells will exhibit an increase in alkaline phosphatase levels during the maturation stage and produce more osteocalcin and osteopontin (Marom *et al.*, 2005) during the matrix mineralisation phase.

Characterisation of MSCs is subject to wide variation among research groups, due to the number of candidate markers ascribed to them in the literature.

However, in recent years, moves have been made to standardise the criteria, and produce a set of minimum requirements to define a multipotent MSC population from human tissue (Dominici *et al.*, 2006). These include adherence to tissue culture plastic when cultured, positive expression of several 'cluster of differentiation' (CD) antigens such as CD105 (endoglin), CD73 (ecto 5' nucleotidase), CD90 (Thy-1), and lack expression of haematopoietic markers CD45, CD34, CD14/CD11b, CD79 alpha or CD19, HLA-DR, and successful *in vitro* differentiation into adipocytes, osteoblasts and chondroblasts. In addition to these, positivity for STRO-1 (Oreffo *et al.*, 1998, Triffitt and Oreffo, 1998) and ALCAM markers have often been used to gauge levels of stemness in MSC populations (Dalby *et al.*, 2007, McMurray *et al.*, 2011). Here, we describe extraction of patient derived mononuclear cells, which include a population of MSCs. Following publishing of the minimum requirement guidelines, expression of CD271 has recently become an indicator for multipotent MSCs (Bühring *et al.*, 2007, Jones *et al.*, 2010, Boxall and Jones, 2012), thus further selection of the adherent bone marrow population for cells containing markers allows for isolation of a cell fraction of increased purity and heterogeneity, which can be then characterised accordingly. Ultimately, MSCs must exhibit multipotency, which can easily be tested by artificial induction of differentiation through the use of different formulations of so-called induction media.

Metabolomics is a fairly recent biological tool that provides a large-scale strategy for identification of small molecules that are within cells at any given time. This metabolomic 'fingerprint' gives an indication of the cellular processes that have taken place (McNamara *et al.*, 2012) and can be thought of as a 'snapshot' of cellular state when cultured under specific conditions, such as incorporation into a gel, following drug treatment, or from stimulation by nanotopographical cues. A metabolomics approach has been adopted in the study of ESCs (Yanes *et al.*, 2010), iPSCs (Panopoulos *et al.*, 2012) and MSCs (McNamara *et al.*, 2011, Tsimbouri *et al.*, 2012). The entire complement of metabolites within a cell at a particular point in time, known as the metabolome, is in a state of constant flux, with biochemical factors being continually produced and degraded, and interactions occurring between molecules. Adopting an untargeted global metabolomics approach lends itself

well to discovery of key metabolites that vary under different conditions, which will be exploited to identify important molecules for self-renewal.

The main aims of this chapter were to successfully isolate and culture a subpopulation of CD271⁺ MSCs from human bone marrow aspirate by magnetic-activated cell sorting selection (MACS), and to determine the optimal conditions for efficient use of the SQ surface, in order to promote self-renewal whilst maintaining maximal retention of stem cell marker expression. Use of the conditions eliciting the largest retention of stemness was then carried forward in assessing the metabolomic profile of these MSCs on the different nanotopographies. Characterisation of the cells and substrate were additionally performed, in order to provide a basic understanding of the key materials utilised in this project.

3.2 Results

3.2.1 Reproducibility of polycarbonate substrates

The substrates used in this thesis were produced in high volume by injection moulding. However, these were manufactured in several batches depending on availability of equipment. Therefore, it was noted that there may be variation introduced between different production runs. In order to assess the extent of such variation, the diameter of pits was measured from SEM images of nanopatterned substrates taken from several batches (*Figure 3-1*).

The results firstly show that injection moulding successfully confers the nanotopography onto the polycarbonate base material. Comparison of the initial shim and the final substrates show that the pit distributions match their respective patterns (*Figure 3-1*). Secondly, there were no significant differences in pit diameter when comparing between five manufacturing batches of SQ and NSQ polycarbonate nanotopographies, and thus the slight variation in dimensions of the features is not an important factor between the two surfaces.

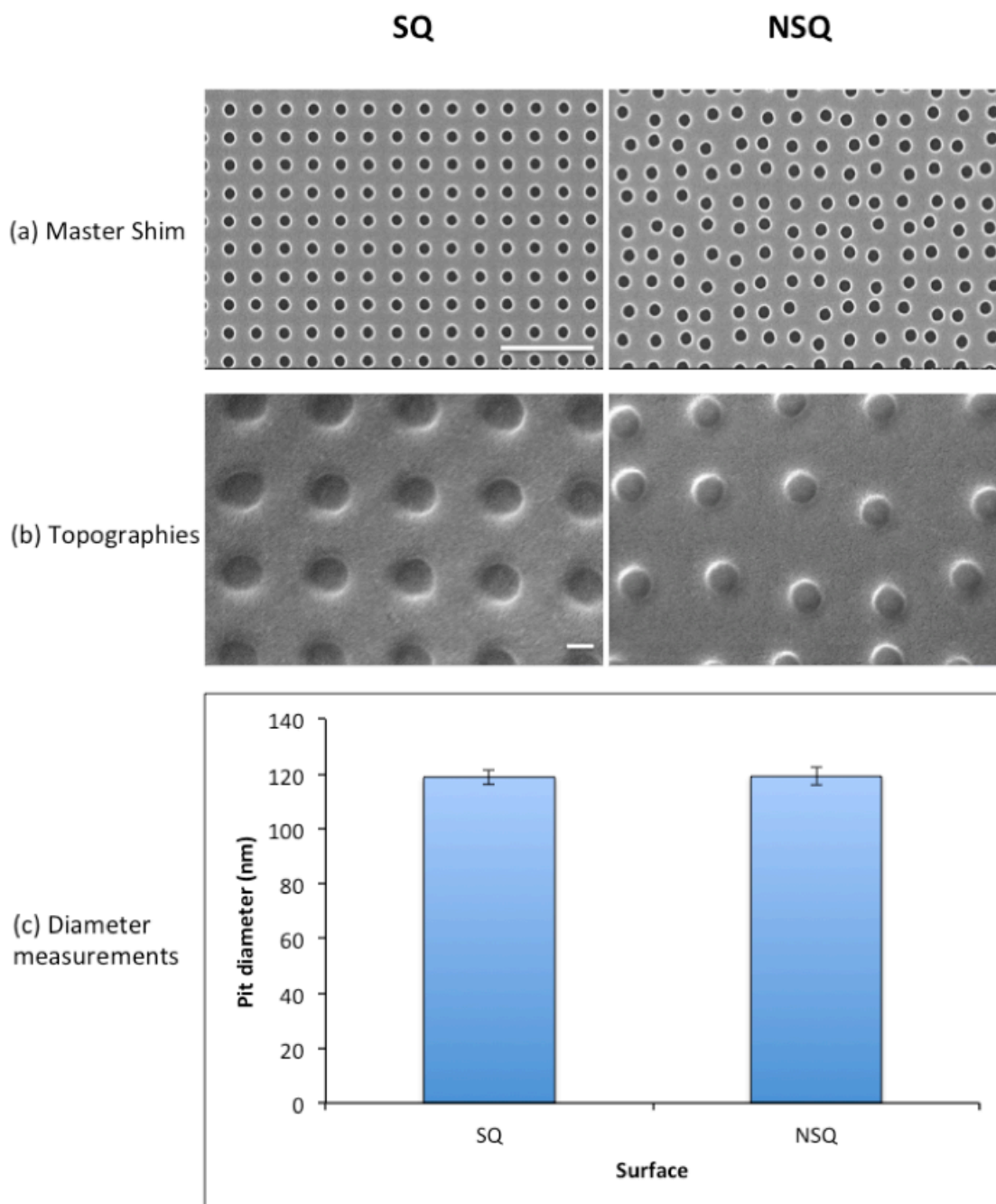


Figure 3-1: Reproducibility of the nanopatterns across batch manufacture. (a) Images of the shims produced by e-beam lithography. These are positive replica images of the master shims used to create SQ (ordered) and NSQ (disordered) nanotopographies. Scale bar: 1 μm (b) Representative SEM images of the surface of the polycarbonate nanotopographies. These are negative replicas. Scale bar: 100 nm (c) Graph showing the average of 54 pit diameter measurements over five different manufacturing batches of nanotopographies. Error bars denote standard deviation. Significance was tested using a student's t-test, with the threshold for statistical significance set at $p < 0.05$. The calculated p-value was $p > 0.5$, suggesting that the difference between pit diameters was not significant.

3.2.2 Plasma cleaning of nanotopographical substrates

The base material of the nanotopographical substrates used in this study was polycarbonate, a transparent and stable polymer with a melting point of 149°C, that has slight hydrophobic properties. Cell adhesion is regarded as a pivotal initial process in tissue engineering, as attachment precedes cell migration and spreading. In addition, as a cell attaches, the formation of focal adhesions can be observed, which can trigger downstream processes such as differentiation (Biggs *et al.*, 2007b). The formation of these adhesions can be influenced by surface properties including surface wettability, which can be regarded in terms of hydrophobicity and hydrophilicity (Lim *et al.*, 2005). Plasma cleaning is a strategy frequently adopted to promote surface oxidation and hydroxylation to assist cell adhesion and overcome the hydrophobicity of tissue culture plasticware and polymers (Ikada, 1994, van Kooten *et al.*, 2004).

Flat, SQ and NSQ surfaces were subjected to a range of plasma treatments and water contact angles (WCAs) were measured and calculated using the Cassie-Baxter equation (*Figure 3-2*).

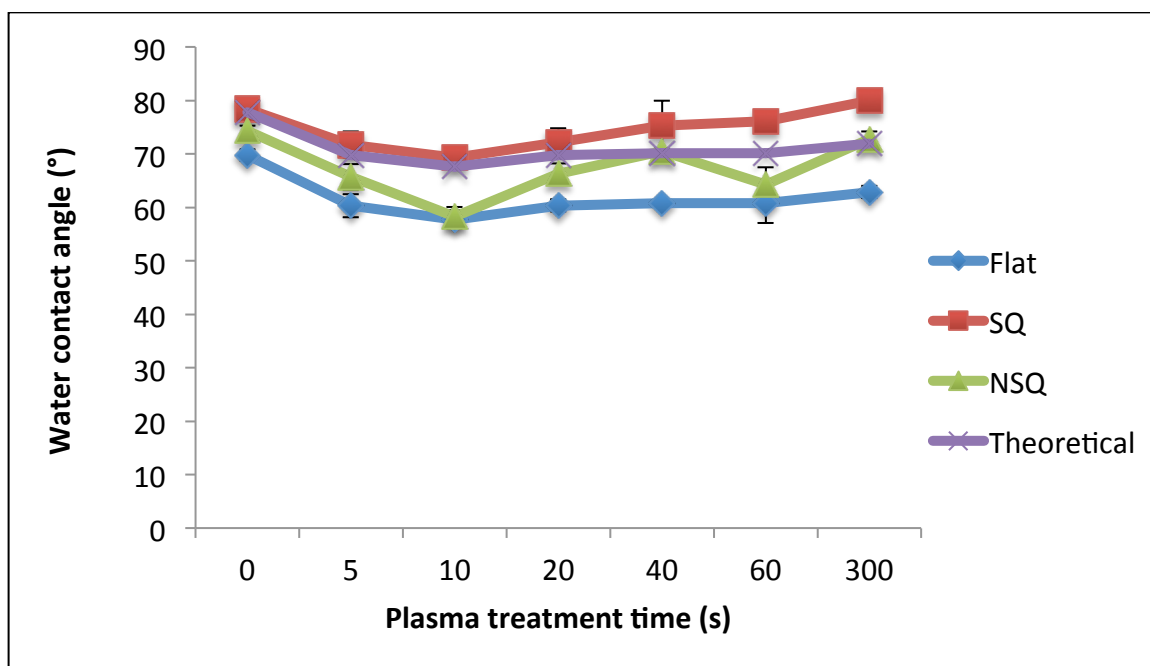
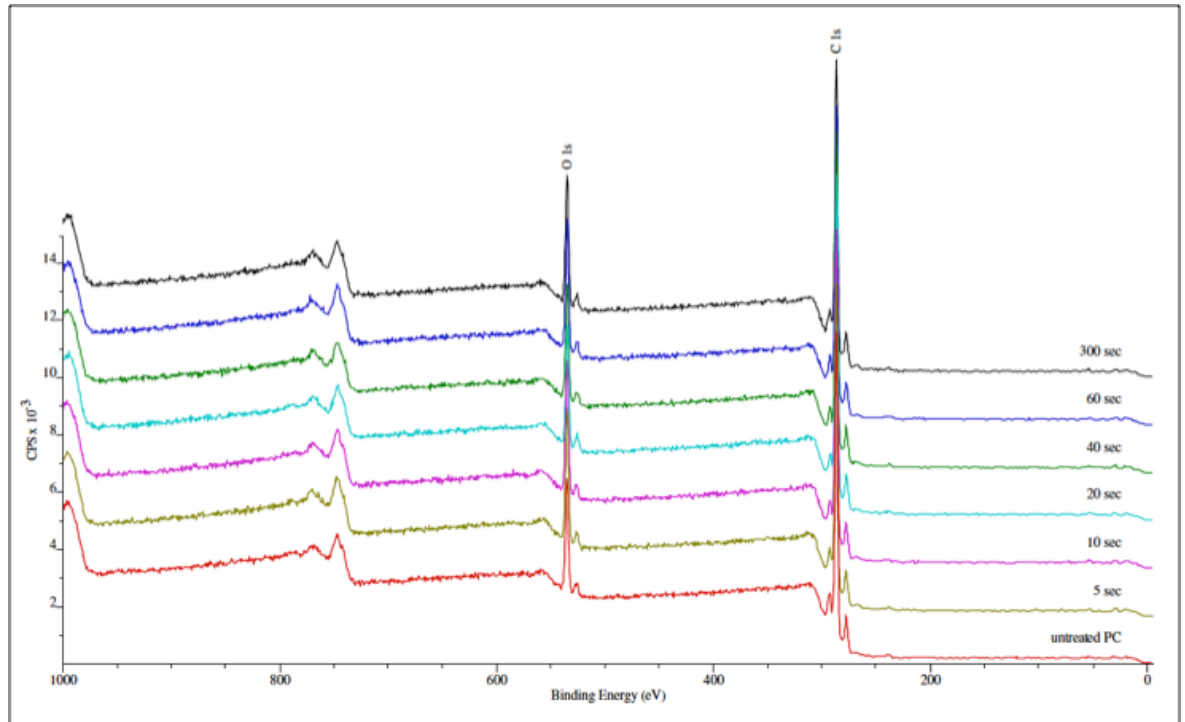


Figure 3-2: Measured and calculated theoretical water contact angles for polycarbonate flat and nanopatterned surfaces. The theoretical water contact angle was calculated using the Cassie-Baxter equation assuming 10% coverage.

The WCAs were observed to immediately decrease upon application of the air plasma treatment, which is expected as more oxygen becomes incorporated into the surface. This indicates a decrease in hydrophobicity. However, the measured WCA increased slightly over time, as it is likely that particles from the ambient air began to deposit on the material surface. For efficient experimental setup, it is desirable to have a relatively short treatment time for preparation of substrates in vast quantities and to avoid this deposition on the surface. It was observed that after 20 seconds plasma treatment, there is a significant difference in WCA when comparing between flat and SQ and flat and NSQ. At this point, the theoretical angle correlates relatively well with the measured WCA values for SQ and NSQ.

For more controlled measurements, X-ray photoelectron spectroscopy (XPS) analysis was carried out to investigate the elemental composition on each of the surfaces following timed oxygen plasma treatment. This confirmed the successful incorporation of oxygen into the material after 10 seconds (*Figure 3-3, Figure 3-4, Table 3-1, Table 3-2*). There appeared to be no significant benefits with prolonged treatment, therefore a short duration of plasma treatment is sufficient to gain an increase in oxygen functionalities.

(a)



(b)

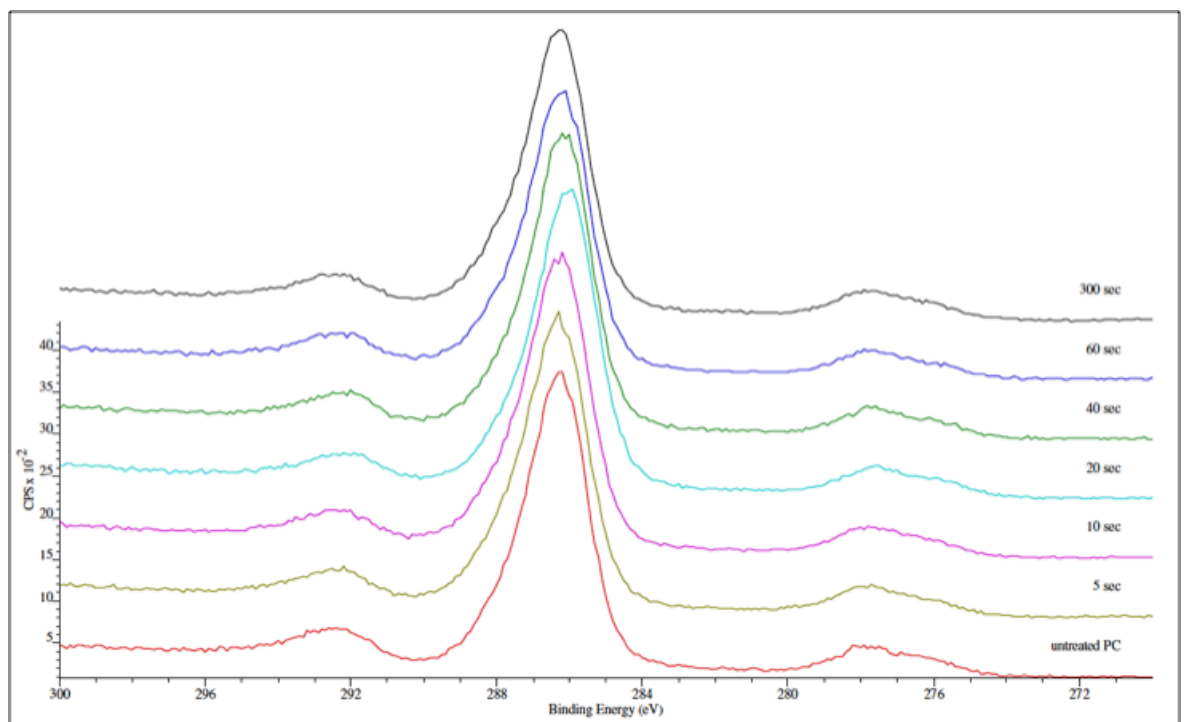
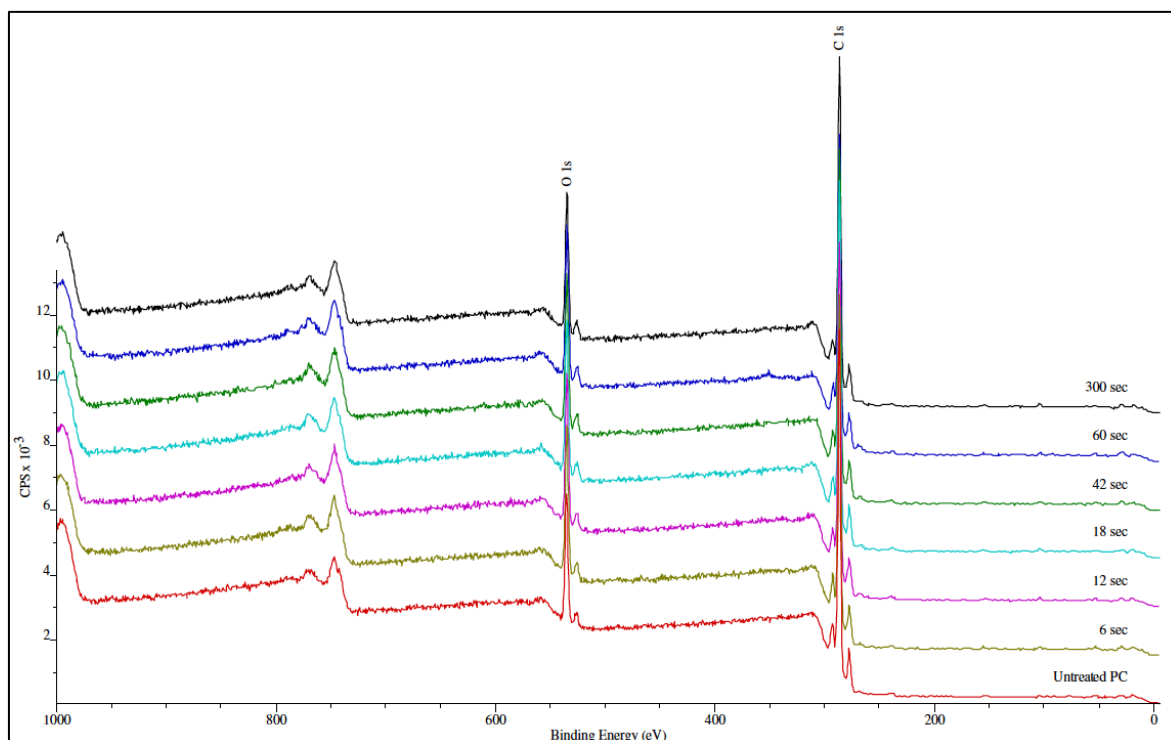


Figure 3-3: XPS analysis of air plasma treated polycarbonate. Time points of treatment are indicated above each trace (a) XPS survey spectrum with peaks corresponding to oxygen and carbon (b) High resolution combined spectra showing only a single photoemission peak corresponding to C1s between the different plasma treated samples. The data for each spectrum in this combined figure are artificially offset on the y-axis for clarity.

(a)



(b)

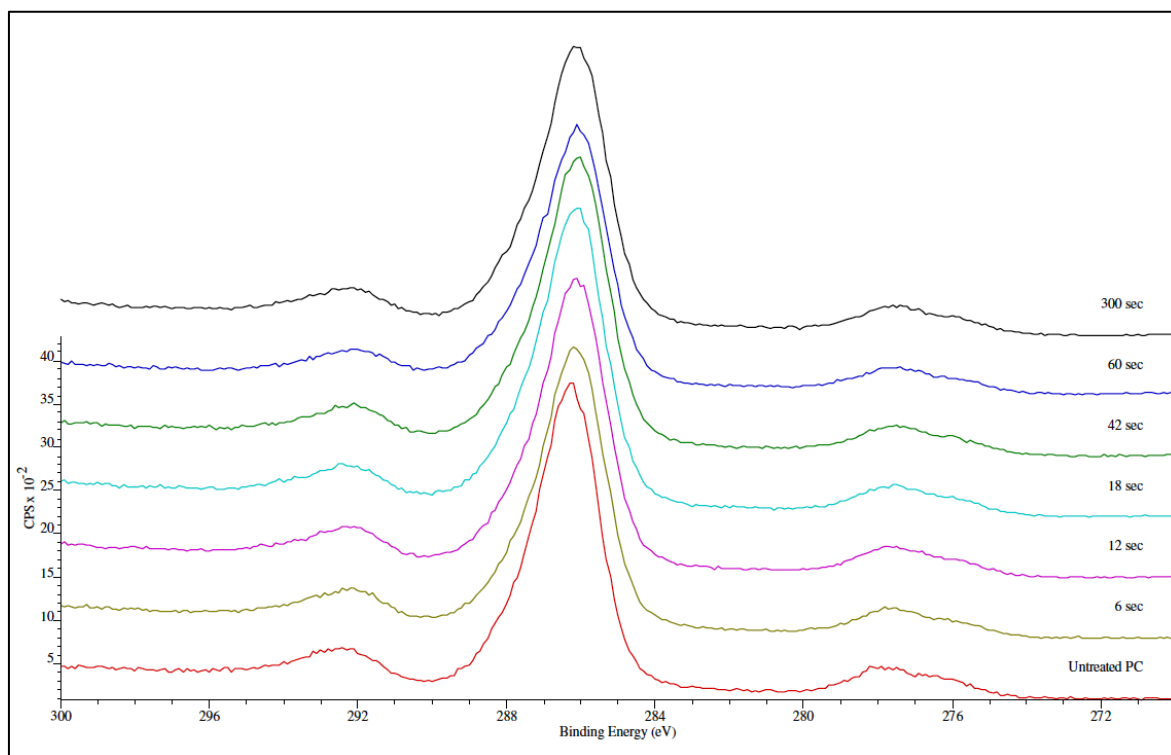


Figure 3-4: XPS analysis of oxygen plasma treated polycarbonate. Time points of treatment are indicated above each trace (a) XPS survey spectrum with peaks corresponding to oxygen and carbon (b) High resolution combined spectra showing only a single photoemission peak corresponding to C1s between the different plasma treated samples. The data for each spectrum in this combined figure are artificially offset on the y-axis for clarity.

Air plasma treatment time (s)	Carbon (%)	Oxygen (%)
0 (No treatment)	87.0	13.0
5	85.0	15.0
10	85.7	14.3
20	86.4	13.6
40	86.7	13.3
60	84.6	15.4
300	85.1	14.9

Table 3-1: Quantification of detailed XPS spectra corresponding to air plasma treated polycarbonate. The table shows the percentage of carbon and oxygen detected on the surface of each sample. XPS analysis was performed by Dr Rasmus Pedersen (University of Glasgow).

Oxygen plasma treatment time (s)	Carbon (%)	Oxygen (%)
0 (No treatment)	87.0	13.0
6	84.8	15.2
12	85.0	15.0
18	84.9	15.1
42	84.6	15.4
60	82.4	17.6
300	85.5	14.5

Table 3-2: Quantification of detailed XPS spectra corresponding to oxygen plasma treated polycarbonate. The table highlights percentages as described for table 1. Oxygen plasma treatment times were kept as close to the air plasma treatment times as possible, within the limits of the machinery. Oxygen plasma treatment was carried out by Daniel Morrison, and XPS analysis was performed by Dr Rasmus Pedersen (University of Glasgow).

In some cases plasma treatment can etch the surface of materials. This was tested for the plasma treatment times used in previous steps of this part of the work. SEM and AFM images (Figure 3-5 and Figure 3-6) did not reveal any distinctive differences as the duration of plasma treatment was increased. In addition there were not any significant changes in pit depth (Figure 3-7).

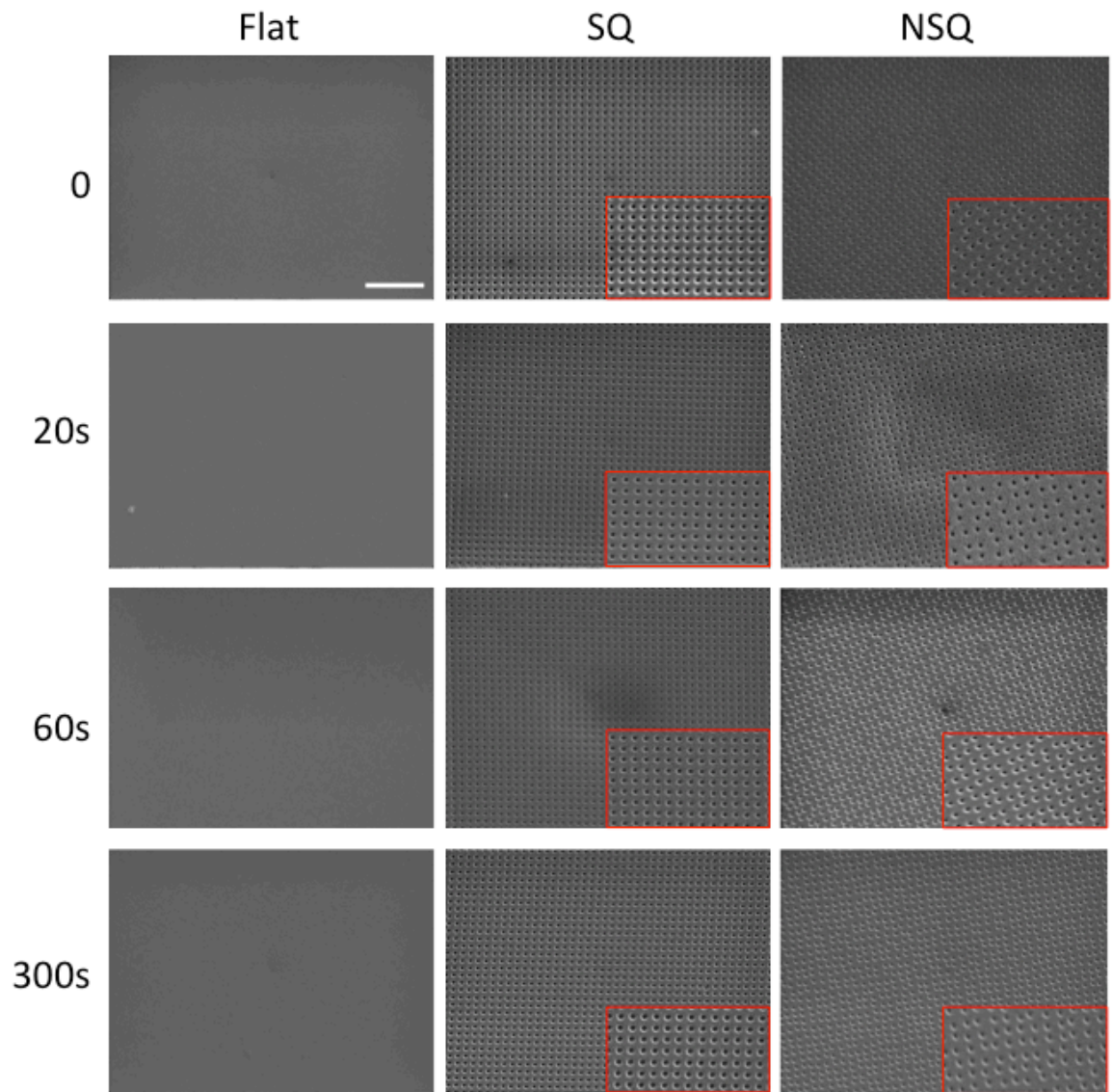


Figure 3-5: SEM images of flat and nanopatterned surfaces following air plasma treatment. Scale bar: $2\mu\text{m}$. Region boxed in red represents an expanded part of the original image.

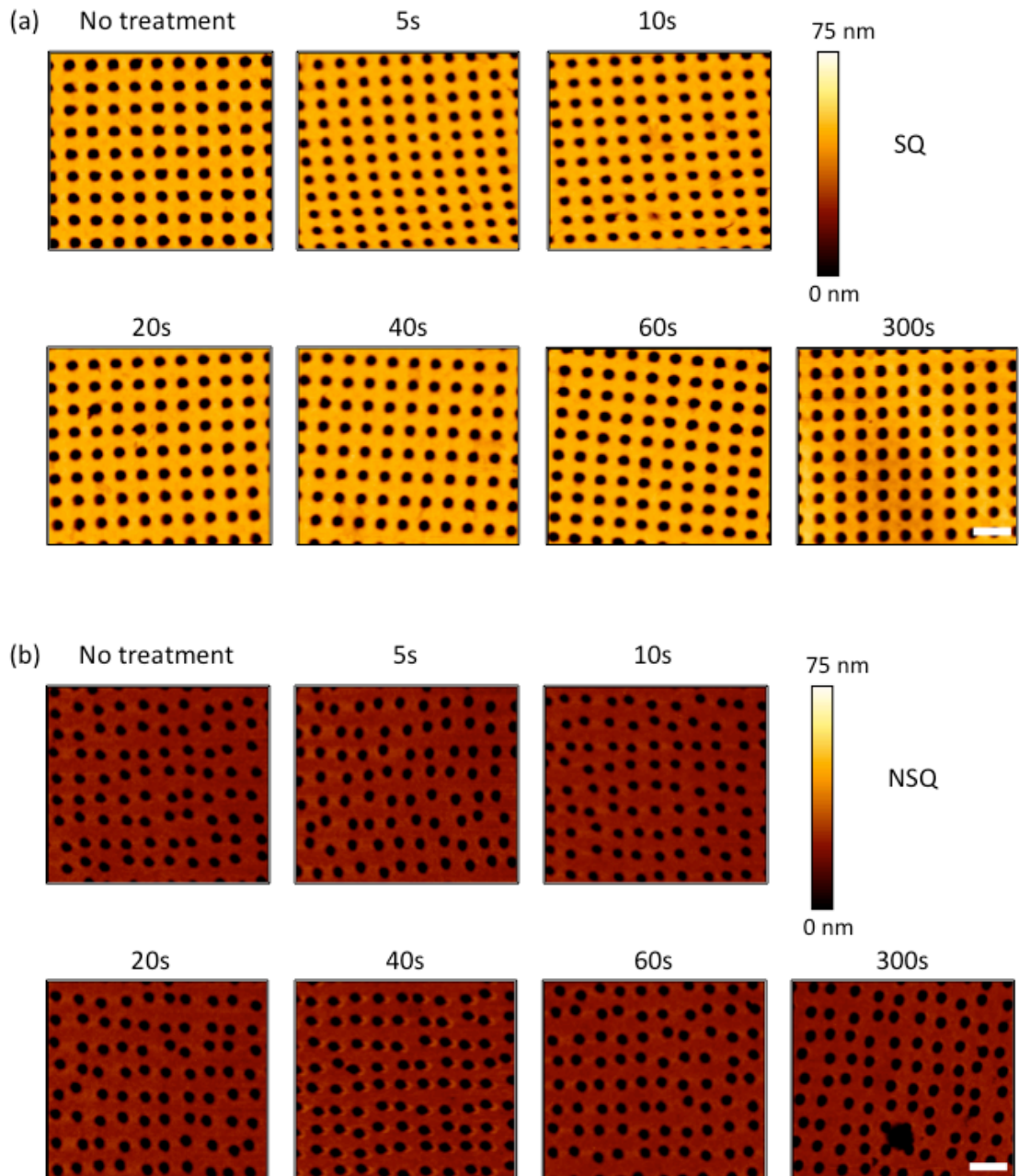


Figure 3-6: Effect of air plasma treatment on nanotopography surfaces assessed by AFM imaging. Samples were subjected to air plasma treatment for the indicated times and imaged using AFM in order to test whether this would have any detrimental effects on validity of the nanopatterns. Imaging was carried out by Dr Alex Winkel (JPK AFM services). Scale bar: 500 nm.

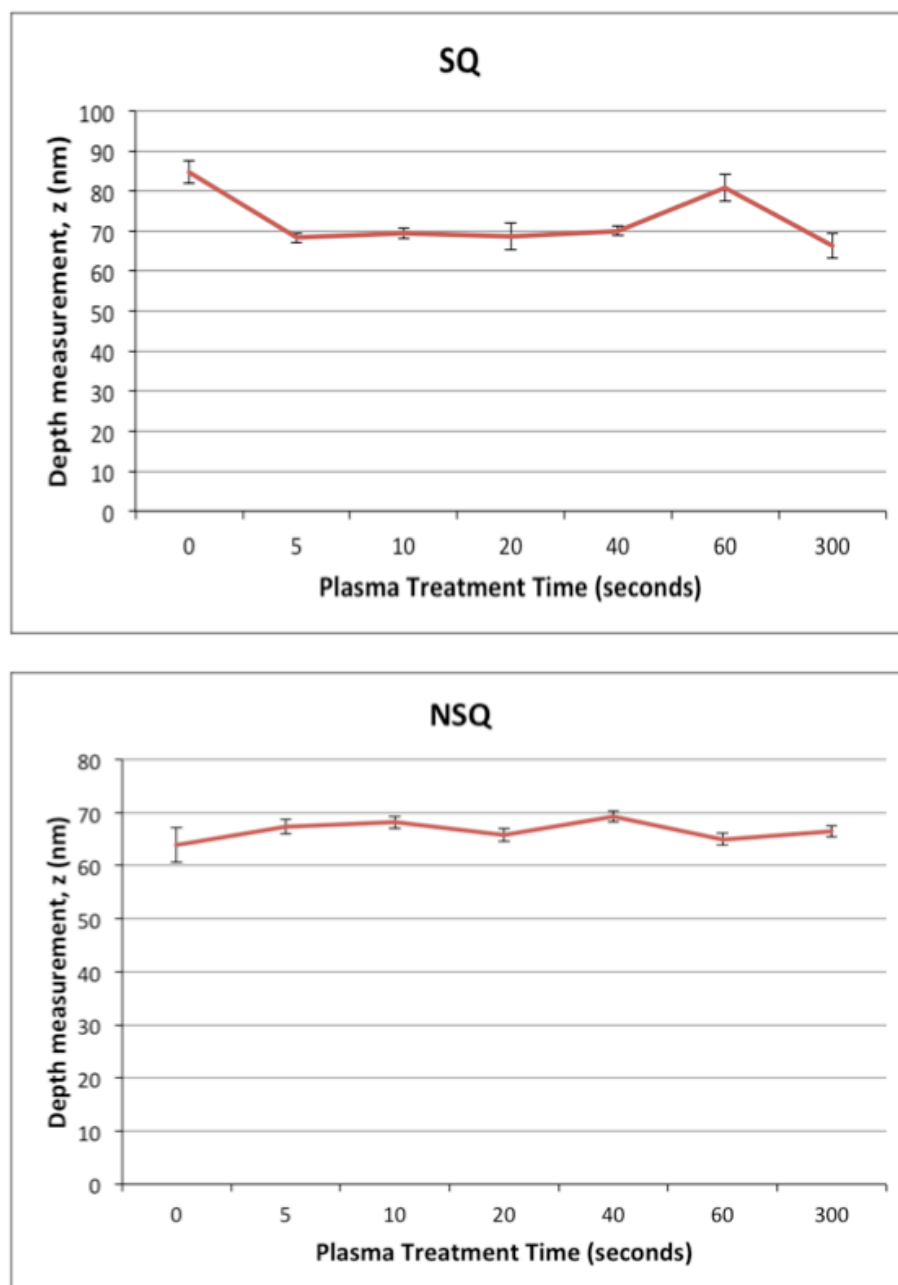


Figure 3-7: Plasma treated nanotopography pit depth measurements derived from AFM images. Pit depth measurements were obtained using Gwyddion open access software. Average depth measurements of pits across the surface of SQ and NSQ plasma treated substrates showed minimal variation in depth with prolonged plasma treatment. Errors bars denote \pm standard deviation.

Based on the results of the plasma cleaning assessment, 20 seconds of air plasma treatment was deemed to be sufficient to assist cell attachment. All polycarbonate surfaces were thus pre-treated in this fashion prior to cell seeding.

3.2.3 Effect of nanotopography on phenotype of MSCs cultured on PCL

The nanoscale pit features described have previously been fabricated in different materials, such as poly(methyl methacrylate) (PMMA) and polycaprolactone (PCL), and were reported to promote either osteogenic differentiation or maintenance of self-renewal of STRO-1 selected MSCs (Dalby *et al.*, 2007, McMurray *et al.*, 2011). To ensure that these nanotopography induced osteogenesis and stem cell maintaining phenotypes were reproducible, SQ and NSQ pit nanotopographies were hot embossed onto PCL and seeded with STRO-1⁺ MSCs, and cultured for 28 days, in an experiment similar to that described by McMurray *et al.* (McMurray *et al.*, 2011). Immunostaining to detect STRO-1 and osteocalcin clearly showed that osteocalcin was indeed higher on NSQ in comparison to SQ and flat, and STRO-1 was higher on SQ in comparison to flat and NSQ (Figure 3-8). These results increased confidence that the nanotopographies selected for study have reproducible effects on bone marrow derived MSCs.

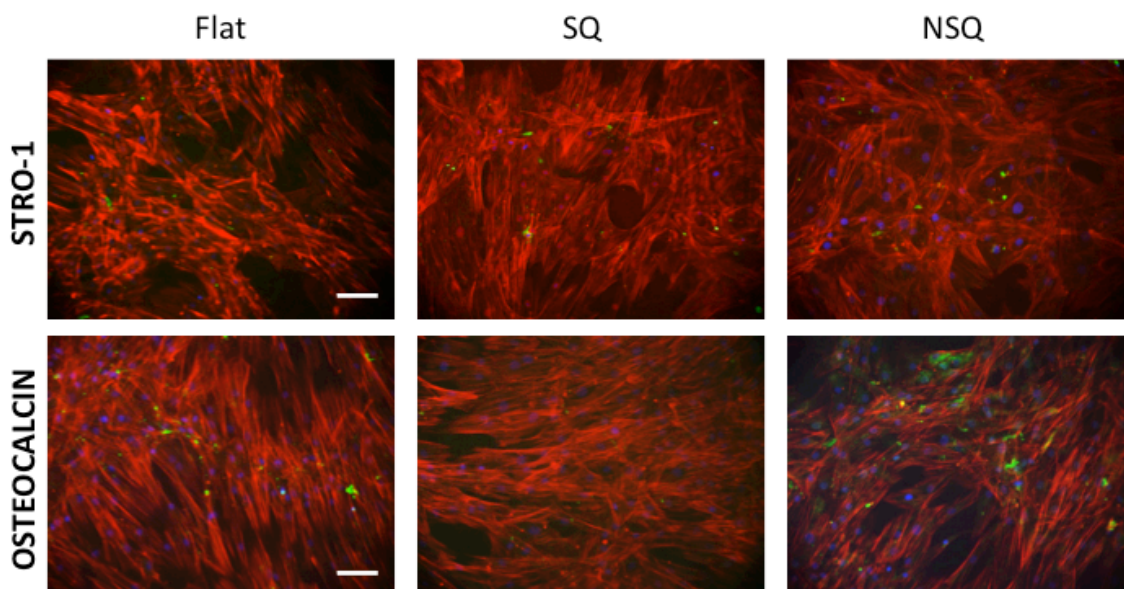


Figure 3-8: Osteogenesis promoting and stem cell maintaining phenotypes induced by nanopit nanotopography on PCL. STRO-1⁺ MSCs were seeded onto flat or hot embossed PCL with SQ/NSQ nanopatterns at 1×10^4 cells/ml as described by McMurray *et al.* Red = F-actin, blue = nuclei, green = STRO-1 or osteocalcin as indicated to the left of each row of images. Scale bar: 100 μ m.

3.2.4 Characterisation of CD271⁺ MSCs

3.2.4.1 Assessment of CD271 selection from bone marrow populations

Following selection of the adherent bone marrow cell population, MACS selection of CD271⁺ cells was incorporated into the existing protocol following selection of the adherent bone marrow cell population, in order to increase the purity or homogeneity of the cells used in experimentation. As such, the selected cells were stained for CD271 to confirm that only positive cells were being selected. CD271 expression was confirmed after 7 days culture following selection

(Figure 3-9).

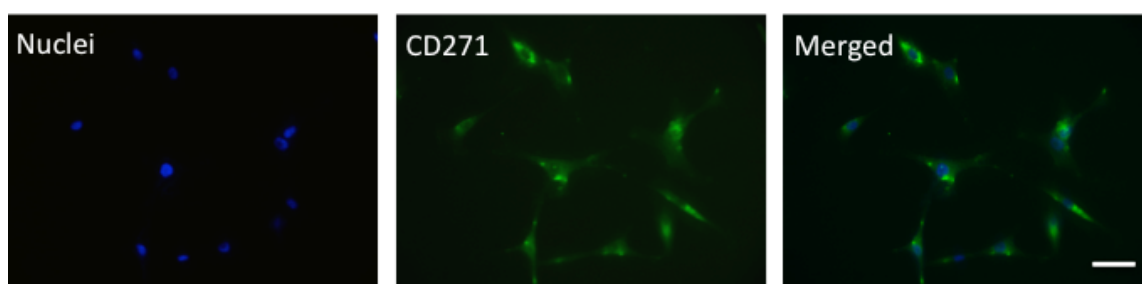


Figure 3-9: Selected MSCs using a CD271 magnetic separation kit stain positive for CD271. Green = CD271, Blue = Nuclei (DAPI stained). Selected cells cultured for 7 days stain positive for CD271. Scale bar: 50 μ m.

3.2.4.2 Characterisation of stem cell phenotypic markers in CD271⁺ MSCs

Aside from adherence to tissue culture plastic, MSCs should stain positively for stem cell markers. Partial characterisation of the selected cells was carried out to determine what positive markers were expressed. The CD271⁺ cell fraction appeared to express several proteins described as being characteristic of stem cells, staining positively for the reported stem cell associated markers STRO-1, CD63 and bone marrow niche marker nestin (Figure 3-10). These results are consistent with the notion that the selected CD271 bone marrow subpopulations contained MSCs.

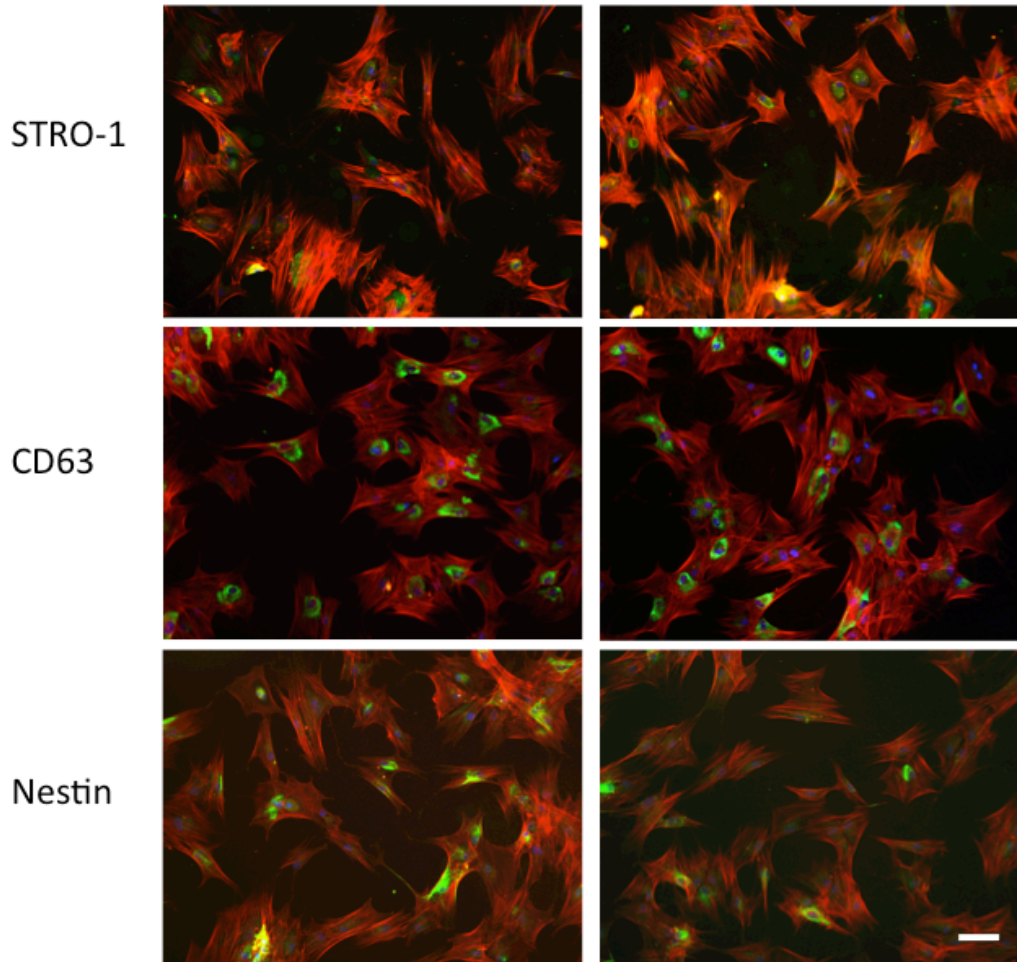
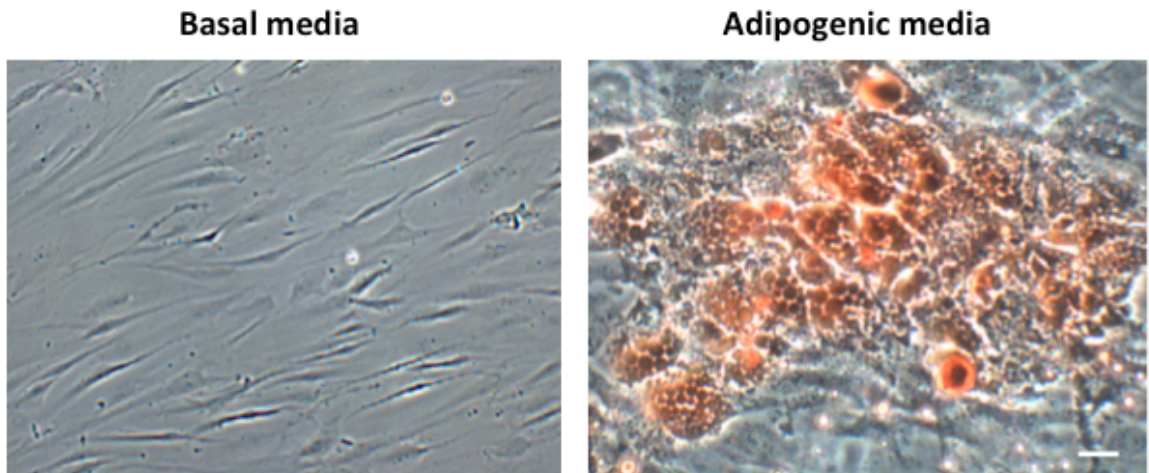


Figure 3-10: The $CD271^+$ MSC population stain positively for stem cell markers *STRO-1*, *CD63*, and niche marker *nestin*. Fluorescence microscopy images of selected MSCs immunostained for the outlined markers after 1 day of culture following selection procedures. *STRO-1*, *CD63* and *nestin* are all reported MSC markers. Two representative images (rows) stained for each marker are shown. Scale bar: 50 μm .

3.2.4.3 Functional characterisation: differentiation into multiple lineages

To prove that the isolated $CD271^+$ cells indeed included an MSC population, they needed to possess the ability to differentiate into mesenchymal lineages. Chemical induction media was added to the cells to drive adipogenic and osteogenic differentiation (*Figure 3-11*).

(a) Adipogenic differentiation



(b) Osteogenic differentiation

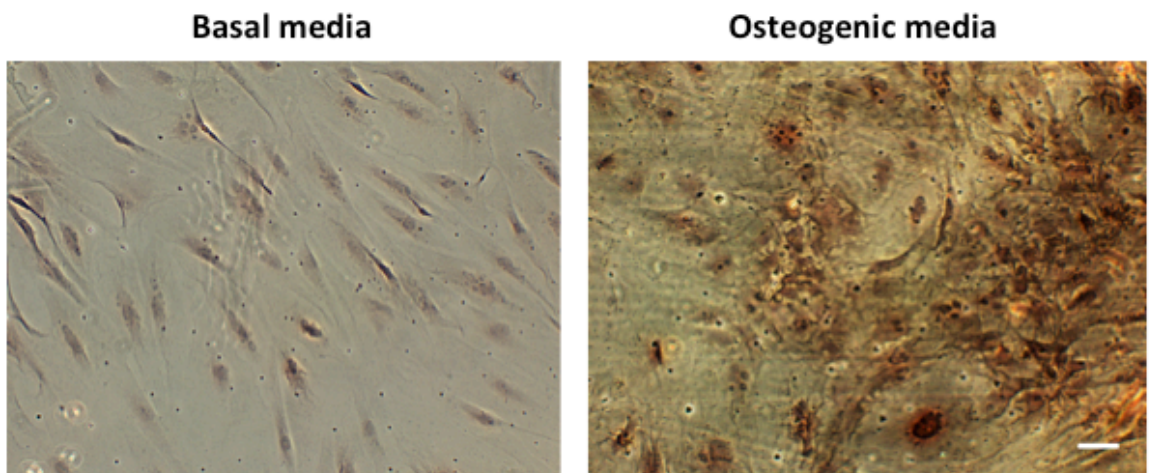


Figure 3-11: Chemically induced osteogenic and adipogenic differentiation of CD271⁺ MSCs. CD271⁺ MSCs were cultured for 6 weeks in osteogenic or adipogenic induction media to drive their differentiation to an osteogenic or adipogenic lineage. (a) Cells cultured in basal media or adipogenic media and stained with Oil Red O to detect lipid droplets. (b) Cells cultured in basal media or osteogenic media and stained with Von Kossa stain and nuclear fast red to indicate phosphate in calcium deposits and nuclei respectively. Scale bar: 100 μ m

Positive staining for lipid droplets and phosphate (as an indicator of calcium phosphate) by histological staining showed that MSCs were present in the CD271⁺ population, confirming successful isolation of MSCs for study.

3.2.5 Optimising seeding density for nanotopography efficiency

Previous seeding protocols involved addition of cells in a suspension to the substrate, which is not very efficient, as some of the cells fall outwith the area of the substrate. Use of a cell seeding device increases nanotopography seeding efficiency by ensuring that the majority of a small volume suspension of cells remains on top of the substrate, rather than falling onto areas of the well that were not covered by the topography (*Figure 3-12*).

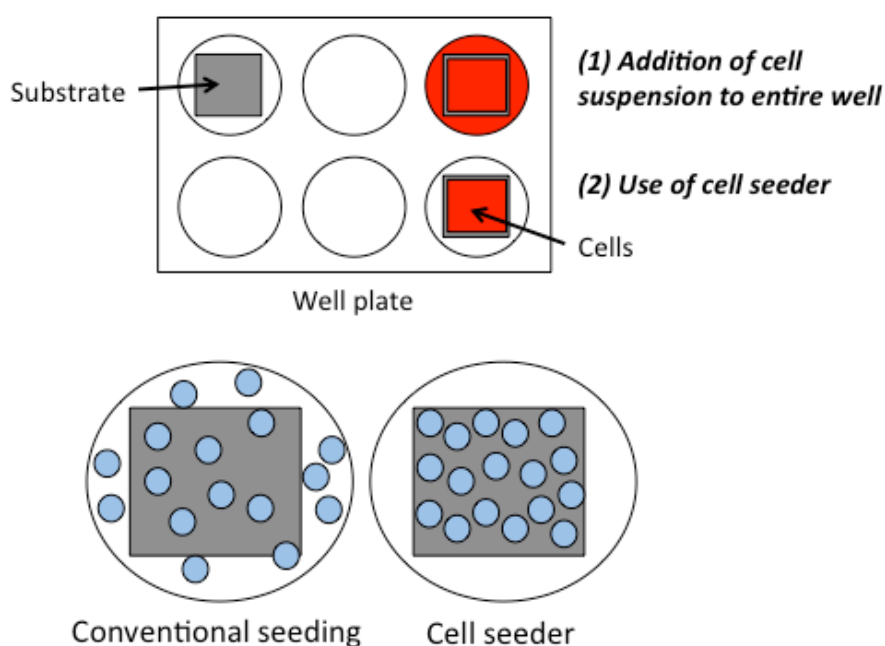


Figure 3-12: Comparison of conventional seeding and seeding with a device. Schematic diagram illustrating the differences between addition of a cell suspension to a well containing a substrate, and use of a cell seeder. Areas coloured red depict regions where the cells within the suspension would reach. The lower panel describes the differences in cell distribution with the two different methods (cells are represented as blue circles). Conventional seeding allows the cells to fall on regions outwith the substrate, whereas use of a cell seeding device contains them on top of the substrate.

However, this in turn increased the degree of cell coverage in comparison to addition of the same cell number held within a much larger volume, thus the number of cells to be added per substrate became a factor to be considered in subsequent experiments. Use of the cell seeder should be more efficient in terms of surface coverage, yet will result in an increased number of cells in direct contact, elevating the risk that they will stop responding to nanotopographical cues. It was hypothesized that the number of cells seeded onto the area of the substrate would be important to the eventual fate of the

MSCs, due to the small size of the patterned features and the strength of such physical cues in comparison to cell-cell contact signalling. That is, an accumulating number of cell-cell contact cues may predominate over the effects of nanotopography. To address this issue, cells were seeded at a number of seeding densities to firstly compare surface coverage. Previous seeding was at 10,000 cells/ml (McMurray *et al.*, 2011, Tsimbouri *et al.*, 2014), which would be equivalent to adding approximately 6000 cells/cm² using the current size of substrate. Initial assessment of cell distribution and coverage was assessed with Coomassie blue protein staining (Figure 3-13). After 7 days surface coverage was relatively high using seeding densities over 2000 cells/cm², and therefore would have increased risk of leading to lots of overlapping cells at early timepoints as the topography influences cell fate.

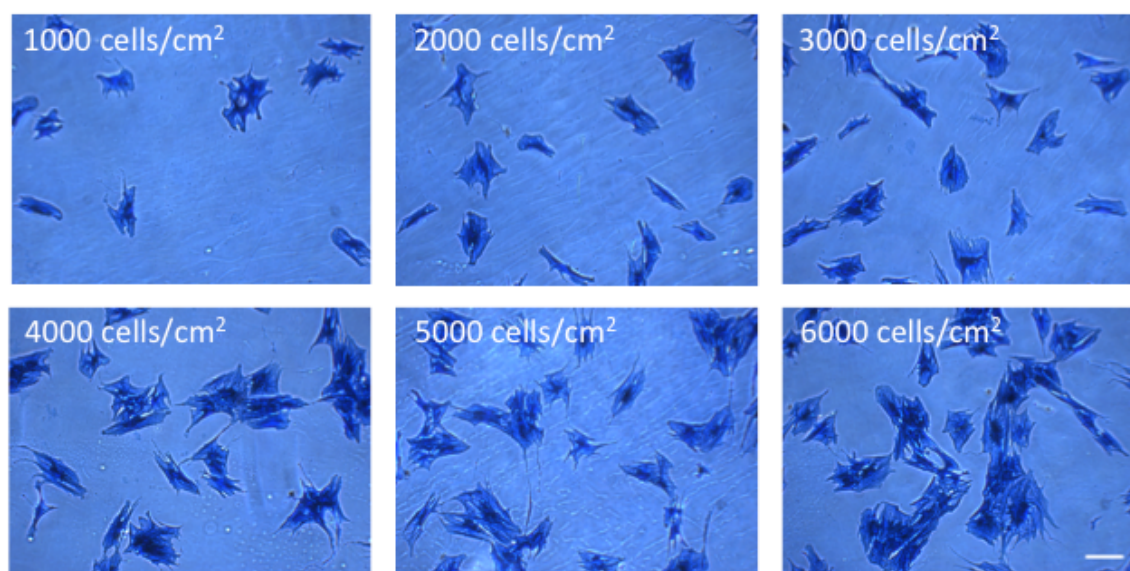
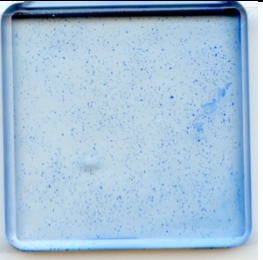
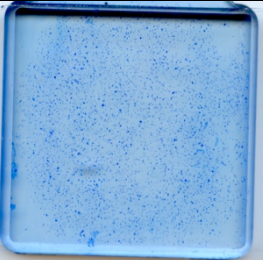
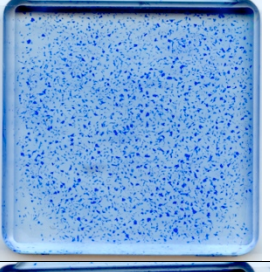


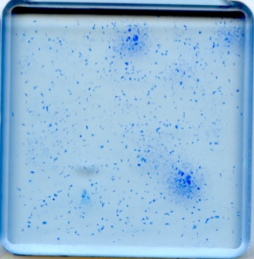
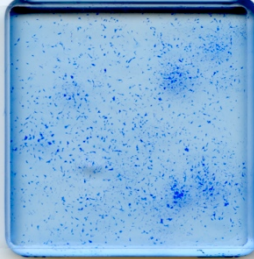
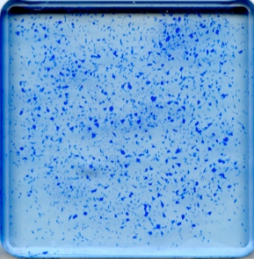
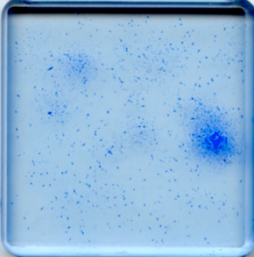
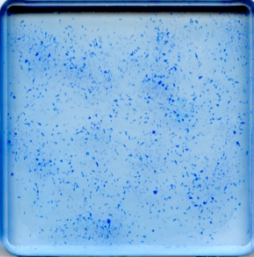
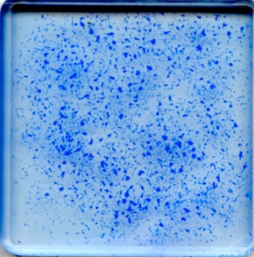
Figure 3-13: Initial assessment of cell spread and coverage when seeding at different densities using a seeding device. Brightfield images of CD271⁺ MSCs seeded onto flat polycarbonate using a cell seeding device at the indicated densities, cultured for 7 days and stained with Coomassie blue. Scale bar: 200 μ m

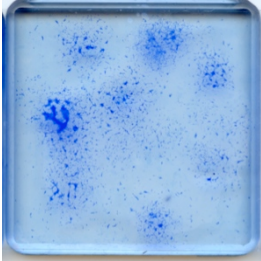
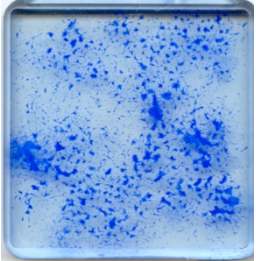
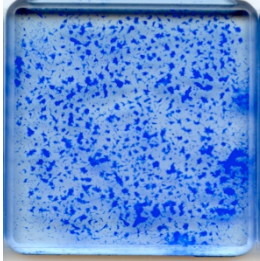
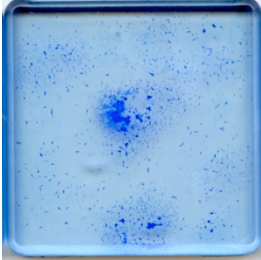
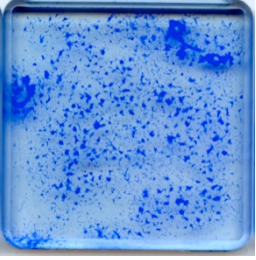
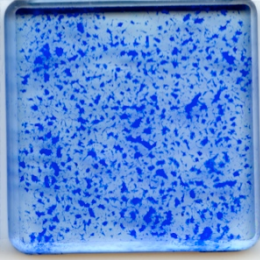
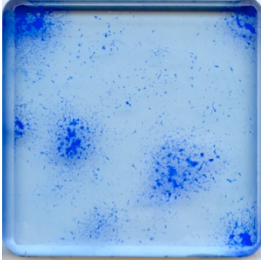
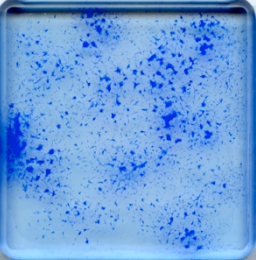
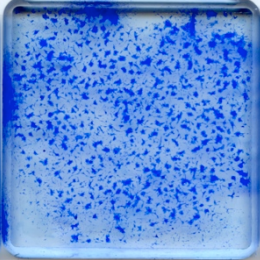
Following these observations, the focus of our study was narrowed to three decreased densities: 500 cells/cm², 1000 cells/cm² and 2000 cells/cm², representing low, medium and high density seeding. The growth patterns were assessed temporally, monitored after growth at 1, 7, 14, 21, and 28 days.

During the initial periods of culture, there were no visible differences between the flat, SQ or NSQ growth patterns. After 21 days, however, it was interesting to note that a number of cell clusters where cells were expanding in colonies (which we termed 'colony growth') was observed only at the low and mid densities, with the lowest density showing the most colony growth (*Figure 3-14*). In the case of the highest density, this appeared to favour uniform coverage of the entire substrate, exhibiting a 'fibroblastic growth' arrangement. After each successive timepoint, it became apparent that the cells grew closer together leaving less space between adjacent cells, and as expected, this was most pronounced with the highest cell density. Cells began to overlap and grow closely together in certain areas of the substrate (*Figure 3-15*).

(a) Day 1			
Nanotopography/ density	500 cells/cm ²	1000 cells/cm ²	2000 cells/cm ²
Flat			
SQ			
NSQ			

(b) Day 7			
Nantopography/ density	500 cells/cm²	1000 cells/cm²	2000 cells/cm²
Flat			
SQ			
NSQ			

(c) Day 14			
Nanotopography/ density	500 cells/cm ²	1000 cells/cm ²	2000 cells/cm ²
Flat			
SQ			
NSQ			

(d) Day 21			
Nanotopography/ density	500 cells/cm ²	1000 cells/cm ²	2000 cells/cm ²
Flat			
SQ			
NSQ			

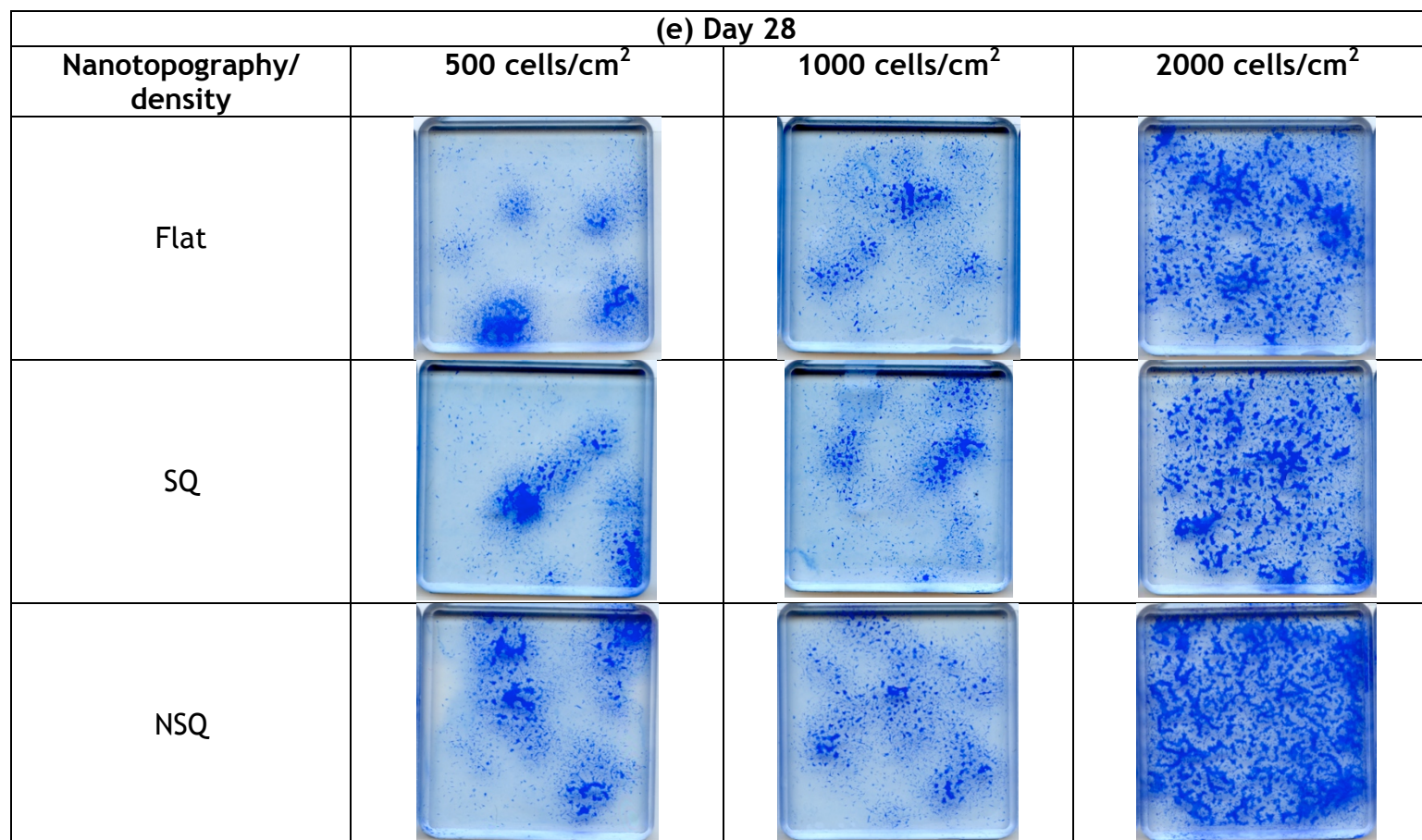


Figure 3-14: CD271⁺ MSCs cultured at different densities exhibit unique cell growth patterns. Whole substrate scans of MSCs cultured for (a) 1 (b) 7 (c) 14 (d) 21 and (e) 28 days, stained with Coomassie blue at densities of 500, 1000 and 2000 cells/cm². Images shown are representative of triplicate material replicates. Cells seeded at the two lower densities expanded as colonies, which began to be noticed after 14 days, whereas those cultured at 2000 cells/cm² grew in a uniform manner, covering the entirety of the surface. These growth patterns occurred independently of the culture surface used, implying that these observations were density-dependent.

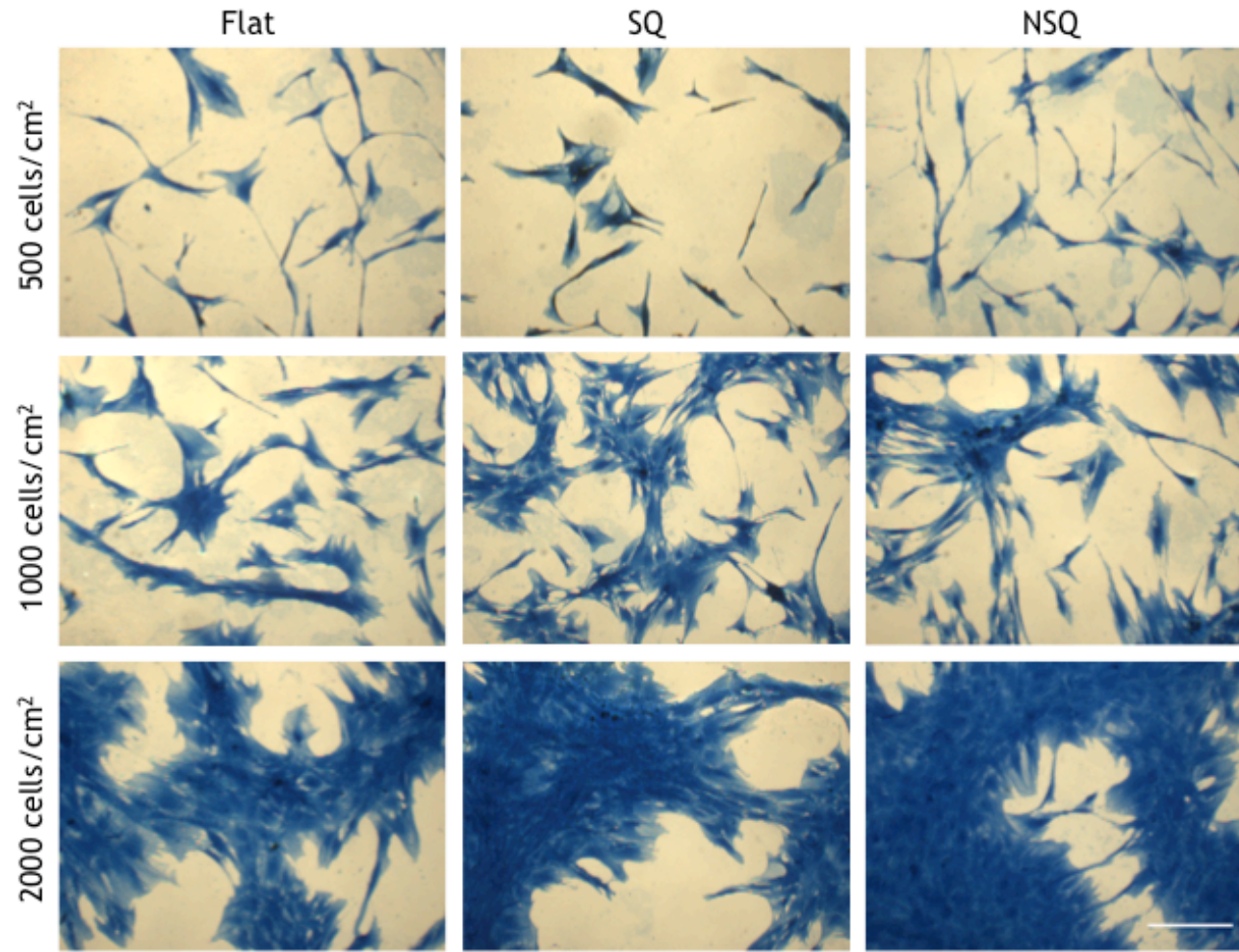


Figure 3-15: Growth and spread of CD271⁺ MSCs on flat and nanopatterned substrates after 28 days culture. Bright-field microscopy images of Coomassie-stained cells after 28 days, taken at 5x magnification. Cells begin to severely overlap at the highest density of 2000 cells/cm². Scale bar: 50 μ m.

Marker expression was tested in MSCs seeded at these densities to investigate a possible relationship between seeding number and phenotype. Western blotting was used as an initial screening technique (Figure 3-16), which revealed that stem cell marker expression was more effectively retained on SQ at the low and medium seeding densities, whereas the highest seeding density favoured osteogenic differentiation and expression of osteopontin on NSQ (Figure 3-17).

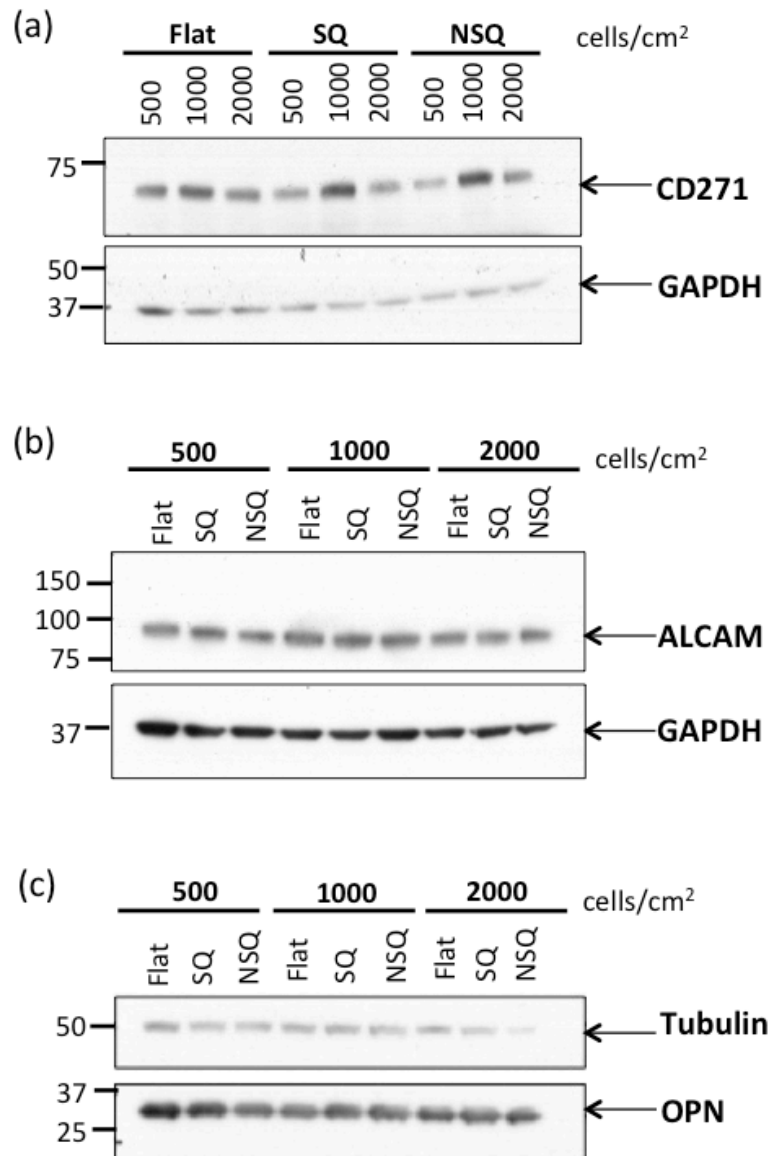


Figure 3-16: Effect of seeding density on protein expression in MSCs seeded on nanotopography. Western blot analysis ($n=1$) of 28 day cultured $CD271^+$ MSC lysates probed for (a) CD271 (b) ALCAM and (c) osteopontin together with loading controls GAPDH or (α) tubulin.

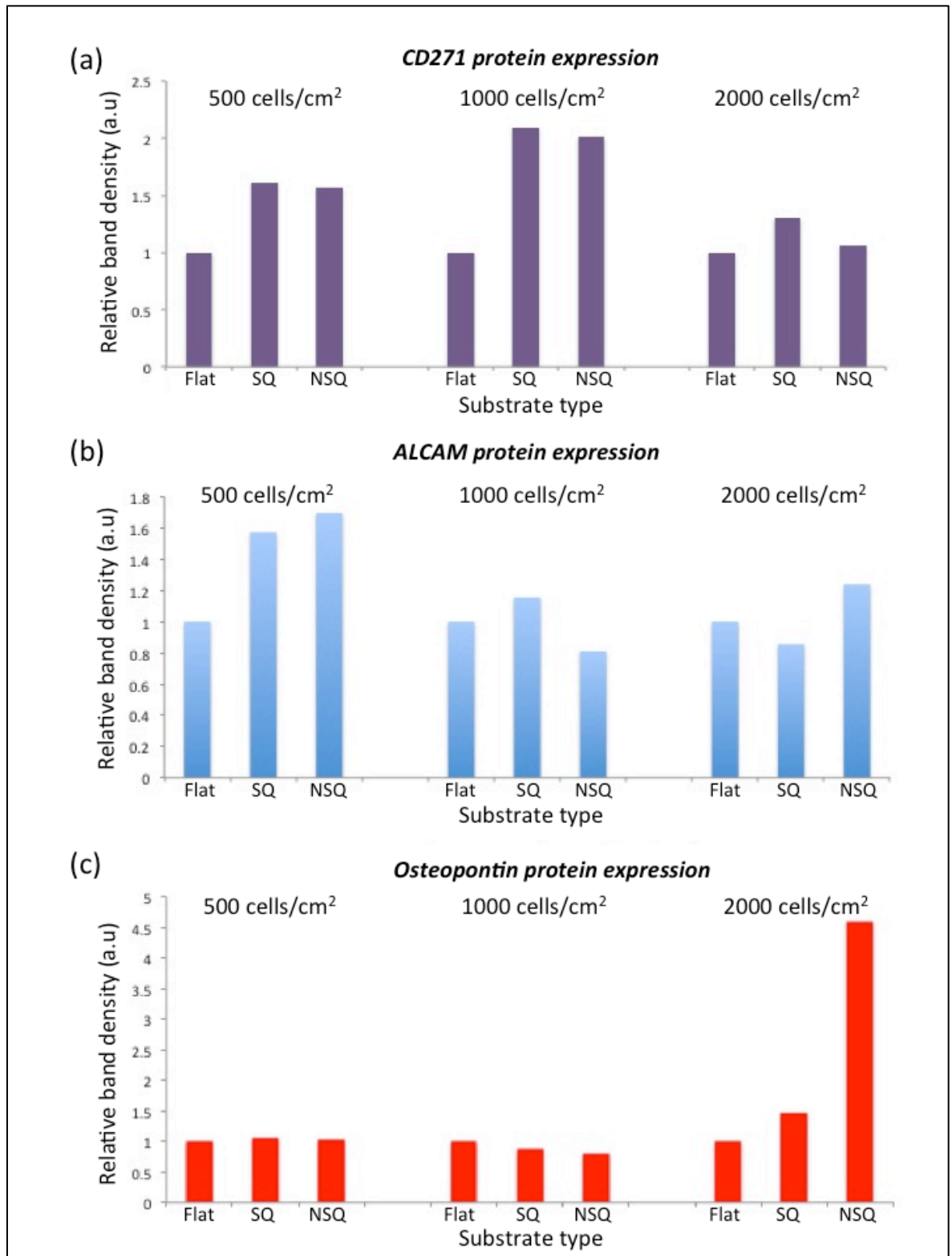
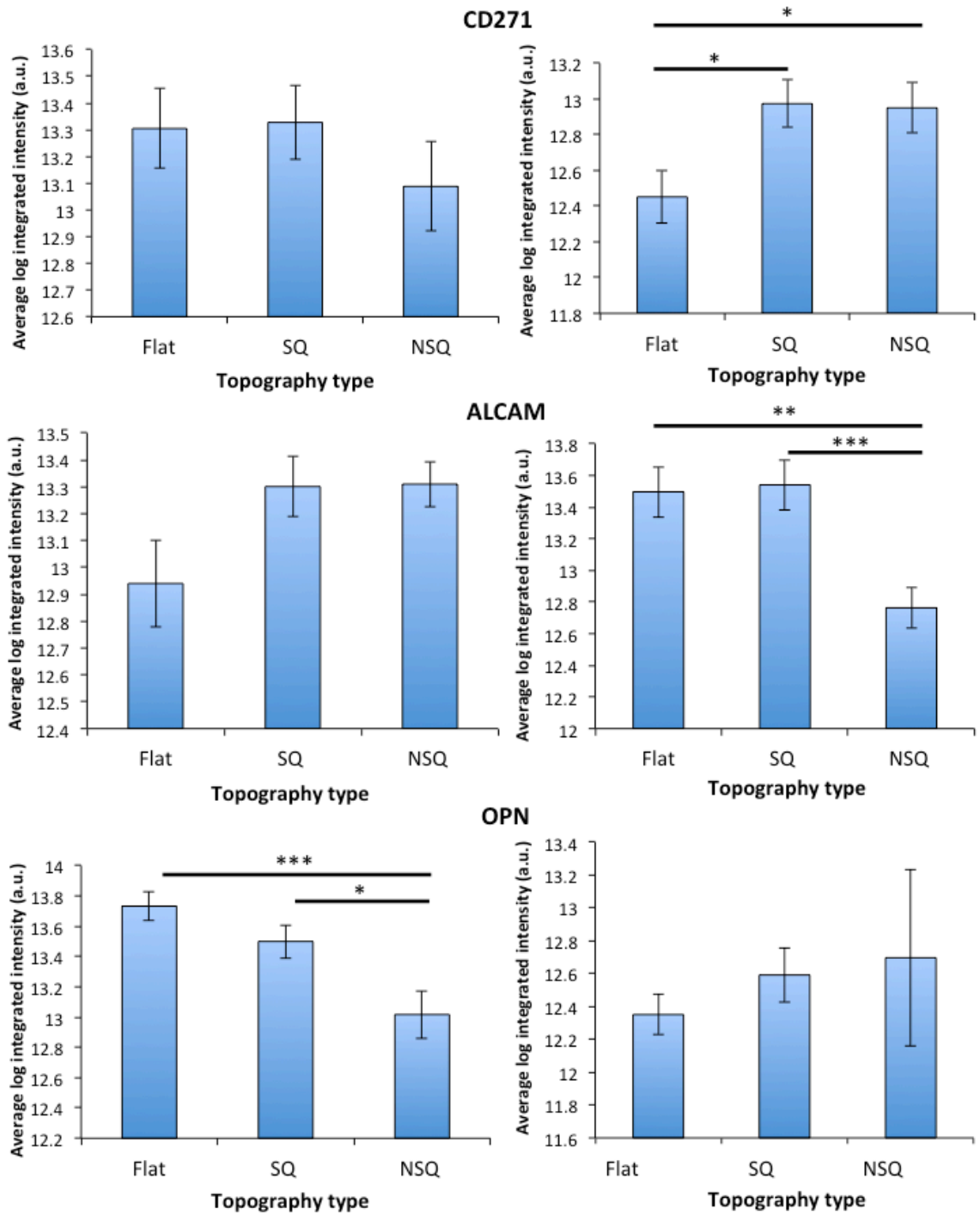


Figure 3-17: Quantified protein expression levels by densitometry. Quantification of bands shown in Figure 3-16, for (a) CD271 (b) ALCAM and (c) osteopontin, and expressed relative to loading control proteins GAPDH or (alpha) tubulin. Relative band densities are expressed in arbitrary units. Sample bands were normalised to the flat surface in each case ($n=1$, therefore no error bars could be included).

As western blotting is a bulk cell analysis, that involves producing a lysate from all of the cells, quantitative analysis of microscopy images was adopted as a method to determine the expression of protein in each cell in high numbers for statistical analysis (*Figure 3-18*). Use of techniques like western blotting involve population analysis and can mask data regarding individual cells. The results paralleled the western blotting data, in that similar trends were observed for stem cell markers CD271 and ALCAM. The seeding density that resulted in highest levels of CD271 and ALCAM on SQ was 1000 cells/cm². It was noted that 500 cells/cm² was also relatively good for stem cell marker levels, however this would pose problems in terms of requiring large numbers of substrates to seed. CD271⁺ MSCs appear to be poor for osteogenesis compared to STRO-1⁺ MSCs and unselected progenitors from bone marrow used in other studies (Rickard *et al.*, 1994, Jones *et al.*, 2002, Dalby *et al.*, 2006c, Biggs *et al.*, 2009a).

(a)

Seeding density of 500 cells/cm² Seeding density of 1000 cells/cm²



(b)

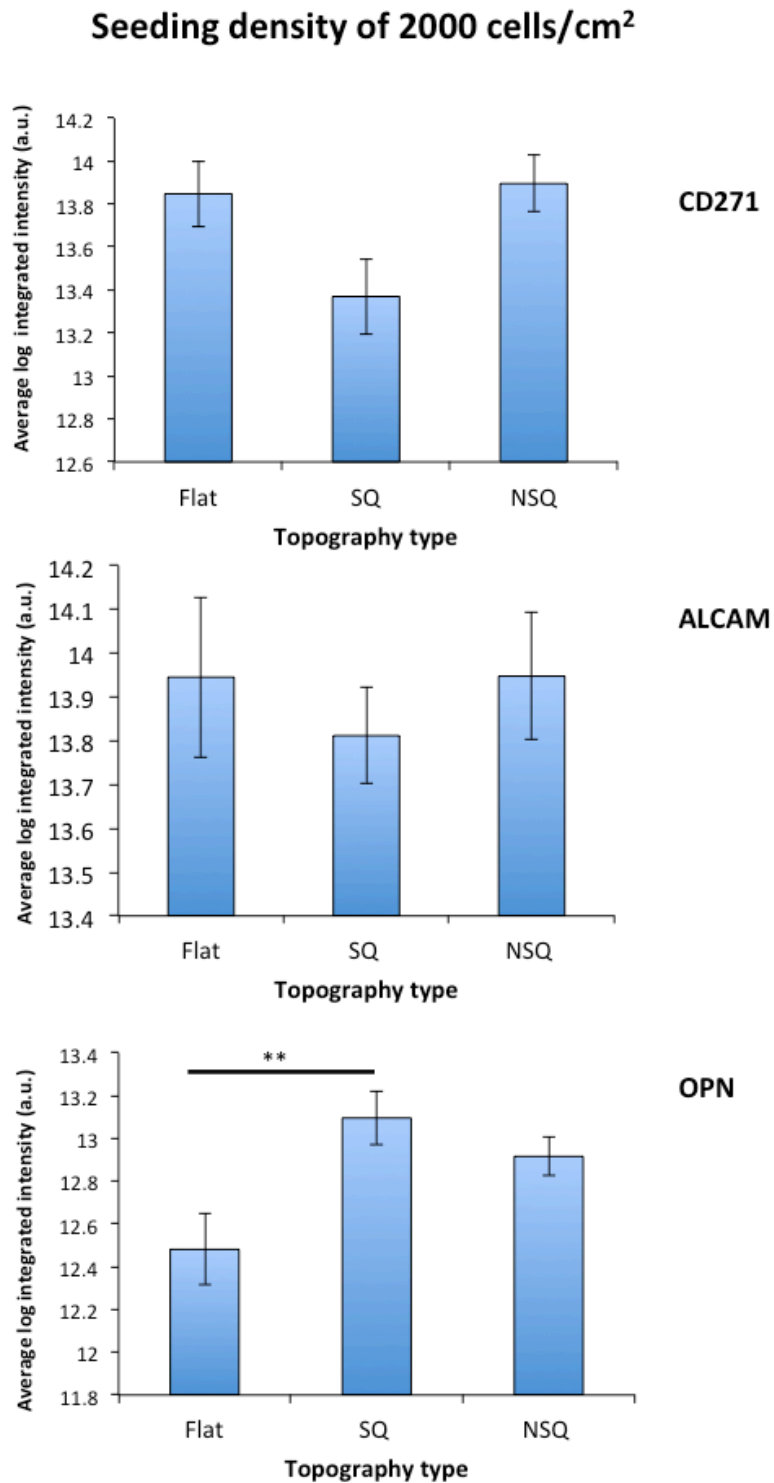


Figure 3-18: Effect of seeding density on protein expression in CD271⁺ MSCs, assessed by image analysis. Cells from 40-60 images were analysed per condition. Levels of CD271, ALCAM and osteopontin (OPN) were measured using CellProfiler image analysis software for cells seeded at (a) 500 cells/cm² and 1000 cells/cm² (b) 2000 cells/cm² on flat/SQ/NSQ. Average log transformations of original data are shown. Error bars represent \pm standard error of the mean. One-way ANOVA with Tukey's post-test, or Kruskal-Wallis test with Dunn's post-test were performed to assess significance. * $p < 0.05$, ** $p < 0.01$, *** $p < 0.001$

3.2.6 MSC proliferation on nanotopography

CD271⁺ MSCs on nanotopographies were assessed for changes in proliferation by bromodeoxyuridine (BrdU) labelling (a structural analog of thymidine) over several timepoints. BrdU added to the media was incorporated into newly synthesised DNA during the synthesis or S phase of the cell cycle in place of thymidine. The results indicate that the number of cells passing through S phase was not significantly different on SQ and NSQ over the timepoints tested, suggesting that proliferation rate was unchanged in the MSCs during self-renewal and differentiation (*Figure 3-19*).

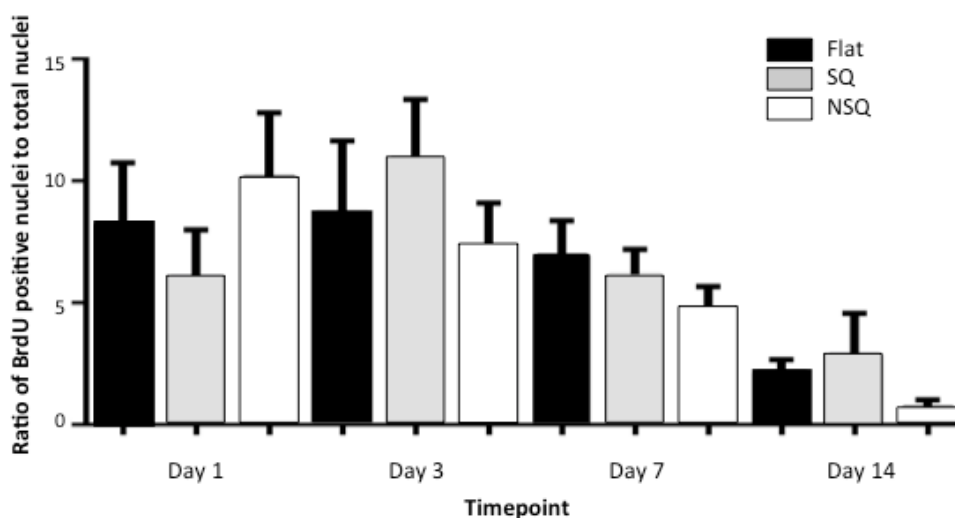


Figure 3-19: BrdU incorporation in CD271⁺ MSCs. Cells were seeded at a density of 1000 cells/cm² and cultured for 1, 3, 7 and 14 days. Results show the average ratio of BrdU positive cells and number of total nuclei from three material replicates. Significance was assessed using a Kruskal Wallis test with Dunn's post-test. Error bars represent standard error of the mean.

Growth (increase in cell number) over the same timepoints on each of the substrates was compared by counting the number of nuclei falling within a grid of pre-defined size. The number of cells on each surface did not show significant changes (*Figure 3-20*).

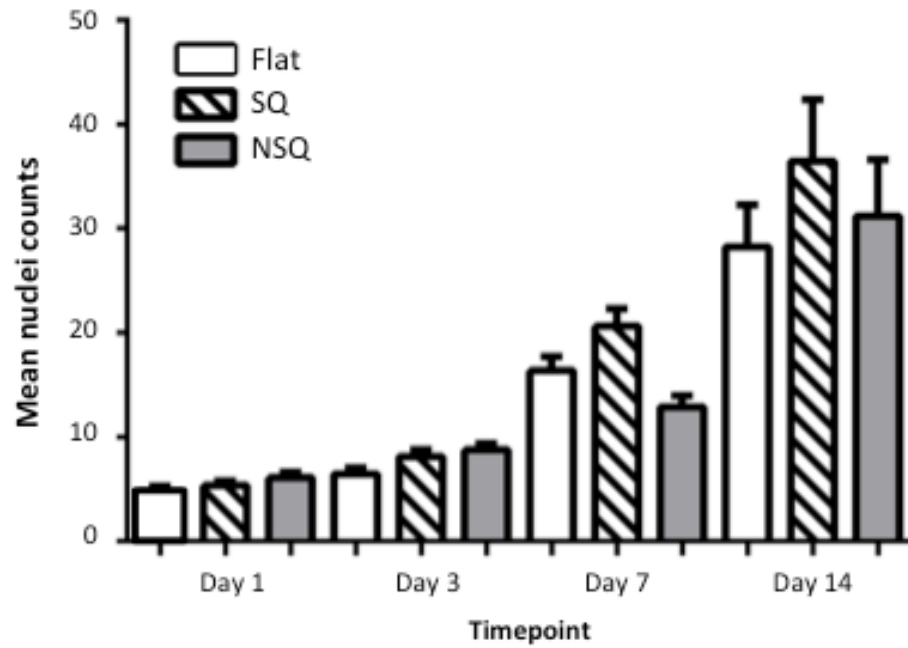


Figure 3-20: Assessment of MSC growth on nanotopographies over time. Cells seeded at a density of 1000 cells/cm² were cultured for 1, 3, 7 and 14 days. Results show the mean number of nuclei counts from 48 images over three material replicates. Significance was assessed using a Kruskal Wallis test with Dunn's post-test. Error bars represent standard error of the mean.

3.2.7 Metabolomic profile of CD271⁺ MSCs

Analysis of the entire cell metabolome offers a strategy for observing the range of molecules that are present within cells at a specific point in time. The metabolite profiles of in-house selected MSCs were assessed following 7 day and 14 day periods in culture. High performance liquid chromatography (HPLC) was used to separate the metabolites within the samples by retention time on the column followed by mass spectrometry to detect the mass/charge (Mz) ratio, from which the mass can be inferred (LC-MS). Data processing was achieved through analysis of derived chromatographic peak intensities using an IDEOM/Mz match Excel interface and various metabolomics data analysis tools.

3.2.7.1 Assessment of cell metabolome after 7 day culture

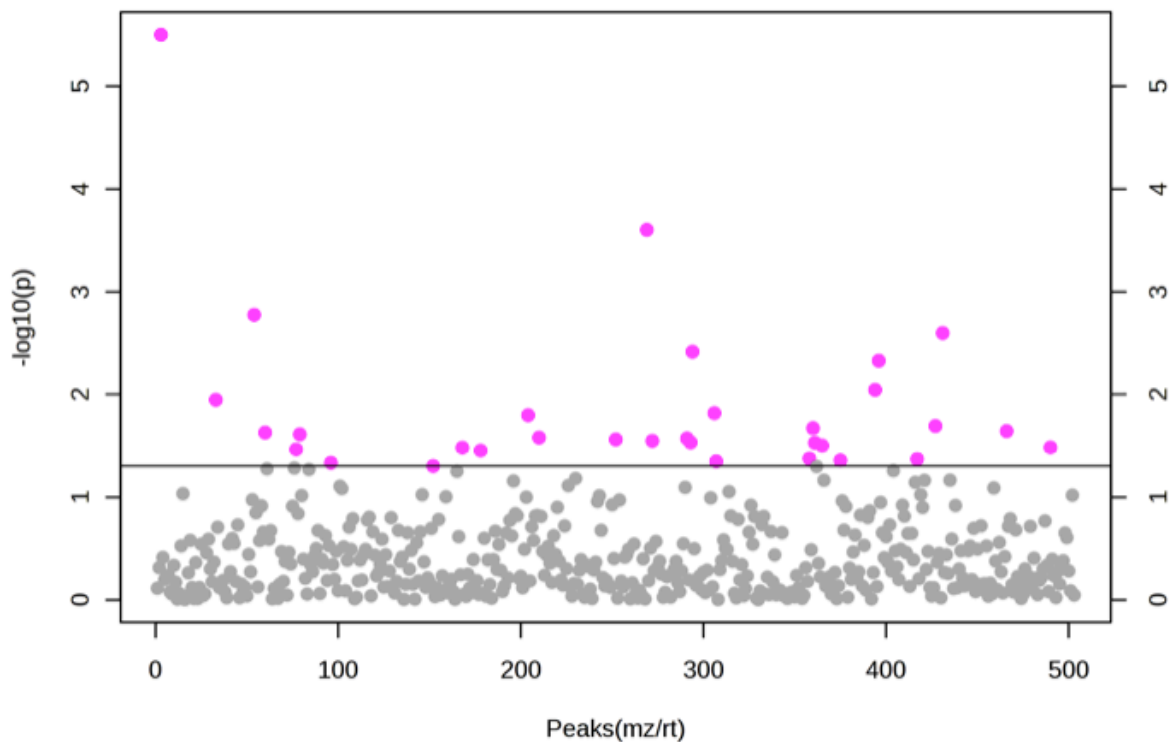
3.2.7.1.1 Overview of data output and activity within metabolic pathways

Looking firstly at the results from cells cultured for one week, it can be observed that a number of significant alterations were detected on the SQ and NSQ samples in comparison to those on flat controls (*Figure 3-21 (a) and (c)*). There appeared to be a balance of increased and decreased relative abundances of metabolites associated with both nanotopographies, with some larger differences detected on NSQ (*Figure 3-21 (b) and (d)*).

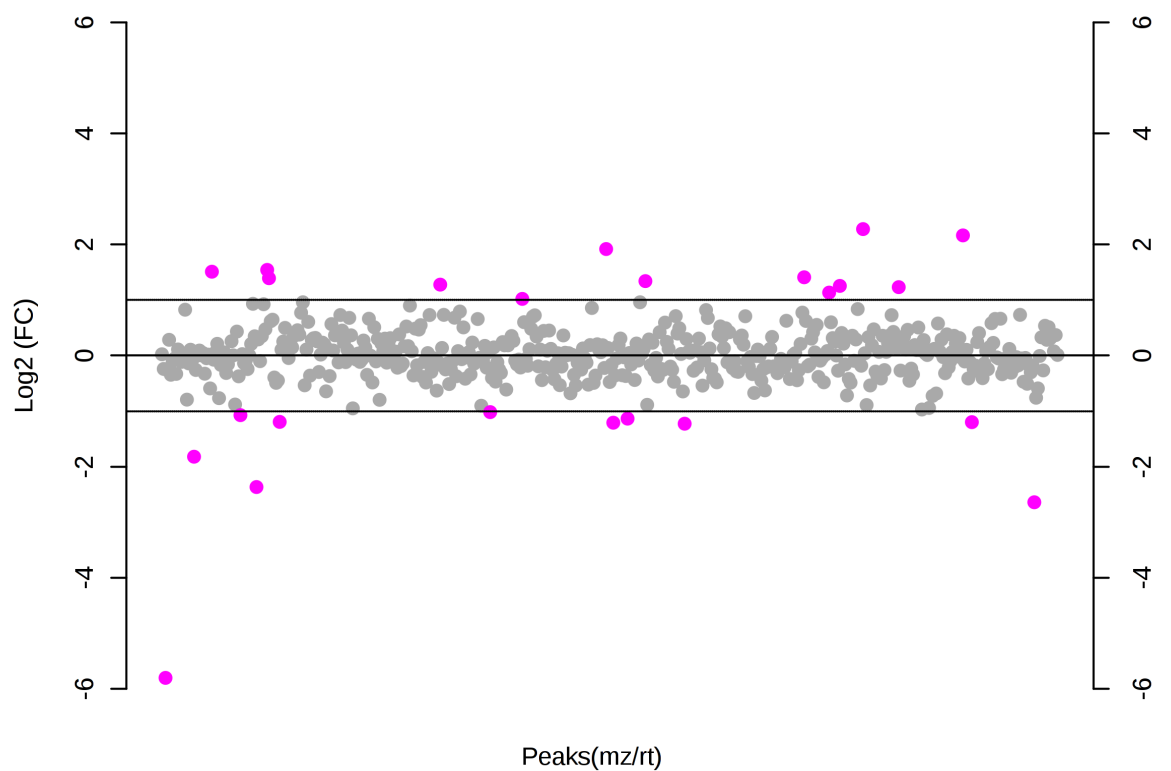
The dataset yielded a list of 670 metabolites that were assigned putative identifications within the IDEOM/Mz match Excel interface, which aided grouping of the metabolites into broad classifications, namely metabolites that could be considered as being nucleotides, amino acids, lipids, secondary metabolites, vitamins and cofactors, and a remaining subset, which were not associated with any known metabolic maps.

Grouping by referencing the maps assigned by IDEOM indicated that the many of the detected metabolites had unknown associations, with the majority of the remaining metabolites being part of lipid and amino acid metabolism, with a smaller number of molecules being part of carbohydrate, nucleotide, and secondary metabolite and cofactor pathways.

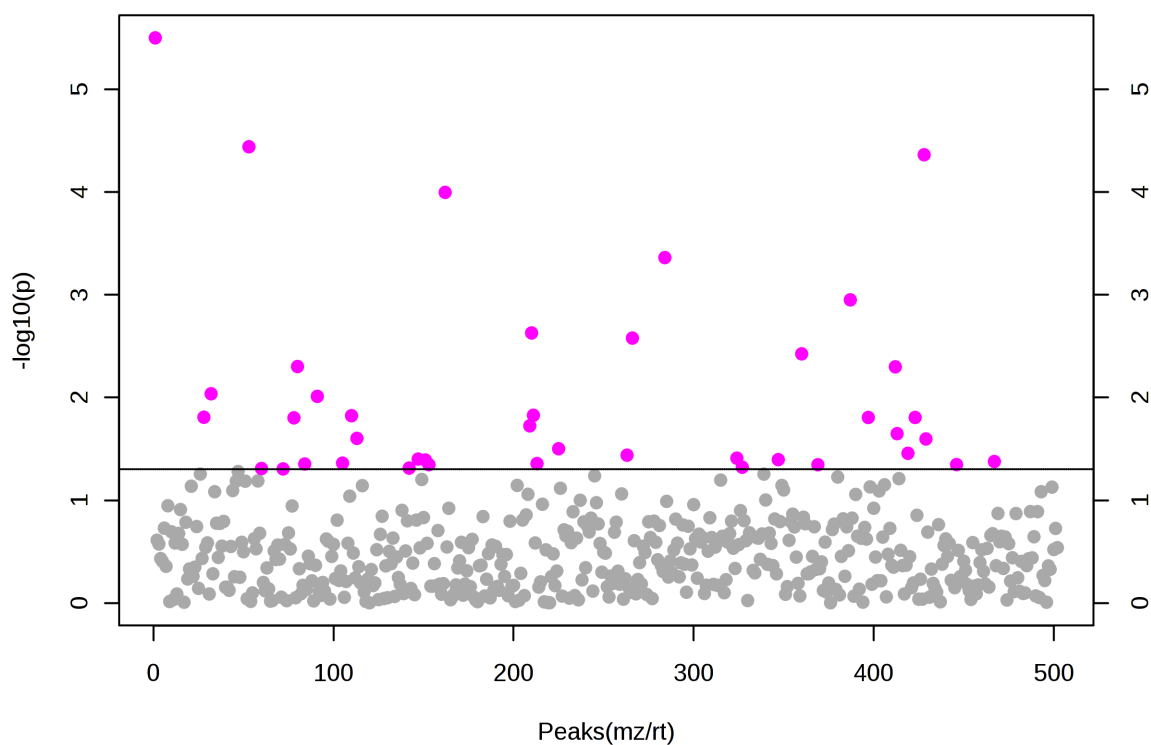
(a) SQ/Flat: T-test



(b) SQ/Flat (fold change)



(c) NSQ/Flat (t-test)



(d) NSQ/Flat (fold change)

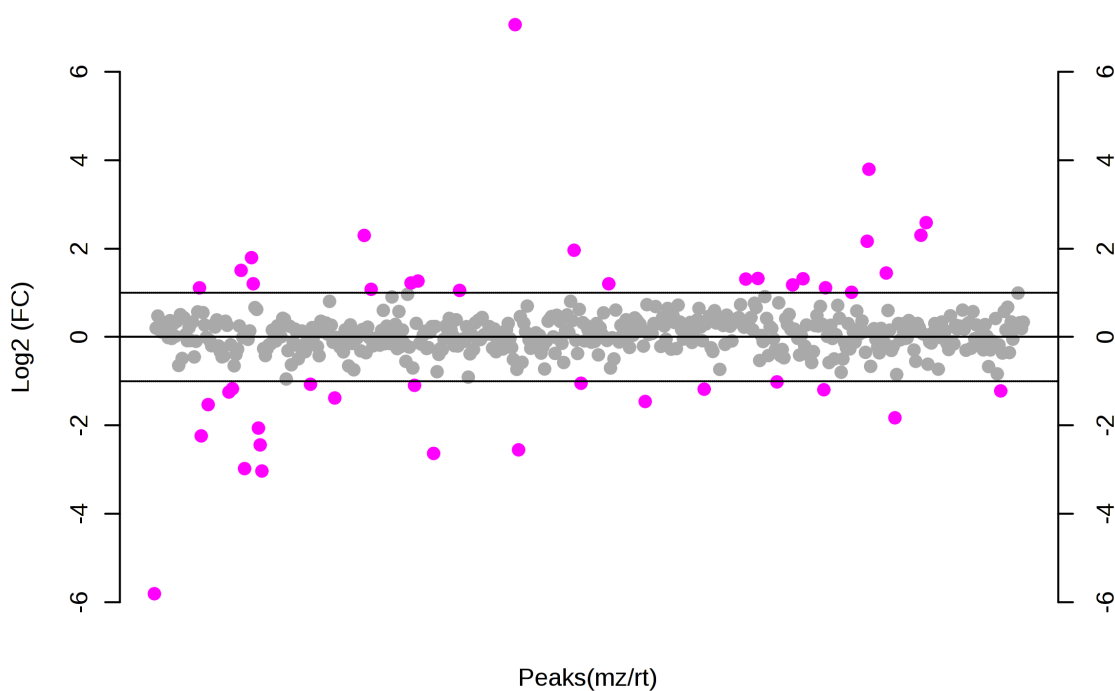


Figure 3-21: Overview of detected and significant metabolites in MSCs on SQ in comparison to flat after 7 days of culture. Identified metabolites from multiple sample replicates ($n = 6$) are indicated by grey circles, with significantly increased or decreased metabolites (relative to the flat control) being denoted by the pink circles. (a) and (c) t-test plots with a significance threshold set at $p < 0.05$ (b) and (d) Fold change plots with cut-off threshold set at 2 fold change. Each of the comparisons yielded a metabolomic 'fingerprint' indicative of the cell state at that particular time point.

Assessment of the fold changes in total metabolite intensity level for each of these pathway groups did not show dramatic changes between SQ and NSQ. However, data appeared suggestive to potential beginnings of a shift in metabolomic activity between the surfaces (*Figure 3-22*). Other studies have mentioned that stem cells are metabolically ‘quiet’ whereas differentiating cells are much more metabolically active (Reyes *et al.*, 2006, Yanes *et al.*, 2010, Tsimbouri *et al.*, 2012).

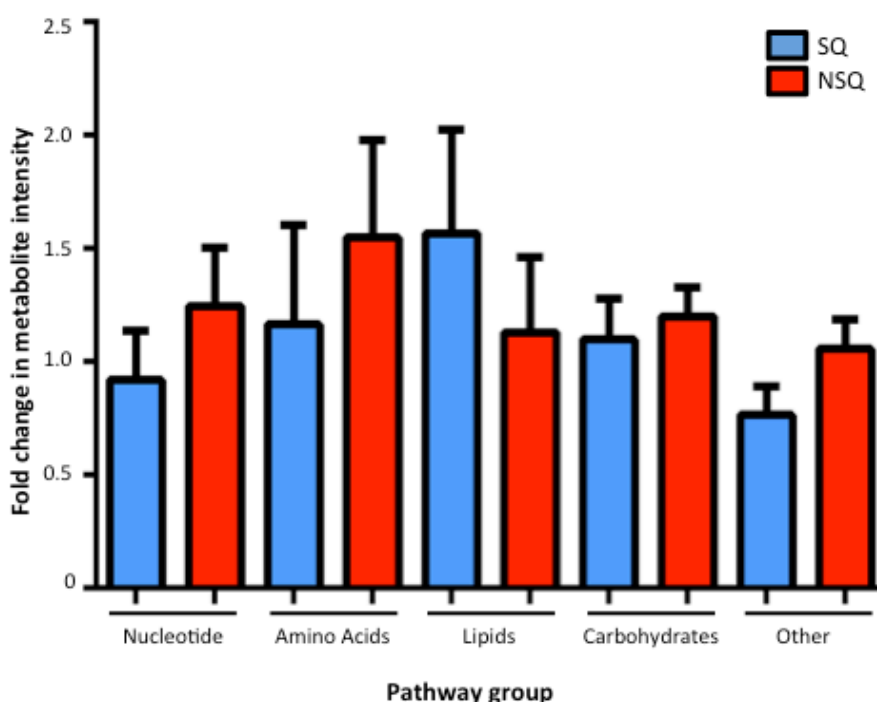


Figure 3-22: Grouped total metabolite fold changes for MSCs cultured on nanotopographies. The peak intensities of all the metabolites classed into each grouping were totalled, averaged and the fold change determined by comparison to flat controls. Amongst the different broad pathway groups, a general trend of lower metabolite abundances were suggested on SQ in comparison to NSQ, with the exception of the lipid group. However, these changes were not found to be statistically significant in this dataset. Material replicates, flat (n=6) SQ (n= 4) and NSQ (n= 5). Error bars: standard error of the mean.

3.2.7.1.2 Visualisation of changes in metabolic groups with heatmap analyses

Investigation into the metabolites within each of the broad groups was taken further by performing fold change calculations for metabolites classed into smaller data clusters. Heat maps were used to visualise the results, and allow fold increases and decreases to be observed more easily. Ranking the metabolites in each of the heat maps from ‘hot’ (increased abundance, red) to ‘cold’ (decreased abundance, blue) gives an indication of whether more fold increases or decreases are favoured on each substrate. In most of the groups,

increases in metabolite abundance were more common on NSQ than SQ (Figure 3-23, Figure 3-24, Figure 3-26), though this trend is reversed with the lipid related metabolites (Figure 3-26). Secondary metabolite, vitamin and cofactor groups, and unmapped metabolites had similar numbers of increases and decreases (Figure 3-27 and Figure 3-28).

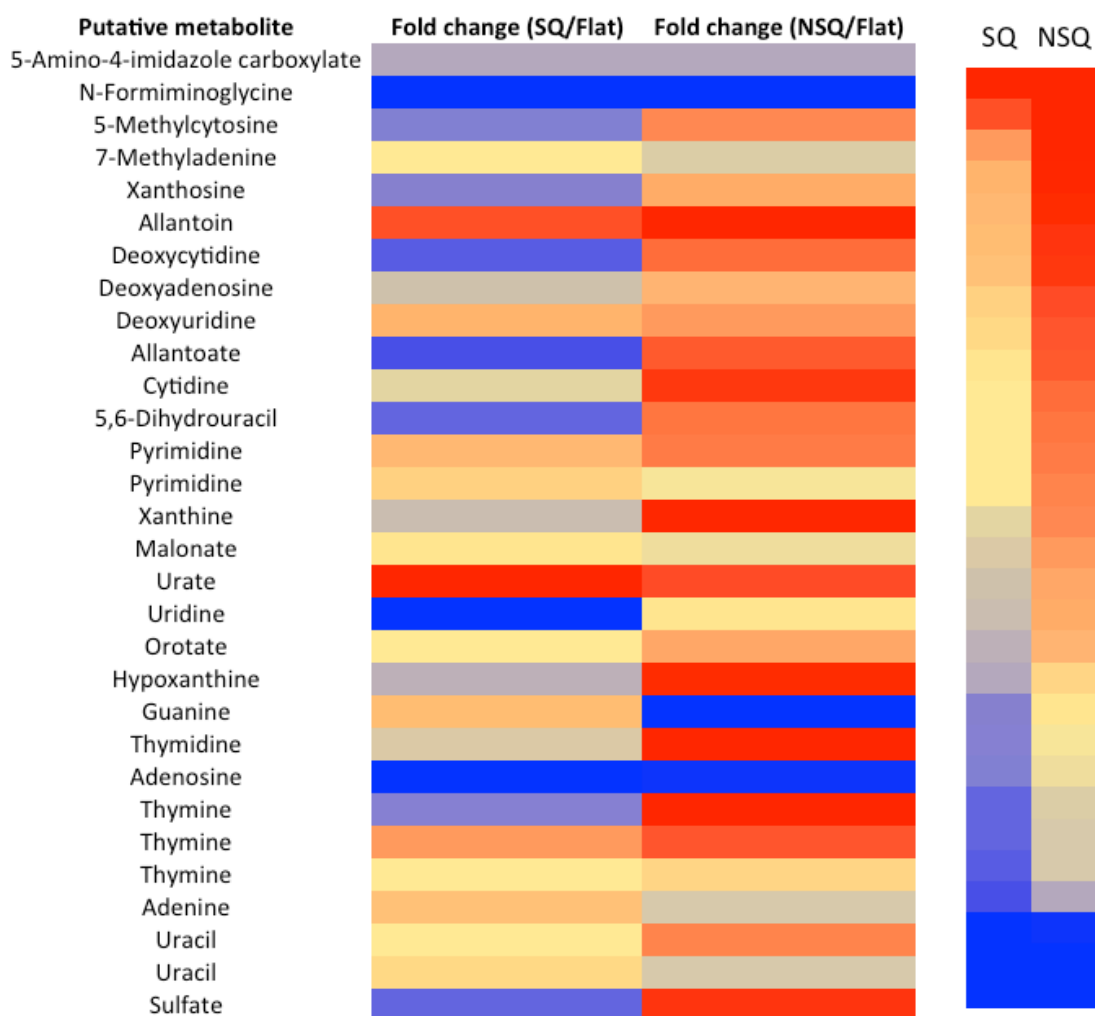


Figure 3-23: Nucleotide metabolite profiles on SQ and NSQ after 7 days of culture. Metabolites classed as being involved in nucleotide metabolism were analysed for both SQ (material replicates, $n=4$) and NSQ ($n=5$). Heat maps were generated from average fold change values with reference to flat controls ($n=6$), assigning a colour scale to the subsequent results. Blue regions signify fold increases, red regions represent fold decreases and yellow regions denote no changes. Values in between these extremes were shaded accordingly. The entire nucleotide dataset sorted from highest to lowest fold change abundance is shown to the right of the main heatmap, highlighting a contrast between SQ and NSQ in terms of the number of metabolites being more abundant and less so, in comparison to flat. NSQ had a higher level of increases in nucleotide metabolites.

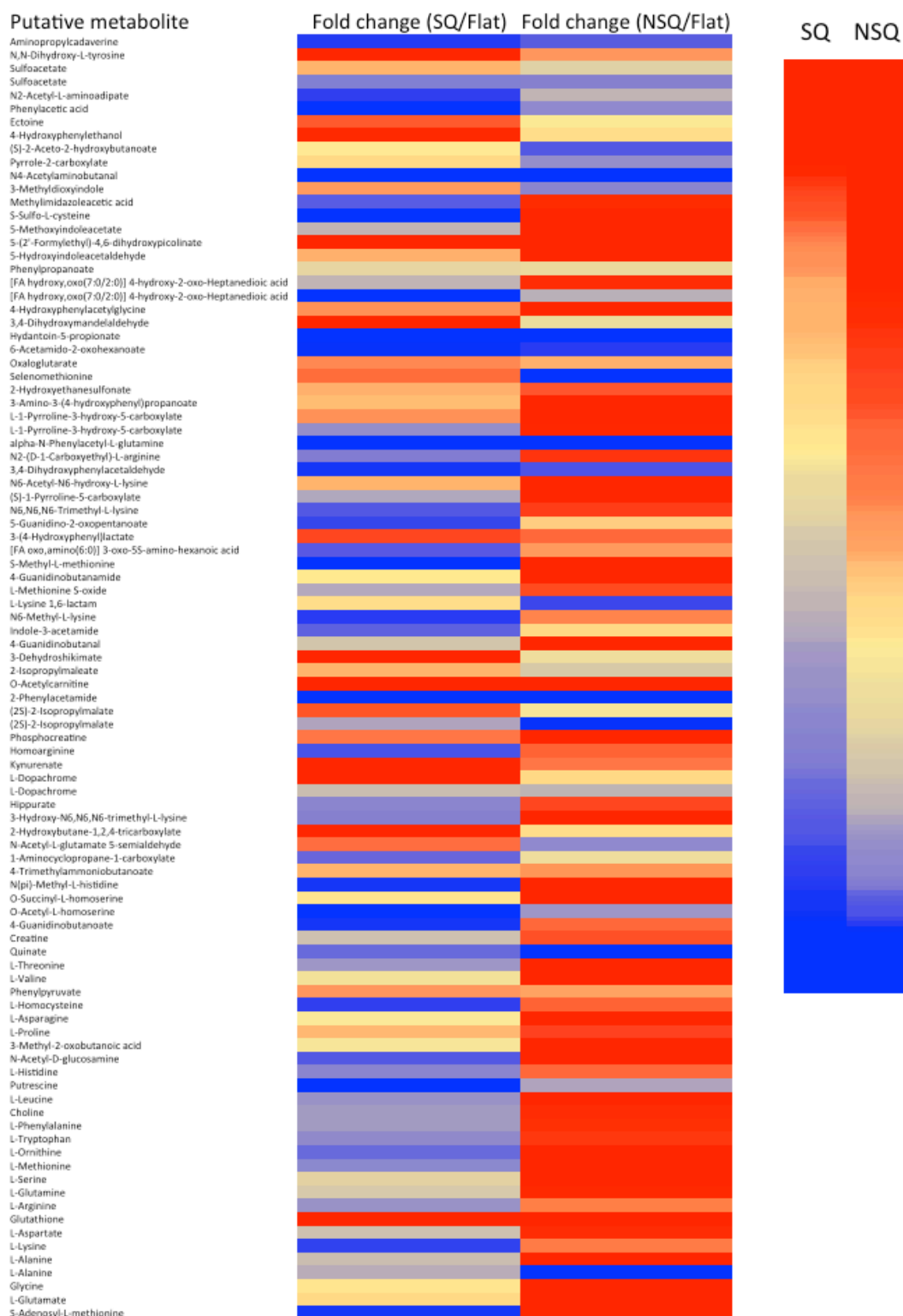


Figure 3-24: Amino acid metabolite profile on SQ and NSQ after 7 days of culture. Metabolites involved in amino acid metabolism were analysed for SQ (material replicates, $n = 4$) and NSQ ($n = 5$). Heat maps were generated from average fold change values with reference to flat controls ($n = 6$), assigning a colour scale to the subsequent results. Blue regions = fold increases, red regions = fold decreases and yellow regions = no change. A truncated list is shown here, as the number of metabolites were quite extensive. The entire amino acid dataset sorted from highest to lowest is shown to the right of the main heatmap, highlighting a contrast between SQ and NSQ in terms of the number of abundant metabolites. Increases in metabolites were more prevalent on NSQ.

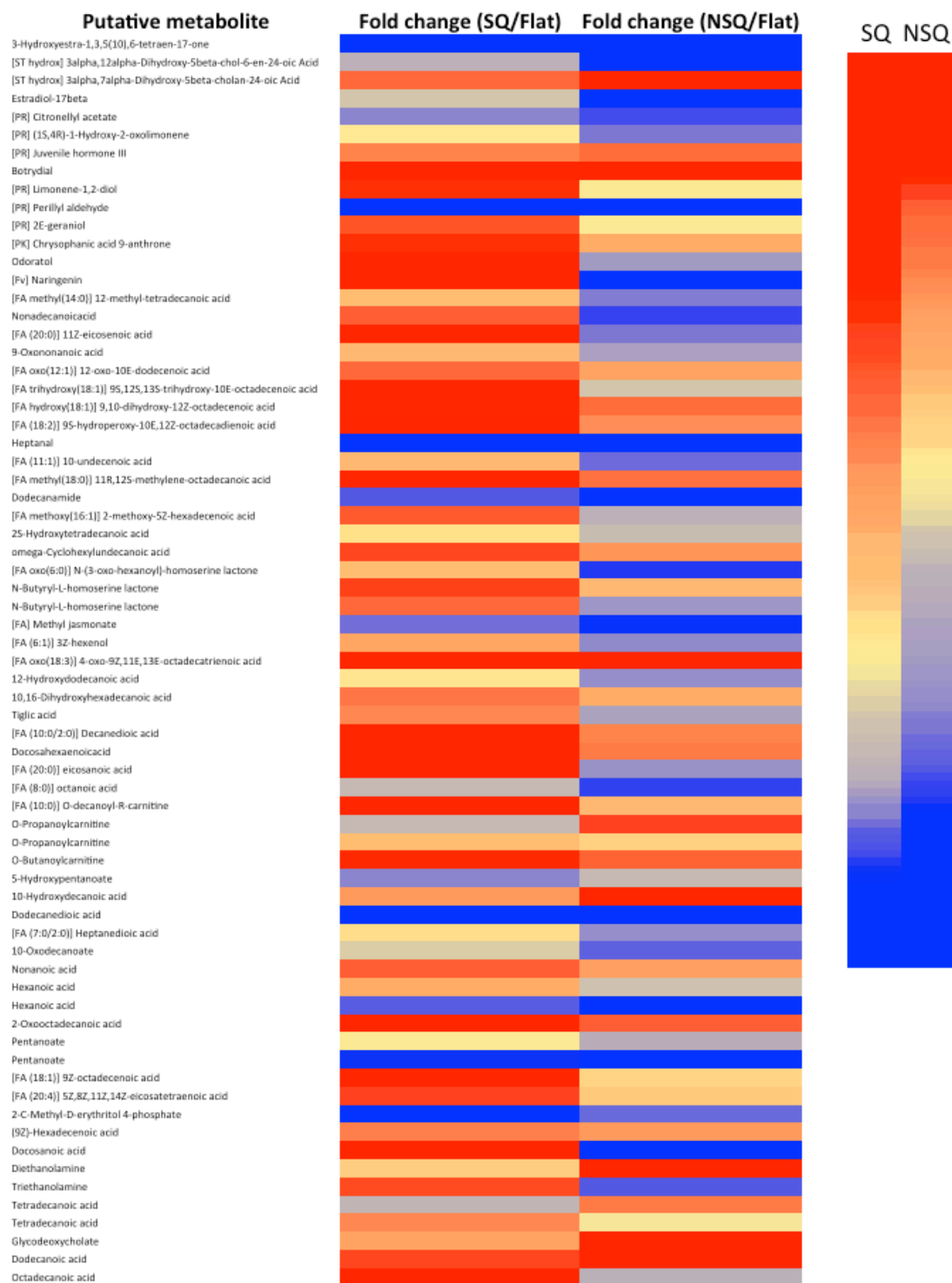


Figure 3-25: Lipid related metabolite profile on SQ and NSQ after 7 days of culture. Metabolites involved in lipid metabolism were analysed for SQ (material replicates, $n = 4$) and NSQ ($n = 5$). Heat maps were generated from average fold change values with reference to flat controls ($n = 6$), assigning a colour scale to the subsequent results. Blue regions = fold increases, red regions = fold decreases and yellow regions = no change. A truncated list is shown here, as the number of metabolites in this class were quite extensive. The entire lipid dataset sorted from highest to lowest is shown to the right of the main heatmap, showing an increased abundance of lipid metabolites on SQ than NSQ.

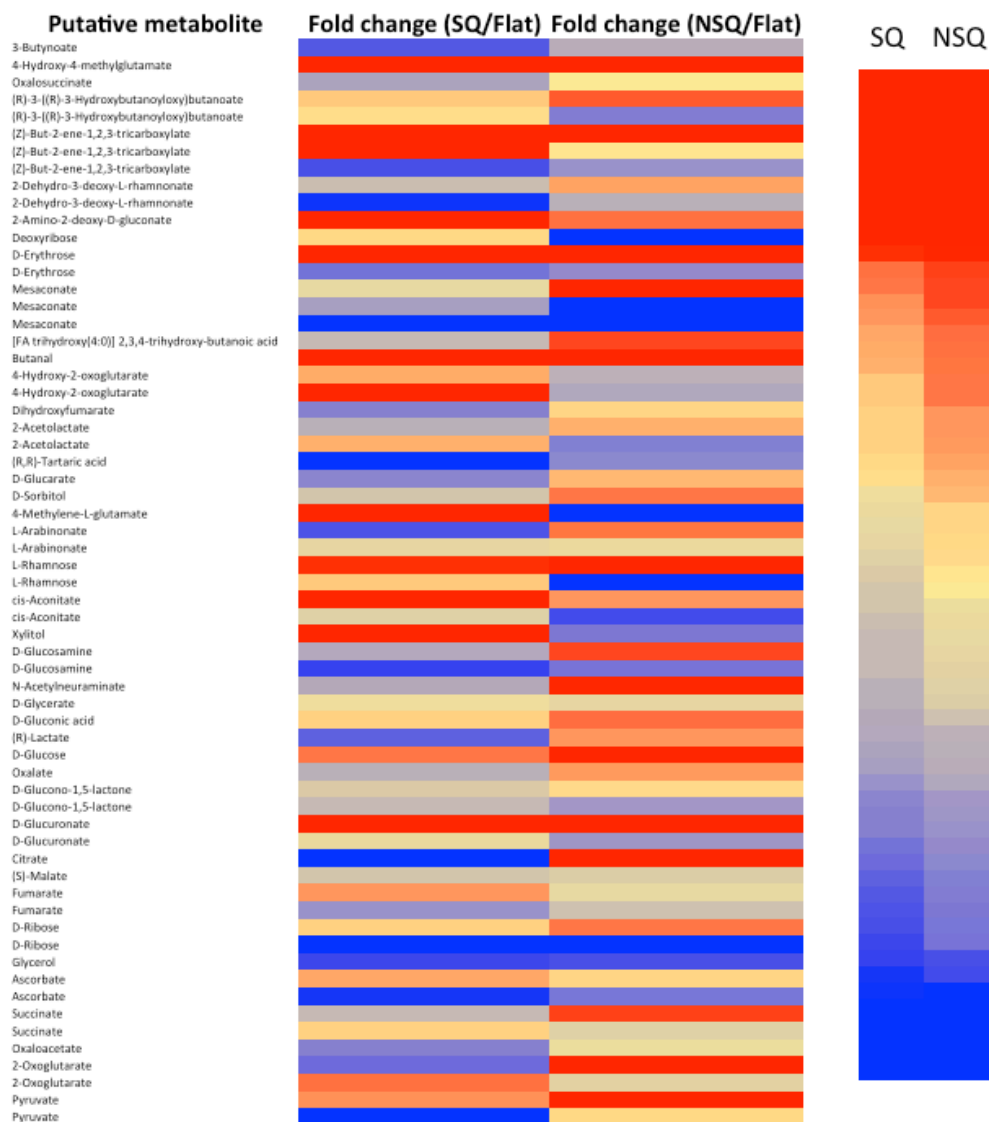


Figure 3-26: Carbohydrate metabolite profiles on SQ and NSQ after 7 day culture. Metabolites classed as being involved in carbohydrate metabolism were analysed for both SQ (material replicates, $n=4$) and NSQ ($n=5$). Heat maps were generated from average fold change values with reference to flat controls ($n=6$), assigning a colour scale to the subsequent results. Blue regions signify fold increases, red regions represent fold decreases and yellow regions denote no changes. Values in between these extremes were shaded accordingly. The entire nucleotide dataset sorted from highest to lowest fold change abundance is shown to the right of the main heatmap, highlighting a contrast between SQ and NSQ in terms of the number of highly abundant and low abundance metabolites. The number of highly abundant carbohydrate metabolites was higher on NSQ.

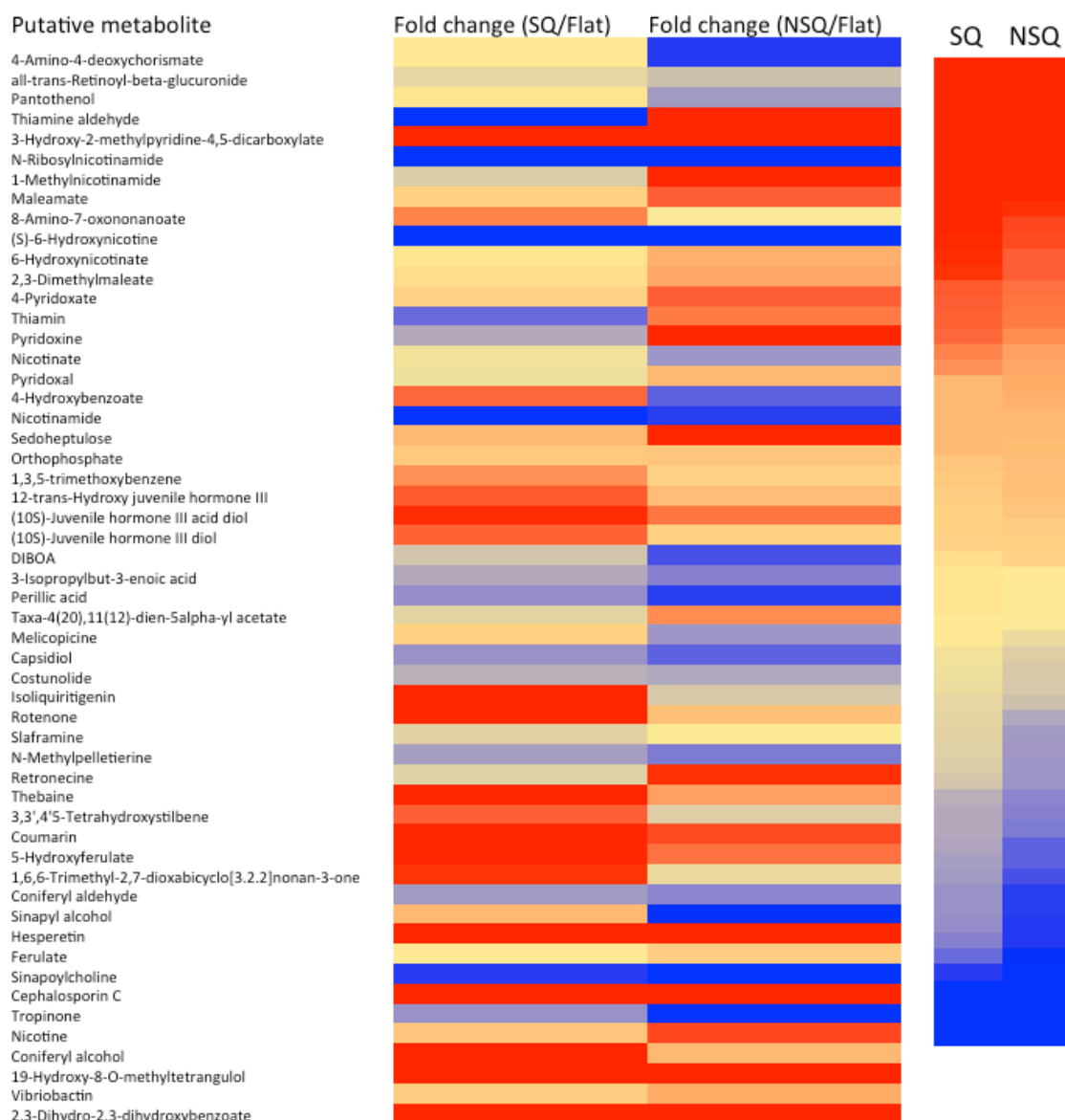


Figure 3-27: Secondary metabolites, vitamins and cofactors (and other remaining smaller groups) profile on SQ and NSQ after 7 days culture. Metabolites classed as being involved in the secondary metabolites category and all other smaller groups for both SQ (material replicates, $n=4$) and NSQ ($n=5$) are shown here (truncated list). Heat maps were generated from average fold change values with reference to flat controls ($n=6$), assigning a colour scale to the subsequent results. Blue regions signify fold increases, red regions represent fold decreases and yellow regions denote no changes. Values in between these extremes were shaded accordingly. The dataset, sorted from highest to lowest fold change abundance can be found to the right of the main heatmap, showing a similar number of low and high abundance metabolites on SQ and NSQ.

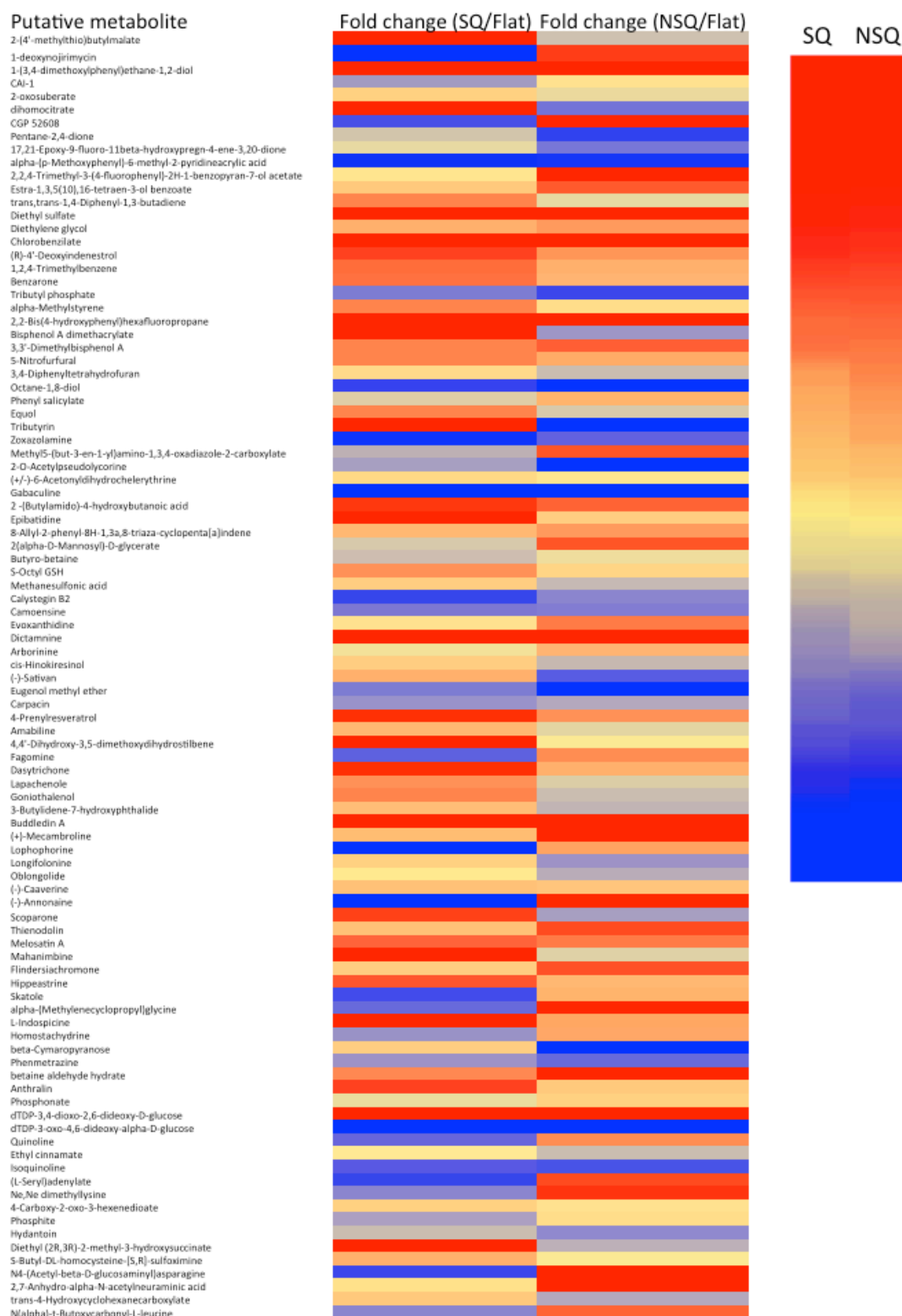


Figure 3-28: Profile of unclassified metabolites on SQ and NSQ after 7 days culture. Metabolites not assigned to any group detected on both SQ (material replicates, $n = 4$) and NSQ ($n = 5$) are shown here (truncated list). Heat maps were generated from average fold change values with reference to flat controls ($n = 6$), assigning a colour scale to the subsequent results. Blue regions signify fold increases, red regions represent fold decreases and yellow regions denote no changes. Values in between these extremes were shaded accordingly. The dataset, sorted from highest to lowest fold change abundance can be found to the right of the main heatmap, showing a similar number of low and high abundance metabolites on SQ and NSQ.

3.2.7.1.3 *Biological relevance of observed changes in metabolic activity*

Following more detailed analysis of the average peak intensities across sample replicates, comparing SQ with the flat surface, 41 annotated peaks were significantly modulated in abundance ($p < 0.05$). Fold changes in peak intensity of NSQ compared to the flat control revealed 42 annotated peaks as having significant changes.

Using identifiers for the putative metabolites in the Kyoto Encyclopaedia for Genes and Genomes (KEGG) database, pathways that contained some of these metabolites were highlighted. Focusing only on the relatively small number of significantly changed metabolites enhances the difficulty in drawing many conclusions, however, an assessment of the identified metabolic pathways was attempted. Noteworthy observations in MSCs on SQ include significant reductions in the abundance of two metabolites involved in nicotinate and nicotinamide metabolism ((S)-6-Hydroxynicotine and nicotinamide-beta-riboside), which are components of oxidative energy pathways, and a significant decrease in O-acetyl-L-homoserine, involved in the metabolism of amino acids cysteine and methionine. This suggests a decreased readiness of cells to participate in differentiation-related or growth-related processes, such as protein synthesis, and mitochondrial oxidative phosphorylation. It appeared that there was a general balance of increases and decreases in arginine and proline metabolism and biosynthesis of amino acids, with similar numbers highlighted in these pathways after input of significantly enhanced and reduced fold change data. With regards to NSQ, a number of elevated metabolites were detected in biosynthesis of amino acids (*Figure 3-29*) and aminoacyl-tRNA biosynthesis pathways.

BIOSYNTHESIS OF AMINO ACIDS

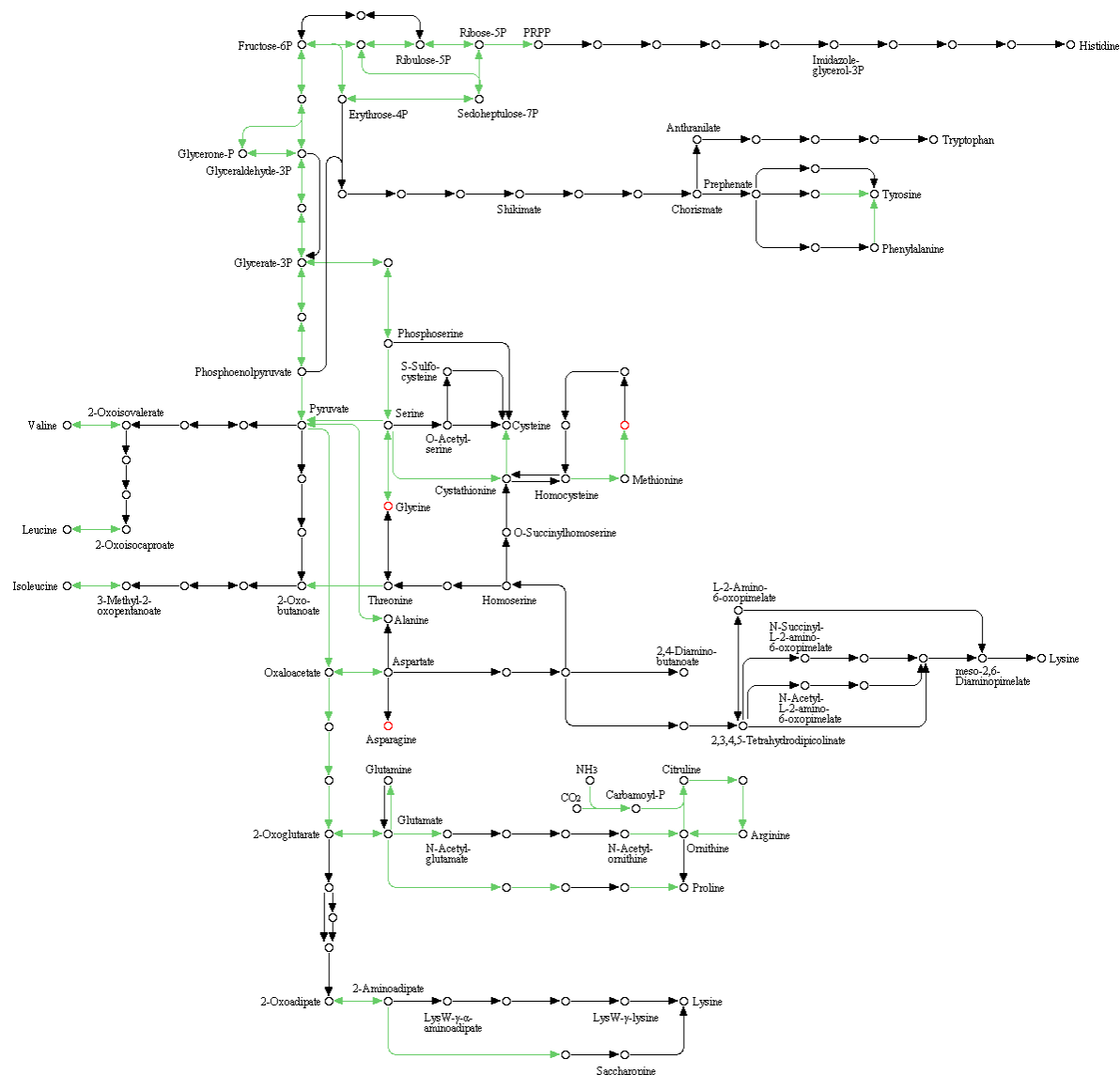


Figure 3-29: Biosynthesis of amino acids KEGG map with elevated NSQ metabolites. Metabolites from NSQ increased fold change data identified within the pathway are represented by red open circles. Map was obtained from KEGG database.

Use of Ingenuity Pathway Analysis (IPA) software allowed for investigation of the datasets in terms of functional processes and wider networks. Firstly, a general assessment was made into the number of up and downregulated gene networks on each nanotopography (Figure 3-30 and Figure 3-31). Processes on SQ were mainly downregulations, whereas those on NSQ were predominantly upregulations, suggesting that MSCs on the latter surface were more metabolically active.

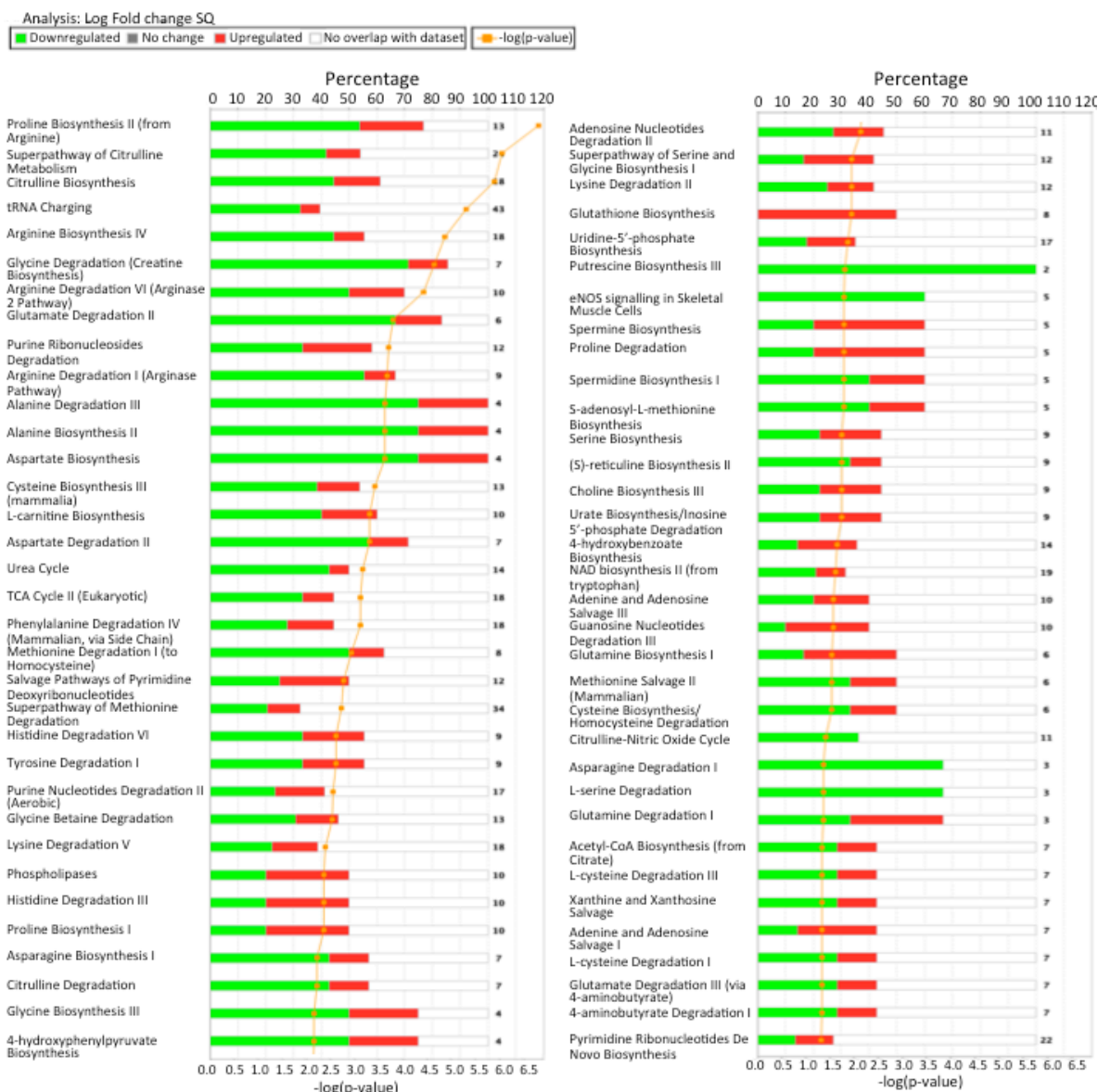


Figure 3-30: Up-regulations and down-regulations in metabolic pathways in MSCs on SQ after 7 days. Green regions of bars represent down-regulations, and red regions represent up-regulations. The number of metabolites in the dataset that are included within each category are shown to the right of the bars. The ratios of detected metabolites to total candidates associated with each grouping of cellular processes are shown in orange. It can be seen that a large degree of metabolites on SQ contribute to decreases in the outlined metabolic pathways, suggesting that MSCs on SQ are more metabolically inactive or 'quiet'. Material replicates, flat (n=6) SQ (n= 4) and NSQ (n= 5).



Figure 3-31: Up-regulations and down-regulations in metabolic pathways on NSQ after 7 days culture. Green regions of bars represent down-regulations, and red regions represent up-regulations. The number of metabolites in the dataset that are included within each category are shown to the right of the bars. The ratios of detected metabolites to total candidates associated with each grouping of cellular processes are shown in orange. It can be seen that a large degree of metabolites on NSQ are involved in up-regulations of metabolic pathways, suggesting that NSQ is more metabolically active. Material replicates, flat ($n=6$) SQ ($n=4$) and NSQ ($n=5$).

Functional networks that contained a high number of candidates from the uploaded datasets on SQ included those involved in cell growth and proliferation, lipid and amino acid metabolism, and cell cycle. In the latter group of networks, of particular interest was that nine molecules including several amino acids were associated with arrest in cell cycle progression and identified on SQ, with their trends suggestive of a reduction in proliferation ($p < 0.0001$). Deprivation of L-methionine, for example, is associated with an

comparison to self-renewing stem cells that make use of anaerobic pathways to avoid damage from reactive oxygen species (Yanes *et al.*, 2010). Indeed, low oxygen conditions can prevent differentiation of human ESCs (Ezashi *et al.*, 2005). Looking more closely at the Krebs cycle (also known as the TCA cycle) on SQ (Figure 3-33), which is an oxidative pathway that occurs in mitochondria, it is interesting to note that the majority of detected Krebs cycle-associated metabolites were decreased in abundance on the SQ surface. It is tempting to speculate that there is reduced activity within this pathway on SQ, as most of the MSCs on this surface are not undergoing differentiation processes and therefore their energy requirements are met without a large shift to mitochondrial oxidative phosphorylation.

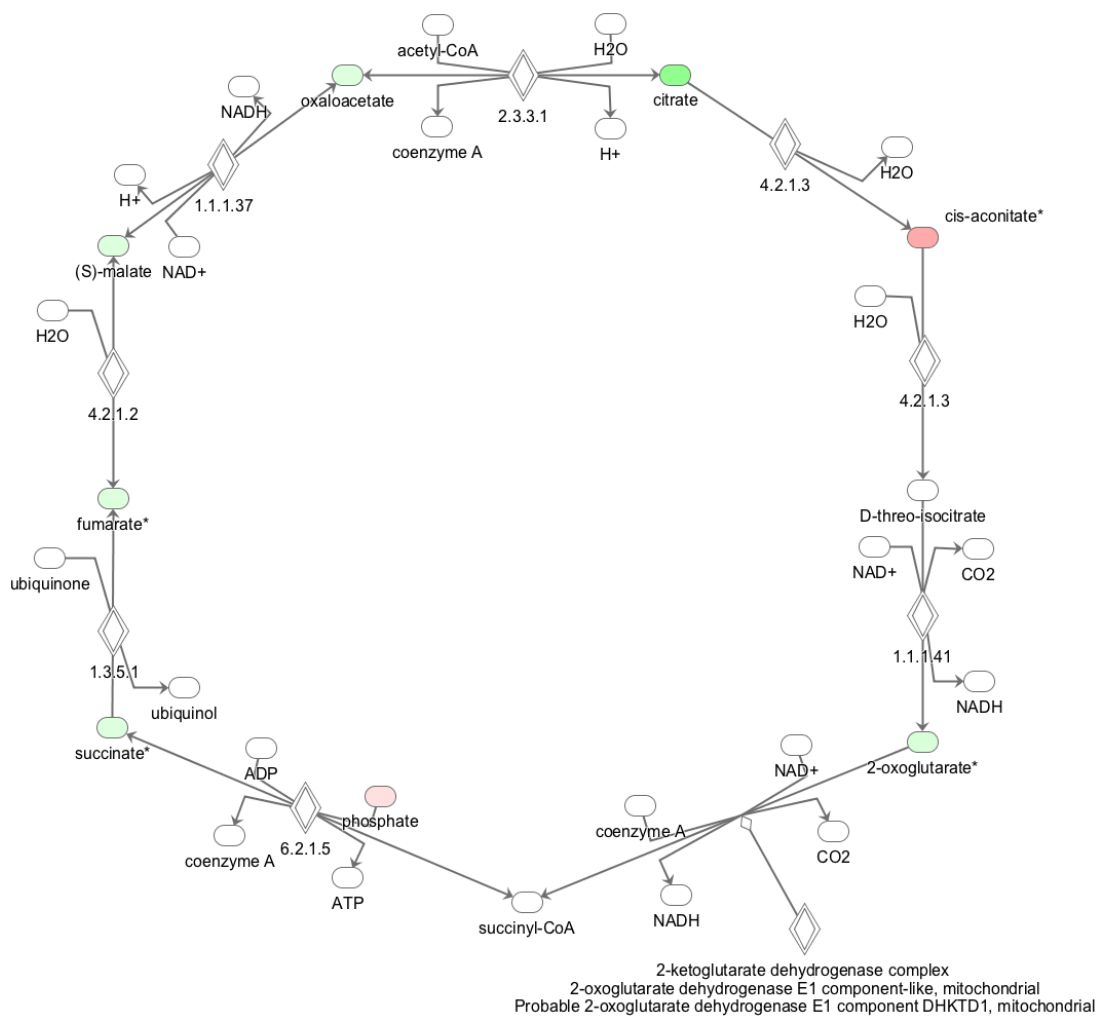


Figure 3-33: Krebs cycle/tricarboxylic acid (TCA) cycle in MSCs on SQ. The Krebs or TCA cycle is a central pathway in metabolism, which takes place in mitochondria, under aerobic conditions. Carbohydrates, proteins and fats are oxidised in a series of reactions, and converge in the TCA cycle for ATP synthesis. It has been reported that oxidative pathways are linked with differentiation; therefore it is interesting that many of the substrates in the cycle are showing decreases on SQ, suggesting a decreased mitochondrial activity in MSCs on this surface.

Functional networks that were proposed likely to be occurring on NSQ included amino acid metabolism, proline, citrulline and arginine biosynthesis, nucleic acid metabolism, and those related to cell growth and proliferation. It can be seen that in the amino acid pathway map, there is a shift towards more upregulations (Figure 3-34) in comparison to the same map on SQ. This elevation in amino acids may be an indicator of a degree of increase in protein synthesis on NSQ, as more basic components are produced in readiness for the process to occur.

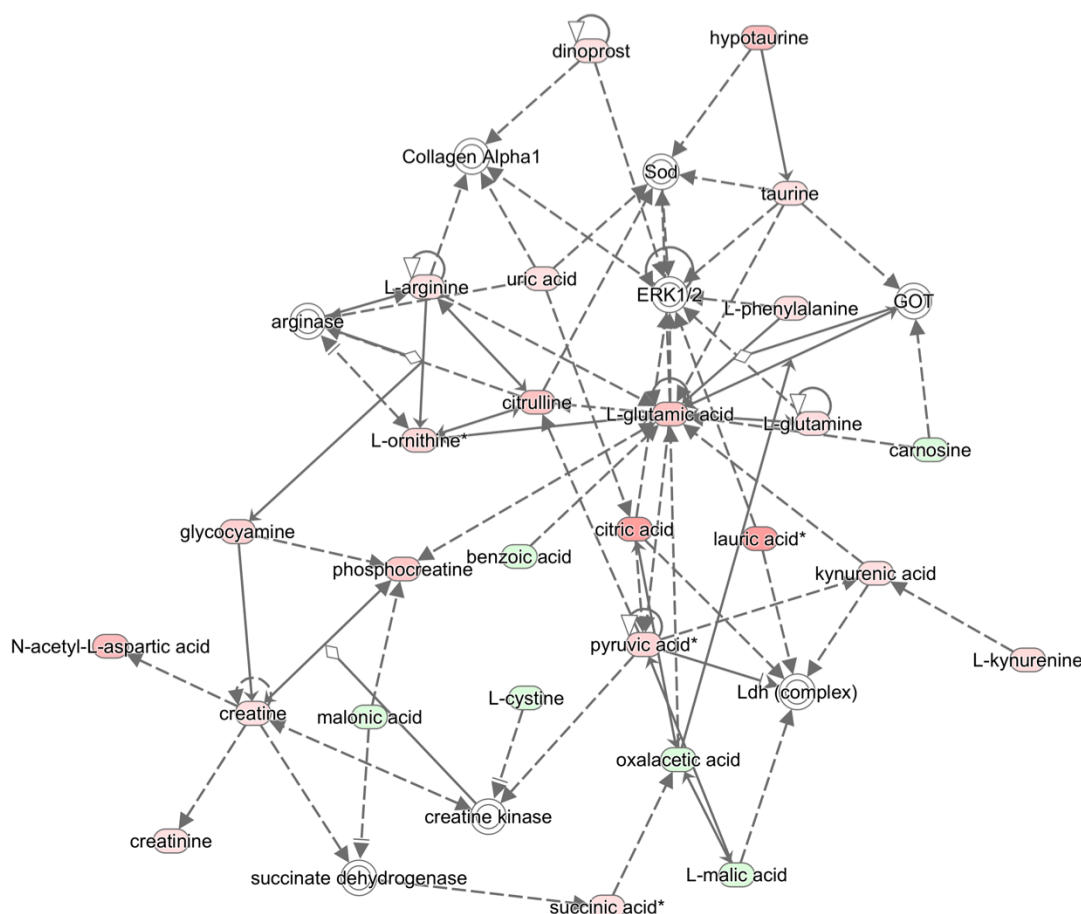


Figure 3-34: Ingenuity pathway highlighting direct and indirect associations for amino acid metabolites in MSCs cultured on NSQ nanotopographies. Metabolites from the uploaded dataset for NSQ are coloured green to signify downregulation, red when upregulated or grey if unchanged. Darker shades represent larger changes. Direct interactions are depicted as unbroken arrows and indirect interactions (via signalling pathways) are depicted as broken arrows. In comparison to the same pathway on SQ, the metabolites show a trend towards being upregulated.

It was additionally promising that IPA predicted an increase in production and activation of alkaline phosphatase in MSCs cultured on NSQ, with identification of L-arginine, L-lysine, ascorbic acid, beta-estradiol, chenodeoxycholic acid, and phosphate from the dataset, which are genes involved in these processes, and occur during osteogenic differentiation.

3.2.7.2 Assessment of cell metabolome after 14 days culture

3.2.7.2.4 Overview of the metabolome after 14 days culture

After 14 days of culture, the metabolic profiles of the MSCs on the surfaces were analysed once more. The portion of the dataset that were assigned putative metabolite identities was taken forward, consisting of a list of 819. General trends were firstly visualised by plotting all the data as a heatmap. A shortened list of some of these showing promising changes between nanotopographies are shown in *Figure 3-35* in order to illustrate the initial reasons for proceeding with the data.

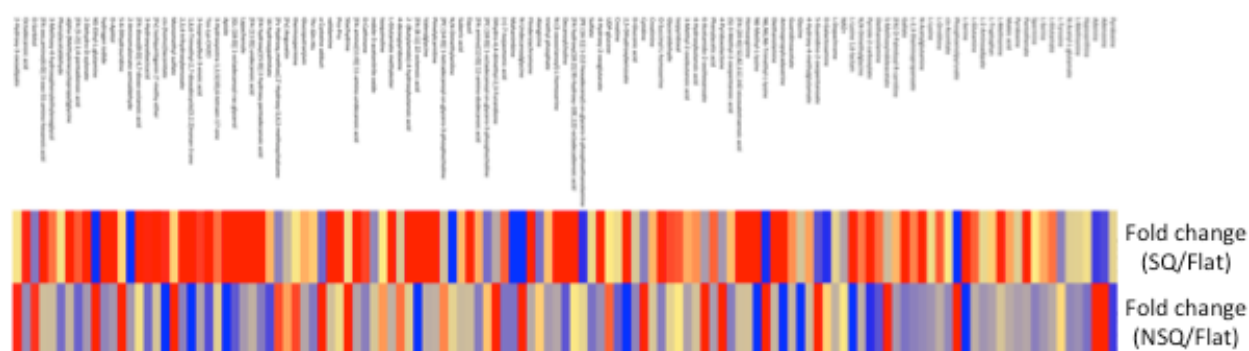


Figure 3-35: Outline of metabolite profile of MSCs after two weeks culture. MSC metabolism on SQ and NSQ surfaces relative to a flat control were visualised using a heatmap. The data displayed consists of a truncated list of metabolites that showed a difference in colour regardless of significance when comparing between fold changes ($n=6$). Decreases are coloured in blue, yellow indicates no change, and increases are designated red. Any values in between these extremes were shaded accordingly.

Even though some of the heatmaps indicated a degree of change in relative abundance between MSCs cultured on the different nanotopographies, with some individual metabolites showing significant differences, the overall combined metabolomic activity within the pathway groups did not appear to show much change at this timepoint (*Figure 3-36*), therefore detailed analysis of each broad grouping was not carried out as extensively as for week 1 and heatmaps generated are not shown here. Nevertheless, significant changes in activity of particular metabolites were looked at in more detail, and there was not much overlap between putative metabolites between the two timepoints. This suggests that stem cells are in a different state after 14 days culture in comparison to 7 days.

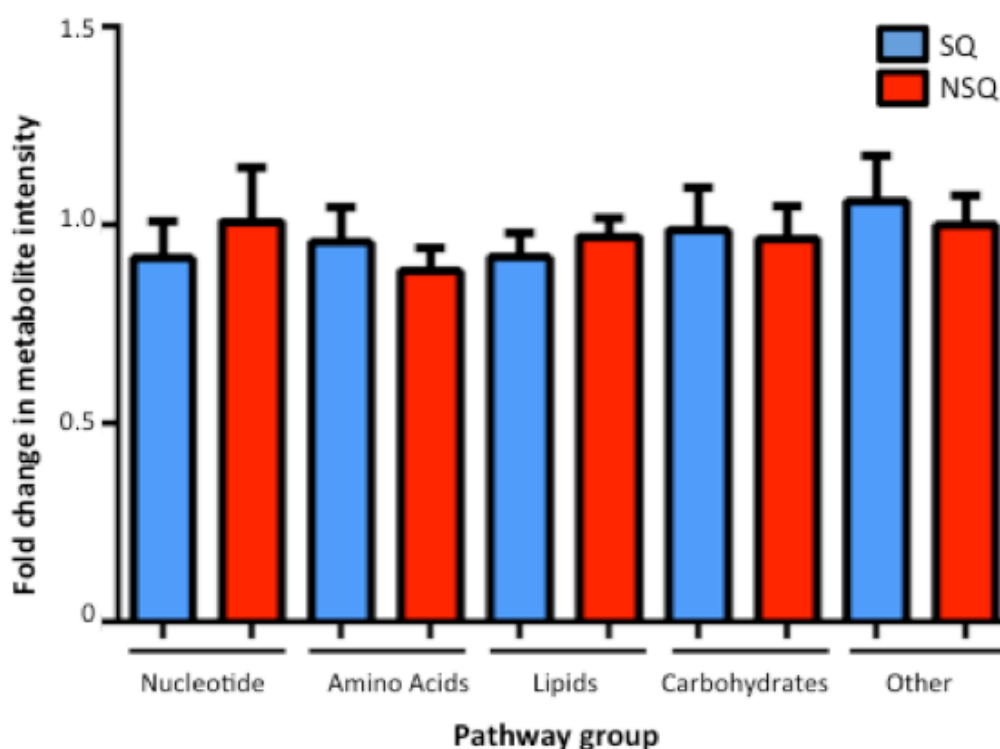


Figure 3-36: Total metabolic intensity fold changes in MSCs cultured on nanotopographies within pathway groups after two weeks. Levels of metabolic activity appear to remain relatively similar between SQ and NSQ at this timepoint, across the nucleotide, amino acid, lipids, vitamins and cofactors, secondary metabolite and other less abundant groupings (including biosynthesis of secondary metabolites, metabolism of vitamins and cofactors, energy metabolism and metabolites with no mapped pathways). Material replicates, flat (n=6) SQ (n= 4) and NSQ (n= 5). Error bars: standard error of the mean.

3.2.7.2.5 Noteworthy differences between SQ and NSQ after 14 days

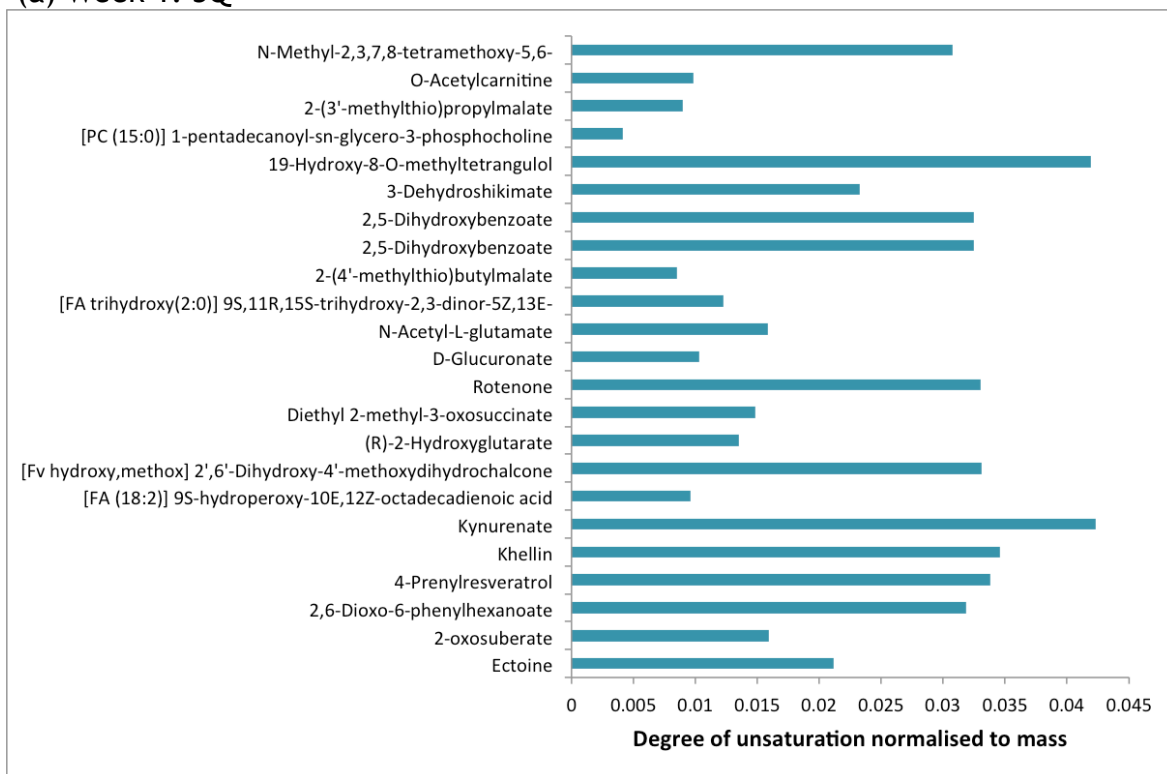
The KEGG database was used to discern whether there was any biological relevance in the metabolites showing the largest differences on SQ and NSQ. Increases in iminoaspartate and maleamate were noticed on SQ, which are involved in nicotinate and nicotinamide metabolism. Several metabolites that could be categorised as being involved in the biosynthesis of secondary metabolites, or metabolism of vitamins and cofactors did not match to any maps, and some had no categories assigned despite having KEGG identifiers, which posed a setback in interpretation of this data.

3.2.7.3 Degree of unsaturation analyses

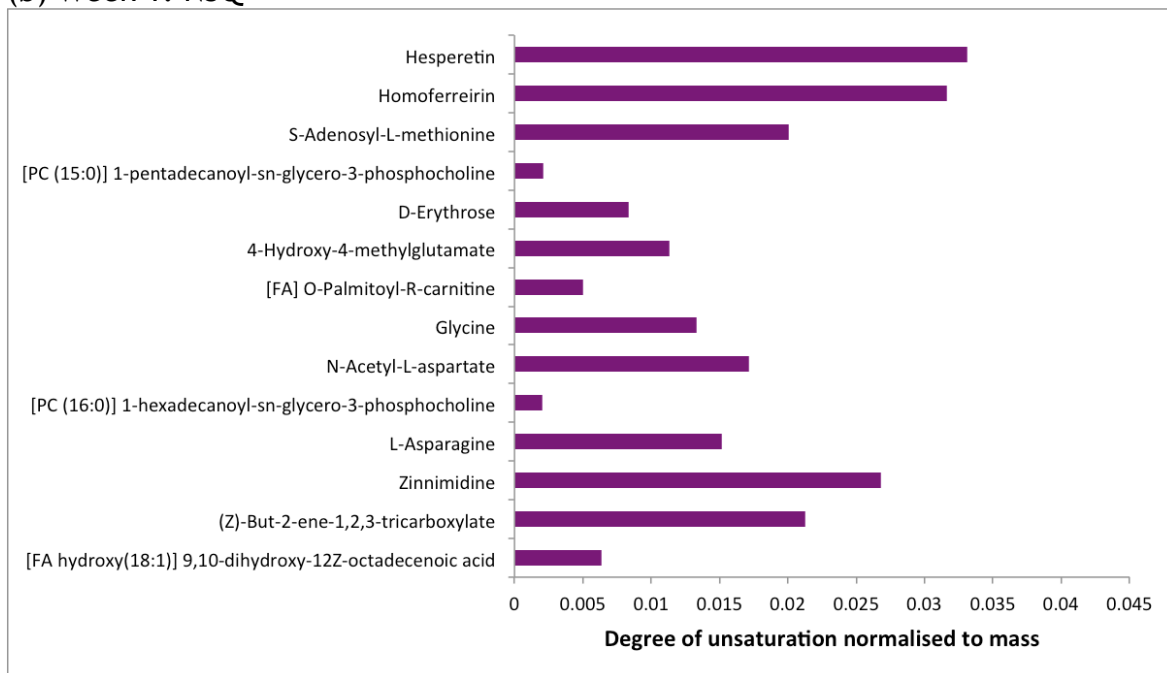
Yanes *et al.* (2010) put forward the concept of a high degree of unsaturated metabolites being associated with pluripotency of ESCs. This was shown to contrast with differentiated cell types, which possessed more saturated metabolites (Yanes *et al.*, 2010). Similarly, the degree of unsaturation within detected metabolites was tested with our MSC dataset, for only those metabolites exhibiting significant up-regulations in comparison to the flat control (fold change), at both of the culture timepoints.

Calculation of a degree of unsaturation score for the significantly up-regulated lipids for SQ and NSQ, showed a higher value for SQ (0.08) compared to NSQ (0.04). This indicates that the lipid profile on SQ is distinct from NSQ and that there is a probable decrease upon nanotopographical induction of differentiation. The calculated values corresponding to each of the individual significantly changed metabolites are shown in *Figure 3-37*. From these, total degree of unsaturation values were determined for each nanotopography, and the results indicate that the MSCs do have higher levels of unsaturated metabolites on SQ (0.51) in comparison to NSQ (0.21) after one week of culture. After two weeks, the value for SQ remained relatively unchanged (0.49), whereas a slight increase was detected on NSQ (0.29).

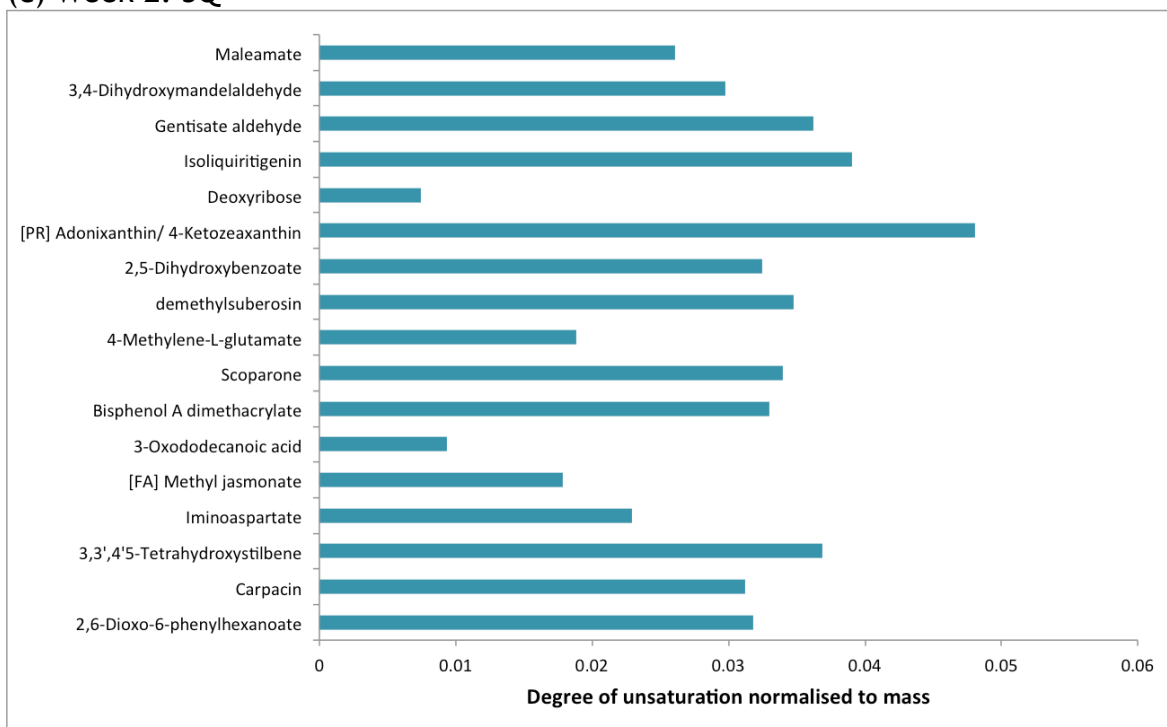
(a) Week 1: SQ



(b) Week 1: NSQ



(c) Week 2: SQ



(d) Week 2: NSQ

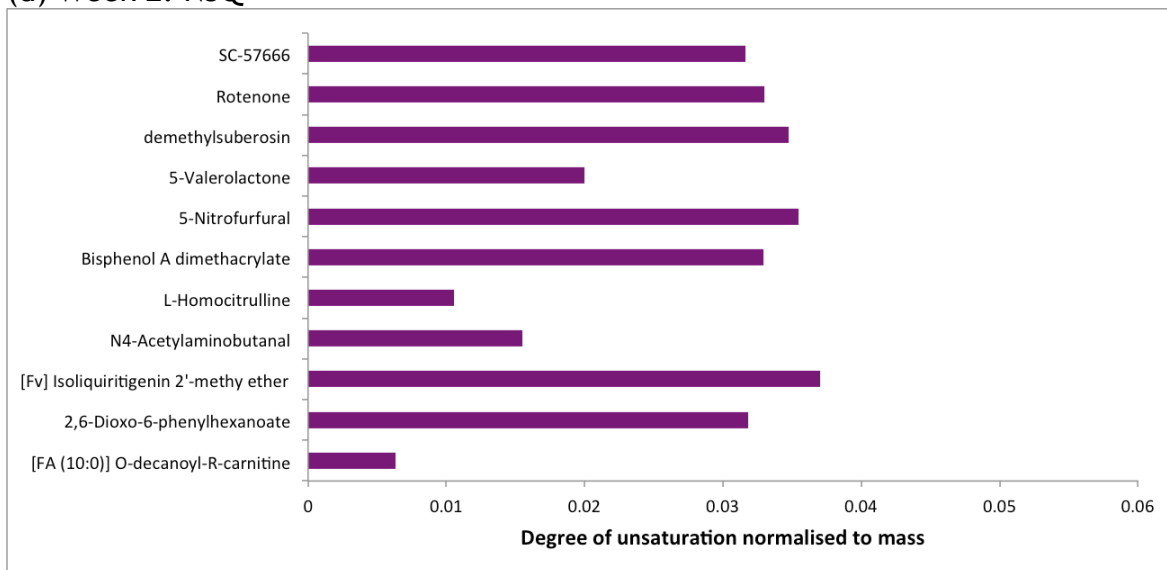


Figure 3-37: Metabolites in MSCs on SQ show an increased number of upregulated metabolites with unsaturated structures. The degree of unsaturation was calculated for all upregulated metabolites on (a) and (d) SQ and (b) and (d) NSQ and normalised to detected masses. Comparisons were made between one and two weeks of culture. Material replicates, flat ($n=6$) SQ ($n=4$) and NSQ ($n=5$).

3.3 Discussion

3.3.1 Characterisation of substrates

The work of this chapter indicated the successful translation of the SQ and NSQ nanotopographies from PCL onto polycarbonate. The necessary conditions and protocols are now in place to best use the surfaces to greatest effect. The initial characterisation of the nanotopography substrates determined that batch-to-batch variation was not a risk when using injection-moulded surfaces in this instance. Ruling out the variation of nanopit diameter was of importance as the distribution of the features should be the sole characteristic that defines each of the nanotopographical substrates. In part, the coating of the substrates for SEM imaging occluded some of the edges of the pits, introducing some difficulties in making diameter measurements with high accuracy, though even this method for comparison did not highlight any large differences between the surface features. Thus, it can be concluded that nanopit features were preserved during different times of manufacture, which is important as experiments had to be setup using multiple batches at times.

Plasma treatment of polymers is a well-established method of assisting cell attachment (Jin Ho *et al.*, 1991, Chu *et al.*, 2002); indeed standard tissue culture plastic (polystyrene) products are treated similarly with surface modification by either gas plasma (Biazar *et al.*, 2011) or corona discharge (Curtis *et al.*, 1983). Various polymers such as polypropylene, polyethylene terephthalate and polycarbonate have been shown to improve surface hydrophilicity following application of plasma (Lai *et al.*, 2006). The technique was implemented in this study, as polycarbonate possesses slightly hydrophobic properties, a common trend of polymers in general (Chu *et al.*, 2002). Plasma treatment was shown to result in an improvement of surface wettability (evidenced by a reduction in water contact angle) thereby rendering the surface more hydrophilic, which should be advantageous in enhancing cell adhesion. This is due to the generation of oxygen functionalities (Hegemann *et al.*, 2003), with incorporation of these into the material surface shown by XPS analysis. Although air plasma treatment is the method that is available for use in this work, it was noted that oxygen plasma treatment applied in a clean room environment would

reduce the 'noise' from contaminants in the air and cause less interference in the XPS results, which is the reasoning for use of oxygen plasma in these tests. Based on the results from both the water contact angle measurements and XPS analysis, adopting plasma treatment of surfaces prior to seeding would be beneficial. Moreover, this type of treatment did not appear to cause any obvious damage to the nanofeatures themselves, even at the longest treatment time tested, though it was observed that some damage in the form of scratches or indentations might occur during transport from the location of manufacture. Subsequent experiments showed that cell attachment occurred after several hours on our treated substrates. Furthermore, use of a seeding device allowed cells to be added directly to the top of each substrate, thereby minimising wastage whilst preserving good seeding distribution. Therefore, this section of work establishes the baseline protocol for preparation and seeding of substrates for the remainder of the study.

3.3.2 Initial seeding density affects response to nanotopography

The level of some MSC surface markers decrease as they differentiate into other cell types, such as STRO-1, CD166/ALCAM, CD90 and CD105 (Lee *et al.*, 2009). It has also been suggested that some markers are subject to influence from donor age, number of passages, and density of culture (Boxall and Jones, 2012). In this part of the study, MSCs positive for the CD271 marker were investigated with regards to seeding density. The advantages of this were two-fold, firstly CD271 could be argued as the most translational marker between species (Boxall and Jones, 2012), thus accumulating evidence for CD271-selected MSCs may be of wide use to the scientific community, and secondly, determining the optimal seeding density will help to standardise use of the nanotopographies, minimising experimental variation, and reducing the number of cells needed without having to add more than necessary to cover the required area. There are reports that cell density may influence MSC phenotype due to constraints on cell morphology, which appear to drive MSC differentiation down specific pathways (McBeath *et al.*, 2004, Lu *et al.*, 2009, Xue *et al.*, 2013). Furthermore, cell density can affect MSC proliferation (Neuhuber *et al.*, 2008) and differentiation (Gobaa *et al.*, 2011). From the three densities tested, expression of phenotypic marker proteins appeared to vary depending on the initial seeding. It was hypothesized

that the optimal cell number to be seeded would be that which enabled a balance between fair coverage of the material surface, yet did not allow too many cell-cell contacts to be established. Cell-cell contact signalling could potentially compete against the nanotopographical instructional cues, which may diminish the effects of the nanotopographies. Certainly, it appeared that lowering cell density elicited enhanced retention of stem cell marker expression. Seeding at 500 cells/cm² and 1000 cells/cm² were effective for stem cell marker expression of CD271 and ALCAM in MSCs cultured on SQ, however using 500 cells/cm² is impractical for experimental purposes (requiring many substrates to be seeded), therefore a compromise between adequate clonal growth and desirable phenotypic marker expression could be achieved by using a density of 1000 cells/cm². This apparent optimal density was maintained for the proceeding experiments described in further chapters.

It was noted that levels of ALCAM were high in MSCs cultured on NSQ after 28 days, though this may be due to the NSQ surface successfully mimicking the endosteal niche in the bone marrow. This microenvironment contains both osteoblasts and MSCs in addition to HSCs that 'home' towards this region of bone marrow, with associative behaviour proving important to support the cell types (Nakamura *et al.*, 2010). Thus it would not be unusual to find a population of MSCs being maintained on NSQ. The CD271 marker was also maintained to a degree on flat, however MSCs on both flat and NSQ were unable to retain expression of both markers as successfully as MSCs on SQ. Thus we conclude that transfer of the SQ nanopattern onto polycarbonate enables MSCs to retain their potential for multipotency.

In light of observing that changes in seeding density affect eventual cell phenotype with regards to marker expression, it is tempting to additionally speculate that the distinct colony growth patterns observed at the lower densities are important in the maintenance of 'stemness', and that a fibroblastic growth pattern favours differentiation into osteoblasts. The appearance of these growth patterns correlates with the aforementioned data regarding marker expression. Initial analysis of the differences between MSCs cultured on flat, SQ and NSQ in terms of proliferation, did not highlight any obvious changes in the number of cells progressing through S phase or in total cell number.

3.3.3 Metabolism of CD271⁺ MSCs on nanotopography

Metabolomic examination of CD271⁺ MSCs yielded a large amount of data. The putative metabolites with assigned KEGG identifiers were taken forward to narrow down the focus of the analysis. Grouping the metabolites into broad pathways suggested that there were more changes at the 7 day timepoint than after 14 days. This suggests that many of the larger changes in the cells undergoing self-renewal and differentiation were occurring early, though the significantly altered metabolites at each timepoint were found to be different, suggesting changes in cell state had occurred as time progressed. There was a trend towards lower total metabolic activity on SQ in comparison to NSQ after 7 days of culture, with the exception of lipids. Neuronal stem cells have shown to be dependent on production of fatty acids and lipids to divide and generate neurons (Knobloch *et al.*, 2013). This signals that the regulation of lipid biosynthesis and metabolism is important in self-renewal and differentiation. Furthermore, fatty acid oxidation has been shown to promote symmetric division in haematopoietic stem cells (Yusuf and Scadden, 2012). Lipid metabolism appears to be linked to stem cell plasticity, thus it may be worthwhile to investigate fatty acids in more detail in future work.

Further investigation showed that many metabolites were downregulated on SQ and upregulated on NSQ after 7 days, suggesting a reduced metabolic activity of MSCs on SQ. This agrees with some of the existing literature and previous work, describing undifferentiated MSCs as being metabolically quiet whereas differentiating cells are generally more metabolically active (McMurray *et al.*, 2011, Tsimbouri *et al.*, 2012).

The metabolites on SQ linked to pathways associated with growth, proliferation and the cell cycle. IPA predicted that arrest in cell cycle progression would be heightened on SQ due to identification of 9 molecules from the dataset known to have roles in this network and based on the peak metabolite intensities of these metabolites when compared to flat controls. However, this is at odds with the results from the BrdU assay and cell counts, as there were no significant differences between surfaces detected. This may be due to some aspect of cell cycle regulation being affected, which prompted further investigations described in the proceeding results chapter. A decrease in L-methionine was noted, which

is of interest as methionine metabolism has a role in regulating maintenance of human pluripotent stem cells (Shiraki *et al.*, 2014). ESCs require methionine to maintain pluripotency, and therefore levels must be regulated (Shiraki *et al.*, 2014). The methionine concept has not been investigated in MSCs as yet, therefore it is possible that MSCs do not require as much methionine to remain multipotent, or that its presence in this stem cell type is subject to some temporal changes, which are not extreme enough to induce differentiation.

Stem cells require an increase in energy requirements as they differentiate, and these energy needs can be provided by oxidative energy pathways such as those that take place in mitochondria (Chung *et al.*, 2007). The data suggested a low likelihood that MSCs on SQ were obtaining their energy from these oxidative processes, suggesting that the cells were not undergoing differentiation, and not requiring the large energy demands associated with maturation into a specified cell type. In addition, utilising anaerobic energy pathways would decrease risk of damage from reactive oxygen species and oxidative stress, which would be detrimental to the maintenance of a stem cell population. MSCs on NSQ showed an increase in amino acids, which may be indicative of an increase in protein synthesis, an important step in stem cell differentiation (Sampath *et al.*, 2008).

Comparison of the upregulated metabolites that were significantly changed on SQ and NSQ, revealed a greater abundance of unsaturated metabolites in MSCs on SQ and a decreased level on NSQ, which is in agreement with the findings of Yanes *et al.* and draws parallels with the group's observations in ESCs. Yanes and colleagues had observed that ESCs contained many unsaturated metabolites and this number would decrease upon differentiation (Yanes *et al.*, 2010). It is promising to observe that after 14 days of culture, the level of unsaturation on SQ is similar to that after 7 days, suggesting a level of maintenance on SQ. In contrast, the degree of unsaturation on NSQ was found to increase slightly after 14 days. This may be due to the MSCs reaching a pre-osteoblast stage, and switching their bioenergetics towards oxidative pathways important for differentiation. Oxidation reactions will increase the number of molecules containing multiple carbon-carbon bonds. There could also be an increase in unsaturated molecules to provide energy to initiate this second wave in differentiation towards an osteoblast phenotype. Unsaturation is known to be

highly reactive under oxidative conditions (Yanes *et al.*, 2010); therefore an accumulation of unsaturated metabolites may be a 'priming' event for MSCs to move past their pre-osteoblastic status. The number of timepoints investigated in this case was restricted to two. However, it may be interesting to investigate earlier and later timepoints to those included in this study to determine when the largest changes on both nanotopographies occur and to see how long SQ can maintain the same level of unsaturated metabolites over time.

Chapter 4

Investigating MSC Cell Cycle using Nanotopography

4 Chapter 4

4.1 Introduction

Cell cycle changes have been associated with the differentiation status of several types of stem cell, including ESCs and HSCs. Mounting evidence indicates that differentiation and self-renewal are coupled to cell cycle regulation. The property of self-renewal can be described as an ability to retain stem cell status in order to undergo either symmetrical or asymmetrical division and generate new daughter cells with similar identities and differentiation capabilities. The inherent link between maintaining self-renewal and cell cycle appears to lie with overlapping signalling pathways and common genes pertaining to both activities (Orford and Scadden, 2008, Viatour, 2012).

Developments into the study of ESC cell cycle have demonstrated that the duration of G1 phase can affect the maintenance of self-renewal and pluripotency. A prolonged G1 phase has been linked with human and mouse ESC differentiation (Li *et al.*, 2012, Calder *et al.*, 2013) whilst a shorter and more limited G1 phase has been proposed to retain pluripotency in ESCs. This was elegantly demonstrated in a study of murine neural stem cells, which normally possess a short G1 phase that becomes longer during differentiation (Lange *et al.*, 2009). These effects were experimentally recapitulated by decreasing CDK4-cyclin D1 expression to lengthen G1, which promoted neurogenic differentiation, or by overexpressing CDK4-cyclin D1 to shorten G1 and achieve the opposite effect (Lange *et al.*, 2009). A restricted G1 phase reduces the time at which a cell remains responsive to differentiation signals, and conversely a lengthened G1 phase provides a sufficient period for activation and deactivation of genes and initiation of various processes allowing differentiation to occur. Despite several reports agreeing with these observations, a study of mouse ESCs with elongated G1 phases reported contradictory findings, reporting that lengthening G1 was not by itself sufficient to drive differentiation (Li *et al.*, 2012).

Interestingly, through use of an adapted real time cell cycle reporter system, whereby human ESCs at different stages of the cell cycle expressed proteins in different colours, Pauklin *et al.* reported that their ESCs could only respond to

differentiation cues at particular stages of G1; those at early G1 expressed markers corresponding to endoderm and mesoderm differentiation, and late G1 ESCs were restricted to neuroectoderm marker expression (Pauklin and Vallier, 2013). In addition, they described a pivotal role for cyclin D in the localisation and subsequent action of Smad2/3; during early G1, low levels of cyclin D would lead to Smad2/3 mediated activation of genes associated with endoderm/mesoderm differentiation, making those cells more susceptible to undergoing differentiation to those lineages (Pauklin and Vallier, 2013). This shows that changes during G1 phase in particular, trigger signalling pathways that impact on the eventual fate of pluripotent stem cells.

The bulk of the literature relating to adult stem cells is based on the study of HSC cell cycle, where it has been postulated that they utilise cell cycle regulation to preserve pools of non-dividing cells in addition to maintaining adequate numbers of actively proliferating cells that will be able to differentiate into tissue-specific cell types (Wilson *et al.*, 2008). Some studies have suggested that HSCs are largely quiescent, and remain dormant until directed to self-renew or differentiate when replacement of mature cell types are needed (Wilson *et al.*, 2008, Zou *et al.*, 2011). The difficulty in discerning the details of HSC regulation is further compounded due to complexities in considering interactions between different cell types found in the *in vivo* niche. Close association between osteoblasts and HSCs, for example, allows thrombopoietin (THPO) expressed by osteoblasts to bind to the THPO surface receptor (MPL) found on the surface of HSCs (Yoshihara *et al.*, 2007) causing dimerisation, and subsequent phosphorylation and activation of JAK2 and downstream effectors (Tortolani *et al.*, 1995). Moreover, application of exogenous THPO resulted in an increase in the number of quiescent HSCs (Yoshihara *et al.*, 2007).

Other factors that may have important roles in the cell cycle of stem cells are retinoblastoma tumour suppressor (RB) and negative regulators. The latter includes members of the cyclin dependent kinase-inhibitory protein/kinase inhibitory protein (CIP/KIP) family. One of these, p27^{kip1}, has been observed to increase during progression of differentiation (Egozi *et al.*, 2007), and its overexpression can cause cell cycle arrest (Menchón *et al.*, 2011). RB is of

interest as it may act to prevent premature senescence of MSCs by promotion of mitotic quiescence (Lin *et al.*, 2014).

In contrast to studies on ESCs and HSCs, research into the cell cycle of MSCs has been rather limited and is poorly understood. This gap in knowledge in the field of stem cell research should be regarded as an important consideration if MSCs are to be viewed seriously as a viable therapeutic option. Beneficial exploitation of regulatory genes and pathways could be utilised to encourage self-renewal over longer periods of time to increase the potential of MSCs for therapy and lessen wastage of MSCs that may have spontaneously differentiated or become senescent during expansion.

From previous research with MSCs cultured on the SQ nanotopography, it can be argued that MSCs on this surface are more efficient at self-renewal whilst maintaining expression of stem cell surface markers, and are thereby primed to favour retention of an MSC-like phenotype. However, the nanotopography-induced mechanisms and processes by which this beneficial self-renewal occurs remain unclear. Filopodia have been described as cellular sensors, allowing cells to probe the physical features of their surroundings, and thus could be involved in an important stage of biomaterial-cell interaction, well-placed to initiate downstream intracellular reactions in response to nanotopography (Dalby *et al.*, 2004a, Dalby *et al.*, 2004b). There may exist an association between the initial recognition of instructional cues and the trigger of events involved in cell cycle. In this chapter, inhibition experiments were used to investigate this association at the level of filopodia and cell cycle protein expression.

Furthering our understanding of SQ induced self-renewal would provide knowledge about the key factors that are important in giving rise to this property, and how the nanotopographical features or distribution may be further improved to exploit this technology to its full capacity in the provision of patient-specific MSCs. To this end, this chapter focuses on investigating potential changes in cell cycle on the nanotopographical surfaces, to determine whether cell cycle regulation could be a causative determinant of eventual MSC fate.

The aims of this chapter are: to begin to elucidate and define the cellular mechanisms at work on SQ that may contribute self-renewal, to investigate the potential changes in cell cycle regulation in MSCs cultured on nanotopography, and to assess the potential link between filopodial interactions with nanotopography and effects on the cell cycle.

4.2 Results

4.2.1 Assessing seeding density for STRO-1+ MSCs

To briefly assess the continued use of the optimised seeding density for MSCs, for STRO-1 selected MSCs (herein referred to as STRO-1⁺ MSCs), western blotting was carried out after 28 days of culture on SQ and NSQ nanotopographies in addition to a flat control, and levels of STRO-1 and OPN were quantified for the initial seeding density of 1000 cells/cm² (Figure 4-1). Comparison of the relative intensities of the bands indicated that continued use of 1000 cells/cm² resulted in an elevated level of STRO-1 (a marker of stemness) on SQ in comparison to the flat control, and an elevated level of OPN (an indicator of osteogenic differentiation) on NSQ in comparison to the flat control.

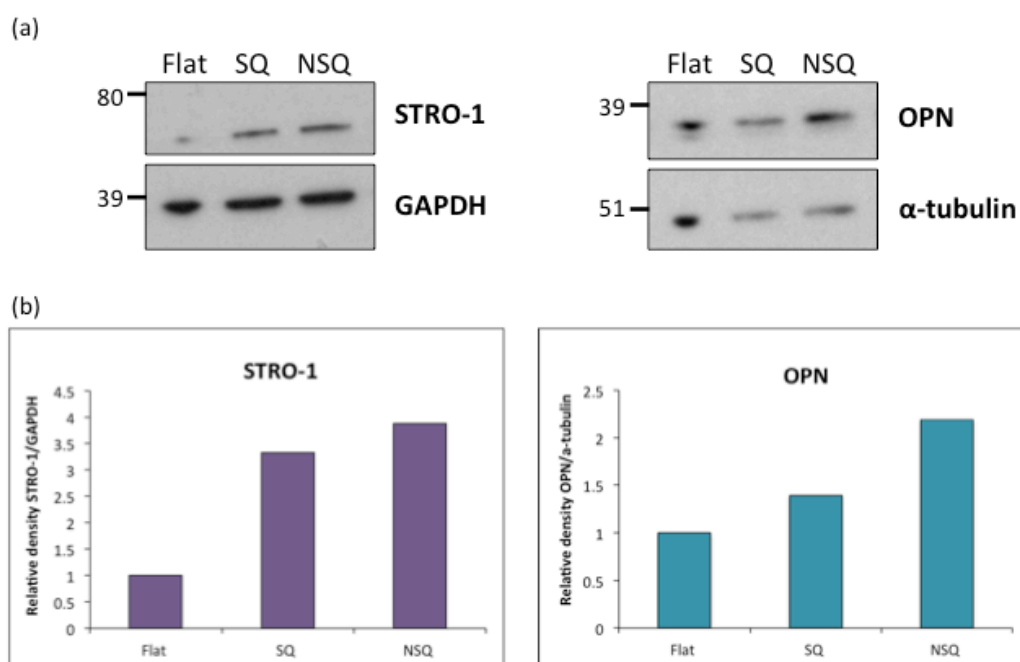


Figure 4-1: Western blotting at a seeding density of 1000 cells/cm² was adequate for use of nanotopographies with STRO-1⁺ MSCs. MSCs were seeded onto flat/SQ/NSQ for 28 days (n=1). (a) Western blots probed for STRO-1/OPN, with GAPDH/α-tubulin used as loading controls (b) Graphs showing quantification of bands at 1000 cells/cm² using Image J. Data was normalised to loading controls. STRO-1 was high on SQ and NSQ in comparison to the flat control at this density, consistent with CD271⁺ MSCs. OPN was highest on the osteogenesis-promoting NSQ surface as would be expected. Taken together, an initial seeding density of 1000 cells/cm² appears adequate for use of STRO-1⁺ MSCs on nanotopographies.

These observations give confidence to further use of this previously optimised seeding density for these MSCs. It is noted that STRO-1 is also increased on NSQ compared to the control and this potentially illustrates a heterogeneous population, which would merit further investigation if time had allowed.

4.2.2 Synchronisation and release of MSCs for analysis of cell cycle

STRO-1⁺ MSCs were seeded on substrates at a density of 1000 cells/cm² and allowed to attach and establish for a period of 48 hours. The cells were washed in serum free media and then incubated for a further 48 hours in 0.1% FBS (low serum) media to induce cell cycle arrest and thereby synchronise the cells. Periods longer than 48 hours appeared to reduce the overall viability of the cells, and many cells were observed to detach.

After this period in low serum media, MSCs were released back into the cycle by replacement of this media with serum containing maintenance media for the required durations for each experiment. A comparison of synchronised and asynchronous cells was carried out with propidium iodide staining and flow cytometry. The results showed that the number of cells in G0/G1 was far greater in the synchronised cells in comparison to those kept in maintenance media (*Figure 4-2*). Thus it can be said with confidence that the majority of the cells were in the G0/G1 stage when cultured in low serum media, and that this was a suitable treatment for synchronisation of MSCs.

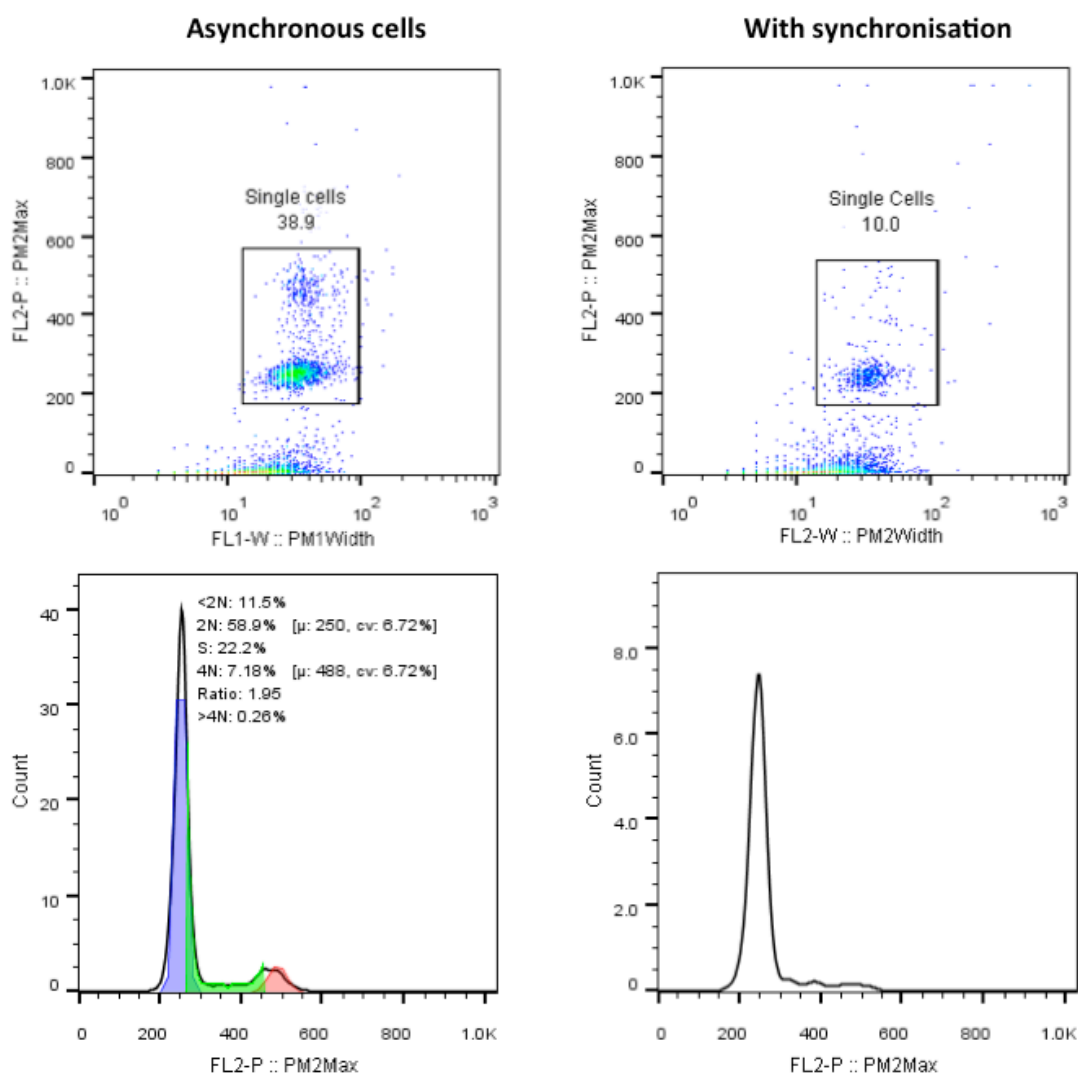


Figure 4-2: Validation of synchronisation procedure using flow cytometry. MSCs were seeded onto flat substrates (60 material replicates per condition) and either kept in maintenance media or subjected to a synchronisation procedure by culture in low serum media. Cells were detached from the substrates and pooled following completion of the treatment, together with the untreated controls, stained with propidium iodide and analysed by Dr Maria C. de Andrés González (University of Southampton) using flow cytometry. The top row of plots show the gating applied. The gated region indicates the population taken forward for analysis, shown in the bottom row of plots. It can be seen that the synchronisation protocol effectively causes all of the MSCs to arrest during G0/G1 phase, confirming that culture in low serum media can be used for synchronisation of MSCs.

4.2.3 Cell cycle screening on nanotopographies

As it appeared that proliferation was not significantly affected by nanotopography (results of BrdU assay, chapter 3), we hypothesized that the differences in eventual cellular phenotype conferred by culture on SQ and NSQ might be at the level of cell cycle regulation. Firstly, quantification of the

protein to be used for normalisation was carried out, to ensure that there were no fluctuations after culture on the different substrates, which would affect the final quantification of the in-cell western (ICW) experiments. The results showed that GAPDH levels were not significantly affected by seeding on different substrates (Figure 4-3).

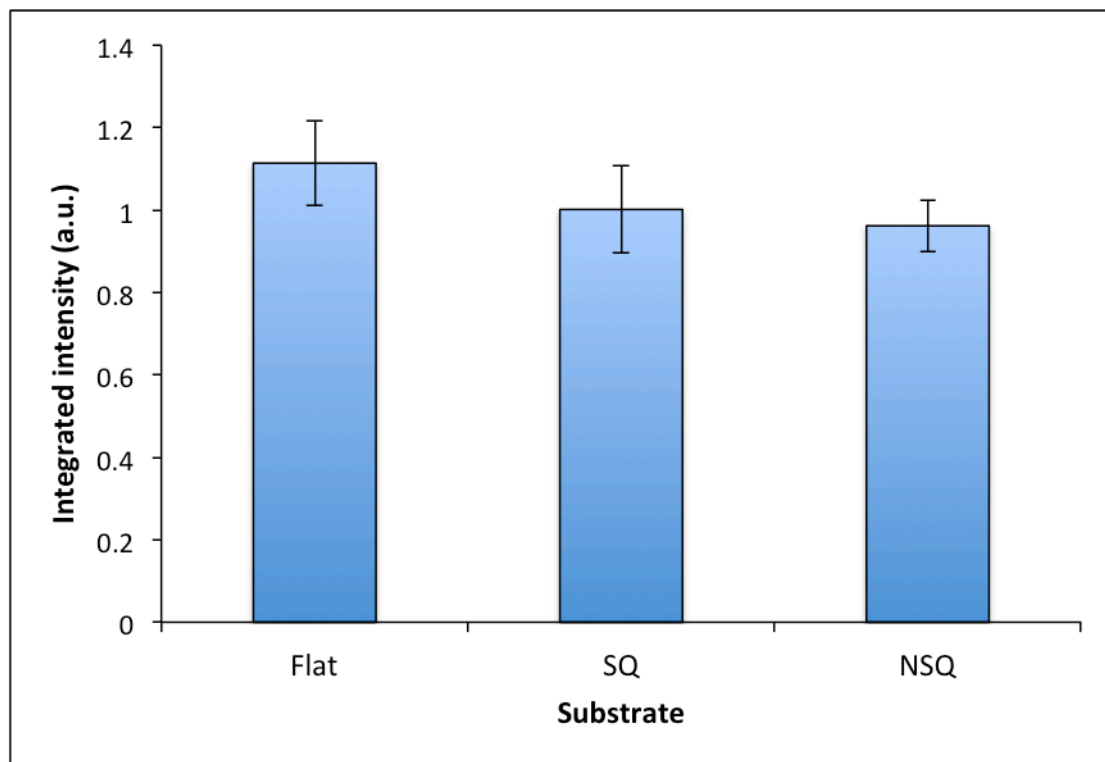


Figure 4-3: Testing GAPDH levels in MSCs cultured on different surfaces. GAPDH levels were assessed in relation to cell number using CellTag stain by ICW. No significant differences in GAPDH protein abundance between surfaces were detected in MSCs, making it suitable for use as a normalisation protein for in cell western experiments. Results shown are average integrated intensity of GAPDH normalised to CellTag for 4 material replicates. Error bars denote \pm standard error of the mean.

A panel of several cell cycle regulatory proteins were examined, with their levels assessed in MSCs cultured on the range of surfaces, to investigate any potential differences that may be occurring as a result of culture on a particular substrate. Phosphorylated proteins were normalised to their total protein equivalents, and testing of one of these, cdc2, also known as CDK1 (Dorée and Hunt, 2002) through comparison to GAPDH, showed that this protein remained at a similar level throughout the experiment for all of the substrates (Figure 4-4).

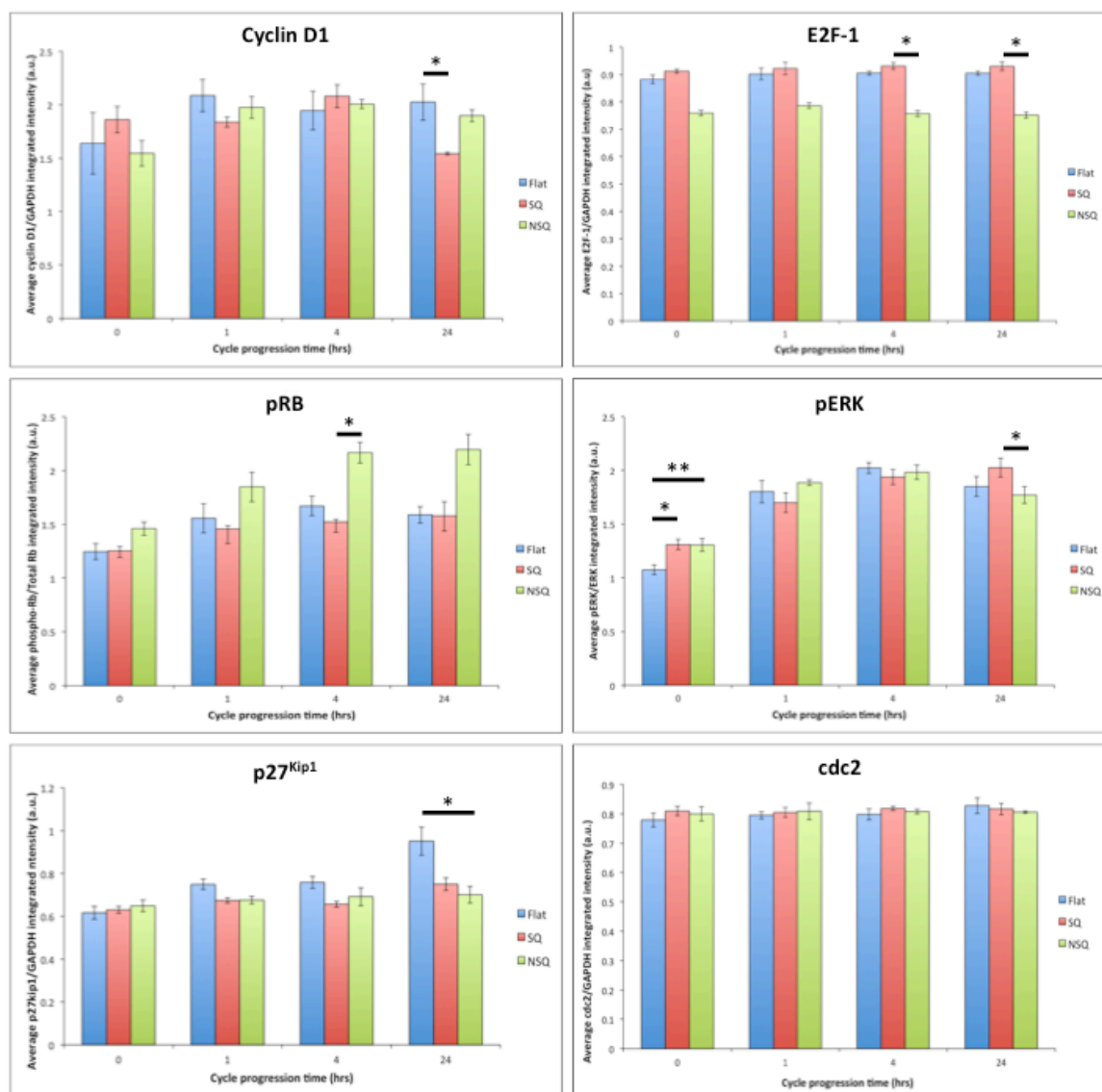


Figure 4-4: Levels of cell cycle proteins assessed in synchronised MSCs on nanotopography. Quantification of candidate cell cycle proteins was achieved using ICW techniques. Bars denote average integrated intensities of at least 4 material replicates, normalised to either GAPDH or the total levels of equivalent protein if the phosphorylated form was stained, and error bars represent \pm standard error of the mean. Values are expressed in arbitrary fluorescence units (a.u.). Blue = flat, red = SQ and green = NSQ. Comparison of protein levels on each type of surface revealed some significant differences at specific timepoints. Statistical significance was tested by Kruskal-Wallis test with Dunn's multiple comparisons post-test for each timepoint. * $p < 0.05$, ** $p < 0.01$.

The CDK6 family of proteins appeared to be potentially interesting, as total CDK6 levels were elevated in MSCs cultured on SQ in comparison to flat and NSQ, and levels remain elevated throughout the 24 hours post-release after synchronisation (Figure 4-5).

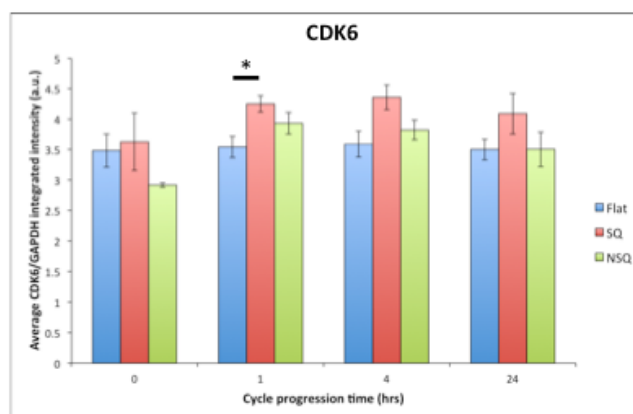


Figure 4-5: Elevated CDK6 protein levels observed on SQ. Quantification of was achieved using ICW techniques. Bars denote average integrated intensities of at least 4 material replicates, normalised to either GAPDH and error bars represent \pm standard error of the mean. Values are expressed in arbitrary fluorescence units (a.u.). Blue = flat, red = SQ and green = NSQ. CDK6 was found to be highest on SQ after 1 hour of culture (post-release into the cell cycle following synchronisation). Statistical significance was tested by Kruskal-Wallis test with Dunn's multiple comparisons post-test for each timepoint. * $p < 0.05$

4.2.4 Analysis of cell cycle stages on SQ using flow cytometry

Flow cytometry allows depiction of the percentage of cells in the phases of the cell cycle. This was carried out for MSCs cultured on SQ and flat substrates following synchronisation (Figure 4-6). Comparison between MSCs on the two surfaces revealed a higher number of cells in G0/G1 phase and a subsequent decrease in S phase. These patterns were found to be reproducible with MSCs isolated from another patient, though patient 2 showed a higher percentage of cells in G2/M phase in comparison to the flat control (Figure 4-7).

The observed trend in G1/G0 and S phases are suggestive of a slower progression through the cell cycle. The effect of SQ nanotopography does not appear to be to induce a complete block as there are still cells found in the latter G2/M stages, and thus these MSCs do not exhibit a pattern indicative of quiescence. This ties in with our hypothesis: that MSCs continue to divide and self-renew on SQ whilst maintaining multipotency, and shows that the time they spend in cell cycle phases is slightly different even though this does not necessarily dramatically affect their overall growth and proliferation.

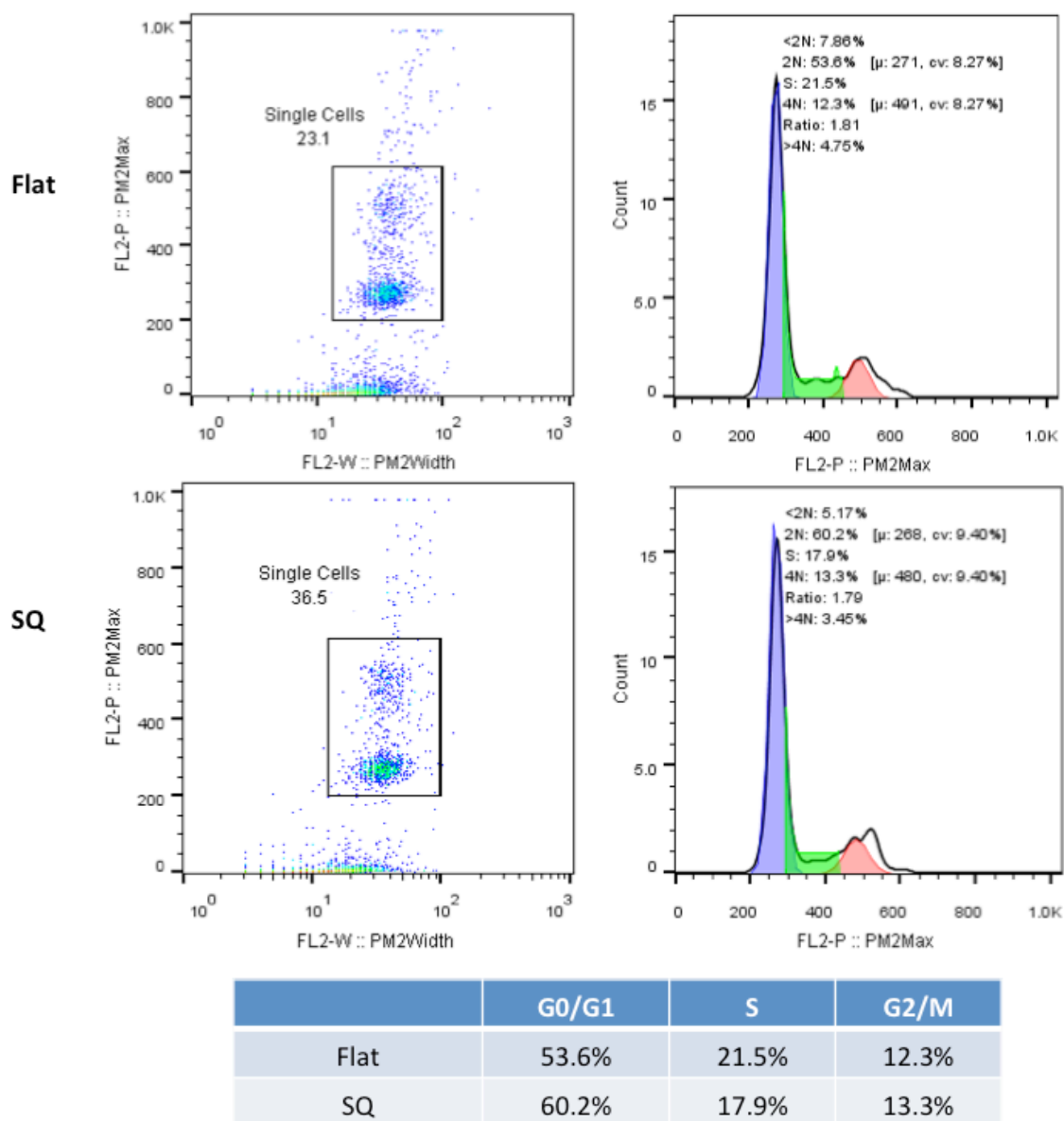


Figure 4-6: Elevated percentage of G0/G1 MSCs observed on SQ (patient 1). Synchronised MSCs were released back into the cell cycle for 24 hours on SQ or a flat control (60 material replicates per condition), detached from all surfaces, pooled, stained with propidium iodide and analysed by flow cytometry. Flow cytometry and associated analyses were performed by Dr Maria C. de Andrés González (University of Southampton). The left column of plots shows the gating applied. The gated region indicates the population taken forward for analysis, shown in the right column of plots. The percentage of cells in G0/G1 was elevated and subsequently lower in S phase of the cell cycle on SQ, which is suggestive of MSCs progressing slower through the cycle in comparison to those on flat surfaces. The results highlight some differences that may reflect changes in the time spent in particular cell cycle phases depending on the type of substrate they are cultured on.

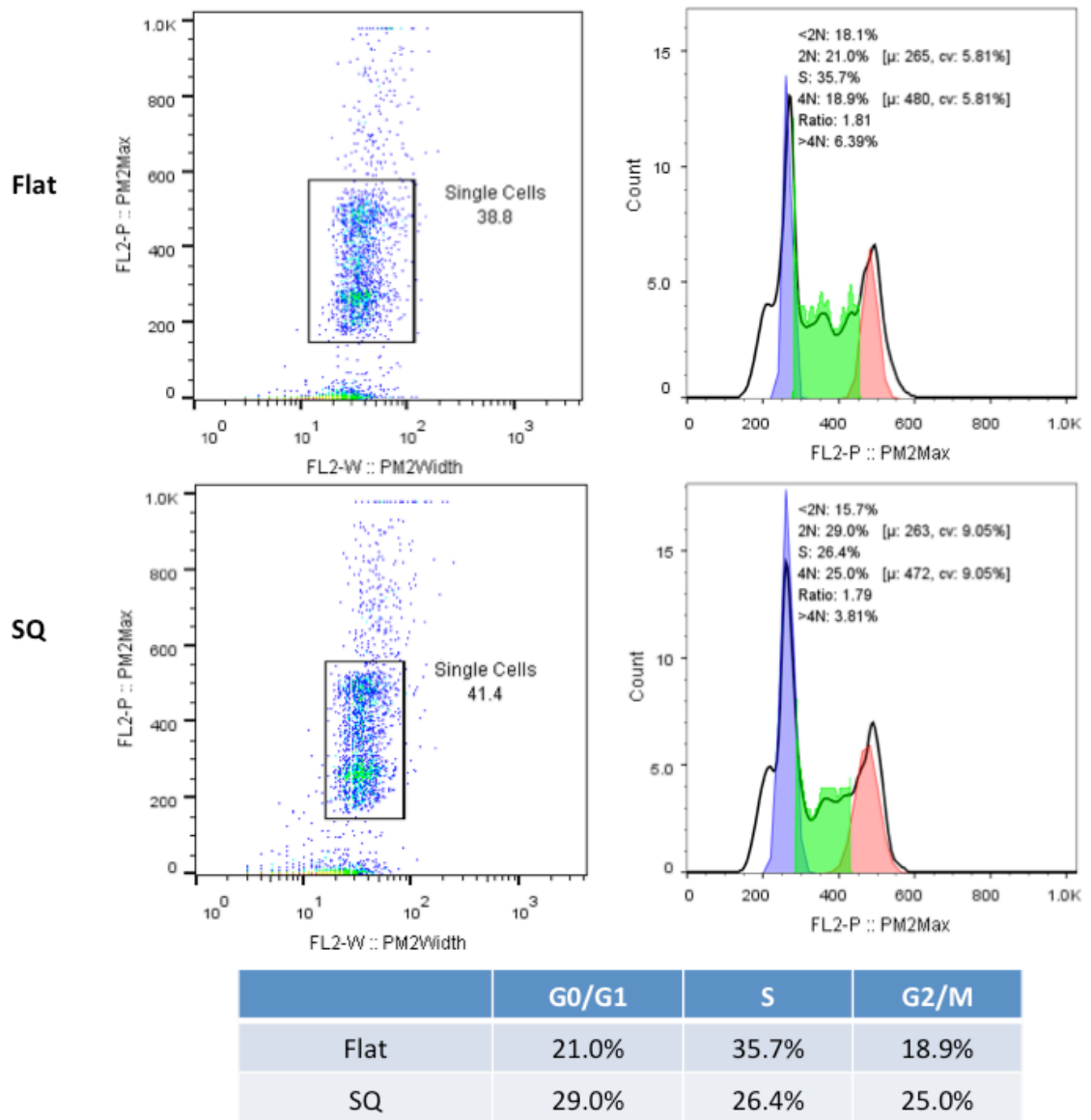


Figure 4-7: Higher percentage of G0/G1 MSCs observed on SQ (patient 2). Synchronised MSCs were released back into the cell cycle for 24 hours on SQ or a flat control (75 material replicates per condition), detached from all surfaces, pooled, stained with propidium iodide, then analysed by flow cytometry. Flow cytometry and associated analyses were performed by Dr Maria C. de Andrés González (University of Southampton). The left column of plots shows the gating applied. The gated region indicates the population taken forward for analysis, shown in the right column of plots. The percentage of cells in G0/G1 was once again elevated and subsequently lower in S phase of the cell cycle on SQ, consistent with patient 1 which is suggestive of MSCs progressing slower through the cycle in comparison to those on flat surfaces. In this patient, there was a higher percentage of MSCs in G2/M on SQ that may account for proliferation being similar on both flat and SQ. The results highlight some differences that may reflect changes in the time spent in particular cell cycle phases depending on the type of substrate they are cultured on.

4.2.5 Observing filopodial spread on nanotopography

There are numerous reports of the role of filopodia in feature sensing on material surfaces in the literature (Biggs *et al.*, 2007a, Hart *et al.*, 2007, Albuschies and Vogel, 2013). We hypothesize that filopodia may undergo changes, perhaps in directionality, or spread as they move across surfaces with differing features on them. Thus, filopodia are ideally placed as initiators of downstream events. In order to investigate this possibility, the spread and directionality of filopodia were observed using SEM (*Figure 4-8 to Figure 4-11*).

Synchronised MSCs did not show much difference in filopodia between surfaces (*Figure 4-8*). Filopodia were observed on flat, SQ and NSQ and were not restricted in their spreading. Interestingly, filopodia on SQ were able to elongate in the spaces between ‘rows’ of pits, and were perhaps restricted by the pits on either side. This behaviour is reminiscent of the effect of grooves, and can be described as a type of ‘contact guidance’ (*Figure 4-9, Figure 4-10, Figure 4-11, central panels corresponding to SQ*). In contrast, filopodia on the flat and NSQ surfaces were more randomly arranged (*Figure 4-9, Figure 4-10, Figure 4-11, lower panels corresponding to NSQ*). Filopodia on flat had no restrictive cues and it would be expected that filopodia would be able to spread in all directions (*Figure 4-9, Figure 4-10, Figure 4-11, uppermost panels corresponding to flat*). On NSQ, the filopodia were also able to grow across the pits (*Figure 4-9, Figure 4-10, Figure 4-11, lower panels corresponding to NSQ*), which could be partially due to the reduced spacing between some of them, as a result of the small offset of the pattern.

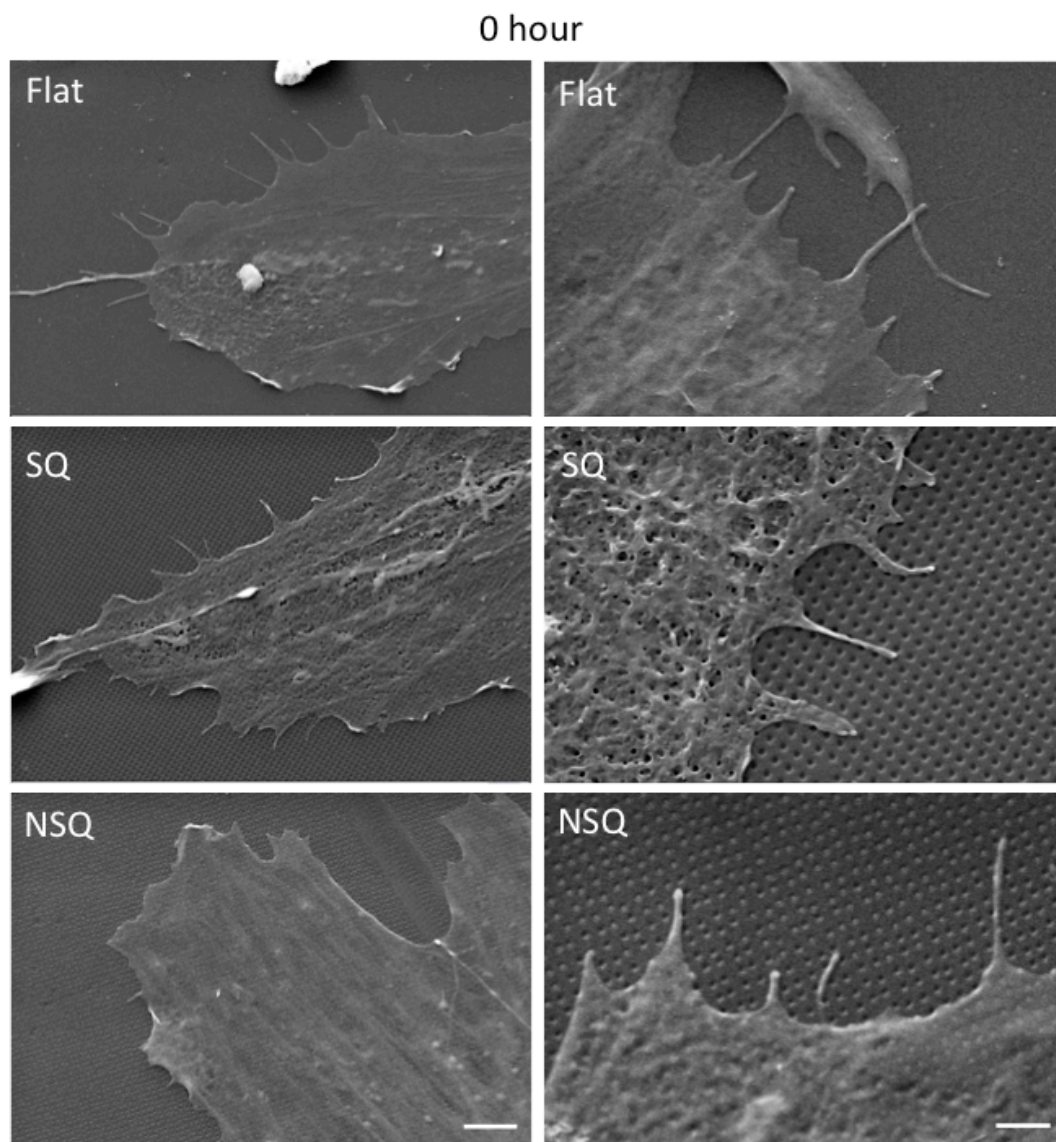


Figure 4-8: Filopodia observed in MSCs following synchronisation. Representative SEM images of MSCs on all surfaces (flat, SQ, NSQ) immediately following synchronisation on nanotopography. Cells were fixed after synchronisation, and imaged after completion of SEM sample processing. The images show that filopodia are present on all substrates. The three panels to the left of each set are images taken at 10,000x magnification, and the three panels to the right of each set are images taken at 30,000x magnification. Left side panels scale bar: 3 μm . Right side panels scale bar: 1 μm . Images were acquired with assistance from Peter Chung (University of Glasgow).

1 hour

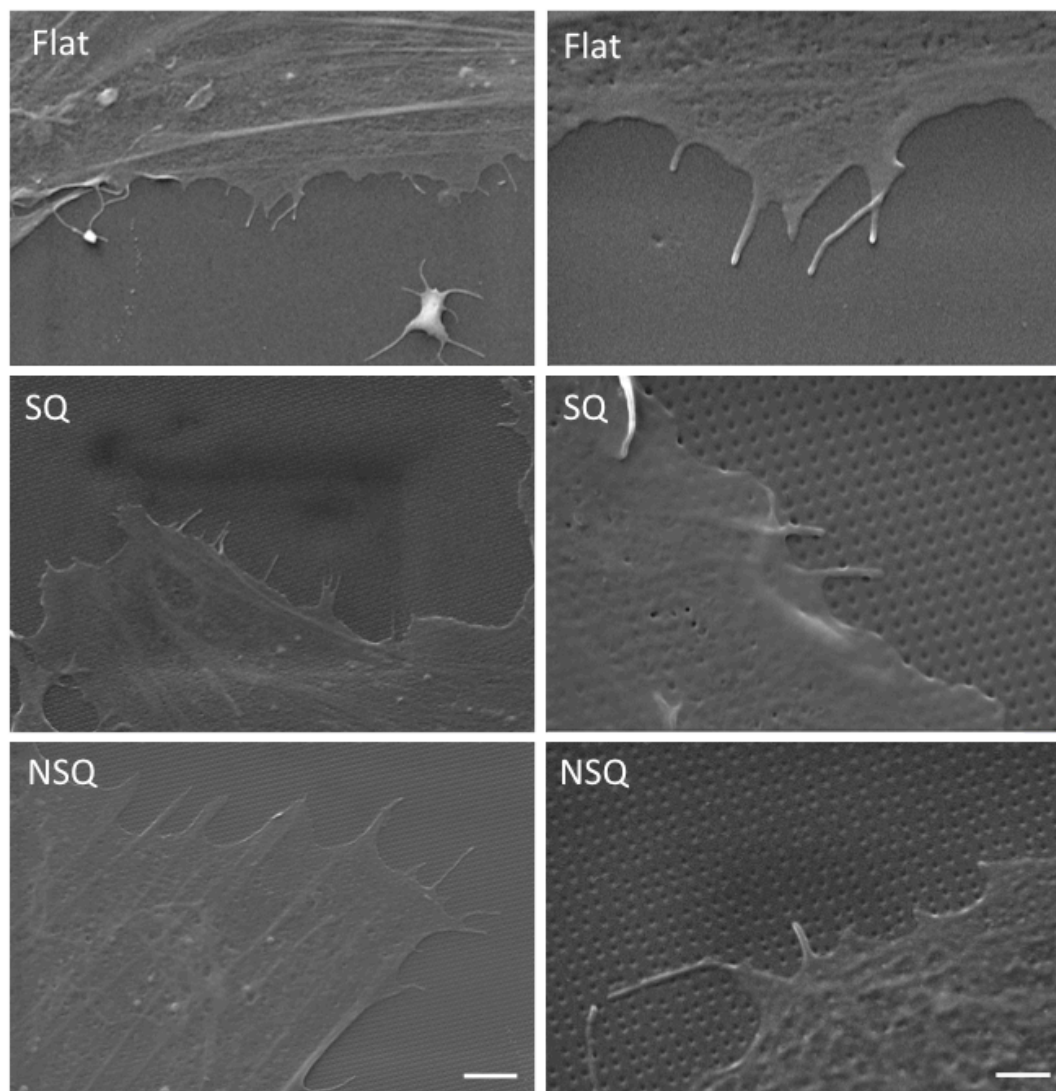


Figure 4-9: Distribution of filopodia after 1 hour release into the cell cycle. Representative SEM images of synchronised MSCs across surfaces (flat, SQ, NSQ) after 1 hour release into the cell cycle. Cells were fixed, and imaged after completion of SEM sample processing. At this stage, filopodia are still present on all surfaces, however there are indications that those on SQ exhibit contact guidance behaviour, and follow the flat spaces between rows of pits. The three panels to the left of each set are images taken at 10,000x magnification, and the three panels to the right of each set are images taken at 30,000x magnification. Left side panels scale bar: 3 μm . Right side panels scale bar: 1 μm . Images were acquired with assistance from Peter Chung (University of Glasgow).

4 hour

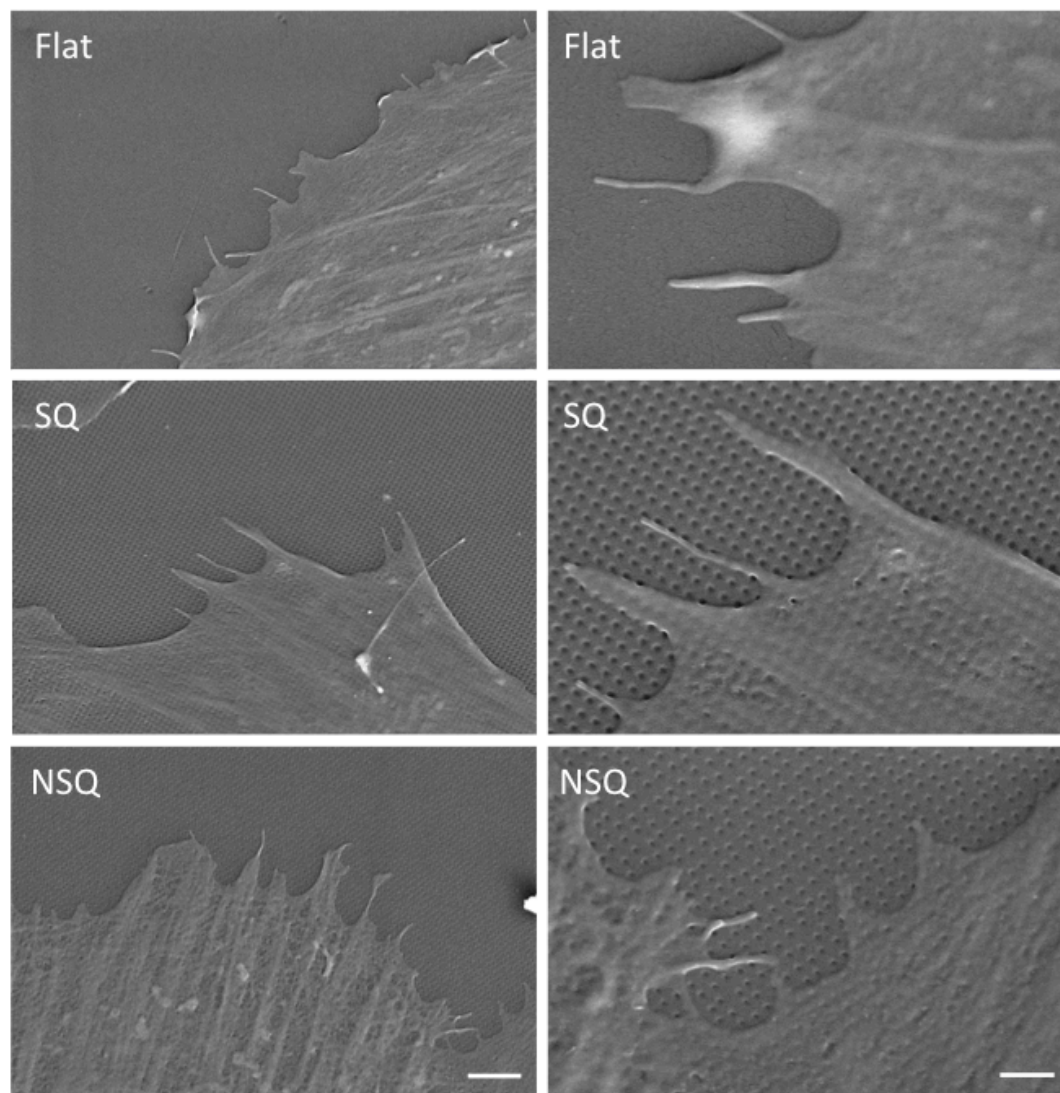


Figure 4-10: Distribution of filopodia after 4 hours release into the cell cycle. Representative SEM images of synchronised MSCs across surfaces (flat, SQ, NSQ) after 4 hours release into the cell cycle. Cells were fixed, and imaged after completion of SEM sample processing. At this timepoint, it is more apparent that contact guidance is only observed on SQ, and that filopodia on flat and NSQ are randomly spread. The three panels to the left of each set are images taken at 10,000x magnification, and the three panels to the right of each set are images taken at 30,000x magnification. Left side panels scale bar: 3 μm . Right side panels scale bar: 1 μm . Images were acquired with assistance from Peter Chung (University of Glasgow).

24 hour

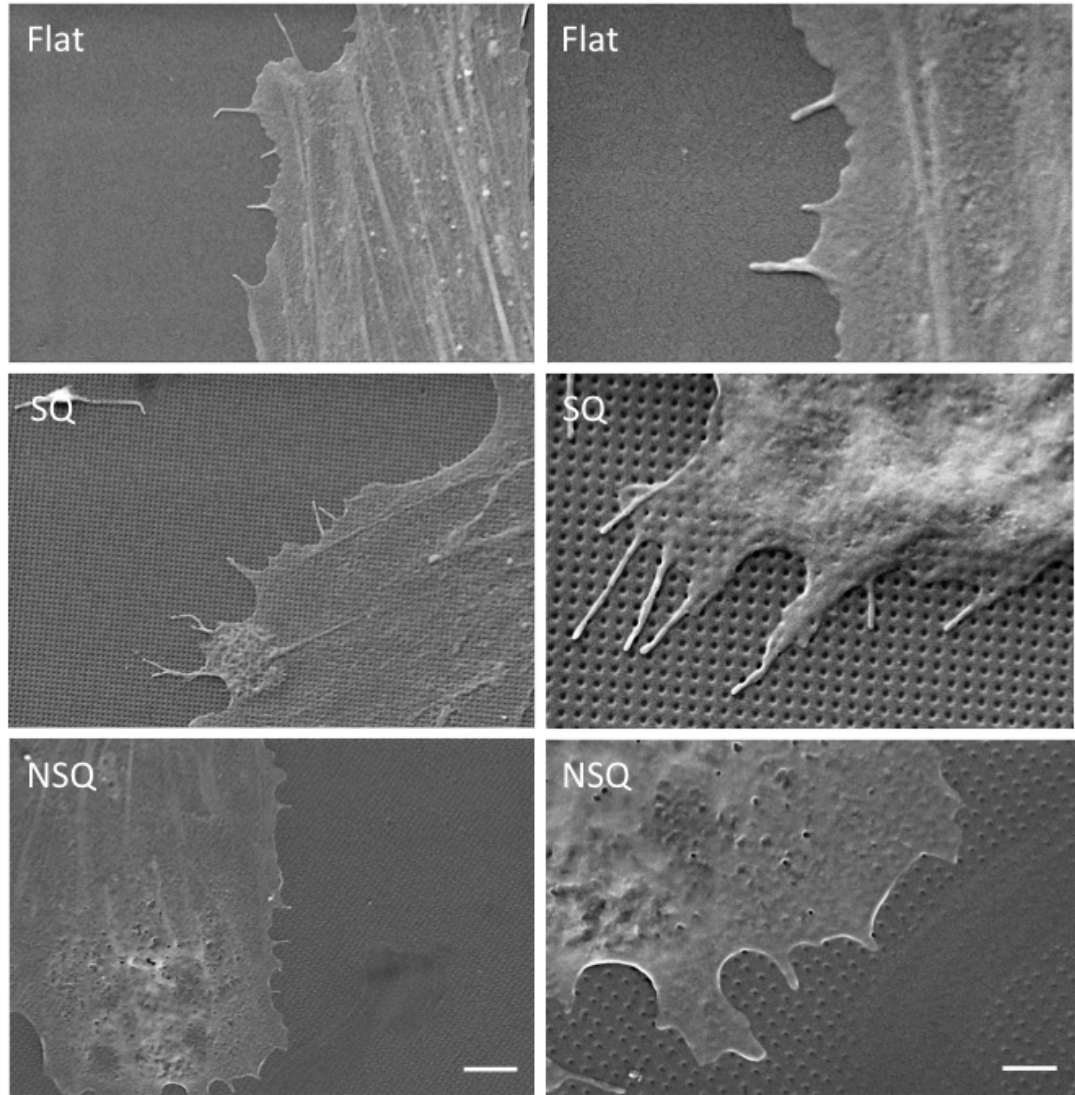


Figure 4-11: Distribution of filopodia after 24 hours release into the cell cycle. Representative SEM images of synchronised MSCs across surfaces (flat, SQ, NSQ) after 24 hours release into the cell cycle. Cells were fixed, and imaged after completion of SEM sample processing. At this timepoint, once again, contact guidance is only observed on SQ, and filopodia on flat and NSQ spread in all directions. The three panels to the left of each set are images taken at 10,000x magnification, and the three panels to the right of each set are images taken at 30,000x magnification. Left side panels scale bar: 3 μm . Right side panels scale bar: 1 μm . Images were acquired with assistance from Peter Chung (University of Glasgow).

4.2.6 Chemical inhibition of filopodia development

Filopodial formation and development is under the control of several genes, one of which is *cdc42*. In order to disrupt filopodial mechanics, a chemical inhibitor of *cdc42* was incorporated into the maintenance media added to the MSCs, to assess the importance/influence of filopodia on intracellular signalling events related to cell cycle regulation.

The inhibitor was initially tested at a range of concentrations after allowing a short period of attachment and time for the establishment of filopodia. Concentrations of 40 μM and above caused cells to detach and die and were not imaged. Qualitative observation of cells (*Figure 4-12*) exposed to inhibitor concentrations of 10-20 μM indicated that the number of filopodia decreased and generally became shorter as the concentration of inhibitor increased, with the optimal concentration being 20 μM . Further observations at this proposed optimal inhibitor concentration were achieved with SEM (*Figure 4-13*), showing that filopodial formation was not impeded entirely in MSCs. However, drawing parallels with the observations of images taken at lower magnifications, the number and length of filopodial protrusions were somewhat inhibited.

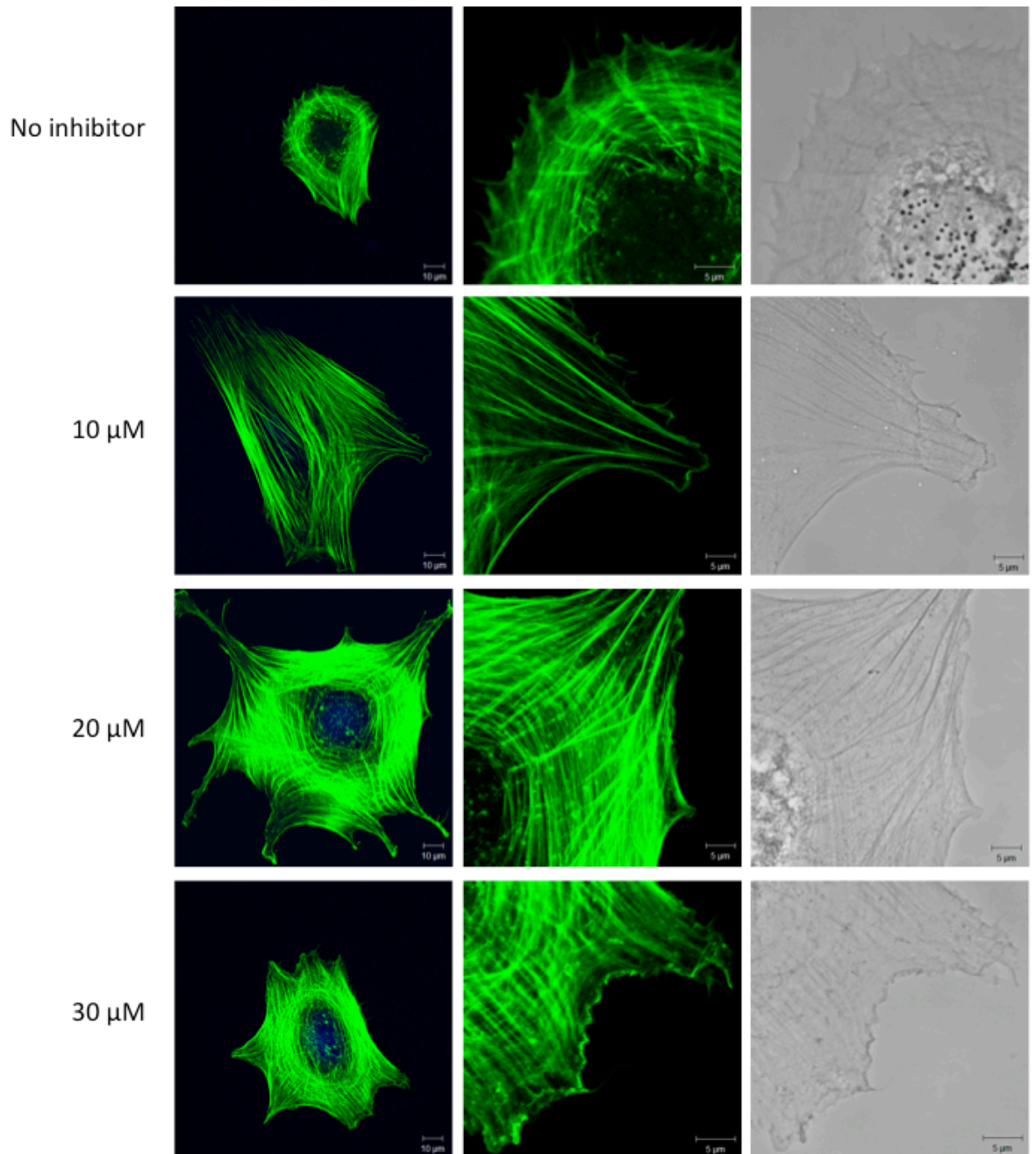


Figure 4-12: Chemical inhibition of filopodia in MSCs. Confocal images of MSCs treated with *cdc42* inhibitor at the outlined concentrations and immunostained to visualise actin and cell nuclei. Images are representative of cells cultured at each concentration. The first panel of each row shows a merged image of a cell (scalebar = 10 μm), the second panel shows an enlarged region within the cell, and the third panel shows a brightfield transmission image of the magnified area (scalebar = 5 μm). All images were taken at 63x magnification. Results indicate that a concentration of 20 μM begins to prevent spreading of filopodia.

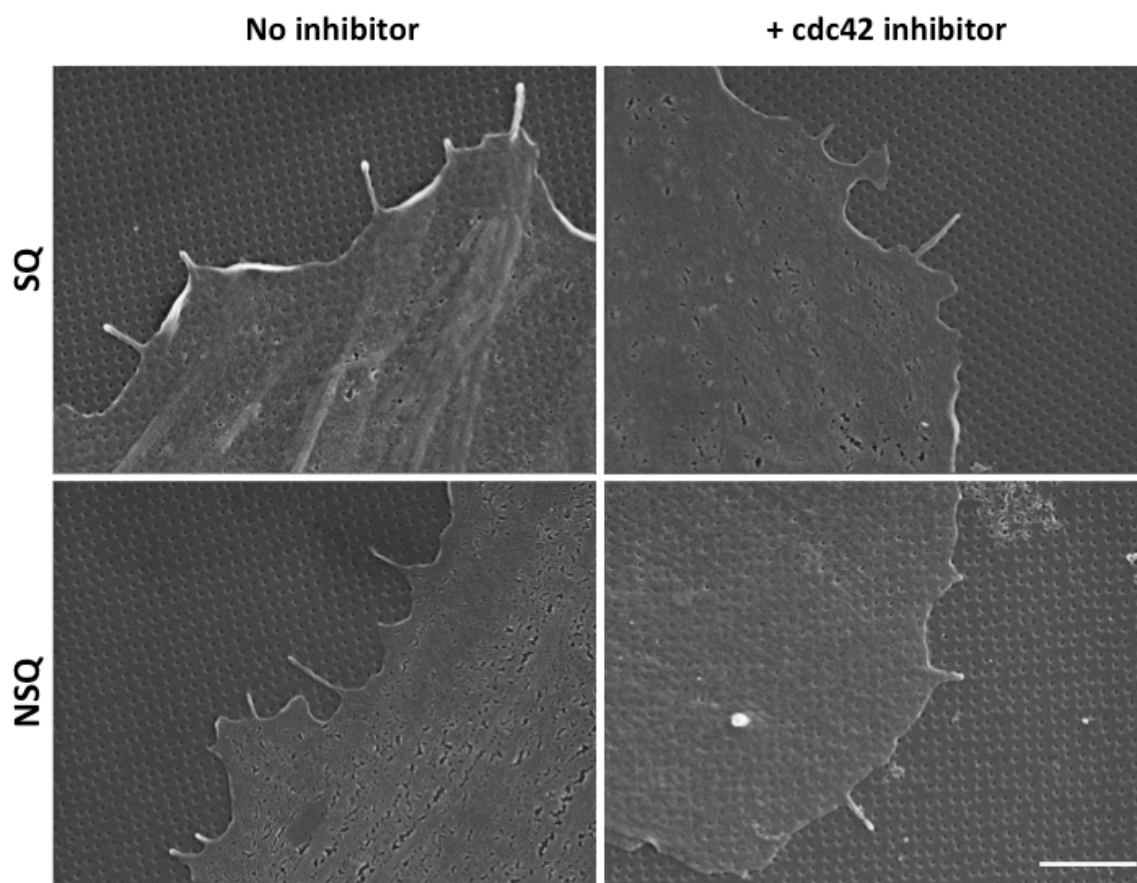


Figure 4-13: Effect of 20 μM *cdc42* inhibitor on filopodial spread on nanotopography. SEM images of MSCs cultured on SQ and NSQ, focusing on edges of the cell that show formation of filopodia. The panels on the left show representative images of controls that did not have any inhibitor added to the culture media. The panels on the right are representative of MSCs that had 20 μM of *cdc42* inhibitor added during their culture. Addition of the inhibitor appeared to reduce the number of filopodia and the length of the extensions. Scale bar: 2 μm .

The inhibitor concentration of 20 μM was taken forward and further tested in experimental conditions, adding the inhibitor to media for the 24 hour incubation period following synchronisation.

4.2.7 Assessment of filopodia inhibition on CDK6 protein expression

Upon successful filopodial inhibition, the next step was to assess the importance of the different filopodial spreading patterns observed on SQ and NSQ, in the eventual expression of cell cycle regulating proteins. Initial work focused on levels of CDK6, as it was a protein that was found to be elevated on our self-renewing surface by ICW. Together with the observation that filopodia on SQ responded to contact guidance cues from the topography itself, there was the

potential that these physical constraints on the cell cytoskeleton might be an initiating event for changes in signalling downstream. Addition of the inhibitor for 24 hours did not have an impact on CDK6 protein levels on SQ; indeed, abundance of CDK6 was relatively similar for flat and SQ even without the addition of the inhibitor (Figure 4-14). This is in contrast with initial observations that there was a trend for CDK6 to be elevated on SQ. It is possible that in waiting to allow sufficient filopodia inhibition, we have missed the early changes occurring within a few hours after release into the cell cycle. Alternatively, this inhibition strategy is not sufficient to prevent formation of filopodia, and thus may mask some of the changes in protein expression so that they were not observed here.

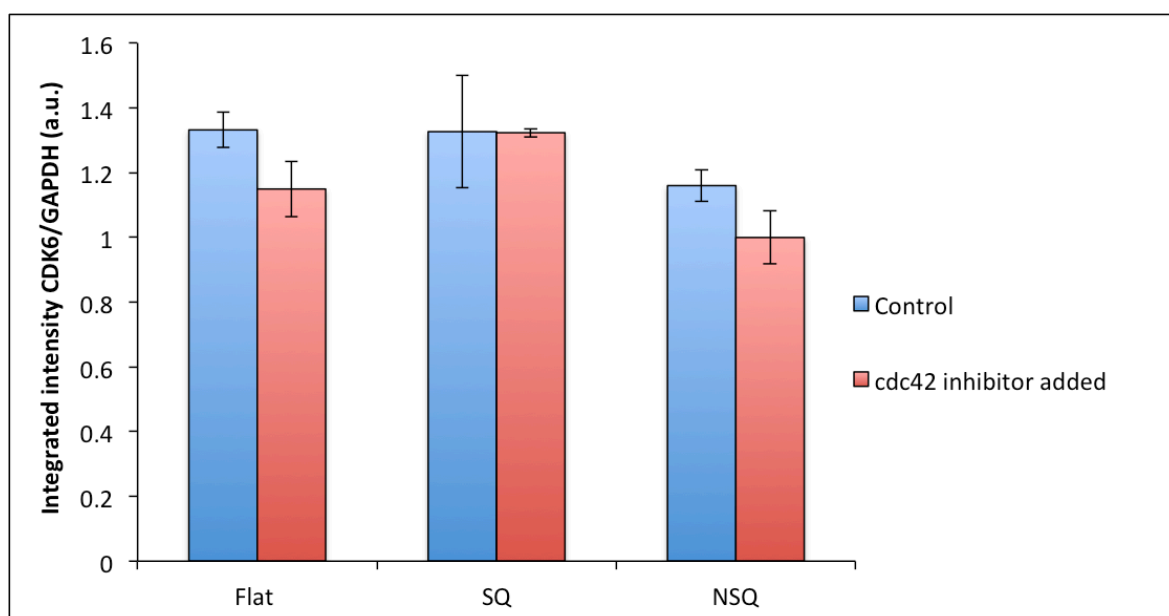


Figure 4-14: CDK6 is not affected in MSCs subjected to cdc42 inhibition. ICW results (ratio of CDK6 and GAPDH integrated intensities expressed in arbitrary fluorescence units) show no significant differences (assessed by unpaired t-test) in CDK6 protein levels between control cells and inhibited cells on each surface. Each bar represents the average integrated intensity ratio of at least 3 technical replicates. Blue bars denote controls and red bars denote inhibited samples. Error bars denote \pm standard error of the mean.

4.2.8 Identifying signalling networks using Next-Generation Sequencing

To add to the information gathered about changes occurring on specific nanotopographies, RNA was extracted from cells that had been synchronised and released into the cycle for 24 hours, and submitted for Next-Generation Sequencing (NGS). Ingenuity Pathway Analysis was utilised to investigate changes

in expression of detected genes for each sample, making use of existing databases to link changes in transcript abundance to known gene regulatory networks.

4.2.8.1 Gene expression in synchronised cells on nanotopographies

Pairwise comparisons of the flat control to each of the nanotopographies directly after synchronisation yielded small numbers of changes, as would be expected in low serum conditions. There were 90 transcript identifiers and abundances accepted for analysis in the SQ comparison and 279 transcript identifiers and abundances accepted for analysis in the NSQ comparison. Pathway analysis of differentially expressed genes showed that trends in functional pathway categories (*Figure 4-15*) were generally similar, with the top pathway on both SQ and NSQ falling into the cell cycle category, presumably due to the highly regulated checks on cell cycle progression preventing cells from progressing past G1 phase in unfavourable conditions. Since it has been shown that stem cell marker expression can be high on NSQ, this indicates the presence of a self-renewing population on this surface too. Therefore it would be expected that cell cycle regulation would be highlighted on NSQ in addition to SQ. The number of indicated pathways and upregulated transcripts were greater on NSQ in comparison to SQ (*Figure 4-16 and Figure 4-17*). Many of these biological processes were indeed related to cell cycle. Although some cell cycle activity was apparent here, evidenced by upregulation of genes related to transcripts in the outlined groupings, the percentage of genes inferred from the dataset that were found in the networks were relatively low.

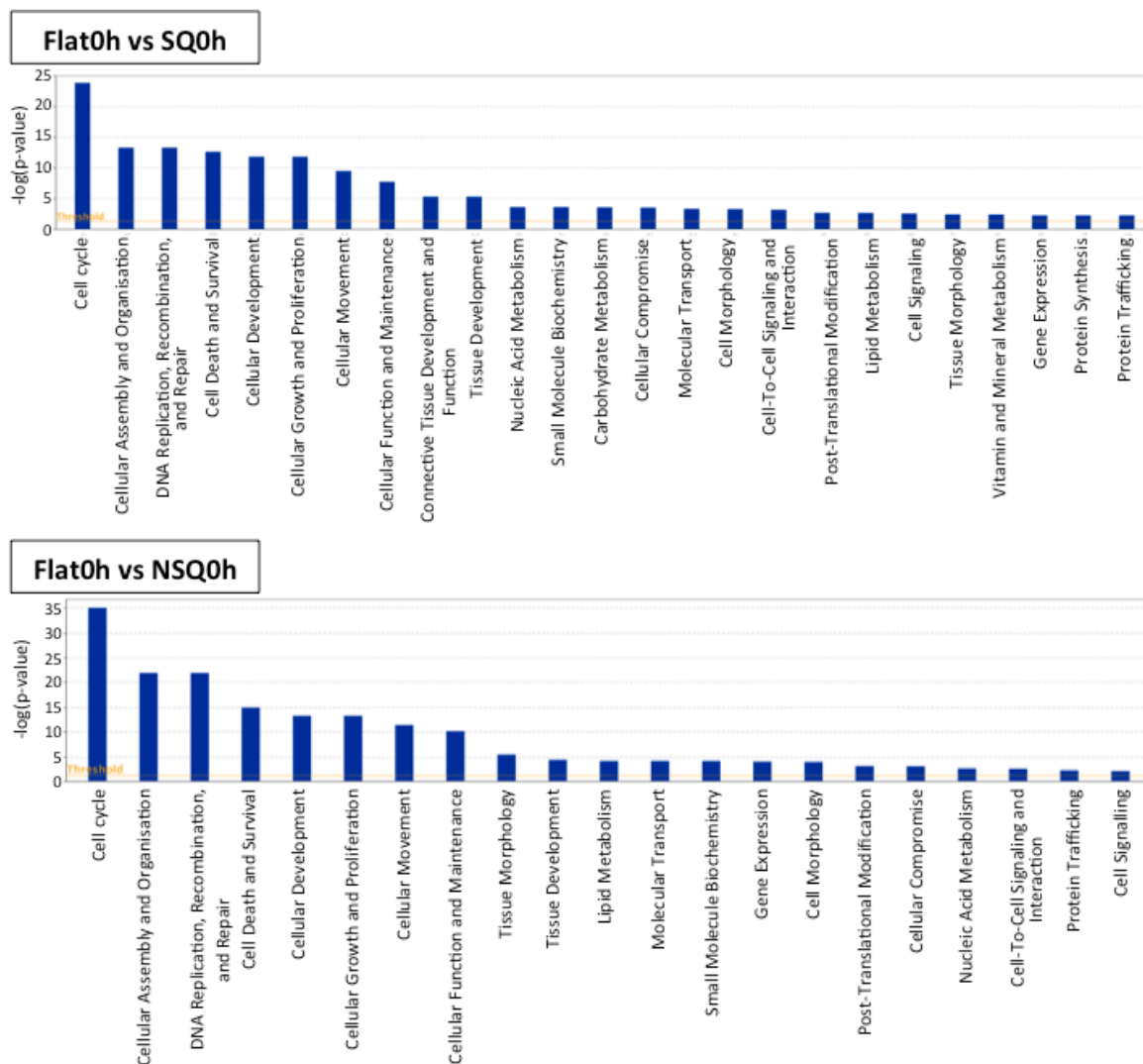


Figure 4-15: Downstream effects analysis of differentially expressed genes in synchronised MSCs cultured on nanotopography. Data generated from NGS was uploaded to IPA software and categorised into functional groupings of expected causal effects derived from literature compiled in the Ingenuity® Knowledge Base. Bar charts shown are for synchronised MSCs, with those cultured on SQ and NSQ nanotopographies compared to flat controls in each instance. The significance threshold applied is represented by the orange line. Significance was calculated using Fischer's exact test (right tailed) in IPA. Taller bars equate to increased significance. The threshold was set at $p < 0.05$.

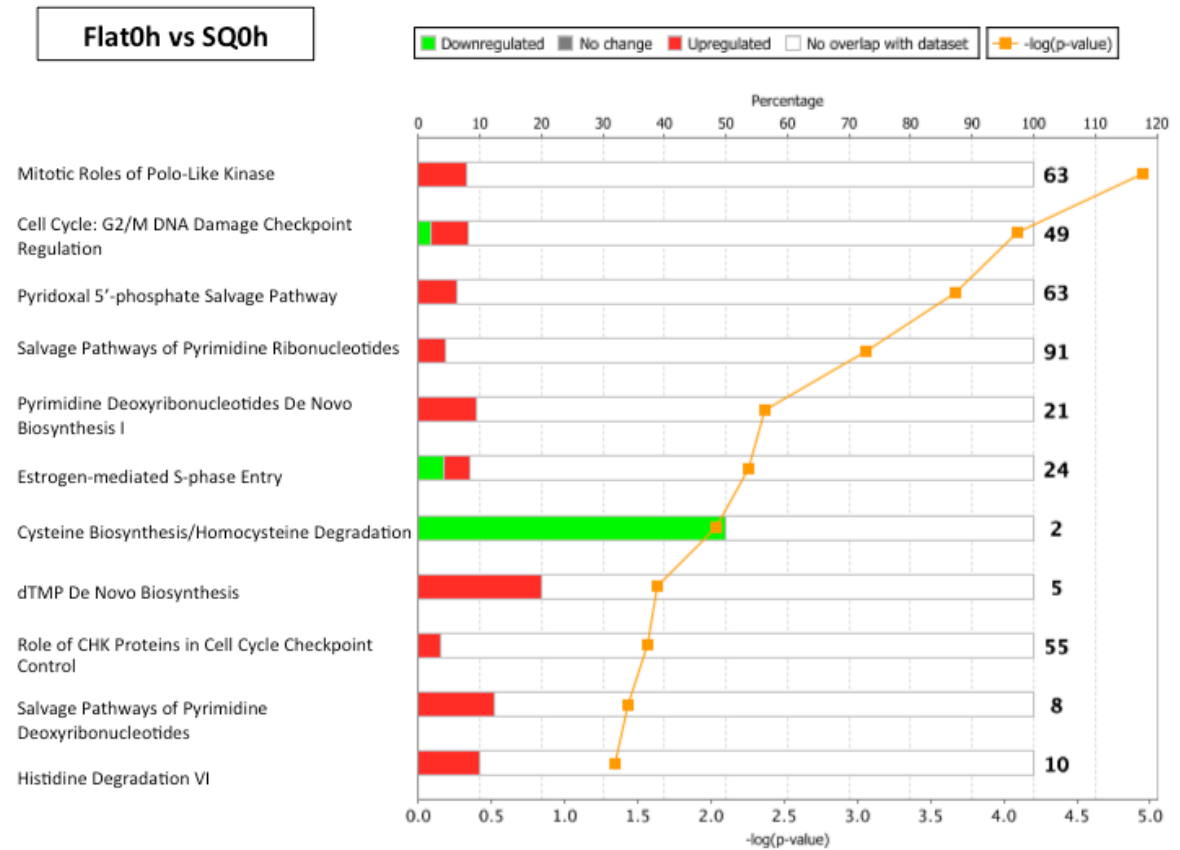


Figure 4-16: Upregulations and downregulations of signalling processes in synchronised MSCs cultured on SQ nanotopography. The number of upregulated and downregulated genes relating to transcripts in each of the named pathways are displayed in red (up) and green (down). A small number of canonical signalling pathways were detected on SQ that were mostly upregulations. A cutoff $-\log(p\text{-value})$ of 1.3 was applied here, thus only pathways with a p value less than 0.05 are shown.

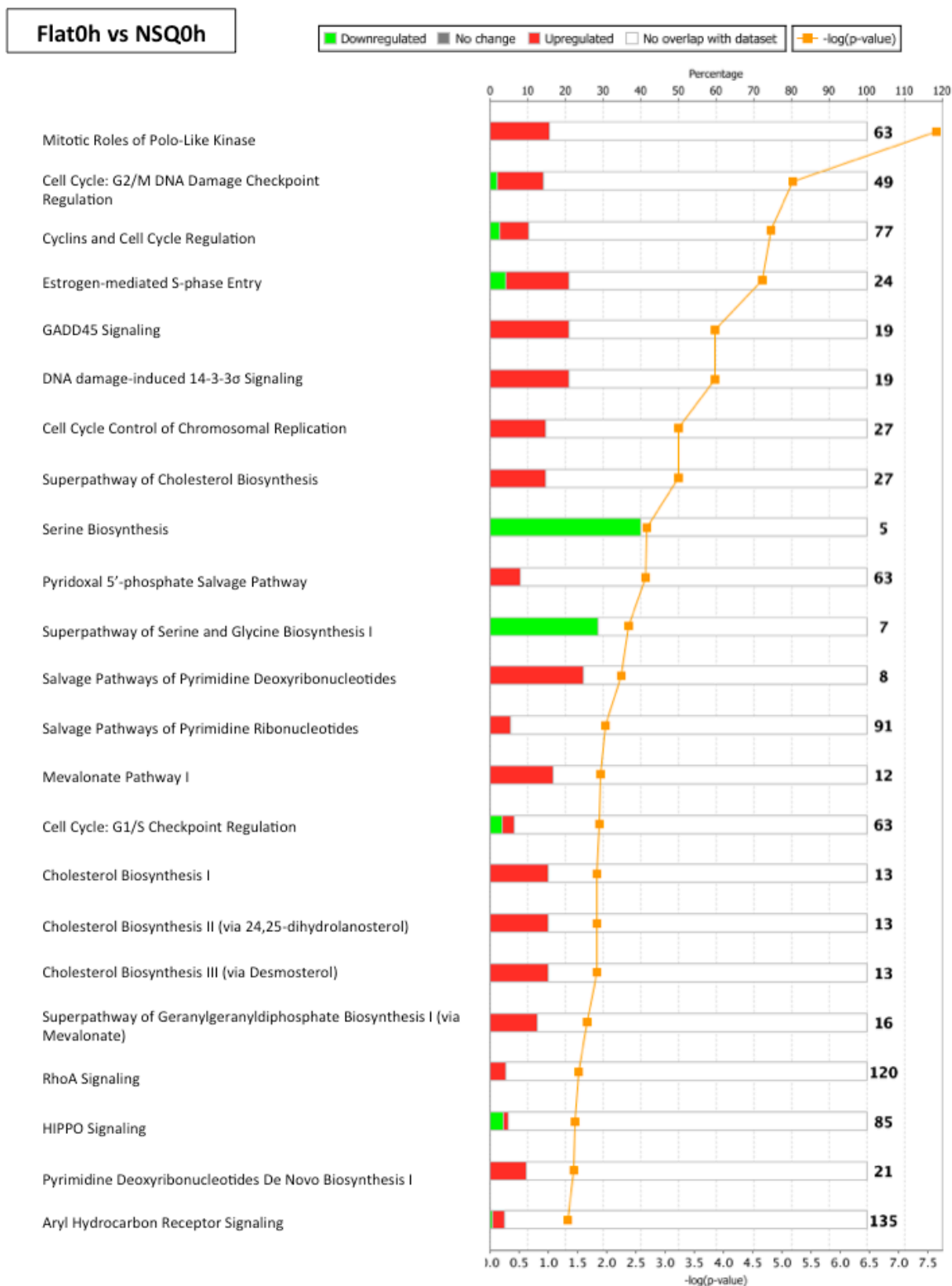


Figure 4-17: Upregulations and downregulations in signalling processes in synchronised MSCs cultured on NSQ nanotopography. The number of upregulated and downregulated genes in each of the named pathways are displayed in red (up) and green (down). A greater number of canonical signalling pathways were detected on NSQ than SQ, though exhibited a similar trend of mostly upregulations. A $-\log(p\text{-value})$ cutoff of 1.3 was applied here, thus only pathways with a p value less than 0.05 are shown.

4.2.8.2 Gene expression changes post-release into cell cycle

The next timepoint investigated was following release of MSCs into the cycle for a period of 24 hours. Several of the same functional signalling groups appeared for both SQ and NSQ, such as cellular growth and proliferation, gene expression, cell cycle, cellular assembly and organisation (Figure 4-18).

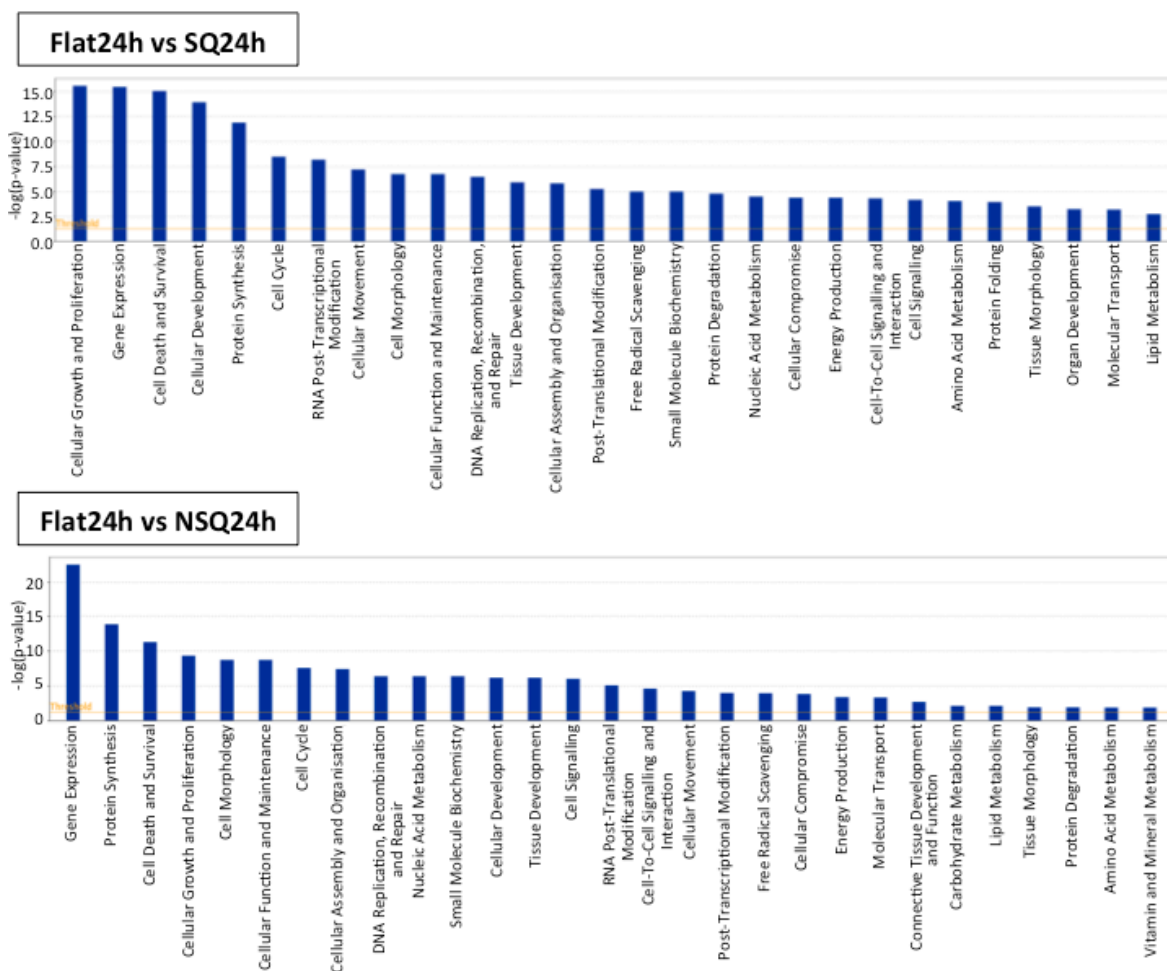


Figure 4-18: Downstream effects analysis of differentially expressed genes in MSCs released into cell cycle for 24 hours on nanotopography. Data generated from NGS was uploaded to IPA software and categorised into functional groupings of expected causal effects derived from literature compiled in the Ingenuity® Knowledge Base. Bar charts shown are for synchronised MSCs released into cell cycle for 24 hours, with those cultured on SQ and NSQ nanotopographies compared to flat controls in each instance. The threshold applied is represented by the orange line. Significance was calculated using Fischer's exact test (right tailed) in IPA. Taller bars equate to increased significance.

However, there were suggestions of differences in the number of genes in each dataset and their expression levels, and thus, further analyses were performed on both datasets. Breakdown of these broad canonical signalling groups into upregulations and downregulations showed that upon progression of MSCs through the cell cycle after synchronisation, a large majority of MSC genes were

downregulated on SQ (*Figure 4-19*). A similar trend was observed on NSQ in terms of most pathways exhibiting downregulations, however, there were more canonical signalling pathways containing up-regulated gene expression in comparison to SQ (*Figure 4-20 and Figure 4-21*). This could be due to a heterogeneous population, containing renewing and differentiating MSCs on NSQ.

It was interesting to note that oxidative phosphorylation appeared to be downregulated to a greater extent on SQ (first bar of *Figure 4-19*) than NSQ (second bar of *Figure 4-20*) at this timepoint, supporting metabolomic data from chapter 3 and existing literature that proposes a decrease in oxidative bioenergetic processes favouring self-renewal (Yanes *et al.*, 2010). Although reduced transcript abundance levels corresponding to a number of genes involved in oxidative phosphorylation were observed in MSCs on NSQ, a lesser percentage of genes were detected in this pathway grouping in comparison to SQ, suggesting that some of these cells are beginning to undergo a switch to differentiation.

Additional support for the initiation of differentiation on NSQ is the indication of increased differential expression of inositol trisphosphate precursors (*Figure 4-21*) that increase entry of calcium across the plasma membrane (Putney *et al.*, 1989), and thereby intracellular calcium levels. This influx of Ca^{2+} may act to enhance calcium signalling with effects on Runx2 that is important for osteogenic differentiation (Zayzafoon, 2006).

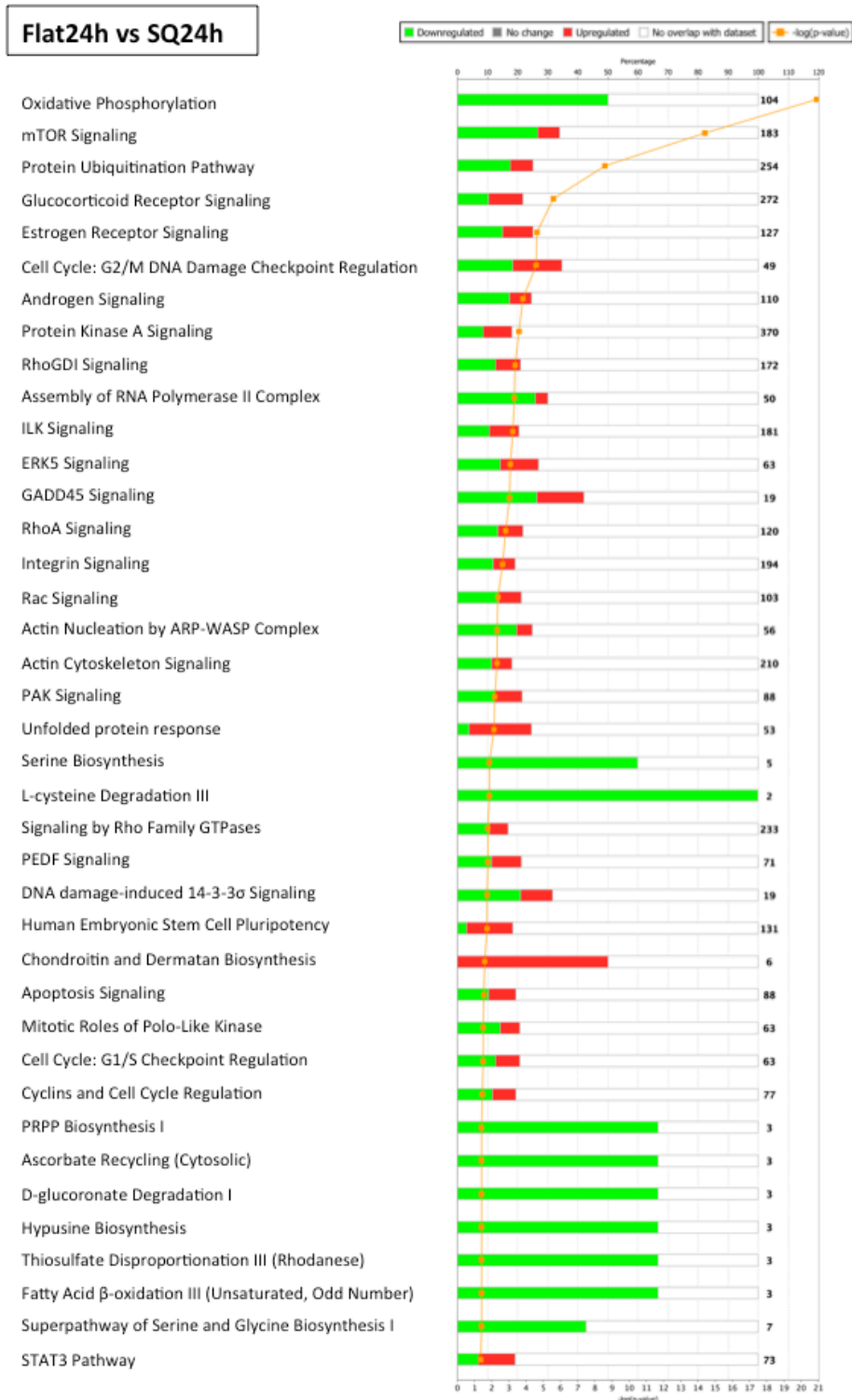


Figure 4-19: Upregulations and downregulations within signaling pathways in MSCs post-release into the cell cycle, cultured on SQ nanotopography. The number of upregulated and downregulated genes in each of the named pathways are displayed in red (up) and green (down). Only pathways with a p value less than 0.05 are shown. The majority of genes are downregulated on SQ after 24 hours, with pathways related to cell cycle, integrin and actin cytoskeleton signalling being highlighted.

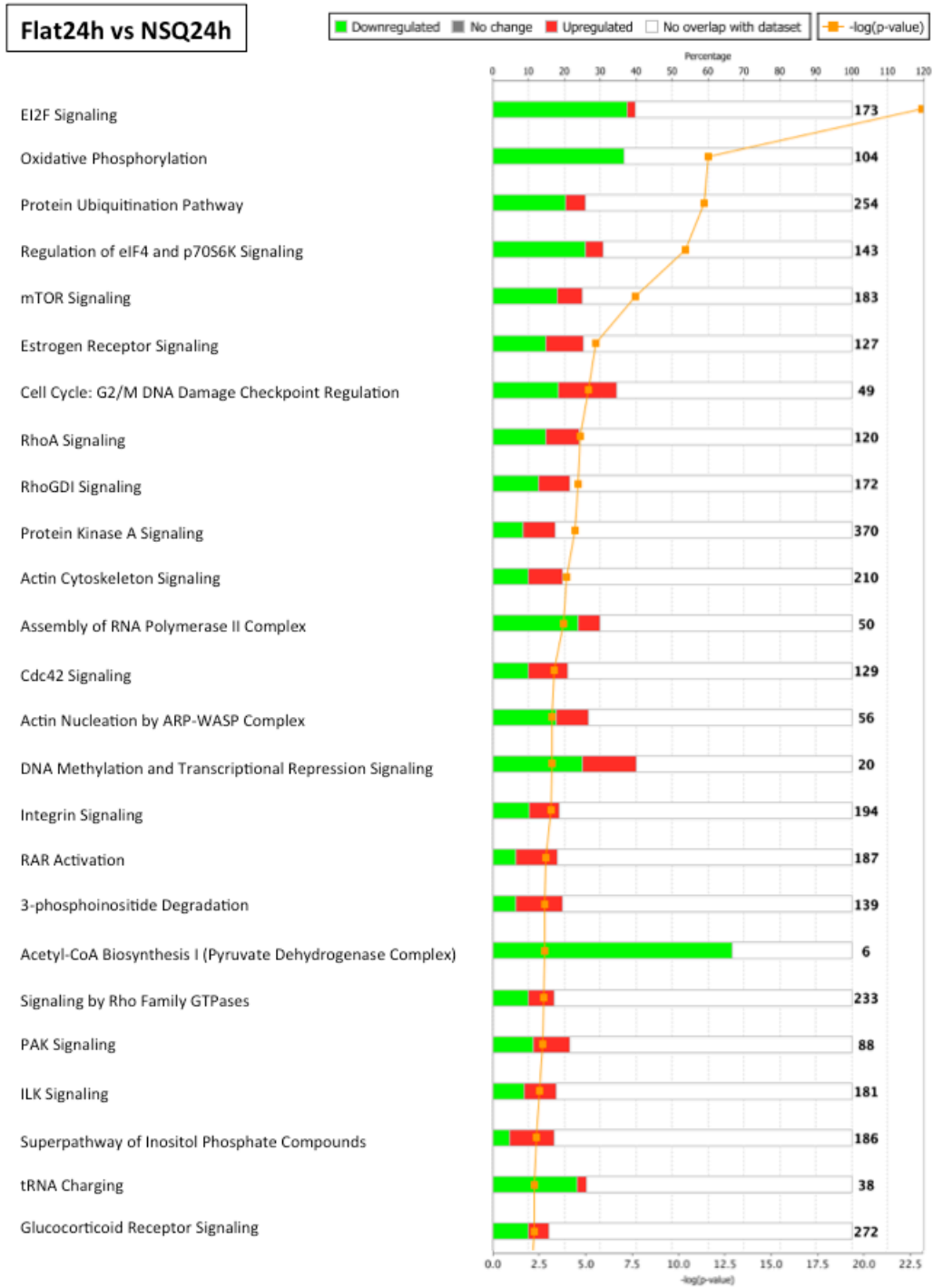


Figure 4-20: Upregulations and downregulations within signalling pathways in MSCs post-release into the cell cycle, cultured on NSQ nanotopography (part 1). The number of upregulated and downregulated genes in each of the named pathways are displayed in red (up) and green (down). Only pathways with a p value less than 0.05 are shown. The NSQ nanotopography induced differential expression of genes involved in more canonical pathways in comparison to SQ. This chart shows the first part of the pathway listing. The majority of genes are downregulated on NSQ after 24 hours, yet there appears to be a greater number of up-regulated genes in comparison to SQ.



Figure 4-21: Upregulations and downregulations within signalling pathways in MSCs post-release into the cell cycle, cultured on NSQ nanotopography (part 2). The number of upregulated and downregulated genes in each of the named pathways are displayed in red (up) and green (down). Only pathways with a p value less than 0.05 are shown. The NSQ nanotopography induced differential expression of genes involved in more canonical pathways in comparison to SQ. This chart shows the second part of the pathway listing. The majority of genes are downregulated on NSQ after 24 hours, yet there appears to be a greater number of upregulated genes in comparison to SQ.

Use of IPA to extrapolate potential phenotypic outcomes (from the transcript data), indicated that a low number of cell cycle-related processes were apparent on SQ after MSCs had been released back into cycle and allowed to progress through each phase. Looking more closely at this data, increases and decreases in differential expression were apparent, with an overall trend towards a decrease in transcript abundance in each case. Adhesion-related signalling processes including RhoA, integrin, Rac, and actin cytoskeleton signalling followed this pattern in a similar way, and were low on SQ.

As more pathway information was available for MSCs released back into the cell cycle, this data was subjected to further analysis, focusing on gene interactions and signalling networks in MSCs on the SQ nanotopography, with some references to those on NSQ. Interpretations of networks deemed to be of particular interest are detailed in the following section.

4.2.8.3 Analysis of interaction networks and pathways

Distinct changes in gene expression in MSCs cultured on SQ and NSQ (in comparison to flat controls) at the later timepoint of 24 hours were classified into networks, and those related to cell cycle and growth were investigated in greater detail. It was noted that *ERK1/2* was found to be downregulated on SQ, which may be important for stem cell renewal (*Figure 4-22*).

With regards to cyclins and cell cycle regulation (*Figure 4-23*), key cyclins (*cyclin D1* and *cyclin B*) and cyclin dependent kinase, (*CDK1*) that are involved in G1 and G2/M phases, were shown to be downregulated on SQ (green). The observation that many negative regulators of the cell cycle were downregulated was not predicted. These included *p21^{Cip1}*, *p19INK4D* and *p18INK4C*. The INK4 family of proteins function to inhibit CDK4 and CDK6 to prevent G1 to S phase transition (Neganova and Lako, 2008).

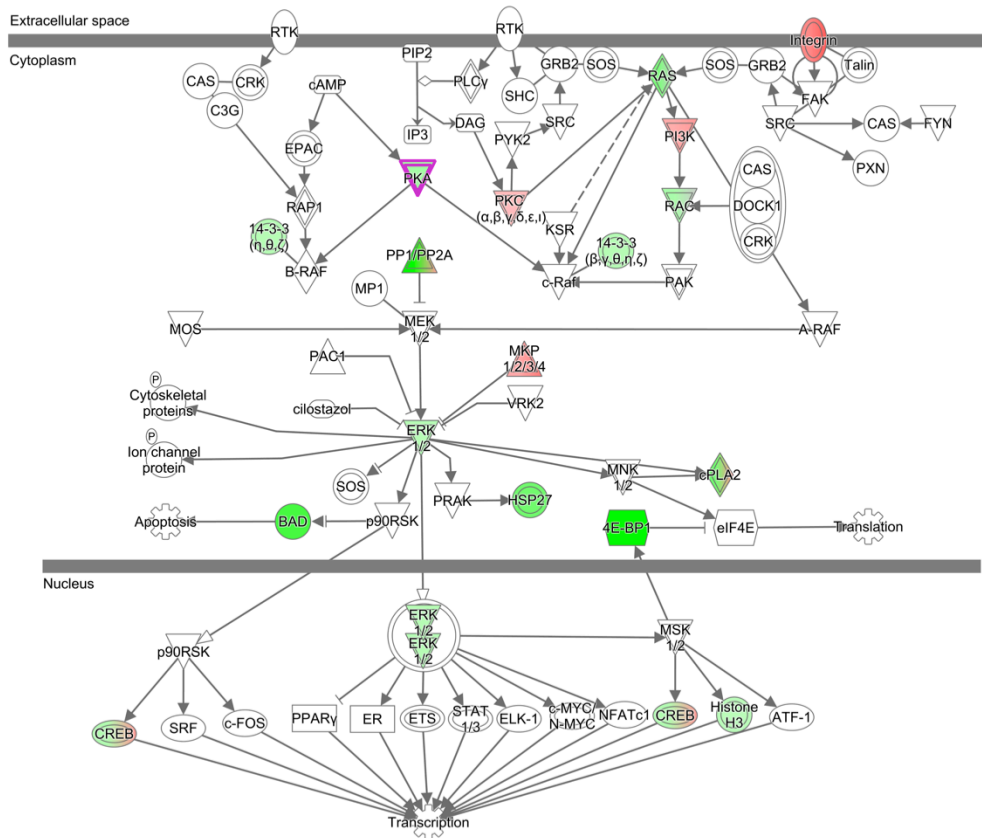


Figure 4-22: ERK/MAPK signalling pathway on SQ nanotopography following release of MSCs into the cell cycle after synchronisation. Identified genes and numerical values corresponding to differential gene expression from the NGS dataset are shown as coloured shapes (downregulated in green and upregulated in red, those displaying two shades of colour contain members that may be differentially regulated). ERK1/2 can be seen as being downregulated (central region in nuclear region and lower central region of cytoplasm), and it is additionally interesting that some element of integrin signalling is being upregulated (top right) on SQ. A two-fold change in abundance threshold was applied.

There is a possibility that other negative regulators that did not pass the threshold criteria are acting to downregulate *cyclin D1* and *CDK4/6*. *Cyclin B* was found to be downregulated on NSQ, together with *CDK7* and *p21^{Cip1}*. This downregulation of the latter two genes could be suggestive of cell cycle progression on NSQ, as *CDK7* has been discussed as being a negative regulator of proliferation (Ganuza *et al.*, 2012). This is at odds with the downregulation of cyclin B activity, which is associated with decreased proliferation. This discrepancy can be explained by considering different subpopulations, with some proliferating (displaying a degree of stem cell retention) and some beginning to transition into differentiation upon reaction to the instructional cues from the NSQ nanotopography.

The *E2F* group of genes encoding transcription factors were shown to be upregulated on both SQ and NSQ, however, IPA did not show any clear

(Figure 4-24), which has downstream effects associated with triggering cell differentiation events in the nucleus (Jaiswal *et al.*, 2000).

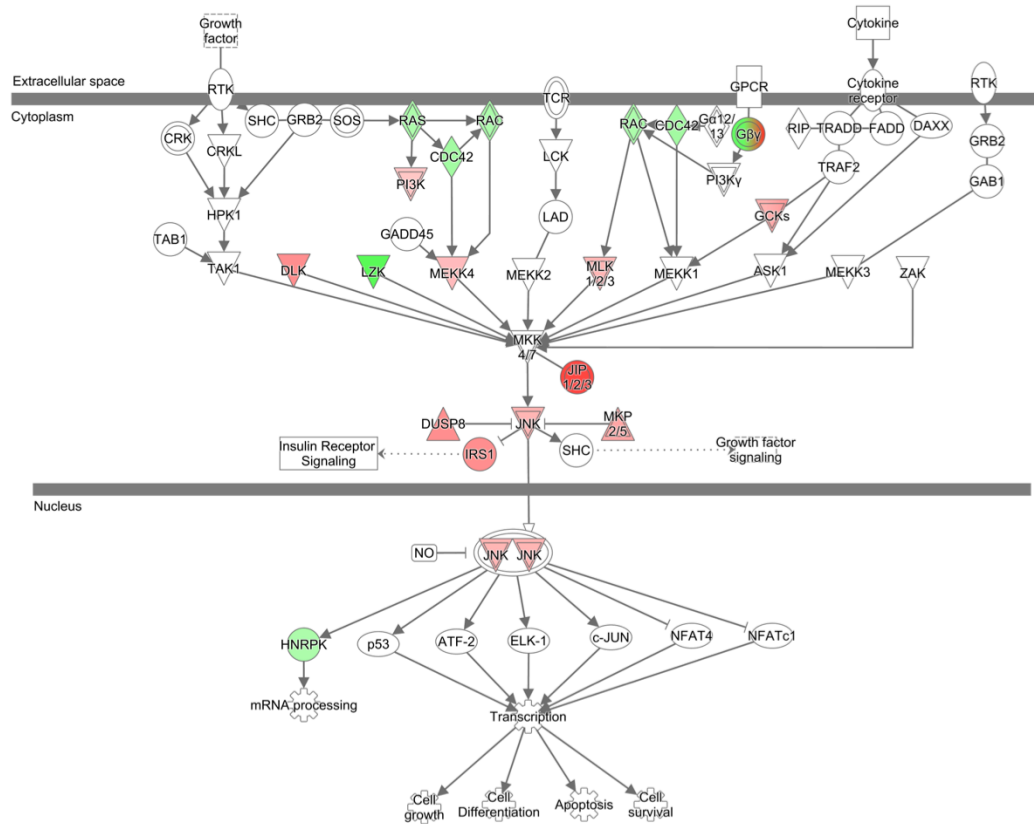


Figure 4-24: Stress-activated protein kinases (SAPK)/Jun amino-terminal kinases (JNK) signalling pathway on NSQ nanotopography following release of MSCs into the cell cycle. Identified genes and numerical values corresponding to differential gene expression from the NGS dataset in relation to flat controls are shown as coloured shapes (downregulated in green and upregulated in red, those displaying two shades of colour contain members that may be differentially regulated).

4.3 Discussion

Current research into the cell cycle of MSCs is very limited, particularly in terms of the contribution of cell cycle regulation to the promotion of symmetrical self-renewal. In this chapter, nanotopography was used as a tool to induce the divergent processes of self-renewal and osteogenic differentiation, and levels of cell cycle related proteins were assessed after synchronising and releasing MSCs into the cell cycle.

4.3.1 Interpretation of cell cycle protein levels analysed by ICW

A trend towards elevated pRB protein levels was consistently observed on NSQ at all the time points tested (*Figure 4-4*), which suggests that G1 to S transition has been repressed at an early stage. This effect appears to be unique to NSQ, as relative pRB levels remained low on both flat and SQ. RB is regulated by phosphorylation; hypophosphorylation of RB during G1 prevents cell entry into S phase, whereas an accumulation of hyperphosphorylation occurs as cell cycle progression unfolds (Ezhevsky *et al.*, 1997). A switch from proliferation to differentiation has been discussed in the literature, reasoning this trend on the NSQ nanotopography in comparison to the other surfaces. The phosphorylation site serine 807/serine 811 has actions on nuclear tyrosine kinase c-Abl (Knudsen and Wang, 1996). In addition, pRb can directly interact with transcription factors such as Runx2 and PPAR γ (Docheva *et al.*, 2008), specific to osteoblasts and adipocytes respectively, therefore an accumulation of pRB may be beneficial during the early stages of differentiation.

Levels of the CDK inhibitor p27^{Kip1} (*Figure 4-4*) were low in MSCs grown on both SQ and NSQ in comparison to the flat controls. A lower level of p27^{Kip1} on NSQ may indicate that some MSCs are proliferating and progressing through the cell cycle. However, this CDK inhibitor being low on SQ would be unexpected if the cells were in a quiescent state during culture. It is possible that inhibitory proteins other than p27^{Kip1} have larger roles than in maintaining a degree of quiescence or slowing progression through the cycle on the self-renewing surface. Alternatively, there is evidence that p27^{Kip1} is important in regulating stem cell progenitor populations (Menchón *et al.*, 2011), therefore it may stand to reason

that levels would be relatively similar on both SQ and NSQ at such an early stage of growth when progenitor cell numbers will be relatively comparable.

Elevation of D type cyclins are generally associated with proliferation, though changes in cyclin D1 levels between surfaces were minimal for the majority of the experimental timepoints (*Figure 4-4*), until the 24 hours timepoint had been reached, whereby the change between flat and SQ began to reach significance. This lowered level of cyclin D1 on SQ is a promising indicator of decreased proliferation. Admittedly, the time constraints of the project restricted the number of cell cycle proteins tested, in addition to those with links to osteogenic differentiation. Runx2, for example, would be expected to show upregulation on NSQ as the onset of osteogenesis commenced, and should correlate with an increase in cyclin D1, whereas the reverse should be true on SQ. It would be of merit to test this in future work, and determine whether some of these proposed concepts and initial hypotheses are robust following further experiments.

A decrease in E2F-1 transcription factor levels was also observed on NSQ at several timepoints (*Figure 4-4*). A link between E2F-1 and Rb exists, with a role for the protein complex in acting as a molecular 'switch' between differentiation and proliferation (Chong *et al.*, 2009). The decrease in E2F-1 correlates with the concomitant increase in pRb, whereby the formation of pRb-E2F-1 complexes results in the sequestration and reduction in E2F-1 transcriptional activity, which has effects on the G1 to S transition (Johnson *et al.*, 1993).

CDK6 protein expression has recently been studied in HSCs, with high CDK6 in a subset of HSCs being correlated to the rapid exit of quiescence and entry into the cycle upon mitogenic stimulation (Laurenti *et al.*, 2015). Intriguingly, two studies by Ogasawara *et al.* have shown that overexpression of CDK6 blocks BMP-2 induced osteoblast differentiation (Ogasawara *et al.*, 2004b), and that there was a requirement for CDK6 levels to fall in order for RANKL-stimulated osteoclast differentiation to occur (Ogasawara *et al.*, 2004a). However, these investigations were carried out on murine cells (RAW264.7 macrophage cell line and MC3T3-E1 osteoblast precursors) and not MSCs.

Nevertheless, in the case of MSCs on SQ, CDK6 levels were elevated on SQ in comparison to flat and NSQ surfaces (*Figure 4-5*), with some significance ($p < 0.05$) in protein level at the 1h timepoint with reference to the flat controls. This increase in CDK6 may have a potential role in repressing differentiation, perhaps even retaining cells in a primed state ready for differentiation. If an abundance of CDK6 is associated with tumour growth, and high levels of CDK6 progress cells through the cell cycle, it stands to reason that the regulation of CDK6 should be important in stem cells. As the observed increase in CDK6 in the experiments carried out in the present study were modest, perhaps this intermediate level of CDK6 is suggestive of a degree of proliferation on SQ, supporting the concept of dynamic stasis on this surface.

4.3.2 Changes in cell signalling networks and cell cycle regulation

Detailed study into the different stages of G1 is outwith the scope of this thesis but it would be interesting to determine which stage is affected with nanotopography, or whether the length of G1 is modulated by the surface. ESCs and HSCs display different mechanisms to preserve self-renewing populations, therefore it may be that MSCs utilise elements of these or even an entirely different process for the purposes of self-renewal. Therefore a wider picture of the effects of SQ and NSQ nanotopographies on gene expression was attempted from analysis of NGS data.

It was interesting to observe that indications of an aerobic bioenergetic profile were present in MSCs on SQ, with oxidative phosphorylation and fatty acid oxidation pathways consisting of downregulations in genes related to the transcripts in the dataset (*Figure 4-19*). Although the differential expression of genes involved in oxidative phosphorylation were shown to be downregulated on NSQ (*Figure 4-20 and Figure 4-21*), this was to a lesser extent, and could perhaps be attributed to the early stages of differentiation where a bioenergetic switch towards oxidative energy processes had not yet taken place, or could indicate a plausible heterogeneous population.

NGS revealed that in networks involving some key cell cycle genes, the majority of genes related to the identified transcripts on SQ were inferred as being downregulated. One example is *CDK1* (Figure 4-23). *CDK1* is known to have roles in mitotic progression (Van Horn *et al.*, 2010), yet in addition to this was shown to have effects on maintenance of pluripotency in human pluripotent stem cells (Neganova *et al.*, 2014). Moreover, the aforementioned $p27^{kip1}$, is thought to play a pivotal role in self-renewal and pluripotency of human ESCs (Menchón *et al.*, 2011), in addition to having a role in the transition stages between proliferation and osteoblast differentiation (Drissi *et al.*, 1999). This indicates that the complexities of cell cycle regulators may extend further than their direct action on cycle progression. Neganova *et al.* studied the effects of *CDK1* by using RNA interference to down-regulate *CDK1* (Neganova *et al.*, 2014). A similar strategy could be utilised to look at the importance of other important cell cycle regulators.

Information about *ERK1/2* and *JNK* on SQ and NSQ was gathered, with *ERK1/2* indicated as being downregulated on SQ (Figure 4-22) and *JNK* being upregulated on NSQ (Figure 4-24). There is evidence consistent with *ERK1/2* and its associated signalling cascade being activated during the differentiation of MSCs towards an osteogenic lineage (Bai *et al.*, 2013), therefore downregulation of *ERK1/2* on SQ may indicate a lack of differentiation on SQ. *JNK* activation has been demonstrated to increase in response to culture in osteogenic media (Jaiswal *et al.*, 2000), and MSCs subjected to geometric cues for enhancement of osteogenesis also point towards elevated *JNK* signalling in addition to elevated *ERK* signalling having roles in promotion of differentiation (Kilian *et al.*, 2010).

4.3.3 Link between filopodia and cell cycle regulation was not established

Following observation that morphology at the level of filopodia was altered, with contact guidance of filopodia being demonstrated on SQ and not on NSQ, it was hypothesized that the directionality of filopodia, and subsequent effect on focal adhesion formation and clustering, may be an important initiating event that triggers signalling processes to progress onset of particular MSC phenotypes.

Other studies have shown that filopodia have roles in topographical sensing (Dalby *et al.*, 2004a), and influence cell adhesion (Albuschies and Vogel, 2013). However, testing of CDK6 levels in MSCs subjected to cdc42 inhibition did not show an appreciative reduction of CDK6 on SQ (Figure 4-14). This may be due to the inhibition method utilised, as the chemical inhibitor that was applied only targeted one protein involved in formation of filopodia, and with less specificity than molecular targeting. An improved strategy would be to use a combination of inhibitors targeting different filopodial targets, to knock out the genes involved in filopodia development or to introduce non-functional versions of proteins (such as a dominant negative), to create a larger cumulative and thereby inhibitory effect. CDK6 was of particular interest as it was elevated on SQ as the cell cycle progressed. Thus, further study into this protein can reveal whether phosphorylation of CDK6 at different sites (both inhibitory or activating sites) is affected by filopodial inhibition, in addition to answering the question of whether associations between any cell cycle proteins and filopodia exist.

4.3.4 Proposed models of self-renewal on SQ in relation to cell cycle

If it is indeed the case that cell cycle regulators act to maintain multipotency or pluripotency, this is in keeping with our hypothesis that MSCs on SQ would be subject to differences in cell cycle regulation. As bone marrow derived MSCs do not appear to show significant changes in proliferation during culture on different nanotopographies, this suggests that MSCs on SQ nanotopography maintain a degree of self-renewal by a mechanism other than keeping reserve populations dormant, as has been proposed for HSCs (Wilson *et al.*, 2008) which are largely used as a model for the study of adult stem cell self-renewal. Li *et al.* suggested that undifferentiated ESCs might progress through G1 at a slower rate (Li *et al.*, 2012), which could be plausible for MSCs, due to a shift in populations in the earlier stages of the cell cycle on SQ (Figure 4-6 and 4-7). It would be interesting to compare SQ with NSQ in the same way; to assess cell cycle related changes in self-renewal against osteogenic differentiation.

It was not possible to reach a definitive conclusion about the mechanism of self-renewal from the current data. However, a potential model for the self-renewal of MSCs on the SQ nanotopography could be that a proportion of cells are undergoing a degree of slow proliferation, yet do not lose their capacity for self-renewal until a substantial amount of time has passed, as demonstrated by previous work using SQ nanotopography carried out at long timepoints of 8 weeks (McMurray *et al.*, 2011). It seems plausible that the increasingly mature subpopulations could be acting to regulate self-renewal of early stage MSCs, akin to a more recent observation for HSCs, though this effect would be lost with the use of synchronised cells (Christopher *et al.*, 2011). Having some heterogeneity within stem cell pools would be more likely than an entirely homogeneous one, as biological systems are rarely found to consist of cells in the same state. If applying the concept of heterogeneity, populations of MSCs may be 'primed' on SQ, in terms of amassing energy to carry out differentiation into a particular lineage, and could be described as being in a mode of dynamic stasis, poised for activation. With regards to cell cycle regulation, some differences are apparent between SQ and NSQ nanotopographies. It appears that MSCs cultured on SQ are subject to regulation to a greater extent. This may be explained by the fact that differentiating cells tend to divert their energies towards greatly energy-consuming differentiation processes to the detriment of those related to proliferation. Thus, regulation pertaining to prevention of cell cycle progression can be relaxed in MSCs cultured on the differentiation-inducing NSQ surface.

Chapter 5

Assessment of Nanotopography for Reprogramming

5 Chapter 5

5.1 Introduction

A large disadvantage to the widespread use of stem cells is their tendency to exhibit uncontrolled and spontaneous differentiation and their limited numbers. In order to generate a source of undifferentiated stem cells, a strategy was formulated to take partially or even terminally differentiated cell types and attempt to revert them back to a stem-like state. This method is now commonly referred to as 'reprogramming'. John Gurdon was an early pioneer in the foundations of this type of research, successfully using nuclear transplantation to transfer an adult frog intestine cell nucleus into an egg cell, resulting in a cloned frog (Gurdon, 1962, Gurdon and Uehlinger, 1966). In doing so, he demonstrated that adult cells retained the information required to form other cells, despite having become specialised, and that differentiation was not irreversible. This caveat was further addressed by Takahashi and Yamanaka in 2006, and became one of the biggest and most publicised success stories of stem cell research. The group were able to take mouse and human fibroblasts and induce pluripotency solely through retroviral introduction of expression of four genes, namely, *Oct3/4*, *Sox2*, *Klf4* and *c-Myc* (Takahashi and Yamanaka, 2006, Takahashi *et al.*, 2007). The resultant iPSCs were shown to possess familiar characteristics of embryonic stem cells (ESCs) in terms of morphology, expression of typical ESC markers, and *in vitro* differentiation capability, proving that some reversion from a differentiated phenotype was achieved (Takahashi and Yamanaka, 2006, Takahashi *et al.*, 2007).

More recent work by Huangfu *et al.* showed that addition of DNA methyltransferase and histone deacetylase (HDAC) inhibitors enhanced reprogramming efficiency of somatic cells into iPSCs (Huangfu *et al.*, 2008a, Huangfu *et al.*, 2008b), which originally takes a long time and has a low success rate (Yamanaka, 2009), likely due to mature cells requiring additional gene activation for reprogramming to take place (Bar-Nur *et al.*, 2014). They described a dramatic increase in reprogramming efficiency with the use of histone deacetylation (HDAC) inhibitor valproic acid (VPA) (Huangfu *et al.*, 2008a). This is thought to be due to the resultant increase in histone acetylation that allows DNA to form an open structure for the binding of transcription

factors. A further study investigating benefits of grooved microtopography on reprogramming efficiency incorporated an experiment with the topography and VPA in tandem, although showing little difference between the presence and absence of VPA with a grooved surface (Downing *et al.*, 2013).

Song *et al.* carried out analyses of MSCs that had differentiated and de-differentiated by addition and subsequent removal of induction media (Song *et al.*, 2006). We proposed that the use of nanotopography instead of reliance solely on chemically-defined media, would be far more advantageous. This posed the question ‘would nanotopographical cues from SQ be strong enough to de-differentiate MSCs that had been partially differentiated?’ This would present a novel application of nanotopography that has not previously been investigated.

Further addressing the issue of reproducing conditions reminiscent of bone marrow, it has been noted that the nanotopographical substrate in isolation would not closely mimic the all aspects of the niche, but rather the topographical features mimic an aspect of a niche component, namely the sinusoidal capillaries that permeate the bone marrow. Intriguingly, the pores of these capillaries (fenestrae) are of similar scale to the size of the nanopits, which supports the use of this type of feature at nanometre dimensions, and is possibly indicative of why these substrates influence MSC phenotype. It has been recently reported that MSCs reside within two microenvironments in the bone marrow, termed the endosteal (bone) niche and the sinusoidal niche, the latter of which comprises the aforementioned sinusoidal capillaries (Ehninger and Trumpp, 2011).

This chapter describes the initial assessment of the SQ nanotopography for “de-differentiation” or specifically to attempt to revert MSCs that have been induced to undergo osteogenesis into an earlier ‘stem-like’ state. Nanotopography was utilised to both induce and reverse phenotype, with the NSQ substrate employed to induce osteogenesis and culture on the SQ substrate used to re-establish stem cell maintenance cues.

5.2 Results

5.2.1 Investigating nanotopography for reprogramming

5.2.1.1 Assessment of de-differentiation with stem cell marker expression

Preliminary experiments assessed the use of nanotopography as a tool for reprogramming of MSCs. MSCs were induced to undergo osteogenic differentiation on the NSQ surface for 14 days, then reseeded onto SQ substrates for a further period of culture (7 or 14 days). Stem cell marker protein levels were used as an indicator of reversion to an earlier stem cell state prior to differentiation. The results unexpectedly showed that levels of CD63 protein decreased on SQ in comparison to CD63 in MSCs on NSQ prior to reseeding (Figure 5-2).

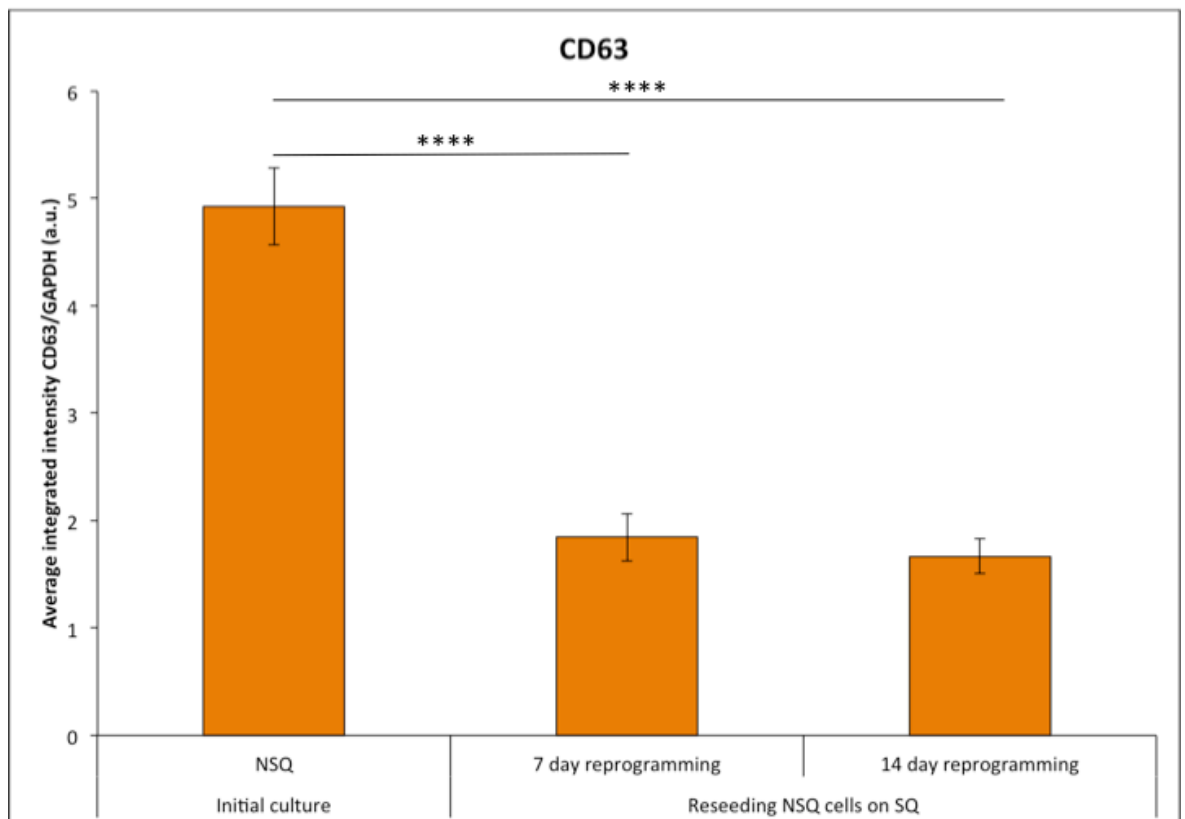


Figure 5-1: CD63 protein levels before and after reprogramming on SQ nanotopography.

Quantification of CD63 protein by ICW. Following reseeding of MSCs that were pre-cultured for 14 days on NSQ onto SQ nanotopography, CD63 levels were assessed again after 7 or 14 days of further culture. Results denote an average integrated intensity normalised to GAPDH expressed in arbitrary fluorescence units, of 4 material replicates for the initial culture period and 5 material replicates for the reseeded cultures. Error bars represent \pm standard error of the mean. CD63 was observed to decrease significantly after reseeding at both timepoints. Statistical significance was tested by one-way ANOVA with Tukey's multiple comparisons test. **** $p < 0.0001$

Results for ALCAM appeared to hold some promise, with a small elevation in ALCAM indicated for the further 7 day culture on SQ following reseeding, which was not observed for the 14 day timepoint (*Figure 5-2*). However, despite the encouraging increase in ALCAM for the 7 day culture, this change was not found to be statistically significant from ALCAM levels measured from the initial NSQ culture.

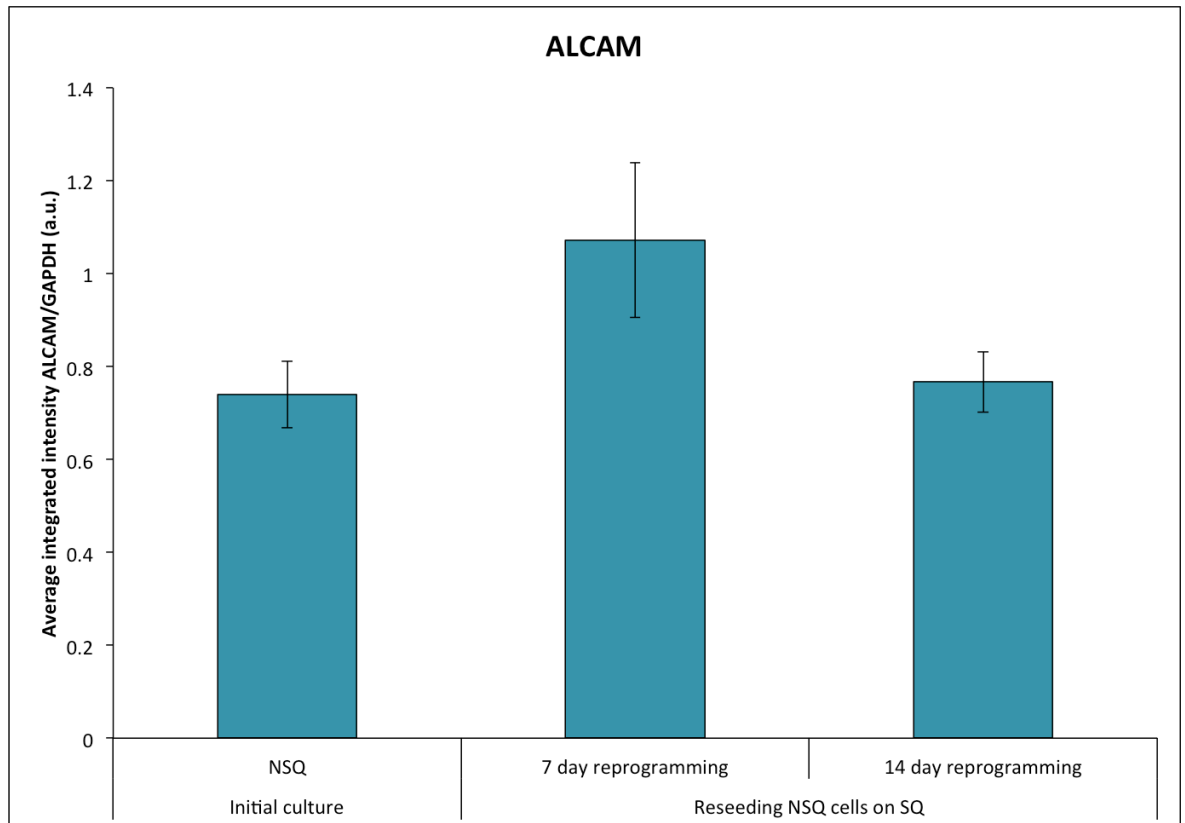


Figure 5-2: ALCAM levels before and after reprogramming on SQ nanotopography.

Quantification of ALCAM protein by ICW. Following reseeding of MSCs that were pre-cultured for 14 days on NSQ onto SQ nanotopography, ALCAM levels were assessed again after 7 or 14 days of further culture. Results denote an average integrated intensity normalised to GAPDH, expressed in arbitrary fluorescence units of 4 material replicates for the initial culture period and 5 material replicates for the reseeded cultures. Error bars represent \pm standard error of the mean. ALCAM levels exhibited a modest increase after reseeding and culture for 7 days on SQ, whereas the longer period of further culture did not appear to have any great effect on ALCAM protein expression. Despite the encouraging trend observed for the 7 day reprogramming culture on SQ, this was not calculated to be statistically significant (one-way ANOVA with Tukey's multiple comparisons test).

Following from these preliminary results, it was thought that performing additional experiments using a culture time of 7 days after reseeding would potentially yield some interesting observations about SQ for this application.

5.2.1.2 Re-evaluation of nanotopography for de-differentiation: incorporation of VPA

As the cues from SQ in isolation did not appear to maximise numbers of MSCs expressing high levels of stem cells markers and override the differentiation signals, VPA, a HDAC inhibitor, was added to enhance the cues from nanotopography. VPA promotes histone acetylation, consequently opening up chromatin into a relaxed structure allowing transcription factors to more readily bind to the DNA (Göttlicher *et al.*, 2001, Kernochan *et al.*, 2005). Intriguingly, cells from another patient responded positively, with results suggesting that reseeded differentiating cells onto SQ nanotopography may be effective in reprogramming cells back into a stem cell-like state, with an increase of STRO-1 protein levels, the marker with which they were isolated, on SQ in comparison to the flat control (Figure 5-3; statistical significance shown in table 5-1). Upon addition of VPA, protein expression of STRO-1 was heightened on both flat and SQ, indicating that use of VPA improves STRO-1 expression on all surfaces regardless of the presence of nanotopographical cues.

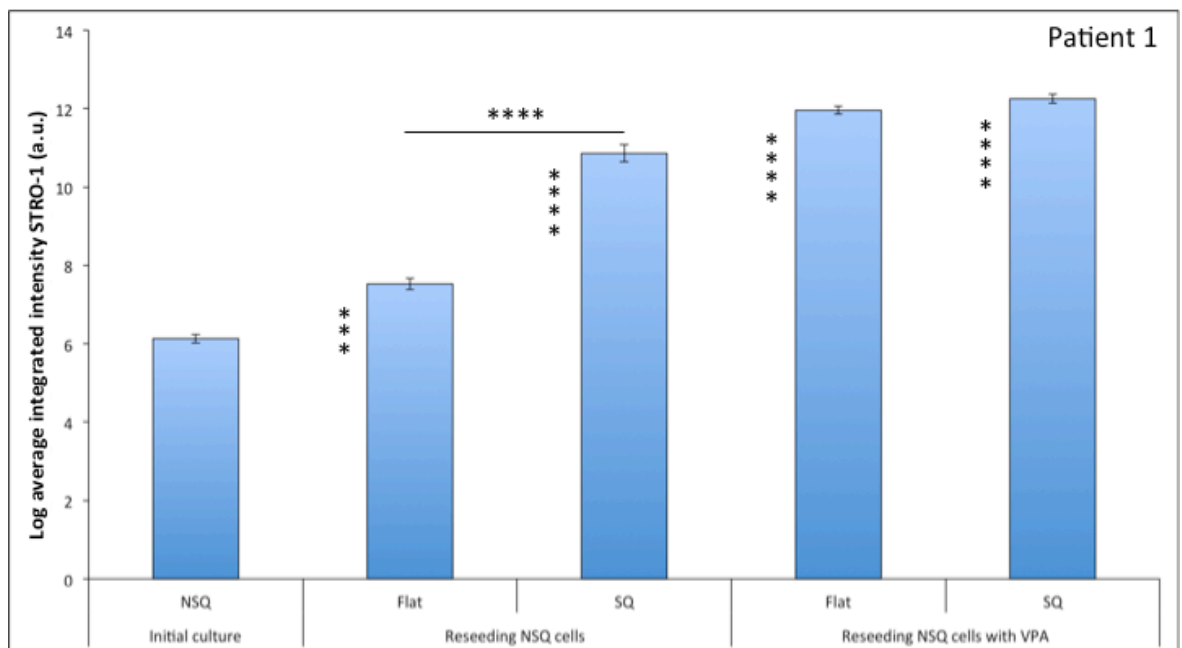


Figure 5-3: STRO-1 protein levels in differentiating MSCs reseeded on SQ to assess reprogramming potential. STRO-1⁺ MSCs were seeded on NSQ and cultured for 21 days, then detached and reseeded onto flat/SQ ± VPA for reprogramming (7 days). Results depict average integrated intensity of cells from patient 1 detected from ≥60 images acquired across 3 material replicates per condition, quantified using CellProfiler imaging software. Error bars represent ± standard error of the mean. Elevated STRO-1 was detected on SQ at a significantly higher level than the flat control. Addition of VPA appeared to heighten STRO-1 protein on both flat and SQ substrates to the same degree. Statistical significance was tested by Kruskal-Wallis test with a Dunn's multiple comparisons post-test. *****p*<0.0001, ****p*<0.001. Stars to the left of bars denote significance when compared to NSQ. Other comparisons are marked with a line.

Comparison	Statistical significance: STRO-1 (Patient 1)
NSQ initial culture vs Reseeded Flat	***
NSQ initial culture vs Reseeded SQ	****
NSQ initial culture vs Reseeded Flat + VPA	****
NSQ initial culture vs Reseeded SQ + VPA	****
Reseeded Flat vs Reseeded SQ	****
Reseeded Flat vs Reseeded Flat + VPA	****
Reseeded SQ vs Reseeded SQ + VPA	No significance
Reseeded Flat + VPA vs Reseeded SQ + VPA	No significance

Table 5-1: Summary of statistical significance calculated for initial assessment of STRO-1.

Details of statistical significance calculated from data acquired by image analysis for MSCs from one donor (Patient 1) in the experimental results depicted in Figure 5-3.

As there were indications that cues from SQ were acting to increase STRO-1 in this instance, further investigation into the consistency of the effect was carried out with MSCs from two additional patients. Some parallels were observed with MSCs from a second donor (*Figure 5-4 upper graph; statistical significance shown in table 5-2*) in that an increase of STRO-1 was demonstrated on SQ, with reseeding on flat leading to a significant drop in STRO-1. Once again, supplementing media with VPA resulted in higher STRO-1 expression to similar levels on flat and SQ. The third assessment of STRO-1 expression (patient 3) showed a detrimental effect with SQ, where the lowest level of STRO-1 was detected (*Figure 5-4 lower graph; statistical significance shown in table 5-3*). STRO-1 was found to be higher on flat with and without VPA. It was observed that VPA increased STRO-1 on SQ, however, this was significantly lower than that measured from the equivalent flat surfaces.

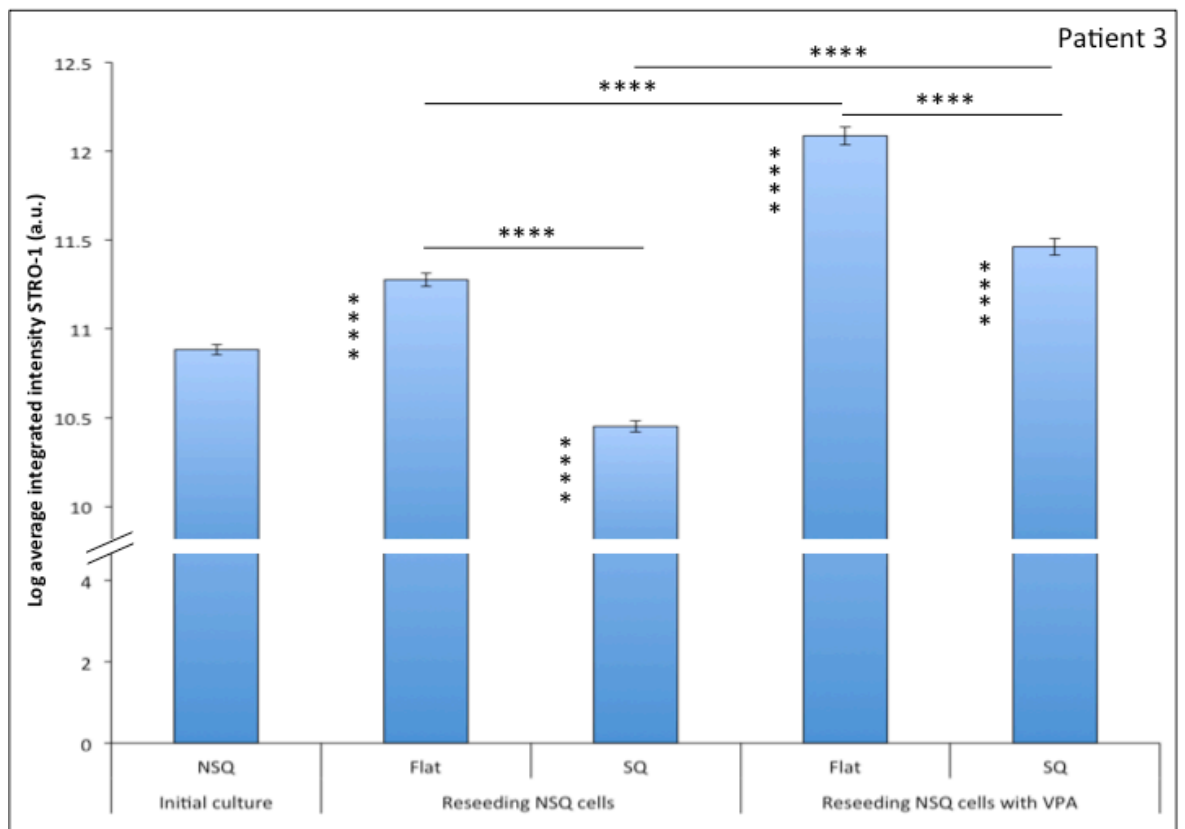
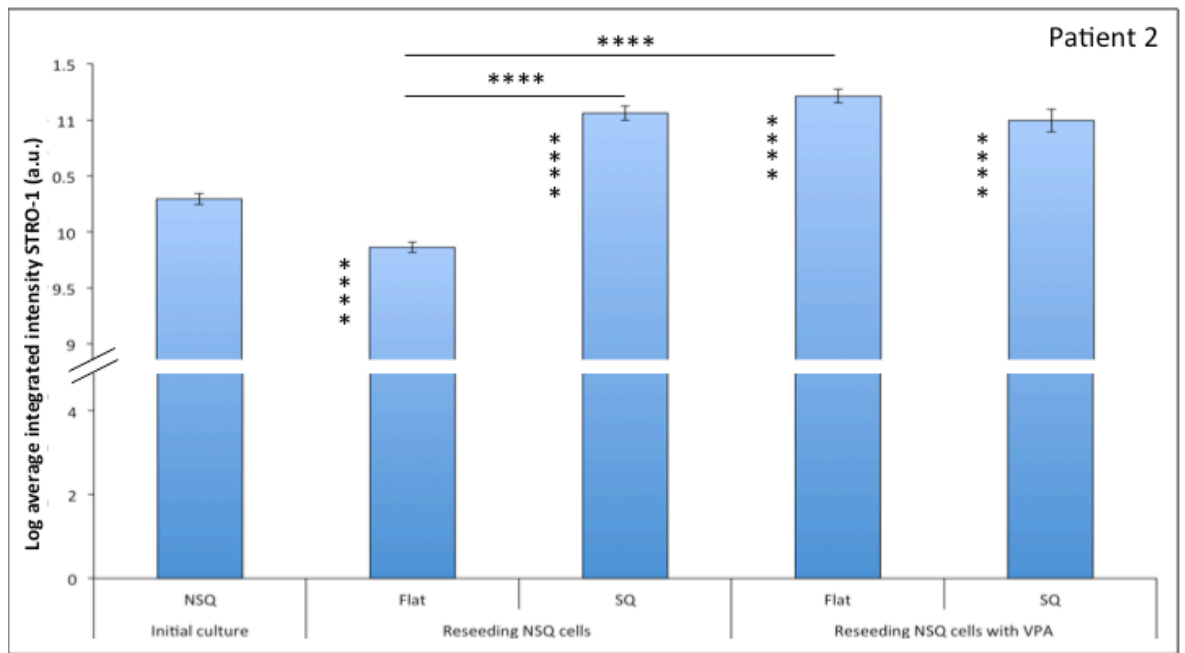


Figure 5-4: Further assessment of STRO-1 protein levels in differentiating MSCs reseeded on SQ. STRO-1⁺ MSCs were seeded on NSQ and cultured for 21 days, then detached and reseeded onto flat/SQ ± VPA for reprogramming (7 days) for 2 different patients (patient 2 and 3; separate graphs displayed per patient). Results depict average integrated intensity of cells detected from ≥60 images acquired across 3 material replicates per condition, quantified using CellProfiler imaging software. Error bars represent ± standard error of the mean. Elevated STRO-1 was detected on SQ at a significantly higher level than the flat control. Addition of VPA appeared to heighten STRO-1 protein on both flat and SQ substrates to the same degree. Statistical significance was tested by Kruskal-Wallis test with a Dunn's multiple comparisons post-test. ****p<0.0001. Stars to the left of bars denote significance when compared to NSQ. Other comparisons are marked with a line. Breaks in the y-axis are indicated with a double line.

Comparison	Statistical significance: STRO-1 (Patient 2)
NSQ initial culture vs Reseeded Flat	***
NSQ initial culture vs Reseeded SQ	****
NSQ initial culture vs Reseeded Flat + VPA	****
NSQ initial culture vs Reseeded SQ + VPA	****
Reseeded Flat vs Reseeded SQ	****
Reseeded Flat vs Reseeded Flat + VPA	****
Reseeded SQ vs Reseeded SQ + VPA	No significance
Reseeded Flat + VPA vs Reseeded SQ + VPA	No significance

Table 5-2: Summary of statistical significance calculated for further assessments of STRO-1 (Patient 2). Details of statistical significance calculated from data acquired by image analysis for MSCs from a second donor in the experimental results depicted in upper graph Figure 5-4.

Comparison	Statistical significance: STRO-1 (Patient 3)
NSQ initial culture vs Reseeded Flat	***
NSQ initial culture vs Reseeded SQ	****
NSQ initial culture vs Reseeded Flat + VPA	****
NSQ initial culture vs Reseeded SQ + VPA	****
Reseeded Flat vs Reseeded SQ	****
Reseeded Flat vs Reseeded Flat + VPA	****
Reseeded SQ vs Reseeded SQ + VPA	No significance
Reseeded Flat + VPA vs Reseeded SQ + VPA	No significance

Table 5-3: Summary of statistical significance calculated for further assessments of STRO-1 (Patient 3). Details of statistical significance calculated from data acquired by image analysis for MSCs from a third donor in the experimental results depicted in the lower graph of Figure 5-4.

It was noted that the observed STRO-1 increases on SQ for two of the experimental results following reseeded could have been due to expansion of the remaining STRO-1 cell population found on NSQ, rather than a result of reprogramming of partially osteo-committed MSCs back to early state MSCs. Therefore, an increased number of substrates were incorporated in the study of MSCs from two other patients (hereby referred to as patient 2 and patient 3), to allow for quantification of ALCAM and osteocalcin (OCN, an osteoblast marker) in addition to STRO-1. Levels of OCN were compared on NSQ following 21 days of culture and on SQ after 7 days post-reseeding. The reasoning was that if OCN levels on SQ subsequently fall, in parallel with a concomitant increase in STRO-1, this would suggest that SQ is presenting lineage reversal cues.

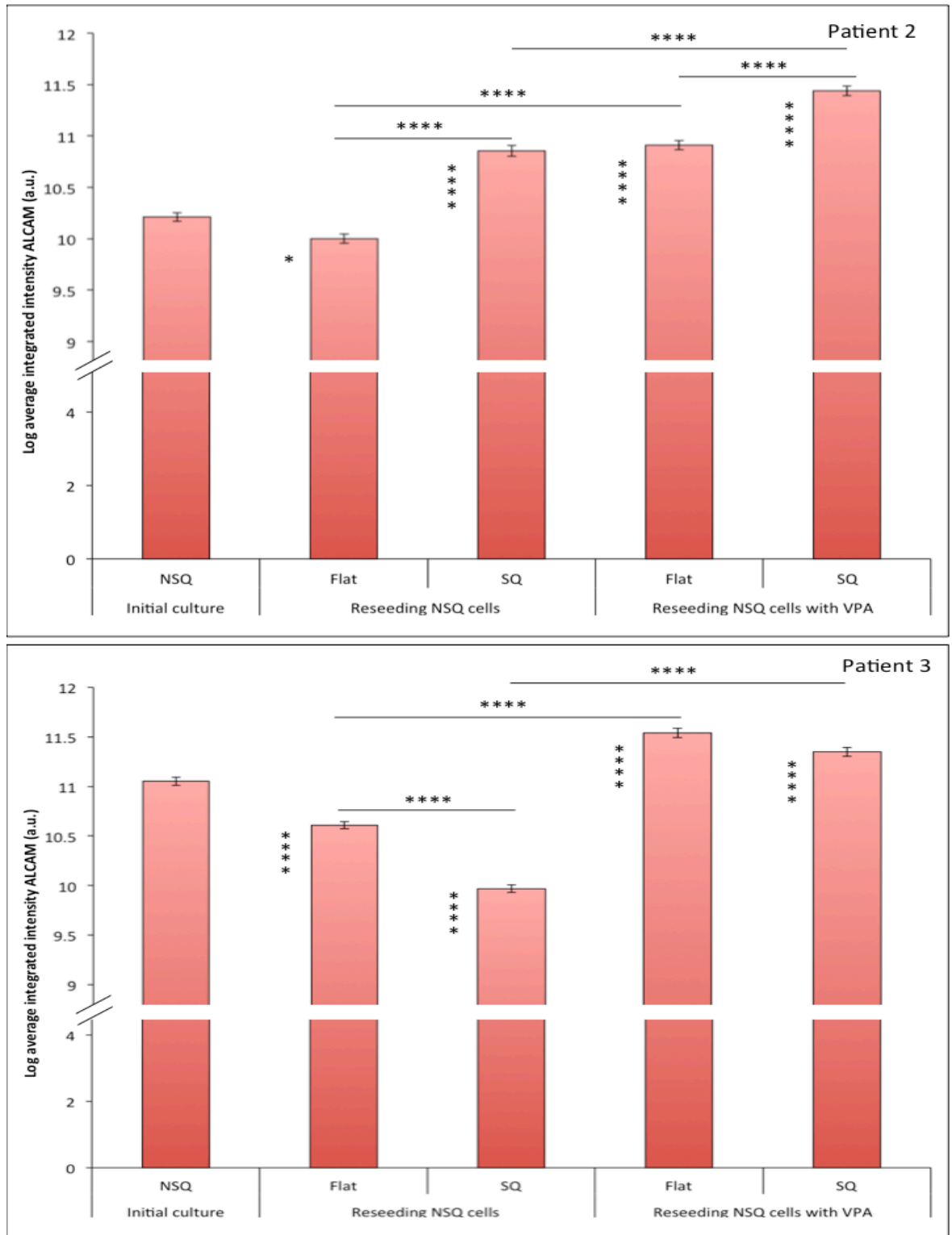


Figure 5-5: ALCAM protein levels following reseeding of NSQ-induced MSCs on SQ and flat substrates. STRO-1⁺ MSCs were seeded on NSQ for 21 days, detached and reseeded onto flat/SQ \pm VPA for reprogramming (7 days) for 2 different patients (Patient 2 and 3; individual graphs displayed per patient). Results depict average integrated intensity of cells detected from ≥ 60 images acquired across 3 material replicates per condition, quantified using CellProfiler. Error bars represent \pm standard error of the mean. ALCAM was significantly higher on SQ than flat for patient 2 but the opposite was observed for patient 3. VPA increased ALCAM on both flat and SQ. Statistical significance was tested by Kruskal-Wallis test with a Dunn's multiple comparisons post-test. **** $p < 0.0001$, * $p < 0.05$. Stars to the left of bars denote significance compared to NSQ. Other comparisons are marked with a line. Breaks in the y-axis are indicated with a double line.

Conversely, if STRO-1 levels were elevated on SQ following reseeding, this would indicate an expansion of a STRO-1⁺ MSC population.

Comparison	Statistical significance: ALCAM (Patient 2)
NSQ initial culture vs Reseeded Flat	*
NSQ initial culture vs Reseeded SQ	****
NSQ initial culture vs Reseeded Flat + VPA	****
NSQ initial culture vs Reseeded SQ + VPA	****
Reseeded Flat vs Reseeded SQ	****
Reseeded Flat vs Reseeded Flat + VPA	****
Reseeded SQ vs Reseeded SQ + VPA	No significance
Reseeded Flat + VPA vs Reseeded SQ + VPA	No significance

Table 5-4: Summary of statistical significance calculated for ALCAM (Patient 2). Details of statistical significance calculated from data acquired by image analysis for MSCs from the second donor in the experimental results depicted in the upper graph (Patient 2) of Figure 5-5.

Comparison	Statistical significance: ALCAM (Patient 3)
NSQ initial culture vs Reseeded Flat	****
NSQ initial culture vs Reseeded SQ	****
NSQ initial culture vs Reseeded Flat + VPA	****
NSQ initial culture vs Reseeded SQ + VPA	****
Reseeded Flat vs Reseeded SQ	****
Reseeded Flat vs Reseeded Flat + VPA	****
Reseeded SQ vs Reseeded SQ + VPA	****
Reseeded Flat + VPA vs Reseeded SQ + VPA	No significance

Table 5-5: Summary of statistical significance calculated for ALCAM (Patient 3). Details of statistical significance calculated from data acquired by image analysis for MSCs from the third donor in the experimental results depicted in the lower graph (Patient 3) of Figure 5-5.

An increase in ALCAM was detected on SQ at a significantly higher level than the flat control for patient 2 but the opposite trend was observed for patient 3 (Figure 5-5, significance shown in tables 5-4 and 5-5). Addition of VPA increased ALCAM on both flat and SQ substrates for each donor in comparison to the initial level on NSQ. In each case, ALCAM marker expression fell when reseeded onto flat substrates without the addition of VPA. MSCs from patient 2 showed a particularly good response to the SQ nanotopography as ALCAM on SQ cultured in the presence or absence of VPA were both significantly elevated in comparison to the corresponding flat controls.

Some variation in results between MSCs derived from different patients was similarly observed for OCN. MSCs from patient 2 appeared to increase after reseeding across all of the substrates in both culture conditions (*Figure 5-6, significance shown in table 5-6*). In contrast, MSCs from patient 3 exhibited a decrease in OCN on SQ that was significantly lower than the comparative flat control (*Figure 5-6, significance shown in table 5-7*). In parallel with STRO-1 and ALCAM, VPA promoted increases in OCN, with similarity between flat and SQ cultured in VPA media.

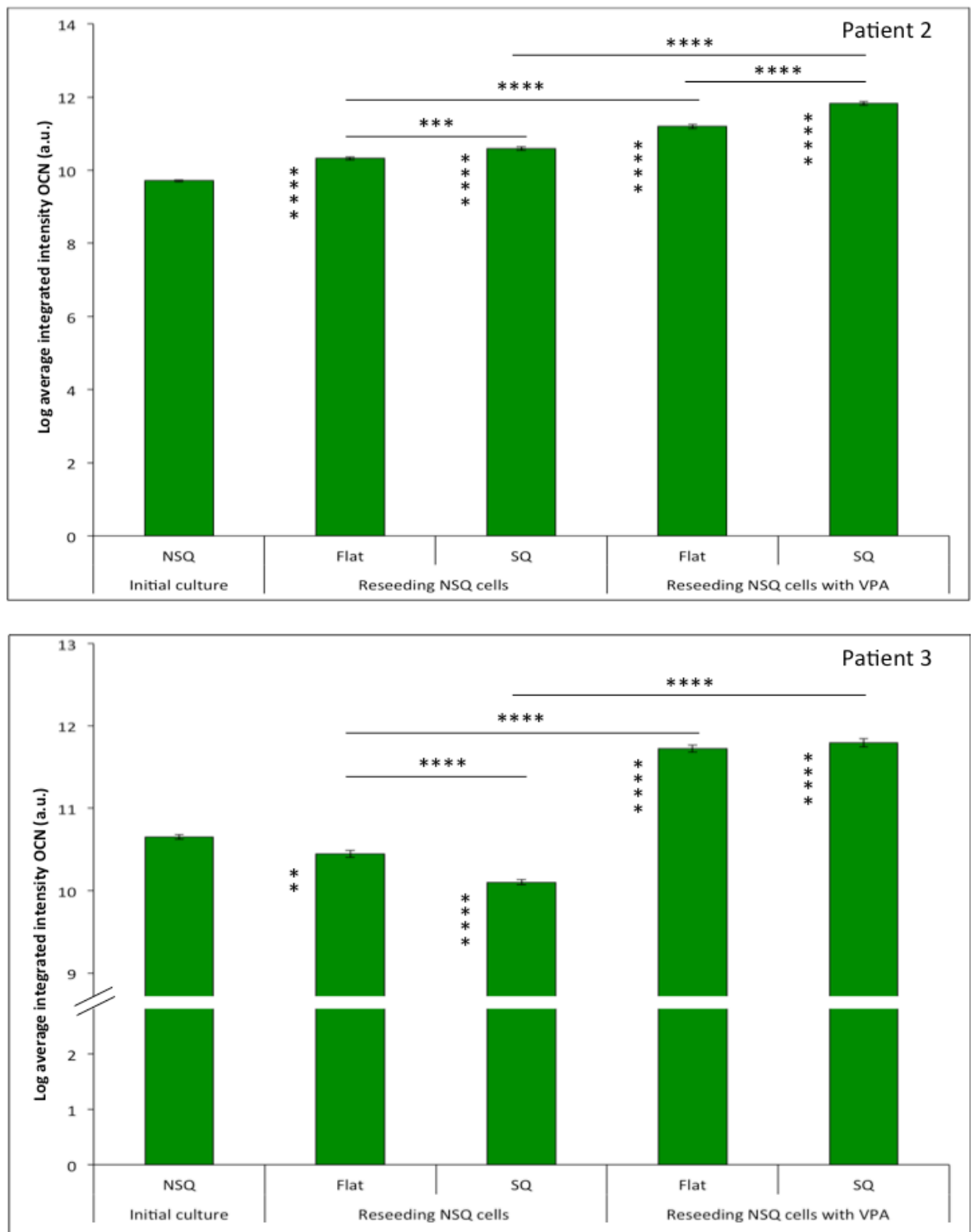


Figure 5-6: OCN protein levels following reseeding of NSQ-induced MSCs on SQ and flat substrates. *STRO-1⁺* MSCs were seeded on NSQ for 21 days, detached and reseeded onto flat/SQ \pm VPA for reprogramming (7 days) for 2 different patients (designated as Patient 2 and 3; individual graphs shown per patient). Results depict average integrated intensity of cells detected from ≥ 60 images acquired across 3 material replicates per condition, quantified using CellProfiler imaging software. Error bars represent \pm standard error of the mean. A slight elevation of OCN was observed across all substrates with MSCs from patient 2 whereas a decrease was detected on SQ for patient 3. OCN levels were high on all surfaces cultured with VPA. Statistical significance was tested by Kruskal-Wallis test with a Dunn's multiple comparisons post-test. **** $p < 0.0001$, *** $p < 0.001$, ** $p < 0.01$. Stars to the left of bars denote significance when compared to NSQ. Other comparisons are marked with a line. Breaks in the y-axis are indicated with a double line.

Comparison	Statistical significance: OCN (Patient 2)
NSQ initial culture vs Reseeded Flat	****
NSQ initial culture vs Reseeded SQ	****
NSQ initial culture vs Reseeded Flat + VPA	****
NSQ initial culture vs Reseeded SQ + VPA	****
Reseeded Flat vs Reseeded SQ	***
Reseeded Flat vs Reseeded Flat + VPA	****
Reseeded SQ vs Reseeded SQ + VPA	****
Reseeded Flat + VPA vs Reseeded SQ + VPA	****

Table 5-6: Summary of statistical significance calculated for OCN (Patient 2). Details of statistical significance calculated from data acquired by image analysis for MSCs from the third donor in the experimental results depicted in the upper graph (Patient 2) of Figure 5-6.

Comparison	Statistical significance: OCN (Patient 3)
NSQ initial culture vs Reseeded Flat	**
NSQ initial culture vs Reseeded SQ	****
NSQ initial culture vs Reseeded Flat + VPA	****
NSQ initial culture vs Reseeded SQ + VPA	****
Reseeded Flat vs Reseeded SQ	****
Reseeded Flat vs Reseeded Flat + VPA	****
Reseeded SQ vs Reseeded SQ + VPA	****
Reseeded Flat + VPA vs Reseeded SQ + VPA	No significance

Table 5-7: Summary of statistical significance calculated for OCN (Patient 3). Details of statistical significance calculated from data acquired by image analysis for MSCs from the third donor in the experimental results depicted in the upper graph (Patient 3) of Figure 5-6.

5.3 Discussion

In this chapter, a novel application of the SQ nanotopography for the reprogramming of differentiating MSCs was investigated. The nanotopography system was used to induce osteogenic differentiation through initial culture of MSCs on the NSQ surface, with subsequent reseeding onto SQ substrates, subjecting the partially differentiated cells to maintenance cues for potential reversion of phenotype to an earlier stem cell state. A desirable outcome would be to obtain a large number of MSCs with a strong degree of stem cell marker expression. It was also deemed pertinent to answer the question of whether the resultant effect was truly in the reprogramming of the differentiating cells, or if the multipotent population was merely expanding.

Early indications suggested that reseeding on SQ might have enhanced the ability of the differentiating MSCs to express ALCAM. However, levels of another stem cell marker, CD63 were not elevated after reseeding, indicating that nanotopographical cues in isolation may not be strong enough to achieve a rescue of stem cell marker expression. In light of these observations, the inclusion of small molecule VPA was tested to determine whether an ‘in conjunction’ nanotopography-chemical approach would be more effective. With the addition of VPA, the expression of the widely recognised STRO-1 marker, which was used to isolate the cells, was found to be amplified on MSCs reseeded on SQ for the preliminary experiment, though this trend was not exclusive to the nanotopographical substrates as cells on the flat control supplemented with VPA exhibited STRO-1 at similar levels. Unexpectedly, in this particular experiment, reseeding differentiated cells onto nanotopography alone was found to elevate levels of STRO-1 in comparison to reseeding onto a flat substrate, suggesting that the STRO-1 selected population of MSCs is more responsive to substrate cues. Thus, it was deemed interesting to determine whether cells from other patients also displayed an increase in STRO-1, and whether additional stem cell markers followed a consistent trend upon reseeding onto SQ substrates. Furthermore, it was decided to investigate the basis of the observed effect: if it was a result of re-direction in expression of markers associated with differentiation to those related to ‘stem-ness’ (de-differentiation) or due to expansion of a multipotent subpopulation amongst the osteogenic cells on the

NSQ surface. Further experimental testing and analyses indicated that cells from different patients displayed variable responses, with cells from one patient showing no response at all.

OCN results proved inconsistent. VPA tended to cause an increase in the expression of this osteo-specific differentiation marker and whilst some patients showed reduction of the marker after reseeding from NSQ, others increased OCN expression. This suggests that the osteogenic populations are either static or are even expanding on SQ and that they continue to expand with VPA. This leads us to hypothesize that reprogramming was not achieved, rather switching between substrates focuses expansion of different subpopulations and that VPA is generally inductive of marker expression as a whole, through the provision of an accessible DNA structure for the binding of transcription factors.

Fluctuations in response are likely dependent on the initial profile of MSCs, reflected in the variable data between patients. Other studies have reported donor-to-donor variability in MSCs (Friedl *et al.*, 2007, Siddappa *et al.*, 2007), reflecting the heterogeneity within stem cell populations. At any given time, there will be populations of multipotent stem cells as well as primitive progenitor cells and those that have progressed further in differentiating to particular lineages, all which will differ in number between donors (Pevsner-Fischer *et al.*, 2011). This issue is reflected in the increased emphasis on development of 'personalised medicine', in which treatments are tailored to individual patients and their biological characteristics rather than attempting to provide a 'blanket' treatment to all (Schork, 2015).

It may be of merit to assess a wider range of markers, such as Runx2, which is an early osteogenic marker (Ducy *et al.*, 1997) in addition to mid or late stage differentiation markers, and to investigate longer periods of culture to assess whether the cues from nanotopography require more time to take effect. An interesting study by Lee *et al.* used a gel strategy for a similar purpose. This involved pre-culturing MSCs on either soft or stiff hydrogels to induce neurogenesis or osteogenesis with subsequent transfer of these cells to hydrogels of opposing stiffnesses to study the reversal of lineage specification defined by the preconditioning period (Lee *et al.*, 2014b). They found that nuclear Runx2

remained elevated after transfer of MSCs to softer gels which suggests that some osteogenic signals become established and become irreversible (Lee *et al.*, 2014b). With this in mind, perhaps it is inevitable to observe an increase in some osteogenic markers to some extent. Moreover, it may stand to reason that greater changes in early markers could be possible with nanotopography.

Taken together, the preliminary results indicate that the use of highly ordered nanopit nanotopography cannot reprogram osteo-committed MSCs. We propose that the SQ substrates are assisting expansion of any remaining STRO-1⁺ MSCs remaining from the initial culture period, and that expression of markers at any given time is likely to vary between patients, which supports the argument for tailoring of stem cell-based therapies. The addition of VPA in conjunction with nanotopography generally increased expression of all markers, and thus did not offer any advantage in targeted elevation of stem cell markers. Nevertheless, the observation that SQ retains the ability to expand small numbers of MSCs even after a relatively long period of time in culture is a promising one, and once more highlights SQ as a useful tool in expansion of MSCs.

Chapter 6

Discussion and Future Work

6 Chapter 6

6.1 General discussion

Stem cells present vast potential in the regeneration of diseased or damaged tissue. In order to best exploit them, knowledge of self-renewal is of particular interest over differentiation, as the former will allow larger-scale investigations to take place in a laboratory setting in addition to generation of increased numbers for implantations for clinical purposes. Success in this regard would overcome the problems associated with limited availability of MSCs from bone marrow aspirate (estimated as being 0.001-0.01%) (Pittenger *et al.*, 1999). Moreover, maintaining multipotency of the MSCs will be important during the expansion period, to ensure that the majority of cells differentiate to the required cell type. Control of these processes will be pivotal, in ensuring that the desired processes are promoted at the correct times, avoiding uncontrolled growth or spontaneous differentiation.

To this end, nanotopography, which attempts to mimic the biophysical component of the cells' extracellular environment or niche, offered a method in which to influence MSC response. Exploration of the mechanisms affected by nanotopography was carried out in this study. Following optimisation to obtain the most efficient response from the substrate of focus, SQ, self-renewal was compared to osteogenesis induced by culture on NSQ. Metabolomic profile, gene expression and cell cycle proteins were assessed and differences between surfaces were analysed. Recognising the complexities of the stem cell niche in bone marrow, a model incorporating nanotopography and other components was trialled in small-scale study, attempting to improve on the existing 2D system. The potential for the SQ nanotopography in reversion of lineage commitment was subjected to preliminary investigation; this was in keeping with the view to exploit nanotopography further for biomedical purposes. This chapter will discuss the main conclusions of each section of work and expand on some of the aforementioned findings and the wider implications of the results demonstrated in this thesis.

6.1.1 Utilising nanotopographies as a tool for study of MSCs

It was demonstrated that nanotopographies could be utilised to induce osteogenesis in addition to maintaining multipotency, thereby are suitable for use as tool to further study these processes in MSCs. These particular nanopatterns chosen were previously tested for induction of these processes (Dalby *et al.*, 2007, McMurray *et al.*, 2011, Tsimbouri *et al.*, 2012), and thus provided important foundations to this work. Although each of these studies were performed on different materials, PMMA, PCL and now polycarbonate, the effects of the pitted nanotopographies on MSC phenotype were shown to be reproducible, possibly indicating that these smaller scale stimuli are combinatorially stronger than the properties of the material itself. However, it stands to reason that the best approach would be to find a material that would markedly enhance the effect of nanotopography.

It was found that cell seeding density was an important factor for the MSC response to nanotopography, which became a concern following implementation of a seeding device for the addition of cells. Although use of the cell seeder minimised the cell number required for each experiment due the ability to seed directly onto the surface of each substrate, using the same number of cells as previous work meant an over-confluence over longer periods of culture. A small number of studies have assessed MSC seeding density (Both *et al.*, 2007), but none have addressed this issue on nanotopography. Seeding number has been indicated to have an effect on proliferation and differentiation, with lower densities being more conducive towards differentiation and higher densities exhibiting a greater degree of proliferation (Pittenger *et al.*, 1999, McBeath *et al.*, 2004, Gobaa *et al.*, 2011), though there are some conflicting reports that lower densities promote faster proliferation (Colter *et al.*, 2000, Sekiya *et al.*, 2002, Both *et al.*, 2007) and retain a higher proportion of multipotent cells (Colter *et al.*, 2000, Sekiya *et al.*, 2002). Some of these findings contrast with the results obtained with nanotopography, whereby the MSCs seeded at higher concentrations were more likely to accumulate OPN, which together with OCN, show increased expression with osteogenic differentiation (Rickard *et al.*, 1994). One of the benefits in determining and defining the number of MSCs seeded in a given area, is that the reproducibility of experiments will be improved, and this

value can be adapted depending on the size of the substrate if this changes in future work.

6.1.2 Metabolomic changes in self-renewing and differentiating MSCs

It was found that some of the metabolomic differences in self-renewing and differentiating MSCs drew parallels with ESCs, specifically studies by Yanes *et al.* which showed that the number of saturated metabolites increased when ESCs were undergoing differentiation (Yanes *et al.*, 2010). Here, more unsaturated metabolites were detected in MSCs cultured on the SQ, which should contain more multipotent MSCs in comparison to NSQ, where the majority of cells should be undergoing differentiation. Global changes in metabolite profile were more evident at the shorter culture time of 7 days, suggesting that differences become established in the earlier stages of cell development. An observed abundance of amino acid metabolites on NSQ were attributed to preparatory stages of an increase in protein production, as many will be required for differentiation processes. Another interesting aspect of this part of the work was a trend towards downregulation of metabolites on SQ, whereas a greater number of upregulations were present on NSQ, contrasting the differences in activity between self-renewing and differentiation states. It has been shown that MSCs undergoing osteogenic differentiation induced by culture in osteogenic medium display increased metabolism (Reyes *et al.*, 2006). Conversely, it is thus plausible that self-renewing MSCs will exhibit low metabolic activity, indications of which have been observed in this metabolic study in agreement with previous work (Reyes *et al.*, 2006, McMurray *et al.*, 2011). This further indicates that metabolic fingerprints are useful in describing the phenotype of MSCs and is in line with other MSC studies.

Lipid metabolism has been investigated largely in HSCs, and has been demonstrated to have links with division and self-renewal (Ito *et al.*, 2012, Yusuf and Scadden, 2012). In this work, it was shown that a high level of metabolic activity in the lipid data grouping was present on SQ, which implies that lipids have an important role in MSC maintenance. However, it is probable that lipids also contribute towards osteogenesis, particularly in terms of levels of

unsaturated fatty acids. A theory that tethers adipogenesis to osteogenesis suggests an inverse relationship between these two pathways of lineage commitment, with one occurring at the expense of the other (James, 2013). This is highlighted by the observation that ablation of OPN encourages adipogenesis to occur (Chen *et al.*, 2014b). It is possible that a point of convergence exists within a stage of both adipogenic and osteogenic differentiation. The level of unsaturated fatty acids should decrease as osteogenesis progresses (showing decreased activation of peroxisome proliferator-activated receptors). Concomitantly, energy demands will steadily increase, leading to bioenergetic switching from anaerobic to oxidative processes (Yanes *et al.*, 2010). It is interesting to note that a level of exposure to unsaturated fatty acids (linoleic and oleic acid) decreased proliferation of MSCs (Smith *et al.*, 2012), a characteristic indicative of the onset of differentiation (Boland *et al.*, 2004) which shows that fatty acids could be used to control the onset of osteogenesis. Further analysis of unsaturated fatty acids is therefore an avenue warranting exploration for continuation of this work.

The metabolomics analyses carried out here did result in a number of metabolites that did not have known identities to linked databases, and conversely, some of those identified may not have active roles in MSCs, therefore validation of putative targets with other techniques and additional assessments would be logical next steps. Nevertheless, metabolomics offers interesting information that may lead to the identification of potentially important metabolites involved in establishment of osteogenesis or maintaining self-renewal. The untargeted metabolomics approach adopted is particularly useful in terms of hypothesis generation. It is recommended that proposed mechanisms and findings warrant further testing for reproducibility and confirmation of hypotheses put forward here.

6.1.3 Influence of nanotopography on cell cycle and gene expression of MSCs

Research pertaining to the cell cycle of MSCs limited and greatly lacking in the context of nanotopography. A recent study carried out by Kulangara *et al.* demonstrated decreased retinoblastoma protein levels and inferred decrease in

proliferation following culture on 350 nm grooves (Kulangara *et al.*, 2014b), indicating that cell cycle is affected upon culture on nanotopographical features.

Investigation into the cell cycle of MSCs on nanotopography yielded some interesting findings. There was evidence to indicate that populations of MSCs were being held in G0/G1 phase on SQ in comparison to those cultured on the flat control. In order to expand MSCs on the SQ substrates, cycle progression is still required through the cell cycle; therefore, it is reassuring to observe a similar proportion of cells in G2/M phase on both surface types. Quantification of cell cycle related proteins appeared to underline these observations, with levels of proteins such as cyclin D1, E2F-1 and pRb showing trends towards a degree of reduced proliferation and progression through the cell cycle on SQ. These observations conflict with results of BrdU assays performed at several time points, which did not reveal any significant differences in the number of cells progressing through S phase. This rules out quiescence on SQ, and large changes in proliferation between substrates. Thus, other possibilities include subpopulations of MSCs undergoing slower progression whilst others cycle normally, with SQ maintaining several pools of cells at the same time in a dynamic system.

In addition, CDK6 was found to be elevated on SQ, however, an association between filopodial spreading and levels of this protein was not proven with inhibition experiments. However, it is possible that inhibition was not wholly efficient, in that filopodia formation was not prevented altogether, therefore other strategies could be employed to better target the genes involved. Assessment of phosphorylated forms of CDK6 would provide more information pertaining to the role of CDK6 on SQ, as some are activatory or inhibitory depending on the phosphorylation site (Kaldis, 1999, Pavletich, 1999). Indirect evidence strongly suggests that nanotopography is highly likely to induce changes in cell cycle. These are related to cellular spreading, integrins, intracellular tension and activation of signalling pathways. Inhibition of spreading has been shown to lead to arrest in G1 phase in growth factor treated cells (Folkman and Moscona, 1978). This is interesting with reference to

nanotopography due to contact guidance being observed on SQ, demonstrating partial inhibition of spreading of filopodia at the cell edges.

Larger integrin-containing focal adhesions are associated with an osteogenic phenotype (Biggs *et al.*, 2009a) and was shown to be the case on NSQ in previous work (Tsimbouri *et al.*, 2014). Furthermore, this increase in focal adhesion size was significantly higher than SQ, showing that MSCs on the self-renewing substrates form smaller adhesions (Tsimbouri *et al.*, 2014). These adhesion structures transmit force through the cytoskeleton, with larger adhesions creating larger forces (Choquet *et al.*, 1997). Focal adhesions also respond to external forces from the surrounding environment (Wang and Ingber, 1995). It therefore follows that changing physical aspects of the MSCs culture environment will lead to adjustments in focal adhesions, altering intracellular tension and having actions on signalling molecules that associate with the cytoskeleton (Miyamoto *et al.*, 1995). Evidence for this putative mechanism includes a study where an increase in ERK-mediated induction of cyclin D1 was demonstrated after increasing intracellular tension using cytochalasin D to disrupt the cytoskeleton (Böhmer *et al.*, 1996). Walker *et al.* proposed a tension-cell cycle model for growth factor stimulated cell signalling, which could be applicable to those cultured on nanotopography. The model illustrates that cells below a certain tension threshold will be unable to progress through the cell cycle due to failure to elicit ERK-dependent activation of cyclin D1 (Walker *et al.*, 2005). Conversely, high levels of tension conferred by actin polymerisation or formation of actin stress fibres would result in Rho-mediated induction of cyclin D1 or prolonged ERK activation leading to recruitment of cyclin D1 respectively (Walker *et al.*, 2005). Synchronised MSCs released into cycle on SQ, showed elevated pERK and lowered cyclin D1 after 24 hours, which suggests transient activation of ERK, which would be insufficient to promote widespread cell cycle progression. This indicates that MSCs on SQ largely display a lower tension phenotype, one that does not exceed the tension threshold required to activate cell cycle related pathways associated with cytoskeletal integrity.

Integrin signalling can trigger activation of focal adhesion kinase, which in turn can activate the MAPK cascade, resulting in activation of ERK (Moreno-Layseca and Streuli, 2014). ERK activity, (ERK 5 and ERK1/2) can affect cell cycle

progression, through regulation of cyclin D1 (Roovers and Assoian, 2000, Mulloy *et al.*, 2003, Legate *et al.*, 2009). It is important to note that ERK requires shuttling to the nucleus through association with anchoring proteins (Moreno-Layseca and Streuli, 2014), therefore, the organisation of the cytoskeleton may become more important in this regard, in allowing or preventing the occurrence of such interactions.

Indeed, links to pivotal signalling effectors ERK and JNK were identified as being up-regulated on NSQ (chapter 4), in agreement with previous work, in which inhibition of ERK and JNK decreased expression of lineage commitment markers (Tsimbouri *et al.*, 2012). Initial indications point towards an increased proportion of cells being held in the early stages of the cell cycle, which is worthy of further investigation. Based on these observations, it is thus tempting to speculate that focus on the G1 phase will be of particular importance, as is the case with well-studied stem cell types, ESCs and HSCs. The duration of ERK activation was not investigated here, however it has been shown that transient and sustained ERK activity results in different actions, namely that sustained ERK signalling is pro-proliferative (Yamamoto *et al.*, 2006), whereas transient ERK signalling prevents entry into the cell cycle (Sharrocks, 2006). The findings in this study show that there is much scope for continuing investigation into the cell cycle of MSCs cultured on nanotopography.

6.1.4 Topography for MSC reprogramming

The potential for nanotopography to redirect the onset of osteogenic differentiation was investigated in this thesis. This idea originated from the basis that stem cells respond to extracellular physical cues in their niche that are likely to assist in the maintenance of pools of self-renewing stem cells. As we postulate that the SQ nanotopography is successfully mimicking an aspect of these cues, there was a possibility that culture on SQ would partially negate the differentiation process. It was hoped that incorporation of nanotopography could be used in the optimisation of reprogramming, which is in itself an inefficient process due to epigenetic barriers including inaccessible chromatin structures (Hanna *et al.*, 2010). However, it was found that marker levels in MSCs cultured on the nanotopographies tended to exhibit variable results from patient to

patient. Nevertheless, some positive indications were observed for the STRO-1 marker, with protein levels increasing following reseeding on SQ for two of the patients, though quantification of bone marker OPN did not provide evidence that reprogramming of differentiating cells was taking place. Inclusion of valproic acid generally led to increases in marker expression regardless of substrate type. Taken together, the SQ nanotopography may not provide sufficiently strong cues for the purposes of reprogramming, yet is able to expand the pool of MSCs that were originally selected for. This is a promising indication that the SQ substrates remain effective on populations of MSCs even after they have been subjected to differentiation cues.

Reprogramming of cells remains a fairly recent concept, with the inclusion of topography being even more so. Polystyrene substrates patterned with micro-gratings or micro-pillars of two diameters and spacing were assessed in terms of efficiency of reprogramming fibroblasts into induced neurons (Kulangara *et al.*, 2014a). Here, the authors indicated that morphological changes, with observations of increased neurite branching and outgrowth on some of these micropatterns, together with expression of neuronal genes demonstrated the potential of topography in reprogramming (Kulangara *et al.*, 2014a). Downing *et al.* compared reprogramming of mouse primary fibroblasts on microtopography to assisted reprogramming using epigenetic modifiers, showing that micron scale grooves increased levels of histone H3 acetylation promoting reprogramming, and could replicate the effect of adding valproic acid and tranylcypromine hydrochloride in the generation of Nanog⁺ colonies (Downing *et al.*, 2013). Use of nanotopography in reprogramming appears to be a growing area of research in recent years, and it would be useful to explore which types of nanopatterns are best for induction of pivotal epigenetic modifications to allow reprogramming to take place most efficiently.

6.2 Thesis conclusion

The research described in this thesis has contributed towards increasing understanding of MSC self-renewal. The results demonstrated that nanotopography could be used in the promotion of either maintenance of multipotency or osteogenic differentiation. MSCs were successfully isolated from

bone marrow (in-house), allowing testing of clinically relevant MSCs (chapter 3) in addition to those from an established source for more detailed aspects of this study (chapters 4 and 5). Colony growth patterns were observed upon seeding at lower initial densities, which may be important in maintaining a self-renewal state. Broad-scale analysis was achieved with metabolomics and next generation sequencing, highlighting that MSCs cultured on the SQ nanotopography may be exhibiting attributes associated with cells that are not undergoing differentiation. Furthermore, these MSCs were not demonstrated to maintain quiescence or a dormant state, but appeared, in some aspects, to be undergoing slowed progression through the cell cycle.

6.3 Recommendations for future work

As a result of the findings in this thesis, there is scope for additional research to take place in exploring the wider implications of culturing cells on nanopit nanotopography and to progress MSC studies still further. It has been shown here that nanotopography can be employed as a tool for study of maintenance of MSC phenotype as well as osteogenic differentiation, which means that mechanistic studies can be carried out in order to determine the importance of particular metabolites, genes or adhesion-related factors for self-renewal. Some suggestions for future work are detailed in the proceeding subsections.

6.3.1 Nanotopography for the culture of MSCs *in vitro*

From a practical view, nanotopography can be easily implemented for widespread use through the application of nanopatterns directly onto tissue culture plastic (polystyrene). The SQ nanopatterning would be of particular interest. If successful, this would potentially open up the possibility of preservation of stemness during expansion *in vitro*, and dampen the loss of markers associated with multipotency. As seeding density has now been optimised for human MSCs extracted from bone marrow, effective seeding conditions in combination with SQ nanotopography should present an attractive application of this work for the scientific community. Furthermore, as alluded to

in section 6.1.1, testing of other materials may enhance the strength of the nanocues further still.

6.3.2 Three-dimensional MSC environments

Much existing work in tissue engineering and regenerative medicine has been carried out on 2D surfaces, though it is increasingly evident that disparities exist between the mechanisms underlying biological processes in these different environments. It is now appreciated that 3D microenvironments offer more complexity than those in 2D, including interactions with multiple cell types, soluble factors, and elements of the ECM, including topographical cues and spatial/structural constraints. An attempt was made to address some of these factors and incorporate them into more physiologically relevant model, in the assessment of a multi-component system to achieve expansion of MSCs that retain a good degree of MSC marker expression. Using MSCs cultured on nanopit nanotopography as a foundation, we propose the addition of collagen and HSCs to increase the degree of MSC marker expression that could be achieved using nanotopography in isolation. This would provide further complexity to better mimic the *in vivo* bone marrow microenvironment.

Initial work, to which lack of time did not allow further progress to be made, demonstrated that nestin expression increased after 7 days of culture with the addition of a collagen gel component, independent of whether nanopatterning, suggesting that this is a stiffness-mediated effect (*Figure 6-1*).

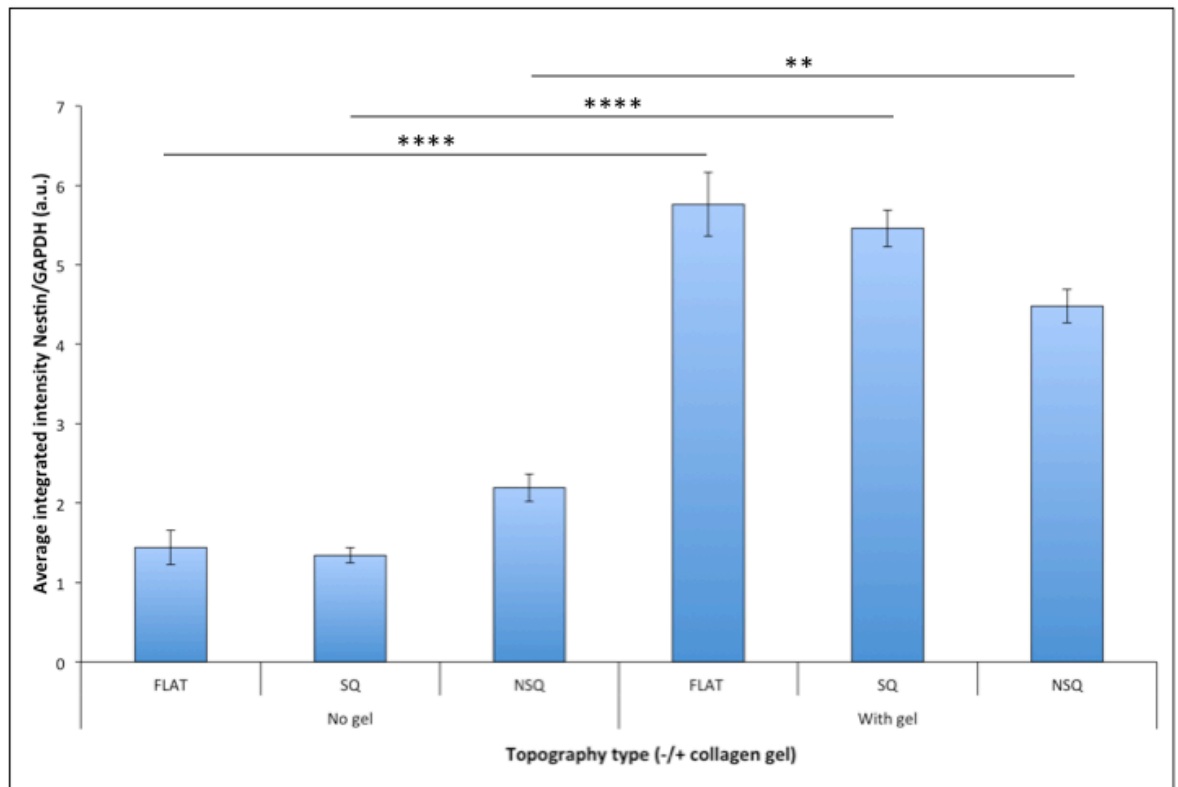


Figure 6-1: Application of a collagen gel increases nestin expression. ICW quantification indicates that use of a collagen gel increases expression of nestin, an effect which was nanotopography independent. Results represent the average integrated intensity of nestin normalised to GAPDH protein levels across 3 material replicates. Error bars denote \pm standard error of the mean. Statistical significance was assessed by one-way ANOVA with Tukey's multiple comparisons test. **** $p < 0.0001$, ** $p < 0.01$

Engler *et al.* showed that nestin expression is stiffness induced, proposing that the soft gels used in their studies promoted commitment towards a neuronal lineage (Engler *et al.*, 2006). Here, we alternatively suggest nestin as a niche marker rather than a neuron-specific marker, as nestin⁺ MSCs located in the bone marrow niche are closely associated with catecholaminergic nerve fibres and HSCs are responsive to the rhythmic oscillations delivered by the sympathetic nervous system (Mendez-Ferrer *et al.*, 2010).

Hypoxia could be a prerequisite factor for the expression of nestin, consistent with low oxygen conditions characteristic of bone marrow (Tsai *et al.*, 2012). Moreover, this would explain the drop in nestin expression when cultured on the nanotopography and control surfaces without the gel. Existing literature supports incorporation of hypoxic conditions in MSC studies, as low oxygen tension has been shown to suppress adipogenic and osteogenic differentiation (Fehrer *et al.*, 2007, Potier *et al.*, 2007) as well as increasing proliferation in

terms of cell number (Grayson *et al.*, 2007) or in the number of population doublings prior to eventual growth arrest (Fehrer *et al.*, 2007).

In addition, stem cell niches contain other cell types, such as osteoblasts and haematopoietic stem cells (HSCs) (Yin and Li, 2006). Cross-talk between the different cell types in the bone marrow appears to be important; an example being that signalling from MSCs are key to maintaining the survival and proliferation of HSC progenitor cells (Walenda *et al.*, 2010). Therefore, the addition of other cell types might bring improvement to the current nanotopography system in terms of efficiently propagating MSCs. Preliminary work incorporated HSCs within the collagen gels that were placed over MSCs seeded on nanotopography, and demonstrated that both cell types remained viable (Figure 6-2).

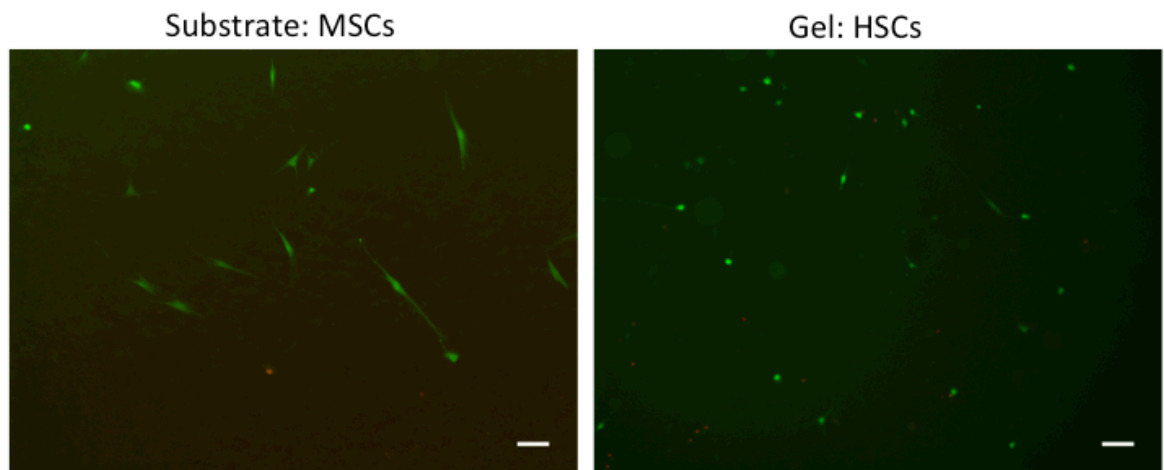


Figure 6-2: Live/dead staining of MSCs and HSCs in the nanotopography-collagen gel system. MSCs that had adhered onto the PCL substrates and were overlaid with collagen gel containing HSCs, were stained with a fluorescence-based live/dead viability stain (which uses calcein acetoxymethyl ester and propidium iodide). The HSCs within the collagen gel were also stained accordingly. Cells labelled green are viable cells, whereas those labelled red are dead. Images were acquired at 4x magnification. Scale bar: 100 μm .

Other studies have utilised aggregates of MSCs, known as ‘spheroids’ or ‘mesenspheres’ (Baraniak and McDevitt, 2012, Alimperti *et al.*, 2014), which can be produced by the hanging drop method, low-binding plates, or forced aggregation by centrifugation, arguing that this is more reminiscent of the *in vivo* environment. Spheroids of adipose-derived stem cells display enhanced survival in nutrient-deprived conditions and proliferation to a lesser extent (Cheng *et al.*, 2012). It is unknown whether MSCs migrating from the

nanotopography into a collagen gel would naturally cluster together if allowed sufficient time. If proven to be the case, this migratory behaviour would be intriguing, as it would indicate that patterns of movement are inherently programmed into MSCs when conditions mimic the bone marrow environment more closely. Therefore, there are avenues to explore in progressing nanotopography into a 3D platform for expansion of multipotent MSCs.

6.3.3 MSCs as supporting cells for regenerative medicine

MSCs themselves are immune privileged, meaning that they do not elicit immune responses when transplanted. This may be due to the fact that they can be found in many different tissues (Meirelles *et al.*, 2006), including brain, dental pulp and even fat, which is now becoming an increasingly common source of MSCs (Zuk *et al.*, 2001, Bunnell *et al.*, 2008, Sun *et al.*, 2009). Furthermore, MSCs have reported immunomodulatory functions on other cells, and it has been shown that they are immunosuppressive (Caplan, 2007, Ankrum and Karp, 2010), which may potentiate the engraftment of other cell types. Immuno-rejection is large limitation with proposed clinical therapies. The premise is that nanotopography-expanded MSCs could be delivered together with the desired cell type for tissue repair for example.

Alternatively, there has been increasing interest in using MSCs to support cells of the haematopoietic system. HSCs are a rare population in bone marrow, and differentiate into mature blood cell types (Orkin and Zon, 2008). The ability to supply blood cells derived from progenitor cells would potentially relieve current pressure on blood donations. It has been demonstrated that co-culture of MSCs with haematopoietic progenitor cells over a period of 5 weeks supported haematopoietic proliferation and differentiation (Majumdar *et al.*, 1998). Co-culture of the two cell types is a logical strategy, as expansion and maintenance of HSCs is dependent on the presence of CXCL12 (Greenbaum *et al.*, 2013), a chemokine produced by bone marrow MSCs (Mishima *et al.*, 2010). Although the concept of MSCs supporting haematopoiesis is not new, MSCs cultured on SQ nanotopography could plausibly support haematopoietic cells over longer periods of culture, as it has been shown that MSCs on SQ expressed stem cell markers after 8 weeks (McMurray *et al.*, 2011). Comparison to the NSQ substrates should

be tested in parallel, as there is evidence to suggest that co-culture with osteogenic differentiated MSCs has a stronger effect on HSC expansion compared to undifferentiated MSCs (Mishima *et al.*, 2010).

6.3.4 Nanotopography as a platform to investigate adhesion and tension

As alluded to previously, it is likely that the nanotopographies affect focal adhesions, influencing their size and distribution, and could affect their stability and downstream effects on signalling pathways. Although focal adhesions were not studied in this project, nanotopography has been shown previously as being implicated in eliciting changes to these anchoring points in a range of cell types (Biggs *et al.*, 2007b, Yim *et al.*, 2010, Chen *et al.*, 2012).

In view of larger focal adhesions being present in MSCs undergoing osteogenesis on NSQ (Tsimbouri *et al.*, 2012), it is plausible that topographies that involve some disruption of FA formation may prevent the highly spread and flattened morphology associated with osteoblasts (McBeath *et al.*, 2004), and additionally abrogate the onset of a high tension state. Indeed, ordered hexagonally arranged nanopits have been reported as reducing adhesion of fibroblasts, characterised by the number of focal contacts and adhesions in comparison to flat controls (Dalby *et al.*, 2006a). The reduction of adhesion could be one reason for the effect of the SQ surface in promotion of self-renewal.

Furthermore, the spacing between features or ligands is important in allowing formation of adhesion bridges (Malmström *et al.*, 2011). This occurs when one adhesion is close enough to join to another and could be important in progression of osteogenic differentiation. Exploration of different nanotopographical features and spacings would reveal information regarding which dimensions would be best for optimisation of MSC self-renewal or osteogenesis.

List of References

- ABDALLAH, B. M. & KASSEM, M. 2007. Human mesenchymal stem cells: from basic biology to clinical applications. *Gene Therapy*, 15, 109-116.
- ABRAMOFF, M. D., MAGALHÃES, P. J. & RAM, S. J. 2004. Image processing with ImageJ. *Biophotonics international*, 11, 33-42.
- AL-NBAHEEN, M., VISHNUBALAJI, R., ALI, D., BOUSLIMI, A., AL-JASSIR, F., MEGGES, M., PRIGIONE, A., ADJAYE, J., KASSEM, M. & ALDAHMAH, A. 2013. Human Stromal (Mesenchymal) Stem Cells from Bone Marrow, Adipose Tissue and Skin Exhibit Differences in Molecular Phenotype and Differentiation Potential. *Stem Cell Reviews*, 9, 32-43.
- ALBRECHT-BUEHLER, G. 1976. Filopodia of spreading 3T3 cells. Do they have a substrate-exploring function? *The Journal of Cell Biology*, 69, 275-286.
- ALBRECHT-BUEHLER, G. 1979. The angular distribution of directional changes of guided 3T3 cells. *The Journal of Cell Biology*, 80, 53-60.
- ALBUSCHIES, J. & VOGEL, V. 2013. The role of filopodia in the recognition of nanotopographies. *Sci. Rep.*, 3.
- ALENGHAT, F. J. & INGBER, D. E. 2002. Mechanotransduction: All Signals Point to Cytoskeleton, Matrix, and Integrins. *Science Signalling*, 2002, pe6-pe6.
- ALI, M. Y., CHUANG, C.-Y. & SAIF, M. T. A. 2014. Reprogramming cellular phenotype by soft collagen gels. *Soft Matter*, 10, 8829-8837.
- ALIMPERTI, S., LEI, P., WEN, Y., TIAN, J., CAMPBELL, A. M. & ANDREADIS, S. T. 2014. Serum-free spheroid suspension culture maintains mesenchymal stem cell proliferation and differentiation potential. *Biotechnology Progress*, 30, 974-983.
- ALTISSIMO, M. 2010. E-beam lithography for micro-/nanofabrication. *Biomicrofluidics*, 4, 026503.
- AMIT, M., MARGULETS, V., SEGEV, H., SHARIKI, K., LAEVSKY, I., COLEMAN, R. & ITSKOVITZ-ELDOR, J. 2003. Human Feeder Layers for Human Embryonic Stem Cells. *Biology of Reproduction*, 68, 2150-2156.
- ANDERS, S. & HUBER, W. 2010. Differential expression analysis for sequence count data. *Genome Biology*, 11, R106.
- ANDERSON, J. M., RODRIGUEZ, A. & CHANG, D. T. 2008. Foreign Body Reaction To Biomaterials. *Seminars in immunology*, 20, 86-100.
- ANDREAS, K., SITTINGER, M. & RINGE, J. 2014. Toward *in situ* tissue engineering: chemokine-guided stem cell recruitment. *Trends in Biotechnology*, 32, 483-492.
- ANKRUM, J. & KARP, J. M. 2010. Mesenchymal stem cell therapy: Two steps forward, one step back. *Trends in molecular medicine*, 16, 203-209.
- APLIN, A. E. & JULIANO, R. L. 1999. Integrin and cytoskeletal regulation of growth factor signaling to the MAP kinase pathway. *Journal of Cell Science*, 112, 695-706.
- ARNOLD, M., CAVALCANTI-ADAM, E. A., GLASS, R., BLÜMMEL, J., ECK, W., KANTLEHNER, M., KESSLER, H. & SPATZ, J. P. 2004. Activation of Integrin Function by Nanopatterned Adhesive Interfaces. *ChemPhysChem*, 5, 383-388.
- ARTIGAS, N., URENA, C., RODRIGUEZ-CARBALLO, E., ROSA, J. L. & VENTURA, F. 2014. Mitogen activated protein kinase (MAPK)-regulated Interactions between Osterix and Runx2 Are Critical for the Transcriptional Osteogenic Program. *Journal of Biological Chemistry*.

- BADDOO, M., HILL, K., WILKINSON, R., GAUPP, D., HUGHES, C., KOPEN, G. C. & PHINNEY, D. G. 2003. Characterization of mesenchymal stem cells isolated from murine bone marrow by negative selection. *Journal of Cellular Biochemistry*, 89, 1235-1249.
- BAI, B., HE, J., LI, Y.-S., WANG, X.-M., AI, H.-J. & CUI, F.-Z. 2013. Activation of the ERK1/2 Signaling Pathway during the Osteogenic Differentiation of Mesenchymal Stem Cells Cultured on Substrates Modified with Various Chemical Groups. *BioMed Research International*, 2013, 361906.
- BAKER, B. M. & CHEN, C. S. 2012. Deconstructing the third dimension - how 3D culture microenvironments alter cellular cues. *Journal of Cell Science*, 125, 3015-3024.
- BALLESTREM, C., HINZ, B., IMHOF, B. A. & WEHRLE-HALLER, B. 2001. Marching at the front and dragging behind: differential α V β 3-integrin turnover regulates focal adhesion behavior. *The Journal of Cell Biology*, 155, 1319-1332.
- BANEYX, G., BAUGH, L. & VOGEL, V. 2002. Fibronectin extension and unfolding within cell matrix fibrils controlled by cytoskeletal tension. *Proceedings of the National Academy of Sciences*, 99, 5139-5143.
- BAR-NUR, O., BRUMBAUGH, J., VERHEUL, C., APOSTOLOU, E., PRUTEANU-MALINICI, I., WALSH, R. M., RAMASWAMY, S. & HOCHEDLINGER, K. 2014. Small molecules facilitate rapid and synchronous iPSC generation. *Nat Meth*, 11, 1170-1176.
- BARANIAK, P. & MCDEVITT, T. 2012. Scaffold-free culture of mesenchymal stem cell spheroids in suspension preserves multilineage potential. *Cell and Tissue Research*, 347, 701-711.
- BARKER, T. H. 2011. The role of ECM proteins and protein fragments in guiding cell behavior in regenerative medicine. *Biomaterials*, 32, 4211-4214.
- BARRIÈRE, C., SANTAMARÍA, D., CERQUEIRA, A., GALÁN, J., MARTÍN, A., ORTEGA, S., MALUMBRES, M., DUBUS, P. & BARBACID, M. 2007. Mice thrive without Cdk4 and Cdk2. *Molecular Oncology*, 1, 72-83.
- BARRY, F., BOYNTON, R. E., LIU, B. & MURPHY, J. M. 2001. Chondrogenic Differentiation of Mesenchymal Stem Cells from Bone Marrow: Differentiation-Dependent Gene Expression of Matrix Components. *Experimental Cell Research*, 268, 189-200.
- BERRY, C. C., CAMPBELL, G., SPADICINO, A., ROBERTSON, M. & CURTIS, A. S. G. 2004. The influence of microscale topography on fibroblast attachment and motility. *Biomaterials*, 25, 5781-5788.
- BERSHADSKY, A. D., TINT, I. S., NEYFAKH JR, A. A. & VASILIEV, J. M. 1985. Focal contacts of normal and RSV-transformed quail cells: Hypothesis of the transformation-induced deficient maturation of focal contacts. *Experimental Cell Research*, 158, 433-444.
- BETTINGER, C., J., LANGER, R. & BORENSTEIN, J. T. 2009. Engineering substrate micro- and nanotopography to control cell function. *Angewandte Chemie International Edition* 48, 5406-5415.
- BHADIRAJU, K. & HANSEN, L. K. 2002. Extracellular Matrix- and Cytoskeleton-Dependent Changes in Cell Shape and Stiffness. *Experimental Cell Research*, 278, 92-100.
- BIAZAR, E., HEIDARI, M., ASEFNEZHAD, A. & MONTAZERI, N. 2011. The relationship between cellular adhesion and surface roughness in polystyrene modified by microwave plasma radiation. *International Journal of Nanomedicine*, 6, 631-639.

- BIGGS, M. J., RICHARDS, R. G., GADEGAARD, N., MCMURRAY, R. J., AFFROSSMAN, S., WILKINSON, C. D., OREFFO, R. O. & DALBY, M. J. 2009a. Interactions with nanoscale topography: adhesion quantification and signal transduction in cells of osteogenic and multipotent lineage. *Journal of Biomedical Materials Research Part A*, 91, 195-208.
- BIGGS, M. J. P. & DALBY, M. J. 2010. Focal adhesions in osteoneogenesis. *Proceedings of the Institution of Mechanical Engineers Part H-Journal of Engineering in Medicine*, 224, 1441-1453.
- BIGGS, M. J. P., RICHARDS, R. G., GADEGAARD, N., WILKINSON, C. D. W. & DALBY, M. J. 2007a. The effects of nanoscale pits on primary human osteoblast adhesion formation and cellular spreading. *Journal of Materials Science-Materials in Medicine*, 18, 399-404.
- BIGGS, M. J. P., RICHARDS, R. G., GADEGAARD, N., WILKINSON, C. D. W. & DALBY, M. J. 2007b. Regulation of implant surface cell adhesion: characterization and quantification of S-phase primary osteoblast adhesions on biomimetic nanoscale substrates. *Journal of Orthopaedic Research*, 25, 273-282.
- BIGGS, M. J. P., RICHARDS, R. G., GADEGAARD, N., WILKINSON, C. D. W., OREFFO, R. O. C. & DALBY, M. J. 2009b. The use of nanoscale topography to modulate the dynamics of adhesion formation in primary osteoblasts and ERK/MAPK signalling in STRO-1+enriched skeletal stem cells. *Biomaterials*, 30, 5094-5103.
- BIGGS, M. J. P., RICHARDS, R. G., MCFARLANE, S., WILKINSON, C. D. W., OREFFO, R. O. C. & DALBY, M. J. 2008. Adhesion formation of primary human osteoblasts and the functional response of mesenchymal stem cells to 330 nm deep microgrooves. *Journal of the Royal Society Interface*, 5, 1231-1242.
- BLANPAIN, C., LOWRY, W. E., GEOGHEGAN, A., POLAK, L. & FUCHS, E. 2004. Self-Renewal, Multipotency, and the Existence of Two Cell Populations within an Epithelial Stem Cell Niche. *Cell*, 118, 635-648.
- BLAU, H. M., BRAZELTON, T. R. & WEIMANN, J. M. 2001. The Evolving Concept of a Stem Cell: Entity or Function? *Cell*, 105, 829-841.
- BLIN, G., LABLACK, N., LOUIS-TISSERAND, M., NICOLAS, C., PICART, C. & PUCÉAT, M. 2010. Nano-scale control of cellular environment to drive embryonic stem cells self-renewal and fate. *Biomaterials*, 31, 1742-1750.
- BOEHLER, R. M., GRAHAM, J. G. & SHEA, L. D. 2011. Tissue engineering tools for modulation of the immune response. *BioTechniques*, 51, 239-passim.
- BÖHMER, R. M., SCHARF, E. & ASSOIAN, R. K. 1996. Cytoskeletal integrity is required throughout the mitogen stimulation phase of the cell cycle and mediates the anchorage-dependent expression of cyclin D1. *Molecular Biology of the Cell*, 7, 101-111.
- BOLAND, G. M., PERKINS, G., HALL, D. J. & TUAN, R. S. 2004. Wnt 3a promotes proliferation and suppresses osteogenic differentiation of adult human mesenchymal stem cells. *Journal of Cellular Biochemistry*, 93, 1210-1230.
- BOSNAKOVSKI, D., MIZUNO, M., KIM, G., ISHIGURO, T., OKUMURA, M., IWANAGA, T., KADOSAWA, T. & FUJINAGA, T. 2004. Chondrogenic differentiation of bovine bone marrow mesenchymal stem cells in pellet cultural system. *Experimental Hematology*, 32, 502-509.
- BOTH, S. K., VAN DER MUIJSENBERG, A. J. C., VAN BLITTERSWIJK, C. A., DE BOER, J. & DE BRUIJN, J. D. 2007. A Rapid and Efficient Method for Expansion of Human Mesenchymal Stem Cells. *Tissue Engineering*, 13, 3-9.

- BOXALL, S. A. & JONES, E. 2012. Markers for Characterization of Bone Marrow Multipotential Stromal Cells. *Stem Cells International*, 2012, 12.
- BRADFORD, M. 1976. A rapid and sensitive method for the quantitation of microgram quantities of protein utilizing the principles of protein-dye binding. *Analytical Biochemistry*, 72, 248-254.
- BREMER, A. & AEBI, U. 1992. The structure of the F-actin filament and the actin molecule. *Current Opinion in Cell Biology*, 4, 20-26.
- BRYDONE, A. S., DALBY, M. J., BERRY, C. C., MEEK, R. M. D. & MCNAMARA, L. E. 2011. Grooved surface topography alters matrix-metalloproteinase production by human fibroblasts. *Biomedical Materials*, 6.
- BÜHRING, H. J., BATTULA, V. L., TREML, S., SCHEWE, B., KANZ, L. & VOGEL, W. 2007. Novel Markers for the Prospective Isolation of Human MSC. *Annals of the New York Academy of Sciences*, 1106, 262-271.
- BUNNELL, B. A., FLAAT, M., GAGLIARDI, C., PATEL, B. & RIPOLL, C. 2008. Adipose-derived Stem Cells: Isolation, Expansion and Differentiation. *Methods (San Diego, Calif.)*, 45, 115-120.
- BURDICK, J. A. & VUNJAK-NOVAKOVIC, G. 2008. Engineered Microenvironments for Controlled Stem Cell Differentiation. *Tissue Engineering Part A*, 15, 205-219.
- CALALB, M. B., POLTE, T. R. & HANKS, S. K. 1995. Tyrosine phosphorylation of focal adhesion kinase at sites in the catalytic domain regulates kinase activity: a role for Src family kinases. *Molecular and Cellular Biology*, 15, 954-963.
- CALDER, A., ROTH-ALBIN, I., BHATIA, S., PILQUIL, C., LEE, J. H., BHATIA, M., LEVADOUX-MARTIN, M., MCNICOL, J., RUSSELL, J., COLLINS, T. & DRAPER, J. S. 2013. Lengthened G1 phase indicates differentiation status in human embryonic stem cells. *Stem Cells and Development* 22, 279-295.
- CALDERWOOD, D. A. 2004. Integrin activation. *Journal of Cell Science*, 117, 657-666.
- CAPLAN, A. I. 1991. Mesenchymal stem cells. *Journal of Orthopaedic Research*, 9, 641-650.
- CAPLAN, A. I. 2007. Adult mesenchymal stem cells for tissue engineering versus regenerative medicine. *Journal of Cellular Physiology*, 213, 341-347.
- CAPLAN, A. I. & DENNIS, J. E. 2006. Mesenchymal stem cells as trophic mediators. *Journal of Cellular Biochemistry*, 98, 1076-1084.
- CÁRCAMO-ORIVE, I., TEJADOS, N., DELGADO, J., GAZTELUMENDI, A., OTAEGUI, D., LANG, V. & TRIGUEROS, C. 2008. ERK2 protein regulates the proliferation of human mesenchymal stem cells without affecting their mobilization and differentiation potential. *Experimental Cell Research*, 314, 1777-1788.
- CAVALCANTI-ADAM, E. A., AYDIN, D., HIRSCHFELD-WARNEKEN, V. C. & SPATZ, J. P. 2008. Cell adhesion and response to synthetic nanopatterned environments by steering receptor clustering and spatial location. *HFSP Journal*, 2, 276-285.
- CAVALCANTI-ADAM, E. A., VOLBERG, T., MICOULET, A., KESSLER, H. & GEIGER, B. 2007. Cell spreading and focal adhesion dynamics are regulated by spacing of integrin ligands. *Biophysical Journal*, 62, 2964-2974.
- CENNI, E., PERUT, F. & BALDINI, N. 2011. *In vitro* models for the evaluation of angiogenic potential in bone engineering. *Acta Pharmacol Sin*, 32, 21-30.

- CHARRAS, G. & SAHAI, E. 2014. Physical influences of the extracellular environment on cell migration. *Nature Reviews Molecular Cell Biology*, 15, 813-824.
- CHASTAIN, S. R., KUNDU, A. K., DHAR, S., CALVERT, J. W. & PUTNAM, A. J. 2006. Adhesion of mesenchymal stem cells to polymer scaffolds occurs via distinct ECM ligands and controls their osteogenic differentiation. *Journal of Biomedical Materials Research Part A*, 78A, 73-85.
- CHEN, H. & LO, S. H. 2003. Regulation of tensin-promoted cell migration by its focal adhesion binding and Src homology domain 2. *Biochemical Journal*, 370, 1039-1045.
- CHEN, H.-C., APPEDDU, P. A., ISODA, H. & GUAN, J.-L. 1996. Phosphorylation of Tyrosine 397 in Focal Adhesion Kinase Is Required for Binding Phosphatidylinositol 3-Kinase. *Journal of Biological Chemistry*, 271, 26329-26334.
- CHEN, J.-L., DUAN, L., ZHU, W., XIONG, J. & WANG, D. 2014a. Extracellular matrix production *in vitro* in cartilage tissue engineering. *Journal of Translational Medicine*, 12, 88.
- CHEN, Q., SHOU, P., ZHANG, L., XU, C., ZHENG, C., HAN, Y., LI, W., HUANG, Y., ZHANG, X., SHAO, C., ROBERTS, A. I., RABSON, A. B., REN, G., ZHANG, Y., WANG, Y., DENHARDT, D. T. & SHI, Y. 2014b. An Osteopontin-Integrin Interaction Plays a Critical Role in Directing Adipogenesis and Osteogenesis by Mesenchymal Stem Cells. *Stem Cells*, 32, 327-337.
- CHEN, W., VILLA-DIAZ, L. G., SUN, Y., WENG, S., KIM, J. K., LAM, R. H. W., HAN, L., FAN, R., KREBSBACH, P. H. & FU, J. 2012. Nanotopography Influences Adhesion, Spreading, and Self-Renewal of Human Embryonic Stem Cells. *ACS Nano*, 6, 4094-4103.
- CHEUNG, N.-C., WANG, S. & YOUNG, T.-H. 2012. The influence of spheroid formation of human adipose-derived stem cells on chitosan films on stemness and differentiation capabilities. *Biomaterials*, 33, 1748-1758.
- CHESHIER, S. H., MORRISON, S. J., LIAO, X. & WEISSMAN, I. L. 1999. In vivo proliferation and cell cycle kinetics of long-term self-renewing hematopoietic stem cells. *Proceedings of the National Academy of Sciences*, 96, 3120-3125.
- CHEUNG, T. H. & RANDO, T. A. 2013. Molecular regulation of stem cell quiescence. *Nat Rev Mol Cell Biol*, 14, 329-340.
- CHONG, J.-L., WENZEL, P. L., SÁENZ-ROBLES, M. T., NAIR, V., FERREY, A., HAGAN, J. P., GOMEZ, Y. M., SHARMA, N., CHEN, H.-Z., OUSEPH, M., WANG, S.-H., TRIKHA, P., CULP, B., MEZACHE, L., WINTON, D. J., SANSOM, O. J., CHEN, D., BREMNER, R., CANTALUPO, P. G., ROBINSON, M. L., PIPAS, J. M. & LEONE, G. 2009. E2f1-3 switch from activators in progenitor cells to repressors in differentiating cells. *Nature*, 462, 930-934.
- CHOQUET, D., FELSENFELD, D. P. & SHEETZ, M. P. 1997. Extracellular Matrix Rigidity Causes Strengthening of Integrin-Cytoskeleton Linkages. *Cell*, 88, 39-48.
- CHRISTOPHER, M. J., RAO, M., LIU, F., WOLOSZYNEK, J. R. & LINK, D. C. 2011. Expression of the G-CSF receptor in monocytic cells is sufficient to mediate hematopoietic progenitor mobilization by G-CSF in mice. *The Journal of Experimental Medicine*, 208, 251-260.
- CHRISTOPHERSON, G. T., SONG, H. & MAO, H.-Q. 2009. The influence of fiber diameter of electrospun substrates on neural stem cell differentiation and proliferation. *Biomaterials*, 30, 556-564.

- CHRZANOWSKA-WODNICKA, M. & BURRIDGE, K. 1996. Rho-stimulated contractility drives the formation of stress fibers and focal adhesions. *The Journal of Cell Biology*, 133, 1403-1415.
- CHU, P. K., CHEN, J. Y., WANG, L. P. & HUANG, N. 2002. Plasma-surface modification of biomaterials. *Materials Science and Engineering: R: Reports*, 36, 143-206.
- CHUNG, S., DZEJA, P. P., FAUSTINO, R. S., PEREZ-TERZIC, C., BEHFAR, A. & TERZIC, A. 2007. Mitochondrial oxidative metabolism is required for the cardiac differentiation of stem cells. *Nature clinical practice. Cardiovascular medicine*, 4, S60-S67.
- CICCIMARO, E., HEVKO, J. & BLAIR, I. A. 2006. Analysis of phosphorylation sites on focal adhesion kinase using nanospray liquid chromatography/multiple reaction monitoring mass spectrometry. *Rapid Communications in Mass Spectrometry*, 20, 3681-3692.
- CLARK, P., CONNOLLY, P., CURTIS, A. S., DOW, J. A. & WILKINSON, C. D. 1987. Topographical control of cell behaviour. I. Simple step cues. *Development*, 99, 439-448.
- CLARK, P., CONNOLLY, P., CURTIS, A. S., DOW, J. A. & WILKINSON, C. D. 1990. Topographical control of cell behaviour: II. Multiple grooved substrata. *Development*, 108, 635-644.
- COLL, J. L., BEN-ZE'EV, A., EZZELL, R. M., RODRÍGUEZ FERNÁNDEZ, J. L., BARIBAULT, H., OSHIMA, R. G. & ADAMSON, E. D. 1995. Targeted disruption of vinculin genes in F9 and embryonic stem cells changes cell morphology, adhesion, and locomotion. *Proceedings of the National Academy of Sciences*, 92, 9161-9165.
- COLTER, D. C., CLASS, R., DIGIROLAMO, C. M. & PROCKOP, D. J. 2000. Rapid expansion of recycling stem cells in cultures of plastic-adherent cells from human bone marrow. *Proceedings of the National Academy of Sciences*, 97, 3213-3218.
- COOPER, N. F. 1985. The intermediate filament proteins. *Biochemical Education*, 13, 154-159.
- CREEK, D. J., JANKEVICS, A., BURGESS, K. E. V., BREITLING, R. & BARRETT, M. P. 2012. IDEOM: an Excel interface for analysis of LC-MS-based metabolomics data. *Bioinformatics*, 28, 1048-1049.
- CURTIS, A. S., FORRESTER, J. V., MCINNES, C. & LAWRIE, F. 1983. Adhesion of cells to polystyrene surfaces. *The Journal of Cell Biology*, 97, 1500-1506.
- CURTIS, A. S. G., GADEGAARD, N., DALBY, M. J., RIEHLE, M. O., WILKINSON, C. D. W. & AITCHISON, G. 2004. Cells react to nanoscale order and symmetry in their surroundings. *IEEE Transactions on Nanobioscience*, 3, 61-65.
- CURTIS, A. S. G. & VARDE, M. 1964. Control of cell behaviour: topological factors. *Journal of the National Cancer Institute*, 33, 15-26.
- DAHÉRON, L., OPITZ, S. L., ZAEHRES, H., LENSCH, W. M., ANDREWS, P. W., ITSKOVITZ-ELDOR, J. & DALEY, G. Q. 2004. LIF/STAT3 Signaling Fails to Maintain Self-Renewal of Human Embryonic Stem Cells. *Stem Cells*, 22, 770-778.
- DAHL, K. N., RIBEIRO, A. J. S. & LAMMERDING, J. 2008. Nuclear Shape, Mechanics, and Mechanotransduction. *Circulation Research*, 102, 1307-1318.

- DAHL, S. L. M., KYPSON, A. P., LAWSON, J. H., BLUM, J. L., STRADER, J. T., LI, Y., MANSON, R. J., TENDE, W. E., DIBERNARDO, L., HENSLEY, M. T., CARTER, R., WILLIAMS, T. P., PRICHARD, H. L., DEY, M. S., BEGELMAN, K. G. & NIKLASON, L. E. 2011. Readily Available Tissue-Engineered Vascular Grafts. *Science Translational Medicine*, 3, 68ra9.
- DALBY, M., GADEGAARD, N., RIEHLE, M. O., WILKINSON, C., SUTHERLAND, D. & AFFROSSMAN, S. 2006a. Nanotopographical stimulation of mesenchymal stem cells. *Comparative Biochemistry and Physiology a-Molecular & Integrative Physiology*, 143, S124-S124.
- DALBY, M. J. 2005. Topographically induced direct cell mechanotransduction. *Medical Engineering & Physics*, 27, 730-742.
- DALBY, M. J., GADEGAARD, N. & OREFFO, R. O. C. 2014. Harnessing nanotopography and integrin-matrix interactions to influence stem cell fate. *Nature Materials*, 13, 558-569.
- DALBY, M. J., GADEGAARD, N., RIEHLE, M. O., WILKINSON, C. D. W. & CURTIS, A. S. G. 2004a. Investigating filopodia sensing using arrays of defined nanopits down to 35 nm diameter in size. *International Journal of Biochemistry & Cell Biology*, 36, 2005-2015.
- DALBY, M. J., GADEGAARD, N., TARE, R., ANDAR, A., RIEHLE, M. O., HERZYK, P., WILKINSON, C. D. W. & OREFFO, R. O. C. 2007. The control of human mesenchymal cell differentiation using nanoscale symmetry and disorder. *Nature Materials*, 6, 997-1003.
- DALBY, M. J., MCCLOY, D., ROBERTSON, M., AGHELI, H., SUTHERLAND, D., AFFROSSMAN, S. & OREFFO, R. O. C. 2006b. Osteoprogenitor response to semi-ordered and random nanotopographies. *Biomaterials*, 27, 2980-2987.
- DALBY, M. J., MCCLOY, D., ROBERTSON, M., WILKINSON, C. D. W. & OREFFO, R. O. C. 2006c. Osteoprogenitor response to defined topographies with nanoscale depths. *Biomaterials*, 27, 1306-1315.
- DALBY, M. J., RIEHLE, M. O., JOHNSTONE, H., AFFROSSMAN, S. & CURTIS, A. S. G. 2004b. Investigating the limits of filopodial sensing: a brief report using SEM to image the interaction between 10 nm high nano-topography and fibroblast filopodia. *Cell Biology International*, 28, 229-236.
- DAMANIK, F. F. R., ROTHUIZEN, T. C., VAN BLITTERSWIJK, C., ROTMANS, J. I. & MORONI, L. 2014. Towards an *in vitro* model mimicking the foreign body response: tailoring the surface properties of biomaterials to modulate extracellular matrix. *Scientific Reports*, 4, 6325.
- DEEG, J. A., LOUBAN, I., AYDIN, D., SELHUBER-UNKEL, C., KESSLER, H. & SPATZ, J. P. 2011. Impact of Local versus Global Ligand Density on Cellular Adhesion. *Nano Letters*, 11, 1469-1476.
- DEL RIO, A., PEREZ-JIMENEZ, R., LIU, R., ROCA-CUSACHS, P., FERNANDEZ, J. M. & SHEETZ, M. P. 2009. Stretching Single Talin Rod Molecules Activates Vinculin Binding. *Science*, 323, 638-641.
- DEMALI, K. A. & BURRIDGE, K. 2003. Coupling membrane protrusion and cell adhesion. *Journal of Cell Science*, 116, 2389-2397.
- DENG, Y., ZHANG, X., ZHAO, X., LI, Q., YE, Z., LI, Z., LIU, Y., ZHOU, Y., MA, H., PAN, G., PEI, D., FANG, J. & WEI, S. 2013. Long-term self-renewal of human pluripotent stem cells on peptide-decorated poly(OEGMA-co-HEMA) brushes under fully defined conditions. *Acta Biomaterialia*, 9, 8840-8850.
- DI MARTINO, A., SITTINGER, M. & RISBUD, M. V. 2005. Chitosan: A versatile biopolymer for orthopaedic tissue-engineering. *Biomaterials*, 26, 5983-5990.

- DOBIN, A., DAVIS, C. A., SCHLESINGER, F., DRENKOW, J., ZALESKI, C., JHA, S., BATUT, P., CHAISSON, M. & GINGERAS, T. R. 2013. STAR: ultrafast universal RNA-seq aligner. *Bioinformatics*, 29, 15-21.
- DOCHEVA, D., PADULA, D., POPOV, C., MUTSCHLER, W., CLAUSEN-SCHAUMANN, H. & SCHIEKER, M. 2008. Researching into the cellular shape, volume and elasticity of mesenchymal stem cells, osteoblasts and osteosarcoma cells by atomic force microscopy. *Journal of Cellular and Molecular Medicine*, 12, 537-552.
- DOETSCH, F. 2003. A niche for adult neural stem cells. *Current Opinion in Genetics & Development*, 13, 543-550.
- DOLDER, J. V. D., SPAUWEN, P. H. M. & JANSEN, J. A. 2003. Evaluation of Various Seeding Techniques for Culturing Osteogenic Cells on Titanium Fiber Mesh. *Tissue Engineering*, 9, 315-325.
- DOMINICI, M., LE BLANC, K., MUELLER, I., SLAPER-CORTENBACH, I., MARINI, F. C., KRAUSE, D. S., DEANS, R. J., KEATING, A., PROCKOP, D. J. & HORWITZ, E. M. 2006. Minimal criteria for defining multipotent mesenchymal stromal cells. The International Society for Cellular Therapy position statement. *Cytotherapy*, 8, 315-317.
- DORÉE, M. & HUNT, T. 2002. From Cdc2 to Cdk1: when did the cell cycle kinase join its cyclin partner? *Journal of Cell Science*, 115, 2461-2464.
- DOS REMEDIOS, C. G., CHHABRA, D., KEKIC, M., DEDOVA, I. V., TSUBAKIHARA, M., BERRY, D. A. & NOSWORTHY, N. J. 2003. Actin Binding Proteins: Regulation of Cytoskeletal Microfilaments. *Physiological Reviews*, 83, 433-473.
- DOWNING, T. L., SOTO, J., MOREZ, C., HOUSSIN, T., FRITZ, A., YUAN, F., CHU, J., PATEL, S., SCHAFFER, D. V. & LI, S. 2013. Biophysical regulation of epigenetic state and cell reprogramming. *Nature Materials*, 12, 1154-1162.
- DREIER, B., GASIOROWSKI, J. Z., MORGAN, J. T., NEALEY, P. F., RUSSELL, P. & MURPHY, C. J. 2013. Early responses of vascular endothelial cells to topographic cues. *American Journal of Physiology-Cell Physiology*, 305, C290-C298.
- DRISSI, H., HUSHKA, D., ASLAM, F., NGUYEN, Q., BUFFONE, E., KOFF, A., VAN WIJNEN, A. J., LIAN, J. B., STEIN, J. L. & STEIN, G. S. 1999. The Cell Cycle Regulator p27kip1 Contributes to Growth and Differentiation of Osteoblasts. *Cancer Research*, 59, 3705-3711.
- DUCY, P., ZHANG, R., GEOFFROY, V., RIDALL, A. L. & KARSENTY, G. 1997. *Osf2/Cbfa1*: A Transcriptional Activator of Osteoblast Differentiation. *Cell*, 89, 747-754.
- DUNN, G. A. & HEATH, J. P. 1976. A new hypothesis of contact guidance in tissue cells. *Experimental Cell Research*, 101, 1-14.
- EGOZI, D., SHAPIRA, M., PAOR, G., BEN-IZHAK, O., SKORECKI, K. & HERSHKO, D. D. 2007. Regulation of the cell cycle inhibitor p27 and its ubiquitin ligase Skp2 in differentiation of human embryonic stem cells. *The FASEB Journal*, 21, 2807-2817.
- EHNINGER, A. & TRUMPP, A. 2011. The bone marrow stem cell niche grows up: mesenchymal stem cells and macrophages move in. *The Journal of Experimental Medicine*, 208, 421-428.
- ENG, G., LEE, B. W., PARSIA, H., CHIN, C. D., SCHNEIDER, J., LINKOV, G., SIA, S. K. & VUNJAK-NOVAKOVIC, G. 2013. Assembly of complex cell microenvironments using geometrically docked hydrogel shapes. *Proceedings of the National Academy of Sciences*, 110, 4551-4556.

- ENGLER, A., BACAKOVA, L., NEWMAN, C., HATEGAN, A., GRIFFIN, M. & DISCHER, D. 2004. Substrate Compliance versus Ligand Density in Cell on Gel Responses. *Biophysical Journal*, 86, 617-628.
- ENGLER, A. J., SEN, S., SWEENEY, H. L. & DISCHER, D. E. 2006. Matrix Elasticity Directs Stem Cell Lineage Specification. *Cell*, 126, 677-689.
- ESEONU, O. I. & DE BARI, C. 2015. Homing of mesenchymal stem cells: mechanistic or stochastic? Implications for targeted delivery in arthritis. *Rheumatology*, 54, 210-218.
- EVANS, N. D. & GENTLEMAN, E. 2014. The role of material structure and mechanical properties in cell-matrix interactions. *Journal of Materials Chemistry B*, 2, 2345-2356.
- EZASHI, T., DAS, P. & ROBERTS, R. M. 2005. Low O₂ tensions and the prevention of differentiation of hES cells. *Proceedings of the National Academy of Sciences of the United States of America*, 102, 4783-4788.
- EZHEVSKY, S. A., NAGAHARA, H., VOCERO-AKBANI, A. M., GIUS, D. R., WEI, M. C. & DOWDY, S. F. 1997. Hypo-phosphorylation of the retinoblastoma protein (pRb) by cyclin D:Cdk4/6 complexes results in active pRb. *Proceedings of the National Academy of Sciences of the United States of America*, 94, 10699-10704.
- FEHRER, C., BRUNAUER, R., LASCHOBBER, G., UNTERLUGGAUER, H., REITINGER, S., KLOSS, F., GÜLLY, C., GASSNE, R. & LEPPERDINGER, G. 2007. Reduced oxygen tension attenuates differentiation capacity of human mesenchymal stem cells and prolongs their lifespan. *Aging Cell*, 6, 745-757.
- FINCHAM, V. J., JAMES, M., FRAME, M. C. & WINDER, S. J. 2000. Active ERK/MAP kinase is targeted to newly forming cell-matrix adhesions by integrin engagement and v-Src. *EMBO J*, 19, 2911-2923.
- FLETCHER, D. A. & MULLINS, R. D. 2010. Cell mechanics and the cytoskeleton. *Nature*, 463, 485-492.
- FOLKMAN, J. & MOSCONA, A. 1978. Role of cell shape in growth control. *Nature*, 273, 345-349.
- FRANTZ, C., STEWART, K. M. & WEAVER, V. M. 2010. The extracellular matrix at a glance. *Journal of Cell Science*, 123, 4195-4200.
- FRENETTE, P. S., PINHO, S., LUCAS, D. & SCHEIERMANN, C. 2013. Mesenchymal Stem Cell: Keystone of the Hematopoietic Stem Cell Niche and a Stepping-Stone for Regenerative Medicine. *Annual Review of Immunology*, 31, 285-316.
- FRIEDENSTEIN, A. J., CHAILAKHJAN, R. K. & LALYKINA, K. S. 1970. The development of fibroblast colonies in monolayer cultures of guinea-pig bone marrow and spleen cells. *Cell Proliferation*, 3, 393-403.
- FRIEDENSTEIN, A. J., CHAILAKHYAN, R. K. & GERASIMOV, U. V. 1987. Bone marrow osteogenic stem cells: in vitro cultivation and transplantation in diffusion chambers. *Cell Proliferation*, 20, 263-272.
- FRIEDL, G., SCHMIDT, H., REHAK, I., KOSTNER, G., SCHAUENSTEIN, K. & WINDHAGER, R. 2007. Undifferentiated human mesenchymal stem cells (hMSCs) are highly sensitive to mechanical strain: transcriptionally controlled early osteo-chondrogenic response in vitro. *Osteoarthritis and Cartilage*, 15, 1293-1300.
- FRINGER, J. & GRINNELL, F. 2001. Fibroblast Quiescence in Floating or Released Collagen Matrices: CONTRIBUTION OF THE ERK SIGNALING PATHWAY AND ACTIN CYTOSKELETAL ORGANIZATION. *Journal of Biological Chemistry*, 276, 31047-31052.

- FUCHS, E., TUMBAR, T. & GUASCH, G. 2004. Socializing with the Neighbors: Stem Cells and Their Niche. *Cell*, 116, 769-778.
- FUCHS, E. & WEBER, K. 1994. Intermediate Filaments: Structure, Dynamics, Function and Disease. *Annual Review of Biochemistry*, 63, 345-382.
- GADEGAARD, N., DALBY, M. J., RIEHLE, M. O. & WILKINSON, C. D. W. 2008. Optimizing substrate disorder for bone tissue engineering of mesenchymal stem cells. *Journal of Vacuum Science & Technology B*, 26, 2554-2557.
- GADEGAARD, N., MARTINES, E., RIEHLE, M. O., SEUNARINE, K. & WILKINSON, C. D. W. 2006. Applications of nano-patterning to tissue engineering. *Microelectronic Engineering*, 83, 1577-1581.
- GADEGAARD, N., THOMS, S., MACINTYRE, D. S., MCGHEE, K., GALLAGHER, J., CASEY, B. & WILKINSON, C. D. W. 2003. Arrays of nano-dots for cellular engineering. *Microelectronic Engineering*, 67-68, 162-168.
- GALBRAITH, C. G., YAMADA, K. M. & SHEETZ, M. P. 2002. The relationship between force and focal complex development. *The Journal of Cell Biology*, 159, 695-705.
- GALLAGHER, J. O., MCGHEE, K. F., WILKINSON, C. D. W. & RIEHLE, M. O. 2002. Interaction of animal cells with ordered nanotopography. *IEEE Transactions on NanoBioscience*, 1, 24-28.
- GANG, E. J., JEONG, J. A., HONG, S. H., HWANG, S. H., KIM, S. W., YANG, I. H., AHN, C., HAN, H. & KIM, H. 2004. Skeletal Myogenic Differentiation of Mesenchymal Stem Cells Isolated from Human Umbilical Cord Blood. *Stem Cells*, 22, 617-624.
- GANUZA, M., SÁIZ-LADERA, C., CAÑAMERO, M., GÓMEZ, G., SCHNEIDER, R., BLASCO, M. A., PISANO, D., PARAMIO, J. M., SANTAMARÍA, D. & BARBACID, M. 2012. Genetic inactivation of Cdk7 leads to cell cycle arrest and induces premature aging due to adult stem cell exhaustion. *The EMBO Journal*, 31, 2498-2510.
- GAUTROT, J. E., MALMSTRÖM, J., SUNDH, M., MARGADANT, C., SONNENBERG, A. & SUTHERLAND, D. S. 2014. The Nanoscale Geometrical Maturation of Focal Adhesions Controls Stem Cell Differentiation and Mechanotransduction. *Nano Letters*, 14, 3945-3952.
- GECKIL, H., XU, F., ZHANG, X., MOON, S. & DEMIRCI, U. 2010. Engineering hydrogels as extracellular matrix mimics. *Nanomedicine (London, England)*, 5, 469-484.
- GEE, A., BAKER, B., SILVERSTEIN, A., MONTERO, G., ESTERHAI, J. & MAUCK, R. 2012. Fabrication and evaluation of biomimetic-synthetic nanofibrous composites for soft tissue regeneration. *Cell and Tissue Research*, 347, 803-813.
- GHARIBI, B., GHUMAN, M. S. & HUGHES, F. J. 2012. Akt- and Erk-mediated regulation of proliferation and differentiation during PDGFRB-induced MSC self-renewal. *Journal of Cellular and Molecular Medicine*, 16, 2789-2801.
- GHULE, P. N., MEDINA, R., LENGNER, C. J., MANDEVILLE, M., QIAO, M., DOMINSKI, Z., LIAN, J. B., STEIN, J. L., VAN WIJNEN, A. J. & STEIN, G. S. 2011. Reprogramming the pluripotent cell cycle: Restoration of an abbreviated G1 phase in human induced pluripotent stem (iPS) cells. *Journal of Cellular Physiology*, 226, 1149-1156.
- GILBERT, P. M., HAVENSTRITE, K. L., MAGNUSSON, K. E. G., SACCO, A., LEONARDI, N. A., KRAFT, P., NGUYEN, N. K., THRUN, S., LUTOLF, M. P. & BLAU, H. M. 2010. Substrate Elasticity Regulates Skeletal Muscle Stem Cell Self-Renewal in Culture. *Science*, 329, 1078-1081.

- GOBAA, S., HOEHNEL, S., ROCCIO, M., NEGRO, A., KOBEL, S. & LUTOLF, M. P. 2011. Artificial niche microarrays for probing single stem cell fate in high throughput. *Nature Methods*, 8, 949-955.
- GOTHARD, D., GREENHOUGH, J., RALPH, E. & OREFFO, R. O. C. 2014. Prospective isolation of human bone marrow stromal cell subsets: A comparative study between Stro-1-, CD146- and CD105-enriched populations. *Journal of Tissue Engineering*, 5, 2041731414551763.
- GÖTTLICHER, M., MINUCCI, S., ZHU, P., KRÄMER, O. H., SCHIMPF, A., GIAVARA, S., SLEEMAN, J. P., LO COCO, F., NERVI, C., PELICCI, P. G. & HEINZEL, T. 2001. Valproic acid defines a novel class of HDAC inhibitors inducing differentiation of transformed cells. *The EMBO Journal*, 20, 6969-6978.
- GRAYSON, W. L., ZHAO, F., BUNNELL, B. & MA, T. 2007. Hypoxia enhances proliferation and tissue formation of human mesenchymal stem cells. *Biochemical and Biophysical Research Communications*, 358, 948-953.
- GREENBAUM, A., HSU, Y.-M. S., DAY, R. B., SCHUETTPELZ, L. G., CHRISTOPHER, M. J., BORGERDING, J. N., NAGASAWA, T. & LINK, D. C. 2013. CXCL12 in early mesenchymal progenitors is required for haematopoietic stem-cell maintenance. *Nature*, 495, 227-230.
- GUNATILLAKE, P. A. & ADHIKARI, R. 2003. Biodegradable synthetic polymers for tissue engineering. *European Cells & Materials*, 5, 1-16.
- GURDON, J. B. 1962. The Developmental Capacity of Nuclei taken from Intestinal Epithelium Cells of Feeding Tadpoles. *Journal of Embryology and Experimental Morphology*, 10, 622-640.
- GURDON, J. B. & UEHLINGER, V. 1966. "Fertile" Intestine Nuclei. *Nature*, 210, 1240-1241.
- HANNA, J. H., SAHA, K. & JAENISCH, R. 2010. Pluripotency and Cellular Reprogramming: Facts, Hypotheses, Unresolved Issues. *Cell*, 143, 508-525.
- HARRISON, R. 1914. The reaction of embryonic cells to solid structures. *J Exp Zool.*, 17, 521-544.
- HART, A., GADEGAARD, N., WILKINSON, C. D. W., OREFFO, R. O. C. & DALBY, M. J. 2007. Osteoprogenitor response to low-adhesion nanotopographies originally fabricated by electron beam lithography. *Journal of Materials Science-Materials in Medicine*, 18, 1211-1218.
- HASELTINE, W. A. 2003. Regenerative Medicine 2003: An Overview. *e-biomed: The Journal of Regenerative Medicine*, 4, 15-18.
- HE, W., YONG, T., TEO, W. E., MA, Z. & RAMAKRISHNA, S. 2005. Fabrication and Endothelialization of Collagen-Blended Biodegradable Polymer Nanofibers: Potential Vascular Graft for Blood Vessel Tissue Engineering. *Tissue Engineering*, 11, 1574-1588.
- HEGEMANN, D., BRUNNER, H. & OEHR, C. 2003. Plasma treatment of polymers for surface and adhesion improvement. *Nuclear Instruments and Methods in Physics Research Section B: Beam Interactions with Materials and Atoms*, 208, 281-286.
- HEINO, J. 2007. The collagen family members as cell adhesion proteins. *BioEssays*, 29, 1001-1010.
- HENCH, L. 1980. Biomaterials. *Science*, 208, 826-831.
- HENCH, L. L. & POLAK, J. M. 2002. Third-Generation Biomedical Materials. *Science*, 295, 1014-1017.
- HIROKAWA, N., NODA, Y., TANAKA, Y. & NIWA, S. 2009. Kinesin superfamily motor proteins and intracellular transport. *Nat Rev Mol Cell Biol*, 10, 682-696.

- HORTON, M. A. 1997. The $\alpha\beta 3$ integrin “vitronectin receptor”. *The International Journal of Biochemistry & Cell Biology*, 29, 721-725.
- HOTULAINEN, P. & LAPPALAINEN, P. 2006. Stress fibers are generated by two distinct actin assembly mechanisms in motile cells. *The Journal of Cell Biology*, 173, 383-394.
- HSU, S.-H., LU, P., NI, H.-C. & SU, C.-H. 2007. Fabrication and evaluation of microgrooved polymers as peripheral nerve conduits. *Biomedical Microdevices*, 9, 665-674.
- HSU, Y.-C., LI, L. & FUCHS, E. 2014. Transit-Amplifying Cells Orchestrate Stem Cell Activity and Tissue Regeneration. *Cell*, 157, 935-949.
- HUANG, S., CHEN, C. S. & INGBER, D. E. 1998. Control of Cyclin D1, p27Kip1, and Cell Cycle Progression in Human Capillary Endothelial Cells by Cell Shape and Cytoskeletal Tension. *Molecular Biology of the Cell*, 9, 3179-3193.
- HUANGFU, D., MAEHR, R., GUO, W., EIJKELENBOOM, A., SNITOW, M., CHEN, A. E. & MELTON, D. A. 2008a. Induction of pluripotent stem cells by defined factors is greatly improved by small-molecule compounds. *Nature Biotechnology*, 26, 795-797.
- HUANGFU, D., OSAFUNE, K., MAEHR, R., GUO, W., EIJKELENBOOM, A., CHEN, S., MUHLESTEIN, W. & MELTON, D. A. 2008b. Induction of pluripotent stem cells from primary human fibroblasts with only Oct4 and Sox2. *Nature Biotechnology*, 26, 1269-1275.
- HUMPHRIES, J. D., BYRON, A. & HUMPHRIES, M. J. 2006. Integrin ligands at a glance. *Journal of Cell Science*, 119, 3901-3903.
- HUMPHRIES, J. D., WANG, P., STREULI, C., GEIGER, B., HUMPHRIES, M. J. & BALLESTREM, C. 2007. Vinculin controls focal adhesion formation by direct interactions with talin and actin. *The Journal of Cell Biology*, 179, 1043-1057.
- HYNES, R. O. 2002. Integrins: Bidirectional, Allosteric Signaling Machines. *Cell*, 110, 673-687.
- IKADA, Y. 1994. Surface modification of polymers for medical applications. *Biomaterials*, 15, 725-736.
- INGBER, D. E. 1993. Cellular tensegrity: defining new rules of biological design that govern the cytoskeleton. *Journal of Cell Science*, 104, 613-627.
- ITO, K., CARRACEDO, A., WEISS, D., ARAI, F., ALA, U., AVIGAN, D. E., SCHAFER, Z. T., EVANS, R. M., SUDA, T., LEE, C.-H. & PANDOLFI, P. P. 2012. A PML-PPAR- δ pathway for fatty acid oxidation regulates hematopoietic stem cell maintenance. *Nature Medicine*, 18, 1350-1358.
- IWASA, J. H. & MULLINS, R. D. 2007. Spatial and Temporal Relationships between Actin-Filament Nucleation, Capping, and Disassembly. *Current Biology*, 17, 395-406.
- JAEJIN, C., EU GENE, P., TAEJUN, C., KEUNHEE, O., SOON-KEUN, K., DONG-SUP, L. & SEUNG BUM, P. 2012. Establishment of High Throughput Screening System Using Human Umbilical Cord-derived Mesenchymal Stem Cells. *International Journal of Oral Biology*, 37, 43-50.
- JAISWAL, R. K., JAISWAL, N., BRUDER, S. P., MBALAVIELE, G., MARSHAK, D. R. & PITTENGER, M. F. 2000. Adult Human Mesenchymal Stem Cell Differentiation to the Osteogenic or Adipogenic Lineage Is Regulated by Mitogen-activated Protein Kinase. *Journal of Biological Chemistry*, 275, 9645-9652.
- JAMES, A. W. 2013. Review of Signaling Pathways Governing MSC Osteogenic and Adipogenic Differentiation. *Scientifica*, 2013, 17.

- JANG, M., LEE, S. T., KIM, J. W., YANG, J. H., YOON, J. K., PARK, J.-C., RYOO, H.-M., VAN DER VLIES, A. J., AHN, J. Y., HUBBELL, J. A., SONG, Y. S., LEE, G. & LIM, J. M. 2013. A feeder-free, defined three-dimensional polyethylene glycol-based extracellular matrix niche for culture of human embryonic stem cells. *Biomaterials*, 34, 3571-3580.
- JIN HO, L., JONG WOO, P. & HAI BANG, L. 1991. Cell adhesion and growth on polymer surfaces with hydroxyl groups prepared by water vapour plasma treatment. *Biomaterials*, 12, 443-448.
- JOHNSON, D. G., SCHWARZ, J. K., CRESS, W. D. & NEVINS, J. R. 1993. Expression of transcription factor E2F1 induces quiescent cells to enter S phase. *Nature*, 365, 349-352.
- JOHNSTONE, S., LINDSAY, S., BARNETT, S. & DALBY, M. 2011. Does Cellular Niche Play an Important Role in Mesenchymal Stem Cell Fate? *Glia*, 59, S120-S120.
- JONES, E., ENGLISH, A., CHURCHMAN, S. M., KOUROUPIS, D., BOXALL, S. A., KINSEY, S., GIANNOUDIS, P. G., EMERY, P. & MCGONAGLE, D. 2010. Large-scale extraction and characterization of CD271+ multipotential stromal cells from trabecular bone in health and osteoarthritis: Implications for bone regeneration strategies based on uncultured or minimally cultured multipotential stromal cells. *Arthritis & Rheumatism*, 62, 1944-1954.
- JONES, E. A., KINSEY, S. E., ENGLISH, A., JONES, R. A., STRASZYNSKI, L., MEREDITH, D. M., MARKHAM, A. F., JACK, A., EMERY, P. & MCGONAGLE, D. 2002. Isolation and characterization of bone marrow multipotential mesenchymal progenitor cells. *Arthritis & Rheumatism*, 46, 3349-3360.
- JOPLING, C., BOUE, S. & BELMONTE, J. C. I. 2011. Dedifferentiation, transdifferentiation and reprogramming: three routes to regeneration. *Nature Reviews Molecular Cell Biology*, 12, 79-89.
- KADAVATH, H., HOFELE, R. V., BIERNAT, J., KUMAR, S., TEPPER, K., URLAUB, H., MANDELKOW, E. & ZWECKSTETTER, M. 2015. Tau stabilizes microtubules by binding at the interface between tubulin heterodimers. *Proceedings of the National Academy of Sciences*, 112, 7501-7506.
- KALDIS, P. 1999. The cdk-activating kinase (CAK): from yeast to mammals. *Cellular and Molecular Life Sciences CMLS*, 55, 284-296.
- KEREVER, A., SCHNACK, J., VELLINGA, D., ICHIKAWA, N., MOON, C., ARIKAWA-HIRASAWA, E., EFIRD, J. T. & MERCIER, F. 2007. Novel Extracellular Matrix Structures in the Neural Stem Cell Niche Capture the Neurogenic Factor Fibroblast Growth Factor 2 from the Extracellular Milieu. *Stem Cells*, 25, 2146-2157.
- KERNOCHAN, L. E., RUSSO, M. L., WOODLING, N. S., HUYNH, T. N., AVILA, A. M., FISCHBECK, K. H. & SUMNER, C. J. 2005. The role of histone acetylation in SMN gene expression. *Human Molecular Genetics*, 14, 1171-1182.
- KILIAN, K. A., BUGARIJA, B., LAHN, B. T. & MRKSICH, M. 2010. Geometric cues for directing the differentiation of mesenchymal stem cells. *Proceedings of the National Academy of Sciences*, 107, 4872-4877.
- KIRCHNER, J., KAM, Z., TZUR, G., BERSHADSKY, A. D. & GEIGER, B. 2003. Live-cell monitoring of tyrosine phosphorylation in focal adhesions following microtubule disruption. *Journal of Cell Science*, 116, 975-986.

- KNOBLOCH, M., BRAUN, S. M. G., ZURKIRCHEN, L., VON SCHOULTZ, C., ZAMBONI, N., ARAUZO-BRAVO, M. J., KOVACS, W. J., KARALAY, O., SUTER, U., MACHADO, R. A. C., ROCCIO, M., LUTOLF, M. P., SEMENKOVICH, C. F. & JESSBERGER, S. 2013. Metabolic control of adult neural stem cell activity by Fasn-dependent lipogenesis. *Nature*, 493, 226-230.
- KNUDSEN, E. S. & WANG, J. Y. J. 1996. Differential Regulation of Retinoblastoma Protein Function by Specific Cdk Phosphorylation Sites. *Journal of Biological Chemistry*, 271, 8313-8320.
- KO, E. & CHO, S.-W. 2013. Biomimetic Polymer Scaffolds to Promote Stem Cell-Mediated Osteogenesis. *International Journal of Stem Cells*, 6, 87-91.
- KO, I. K., LEE, S. J., ATALA, A. & YOO, J. J. 2013. *In situ* tissue regeneration through host stem cell recruitment. *Experimental & Molecular Medicine*, 45, e57.
- KOLIOS, G. & MOODLEY, Y. 2013. Introduction to Stem Cells and Regenerative Medicine. *Respiration*, 85, 3-10.
- KUBLER, M. D., JORDAN, P. W., O'NEILL, C. H. & WATT, F. M. 1991. Changes in the abundance and distribution of actin and associated proteins during terminal differentiation of human epidermal keratinocytes. *Journal of Cell Science*, 100, 153-165.
- KULANGARA, K., ADLER, A. F., WANG, H., CHELLAPPAN, M., HAMMETT, E., YASUDA, R. & LEONG, K. W. 2014a. The effect of substrate topography on direct reprogramming of fibroblasts to induced neurons. *Biomaterials*, 35, 5327-5336.
- KULANGARA, K., YANG, J., CHELLAPPAN, M., YANG, Y. & LEONG, K. W. 2014b. Nanotopography Alters Nuclear Protein Expression, Proliferation and Differentiation of Human Mesenchymal Stem/Stromal Cells. *PLoS ONE*, 9, e114698.
- KULTERER, B., FRIEDL, G., JANDROSITZ, A., SANCHEZ-CABO, F., PROKESCH, A., PAAR, C., SCHEIDELER, M., WINDHAGER, R., PREISEGGER, K.-H. & TRAJANOSKI, Z. 2007. Gene expression profiling of human mesenchymal stem cells derived from bone marrow during expansion and osteoblast differentiation. *BMC Genomics*, 8, 70.
- KUNISAKI, Y., BRUNS, I., SCHEIERMANN, C., AHMED, J., PINHO, S., ZHANG, D., MIZOGUCHI, T., WEI, Q., LUCAS, D., ITO, K., MAR, J. C., BERGMAN, A. & FRENETTE, P. S. 2013. Arteriolar niches maintain haematopoietic stem cell quiescence. *Nature*, 502, 637-643.
- KWAN, A. P., CUMMINGS, C. E., CHAPMAN, J. A. & GRANT, M. E. 1991. Macromolecular organization of chicken type X collagen in vitro. *The Journal of Cell Biology*, 114, 597-604.
- LAEMMLI, U. K. 1970. Cleavage of Structural Proteins during the Assembly of the Head of Bacteriophage T4. *Nature*, 227, 680-685.
- LAI, J., SUNDERLAND, B., XUE, J., YAN, S., ZHAO, W., FOLKARD, M., MICHAEL, B. D. & WANG, Y. 2006. Study on hydrophilicity of polymer surfaces improved by plasma treatment. *Applied Surface Science*, 252, 3375-3379.
- LAMERS, E., FRANK WALBOOMERS, X., DOMANSKI, M., TE RIET, J., VAN DELFT, F. C. M. J. M., LUTTGE, R., WINNUBST, L. A. J. A., GARDENIERS, H. J. G. E. & JANSEN, J. A. 2010. The influence of nanoscale grooved substrates on osteoblast behavior and extracellular matrix deposition. *Biomaterials*, 31, 3307-3316.

- LANDER, A., KIMBLE, J., CLEVERS, H., FUCHS, E., MONTARRAS, D., BUCKINGHAM, M., CALOF, A., TRUMPP, A. & OSKARSSON, T. 2012. What does the concept of the stem cell niche really mean today? *BMC Biology*, 10, 19.
- LANGE, C., HUTTNER, W. B. & CALEGARI, F. 2009. Cdk4/CyclinD1 Overexpression in Neural Stem Cells Shortens G1, Delays Neurogenesis, and Promotes the Generation and Expansion of Basal Progenitors. *Cell Stem Cell*, 5, 320-331.
- LANGER, R. & TIRRELL, D. A. 2004. Designing materials for biology and medicine. *Nature*, 428, 487-492.
- LANGER, R. & VACANTI, J. 1993. Tissue engineering. *Science*, 260, 920-926.
- LAURENTI, E., FRELIN, C., XIE, S., FERRARI, R., DUNANT, CYRILLE F., ZANDI, S., NEUMANN, A., PLUMB, I., DOULATOV, S., CHEN, J., APRIL, C., FAN, J.-B., ISCOVE, N. & DICK, JOHN E. 2015. CDK6 Levels Regulate Quiescence Exit in Human Hematopoietic Stem Cells. *Cell Stem Cell*, 16, 302-313.
- LAWSON, C., LIM, S.-T., URYU, S., CHEN, X. L., CALDERWOOD, D. A. & SCHLAEPFER, D. D. 2012. FAK promotes recruitment of talin to nascent adhesions to control cell motility. *The Journal of Cell Biology*, 196, 223-232.
- LAZARIDES, E. 1976. Actin, alpha-actinin, and tropomyosin interaction in the structural organization of actin filaments in nonmuscle cells. *The Journal of Cell Biology*, 68, 202-219.
- LEE, H. J., CHOI, B. H., MIN, B.-H. & PARK, S. R. 2009. Changes in surface markers of human mesenchymal stem cells during the chondrogenic differentiation and dedifferentiation processes in vitro. *Arthritis & Rheumatism*, 60, 2325-2332.
- LEE, J., ABDEEN, A. A., HUANG, T. H. & KILIAN, K. A. 2014a. Controlling cell geometry on substrates of variable stiffness can tune the degree of osteogenesis in human mesenchymal stem cells. *Journal of the Mechanical Behavior of Biomedical Materials*, 38, 209-218.
- LEE, J., ABDEEN, A. A. & KILIAN, K. A. 2014b. Rewiring mesenchymal stem cell lineage specification by switching the biophysical microenvironment. *Scientific Reports*, 4, 5188.
- LEGATE, K. R., WICKSTRÖM, S. A. & FÄSSLER, R. 2009. Genetic and cell biological analysis of integrin outside-in signaling. *Genes & Development*, 23, 397-418.
- LI, J., WANG, G., WANG, C., ZHAO, Y., ZHANG, H., TAN, Z., SONG, Z., DING, M. & DENG, H. 2007. MEK/ERK signaling contributes to the maintenance of human embryonic stem cell self-renewal. *Differentiation*, 75, 299-307.
- LI, L. & CLEVERS, H. 2010. Coexistence of Quiescent and Active Adult Stem Cells in Mammals. *Science (New York, N.Y.)*, 327, 542-545.
- LI, V. C., BALLABENI, A. & KIRSCHNER, M. W. 2012. Gap 1 phase length and mouse embryonic stem cell self-renewal. *Proceedings of the National Academy of Sciences*, 109, 12550-12555.
- LIM, J. Y., HANSEN, J. C., SIEDLECKI, C. A., HENGSTEBECK, R. W., CHENG, J., WINOGRAD, N. & DONAHUE, H. J. 2005. Osteoblast Adhesion on Poly(l-lactic Acid)/Polystyrene Demixed Thin Film Blends: Effect of Nanotopography, Surface Chemistry, and Wettability. *Biomacromolecules*, 6, 3319-3327.
- LIN, L., CHOW, K. L. & LENG, Y. 2009. Study of hydroxyapatite osteoinductivity with an osteogenic differentiation of mesenchymal stem cells. *Journal of Biomedical Materials Research Part A*, 89A, 326-335.

- LIN, S.-P., CHIU, F.-Y., WANG, Y., YEN, M.-L., KAO, S.-Y. & HUNG, S.-C. 2014. RB Maintains Quiescence and Prevents Premature Senescence through Upregulation of DNMT1 in Mesenchymal Stromal Cells. *Stem Cell Reports*, 3, 975-986.
- LOESBERG, W. A., TE RIET, J., VAN DELFT, F. C. M. J. M., SCHÖN, P., FIGDOR, C. G., SPELLER, S., VAN LOON, J. J. W. A., WALBOOMERS, X. F. & JANSEN, J. A. 2007. The threshold at which substrate nanogroove dimensions may influence fibroblast alignment and adhesion. *Biomaterials*, 28, 3944-3951.
- LU, H., GUO, L., WOZNIAK, M. J., KAWAZOE, N., TATEISHI, T., ZHANG, X. & CHEN, G. 2009. Effect of cell density on adipogenic differentiation of mesenchymal stem cells. *Biochemical and Biophysical Research Communications*, 381, 322-327.
- LUKASHEV, M. E. & WERB, Z. 1998. ECM signalling: orchestrating cell behaviour and misbehaviour. *Trends in Cell Biology*, 8, 437-441.
- LUNA, E. J. & HITT, A. L. 1992. Cytoskeleton-plasma membrane interactions. *Science*, 258, 955-964.
- LUTOLF, M. P., GILBERT, P. M. & BLAU, H. M. 2009. Designing materials to direct stem-cell fate. *Nature*, 462, 433-441.
- MA, P. X. 2008. Biomimetic Materials for Tissue Engineering. *Advanced drug delivery reviews*, 60, 184-198.
- MA, P. X., ZHANG, R., XIAO, G. & FRANCESCHI, R. 2001. Engineering new bone tissue *in vitro* on highly porous poly(α -hydroxyl acids)/hydroxyapatite composite scaffolds. *Journal of Biomedical Materials Research*, 54, 284-293.
- MACCHIARINI, P., JUNGEBLUTH, P., GO, T., ASNAGHI, M. A., REES, L. E., COGAN, T. A., DODSON, A., MARTORELL, J., BELLINI, S., PARNIGOTTO, P. P., DICKINSON, S. C., HOLLANDER, A. P., MANTERO, S., CONCONI, M. T. & BIRCHALL, M. A. 2008. Clinical transplantation of a tissue-engineered airway. *The Lancet*, 372, 2023-2030.
- MAJUMDAR, M. K., THIEDE, M. A., MOSCA, J. D., MOORMAN, M. & GERSON, S. L. 1998. Phenotypic and functional comparison of cultures of marrow-derived mesenchymal stem cells (MSCs) and stromal cells. *Journal of Cellular Physiology*, 176, 57-66.
- MALMSTRÖM, J., LOVMAND, J., KRISTENSEN, S., SUNDH, M., DUCH, M. & SUTHERLAND, D. S. 2011. Focal Complex Maturation and Bridging on 200 nm Vitronectin but Not Fibronectin Patches Reveal Different Mechanisms of Focal Adhesion Formation. *Nano Letters*, 11, 2264-2271.
- MALUMBRES, M. & BARBACID, M. 2005. Mammalian cyclin-dependent kinases. *Trends in Biochemical Sciences*, 30, 630-641.
- MANO, J. F. 2015. Designing biomaterials for tissue engineering based on the deconstruction of the native cellular environment. *Materials Letters*, 141, 198-202.
- MAROM, R., SHUR, I., SOLOMON, R. & BENAYAHU, D. 2005. Characterization of adhesion and differentiation markers of osteogenic marrow stromal cells. *Journal of Cellular Physiology*, 202, 41-48.
- MARTHIENS, V., KAZANIS, I., MOSS, L., LONG, K. & FFRENCH-CONSTANT, C. 2010. Adhesion molecules in the stem cell niche - more than just staying in shape? *Journal of Cell Science*, 123, 1613-1622.
- MASON, M. D., DAVIES, G. & JIANG, W. G. Cell adhesion molecules and adhesion abnormalities in prostate cancer. *Critical Reviews in Oncology / Hematology*, 41, 11-28.

- MATSUMOTO, A. & NAKAYAMA, K. I. 2013. Role of key regulators of the cell cycle in maintenance of hematopoietic stem cells. *Biochimica et Biophysica Acta (BBA) - General Subjects*, 1830, 2335-2344.
- MATSUMURA, G., MIYAGAWA-TOMITA, S., SHIN'OKA, T., IKADA, Y. & KUROSAWA, H. 2003. First Evidence That Bone Marrow Cells Contribute to the Construction of Tissue-Engineered Vascular Autografts *In Vivo*. *Circulation*, 108, 1729-1734.
- MATSUSHIME, H., QUELLE, D. E., SHURTLEFF, S. A., SHIBUYA, M., SHERR, C. J. & KATO, J. Y. 1994. D-type cyclin-dependent kinase activity in mammalian cells. *Molecular and Cellular Biology*, 14, 2066-2076.
- MCBEATH, R., PIRONE, D. M., NELSON, C. M., BHADRIRAJU, K. & CHEN, C. S. 2004. Cell Shape, Cytoskeletal Tension, and RhoA Regulate Stem Cell Lineage Commitment. *Developmental Cell*, 6, 483-495.
- MCMURRAY, R. J., GADEGAARD, N., TSIMBOURI, P. M., BURGESS, K. V., MCNAMARA, L. E., TARE, R., MURAWSKI, K., KINGHAM, E., OREFFO, R. O. C. & DALBY, M. J. 2011. Nanoscale surfaces for the long-term maintenance of mesenchymal stem cell phenotype and multipotency. *Nature Materials*, 10, 637-644.
- MCNAMARA, L. E., MCMURRAY, R., J., BIGGS, M. J. P., KANTAWONG, F., OREFFO, R. O. C. & DALBY, M. J. 2010. Nanotopographical control of stem cell differentiation. *Journal of Tissue Engineering*, 1, 1-13.
- MCNAMARA, L. E., SJOSTROM, T., BURGESS, K. E. V., KIM, J. J. W., LIU, E., GORDONOV, S., MOGHE, P. V., MEEK, R. M. D., OREFFO, R. O. C., SU, B. & DALBY, M. J. 2011. Skeletal stem cell physiology on functionally distinct titania nanotopographies. *Biomaterials*, 32, 7403-7410.
- MCNAMARA, L. E., SJÖSTRÖM, T., MEEK, R. M. D., OREFFO, R. O. C., SU, B., DALBY, M. J. & BURGESS, K. E. V. 2012. Metabolomics: a valuable tool for stem cell monitoring in regenerative medicine. *Journal of The Royal Society Interface*.
- MEIRELLES, L. D. S., CHAGASTELLES, P. C. & NARDI, N. B. 2006. Mesenchymal stem cells reside in virtually all post-natal organs and tissues. *Journal of Cell Science*, 119, 2204-2213.
- MELCHELS, F. P. W., BARRADAS, A. M. C., VAN BLITTERSWIJK, C. A., DE BOER, J., FEIJEN, J. & GRIJPM, D. W. 2010. Effects of the architecture of tissue engineering scaffolds on cell seeding and culturing. *Acta Biomaterialia*, 6, 4208-4217.
- MELTON, C. & BLELLOCH, R. 2010. MicroRNA Regulation of Embryonic Stem Cell Self-Renewal and Differentiation. In: MESHORER, E. & PLATH, K. (eds.) *The Cell Biology of Stem Cells*. Springer US.
- MELTON, C., JUDSON, R. L. & BLELLOCH, R. 2010. Opposing microRNA families regulate self-renewal in mouse embryonic stem cells. *Nature*, 463, 621-626.
- MENCHÓN, C., EDEL, M. J. & IZPISUA BELMONTE, J. C. 2011. The cell cycle inhibitor p27Kip1 controls self-renewal and pluripotency of human embryonic stem cells by regulating the cell cycle, Brachyury and Twist. *Cell Cycle*, 10, 1435-1447.
- MENDEZ-FERRER, S., MICHURINA, T. V., FERRARO, F., MAZLOOM, A. R., MACARTHUR, B. D., LIRA, S. A., SCADDEN, D. T., MA'AYAN, A., ENIKOLOPOV, G. N. & FRENETTE, P. S. 2010. Mesenchymal and haematopoietic stem cells form a unique bone marrow niche. *Nature*, 466, 829-834.

- MICHAILOVICI, I., HARRINGTON, H. A., AZOGUI, H. H., YAHALOM-RONEN, Y., PLOTNIKOV, A., CHING, S., STUMPF, M. P. H., KLEIN, O. D., SEGER, R. & TZAHOR, E. 2014. Nuclear to cytoplasmic shuttling of ERK promotes differentiation of muscle stem/progenitor cells. *Development*, 141, 2611-2620.
- MICHOLT, L., GÄRTNER, A., PRODANOV, D., BRAEKEN, D., DOTTI, C. G. & BARTIC, C. 2013. Substrate Topography Determines Neuronal Polarization and Growth In vitro. *PLoS ONE*, 8, e66170.
- MIKHAYLOVA, M., CLOIN, B. M. C., FINAN, K., VAN DEN BERG, R., TEEUW, J., KIJANKA, M. M., SOKOLOWSKI, M., KATRUKHA, E. A., MAIDORN, M., OPAZO, F., MOUTEL, S., VANTARD, M., PEREZ, F., VAN BERGEN EN HENEGOUWEN, P. M. P., HOOGENRAAD, C. C., EWERS, H. & KAPITEIN, L. C. 2015. Resolving bundled microtubules using anti-tubulin nanobodies. *Nat Commun*, 6.
- MISHIMA, S., NAGAI, A., ABDULLAH, S., MATSUDA, C., TAKETANI, T., KUMAKURA, S., SHIBATA, H., ISHIKURA, H., KIM, S. U. & MASUDA, J. 2010. Effective ex vivo expansion of hematopoietic stem cells using osteoblast-differentiated mesenchymal stem cells is CXCL12 dependent. *European Journal of Haematology*, 84, 538-546.
- MITSUI, K., TOKUZAWA, Y., ITOH, H., SEGAWA, K., MURAKAMI, M., TAKAHASHI, K., MARUYAMA, M., MAEDA, M. & YAMANAKA, S. 2003. The Homeoprotein Nanog Is Required for Maintenance of Pluripotency in Mouse Epiblast and ES Cells. *Cell*, 113, 631-642.
- MIYAMOTO, S., TERAMOTO, H., COSO, O. A., GUTKIND, J. S., BURBELO, P. D., AKIYAMA, S. K. & YAMADA, K. M. 1995. Integrin function: molecular hierarchies of cytoskeletal and signaling molecules. *The Journal of Cell Biology*, 131, 791-805.
- MORENO-LAYSECA, P. & STREULI, C. H. 2014. Signalling pathways linking integrins with cell cycle progression. *Matrix Biology*, 34, 144-153.
- MORRISON, S. J. & KIMBLE, J. 2006. Asymmetric and symmetric stem-cell divisions in development and cancer. *Nature*, 441, 1068-1074.
- MOUW, J. K., OU, G. & WEAVER, V. M. 2014. Extracellular matrix assembly: a multiscale deconstruction. *Nature Reviews Molecular Cell Biology*, 15, 771-785.
- MULLOY, R., SALINAS, S., PHILIPS, A. & HIPSKIND, R. A. 2003. Activation of cyclin D1 expression by the ERK5 cascade. *Oncogene*, 22, 5387-5398.
- MURAGLIA, A., CANCEDDA, R. & QUARTO, R. 2000. Clonal mesenchymal progenitors from human bone marrow differentiate in vitro according to a hierarchical model. *Journal of Cell Science*, 113, 1161-1166.
- MURPHY, S. M., PREBLE, A. M., PATEL, U. K., O'CONNELL, K. L., DIAS, D. P., MORITZ, M., AGARD, D., STULTS, J. T. & STEARNS, T. 2001. GCP5 and GCP6: Two New Members of the Human γ -Tubulin Complex. *Molecular Biology of the Cell*, 12, 3340-3352.
- NAIR, L. S. & LAURENCIN, C. T. 2007. Biodegradable polymers as biomaterials. *Progress in Polymer Science*, 32, 762-798.
- NAKAMURA, R., NAKAMURA, F. & FUKUNAGA, S. 2014. Changes in the composition of the extracellular matrix accumulated by mesenchymal stem cells during *in vitro* expansion. *Animal Science Journal*, 85, 706-713.
- NAKAMURA, Y., ARAI, F., IWASAKI, H., HOSOKAWA, K., KOBAYASHI, I., GOMEI, Y., MATSUMOTO, Y., YOSHIHARA, H. & SUDA, T. 2010. Isolation and characterization of endosteal niche cell populations that regulate hematopoietic stem cells. *Blood*, 116, 1422-1432.

- NARUSE, K., URABE, K., MUKAIDA, T., UENO, T., MIGISHIMA, F., OIKAWA, A., MIKUNI-TAKAGAKI, Y. & ITOMAN, M. 2004. Spontaneous differentiation of mesenchymal stem cells obtained from fetal rat circulation. *Bone*, 35, 850-858.
- NAUMANEN, P., LAPPALAINEN, P. & HOTULAINEN, P. 2008. Mechanisms of actin stress fibre assembly. *Journal of Microscopy*, 231, 446-454.
- NAVARRO, M., MICHIARDI, A., CASTAÑO, O. & PLANELL, J. A. 2008. Biomaterials in orthopaedics. *Journal of the Royal Society Interface*, 5, 1137-1158.
- NEGANOVA, I. & LAKO, M. 2008. G1 to S phase cell cycle transition in somatic and embryonic stem cells. *Journal of Anatomy*, 213, 30-44.
- NEGANOVA, I., TILGNER, K., BUSKIN, A., PARASKEVOPOULOU, I., ATKINSON, S. P., PEBERDY, D., PASSOS, J. F. & LAKO, M. 2014. CDK1 plays an important role in the maintenance of pluripotency and genomic stability in human pluripotent stem cells. *Cell Death & Disease*, 5, e1508.
- NERMUT, M. V., GREEN, N. M., EASON, P., YAMADA, S. S. & YAMADA, K. M. 1988. Electron microscopy and structural model of human fibronectin receptor. *The EMBO Journal*, 7, 4093-4099.
- NEUHUBER, B., SWANGER, S. A., HOWARD, L., MACKAY, A. & FISCHER, I. 2008. Effects of plating density and culture time on bone marrow stromal cell characteristics. *Experimental Hematology*, 36, 1176-1185.
- NICHOLS, J. & SMITH, A. 2012. Pluripotency in the Embryo and in Culture. *Cold Spring Harbor perspectives in biology*, 4.
- NOBES, C. D. & HALL, A. 1995. Rho, Rac, and Cdc42 GTPases regulate the assembly of multimolecular focal complexes associated with actin stress fibers, lamellipodia, and filopodia. *Cell*, 81, 53-62.
- NOMURA, S. & TAKANO-YAMAMOTO, T. 2000. Molecular events caused by mechanical stress in bone. *Matrix Biology*, 19, 91-96.
- ODA, T., IWASA, M., AIHARA, T., MAEDA, Y. & NARITA, A. 2009. The nature of the globular- to fibrous-actin transition. *Nature*, 457, 441-445.
- OGASAWARA, T., KATAGIRI, M., YAMAMOTO, A., HOSHI, K., TAKATO, T., NAKAMURA, K., TANAKA, S., OKAYAMA, H. & KAWAGUCHI, H. 2004a. Osteoclast Differentiation by RANKL Requires NF- κ B-Mediated Downregulation of Cyclin-Dependent Kinase 6 (Cdk6). *Journal of Bone and Mineral Research*, 19, 1128-1136.
- OGASAWARA, T., KAWAGUCHI, H., JINNO, S., HOSHI, K., ITAKA, K., TAKATO, T., NAKAMURA, K. & OKAYAMA, H. 2004b. Bone Morphogenetic Protein 2-Induced Osteoblast Differentiation Requires Smad-Mediated Down-Regulation of Cdk6. *Molecular and Cellular Biology*, 24, 6560-6568.
- OKITA, K., ICHISAKA, T. & YAMANAKA, S. 2007. Generation of germline-competent induced pluripotent stem cells. *Nature*, 448, 313-317.
- OREFFO, R. O. C., BORD, S. & TRIFFITT, J. T. 1998. Skeletal Progenitor Cells and Ageing Human Populations. *Clinical Science*, 94, 549-555.
- ORFORD, K. W. & SCADDEN, D. T. 2008. Deconstructing stem cell self-renewal: genetic insights into cell-cycle regulation. *Nature Reviews Genetics*, 9, 115-128.
- ORKIN, S. H. & ZON, L. I. 2008. Hematopoiesis: An Evolving Paradigm for Stem Cell Biology. *Cell*, 132, 631-644.
- ORLIC, D. 2003. Adult stem cells: can they transdifferentiate? *Blood*, 102, 4249-4250.

- PANOPOULOS, A. D., YANES, O., RUIZ, S., KIDA, Y. S., DIEP, D., TAUTENHAHN, R., HERRERIAS, A., BATCHELDER, E. M., PLONGTHONGKUM, N., LUTZ, M., BERGGREN, W. T., ZHANG, K., EVANS, R. M., SIUZDAK, G. & BELMONTE, J. C. I. 2012. The metabolome of induced pluripotent stem cells reveals metabolic changes occurring in somatic cell reprogramming. *Cell Res*, 22, 168-177.
- PAUKLIN, S. & VALLIER, L. 2013. The Cell-Cycle State of Stem Cells Determines Cell Fate Propensity. *Cell*, 155, 135-147.
- PAVLETICH, N. P. 1999. Mechanisms of cyclin-dependent kinase regulation: structures of cdks, their cyclin activators, and cip and INK4 inhibitors1,2. *Journal of Molecular Biology*, 287, 821-828.
- PELHAM, R. J. & WANG, Y.-L. 1997. Cell locomotion and focal adhesions are regulated by substrate flexibility. *Proceedings of the National Academy of Sciences*, 94, 13661-13665.
- PERINPANAYAGAM, H., ZAHARIAS, R., STANFORD, C., BRAND, R., KELLER, J. & SCHNEIDER, G. 2001. Early cell adhesion events differ between osteoporotic and non-osteoporotic osteoblasts. *Journal of Orthopaedic Research*, 19, 993-1000.
- PEVSNER-FISCHER, M., LEVIN, S. & ZIPORI, D. 2011. The Origins of Mesenchymal Stromal Cell Heterogeneity. *Stem Cell Reviews and Reports*, 7, 560-568.
- PISCIOTTA, A., CARNEVALE, G., MELONI, S., RICCIO, M., DE BIASI, S., GIBELLINI, L., FERRARI, A., BRUZZESI, G. & DE POL, A. 2015. Human Dental pulp stem cells (hDPSCs): isolation, enrichment and comparative differentiation of two sub-populations. *BMC Developmental Biology*, 15, 14.
- PITTINGER, M. F., MACKAY, A. M., BECK, S. C., JAISWAL, R. K., DOUGLAS, R., MOSCA, J. D., MOORMAN, M. A., SIMONETTI, D. W., CRAIG, S. & MARSHAK, D. R. 1999. Multilineage Potential of Adult Human Mesenchymal Stem Cells. *Science*, 284, 143-147.
- POLLARD, T. D. 2003. The cytoskeleton, cellular motility and the reductionist agenda. *Nature*, 422, 741-745.
- POTIER, E., FERREIRA, E., ANDRIAMANALIJAONA, R., PUJOL, J.-P., OUDINA, K., LOGEART-AVRAMOGLU, D. & PETITE, H. 2007. Hypoxia affects mesenchymal stromal cell osteogenic differentiation and angiogenic factor expression. *Bone*, 40, 1078-1087.
- PRAGER-KHOUTORSKY, M., LICHTENSTEIN, A., KRISHNAN, R., RAJENDRAN, K., MAYO, A., KAM, Z., GEIGER, B. & BERSHADSKY, A. D. 2011. Fibroblast polarization is a matrix-rigidity-dependent process controlled by focal adhesion mechanosensing. *Nature Cell Biology*, 13, 1457-1465.
- PUTNEY, J. W., TAKEMURA, H., HUGHES, A. R., HORSTMAN, D. A. & THASTRUP, O. 1989. How do inositol phosphates regulate calcium signaling? *The FASEB Journal*, 3, 1899-905.
- QIAN, H., LE BLANC, K. & SIGVARDSSON, M. 2012. Primary Mesenchymal Stem and Progenitor Cells from Bone Marrow Lack Expression of CD44 Protein. *Journal of Biological Chemistry*, 287, 25795-25807.
- QUYN, A. J., APPLETON, P. L., CAREY, F. A., STEELE, R. J. C., BARKER, N., CLEVERS, H., RIDGWAY, R. A., SANSOM, O. J. & NÄTHKE, I. S. 2010. Spindle Orientation Bias in Gut Epithelial Stem Cell Compartments Is Lost in Precancerous Tissue. *Cell Stem Cell*, 6, 175-181.
- RADUCANU, A., HUNZIKER, E. B., DROSSE, I. & ASZÓDI, A. 2009. B1 Integrin Deficiency Results in Multiple Abnormalities of the Knee Joint. *Journal of Biological Chemistry*, 284, 23780-23792.

- REILLY, G. C., RADIN, S., CHEN, A. T. & DUCHEYNE, P. 2007. Differential alkaline phosphatase responses of rat and human bone marrow derived mesenchymal stem cells to 45S5 bioactive glass. *Biomaterials*, 28, 4091-4097.
- REISKE, H. R., KAO, S.-C., CARY, L. A., GUAN, J.-L., LAI, J.-F. & CHEN, H.-C. 1999. Requirement of Phosphatidylinositol 3-Kinase in Focal Adhesion Kinase-promoted Cell Migration. *Journal of Biological Chemistry*, 274, 12361-12366.
- REUBINOFF, B. E., PERA, M. F., FONG, C.-Y., TROUNSON, A. & BONGSO, A. 2000. Embryonic stem cell lines from human blastocysts: somatic differentiation in vitro. *Nat Biotech*, 18, 399-404.
- REYES, J. M. G., FERMANIAN, S., YANG, F., ZHOU, S.-Y., HERRETES, S., MURPHY, D. B., ELISSEFF, J. H. & CHUCK, R. S. 2006. Metabolic Changes in Mesenchymal Stem Cells in Osteogenic Medium Measured by Autofluorescence Spectroscopy. *Stem Cells*, 24, 1213-1217.
- RICKARD, D. J., SULLIVAN, T. A., SHENKER, B. J., LEBOY, P. S. & KAZHDAN, I. 1994. Induction of Rapid Osteoblast Differentiation in Rat Bone Marrow Stromal Cell Cultures by Dexamethasone and BMP-2. *Developmental Biology*, 161, 218-228.
- RIDLEY, A. J. & HALL, A. 1992. The small GTP-binding protein rho regulates the assembly of focal adhesions and actin stress fibers in response to growth factors. *Cell*, 70, 389-399.
- RIDLEY, A. J., PATERSON, H. F., JOHNSTON, C. L., DIEKMANN, D. & HALL, A. 1992. The small GTP-binding protein rac regulates growth factor-induced membrane ruffling. *Cell*, 70, 401-410.
- RIVELINE, D., ZAMIR, E., BALABAN, N. Q., SCHWARZ, U. S., ISHIZAKI, T., NARUMIYA, S., KAM, Z., GEIGER, B. & BERSHADSKY, A. D. 2001. Focal Contacts as Mechanosensors: Externally Applied Local Mechanical Force Induces Growth of Focal Contacts by an mDia1-Dependent and ROCK-Independent Mechanism. *The Journal of Cell Biology*, 153, 1175-1186.
- ROOVERS, K. & ASSOIAN, R. K. 2000. Integrating the MAP kinase signal into the G1 phase cell cycle machinery. *BioEssays*, 22, 818-826.
- RUSTAD, K. C. & GURTNER, G. C. 2012. Mesenchymal Stem Cells Home to Sites of Injury and Inflammation. *Advances in Wound Care*, 1, 147-152.
- SAIKIA, K. C., BHATTACHARYA, T. D., BHUYAN, S. K., TALUKDAR, D. J., SAIKIA, S. P. & JITESH, P. 2008. Calcium phosphate ceramics as bone graft substitutes in filling bone tumor defects. *Indian Journal of Orthopaedics*, 42, 169-172.
- SALEH, F. A., FRITH, J. E., LEE, J. A. & GENEVER, P. G. 2012. Three-Dimensional In Vitro Culture Techniques for Mesenchymal Stem Cells. In: MACE, K. A. & BRAUN, K. M. (eds.) *Progenitor Cells*. Humana Press.
- SALGADO, A. J., OLIVEIRA, J. M., MARTINS, A., TEIXEIRA, F. G., SILVA, N. A., NEVES, N. M., SOUSA, N. & REIS, R. L. 2013. Chapter One - Tissue Engineering and Regenerative Medicine: Past, Present, and Future. In: STEFANO GEUNA, I. P. P. T. & BRUNO, B. (eds.) *International Review of Neurobiology*. Academic Press.
- SALVI, J. D., YUL LIM, J. & DONAHUE, H. J. 2010. Increased mechanosensitivity of cells cultured on nanotopographies. *Journal of Biomechanics*, 43, 3058-3062.

- SAMPATH, P., PRITCHARD, D. K., PABON, L., REINECKE, H., SCHWARTZ, S. M., MORRIS, D. R. & MURRY, C. E. 2008. A Hierarchical Network Controls Protein Translation during Murine Embryonic Stem Cell Self-Renewal and Differentiation. *Cell Stem Cell*, 2, 448-460.
- SANTAMARIA, D., BARRIERE, C., CERQUEIRA, A., HUNT, S., TARDY, C., NEWTON, K., CACERES, J. F., DUBUS, P., MALUMBRES, M. & BARBACID, M. 2007. Cdk1 is sufficient to drive the mammalian cell cycle. *Nature*, 448, 811-815.
- SARUGASER, R., HANOUN, L., KEATING, A., STANFORD, W. L. & DAVIES, J. E. 2009. Human Mesenchymal Stem Cells Self-Renew and Differentiate According to a Deterministic Hierarchy. *PLoS ONE*, 4, e6498.
- SATYANARAYANA, A. & KALDIS, P. 2009. Mammalian cell-cycle regulation: several Cdks, numerous cyclins and diverse compensatory mechanisms. *Oncogene*, 28, 2925-2939.
- SCADDEN, D. T. 2006. The stem-cell niche as an entity of action. *Nature*, 441, 1075-1079.
- SCHELTEMA, R. A., JANKEVICS, A., JANSEN, R. C., SWERTZ, M. A. & BREITLING, R. 2011. PeakML/mzMatch: A File Format, Java Library, R Library, and Tool-Chain for Mass Spectrometry Data Analysis. *Analytical Chemistry*, 83, 2786-2793.
- SCHLAEPFER, D. D., JONES, K. C. & HUNTER, T. 1998. Multiple Grb2-Mediated Integrin-Stimulated Signaling Pathways to ERK2/Mitogen-Activated Protein Kinase: Summation of Both c-Src- and Focal Adhesion Kinase-Initiated Tyrosine Phosphorylation Events. *Molecular and Cellular Biology*, 18, 2571-2585.
- SCHNEIDER, C. A., RASBAND, W. S. & ELICEIRI, K. W. 2012. NIH Image to ImageJ: 25 years of image analysis. *Nature Methods*, 9, 671-675.
- SCHOFIELD, R. 1978. The relationship between the spleen colony-forming cell and the haemopoietic stem cell. *Blood Cells*, 4, 7-25.
- SCHORK, N. J. 2015. Personalized medicine: Time for one-person trials. *Nature*, 520, 609-611.
- SCHWARTZ, M. 2004. Rho signalling at a glance. *Journal of Cell Science*, 117, 5457-5458.
- SEKIYA, I., LARSON, B. L., SMITH, J. R., POCHAMPALLY, R., CUI, J.-G. & PROCKOP, D. J. 2002. Expansion of Human Adult Stem Cells from Bone Marrow Stroma: Conditions that Maximize the Yields of Early Progenitors and Evaluate Their Quality. *Stem Cells*, 20, 530-541.
- SELHUBER-UNKEL, C., ERDMANN, T., LÓPEZ-GARCÍA, M., KESSLER, H., SCHWARZ, U. S. & SPATZ, J. P. 2010. Cell Adhesion Strength Is Controlled by Intermolecular Spacing of Adhesion Receptors. *Biophysical Journal*, 98, 543-551.
- SHAH, N. J., HYDER, M. N., QUADIR, M. A., DORVAL COURCHESNE, N.-M., SEEHERMAN, H. J., NEVINS, M., SPECTOR, M. & HAMMOND, P. T. 2014. Adaptive growth factor delivery from a polyelectrolyte coating promotes synergistic bone tissue repair and reconstruction. *Proceedings of the National Academy of Sciences*, 111, 12847-12852.
- SHAHIN, K. & DORAN, P. M. 2011. Improved seeding of chondrocytes into polyglycolic acid scaffolds using semi-static and alginate loading methods. *Biotechnology Progress*, 27, 191-200.
- SHARROCKS, A. D. 2006. Cell Cycle: Sustained ERK Signalling Represses the Inhibitors. *Current Biology*, 16, R540-R542.

- SHERR, C. J. & ROBERTS, J. M. 1999. CDK inhibitors: positive and negative regulators of G1-phase progression. *Genes & Development*, 13, 1501-1512.
- SHIMAOKA, M., LU, C., PALFRAMAN, R. T., VON ANDRIAN, U. H., MCCORMACK, A., TAKAGI, J. & SPRINGER, T. A. 2001. Reversibly locking a protein fold in an active conformation with a disulfide bond: Integrin α L I domains with high affinity and antagonist activity in vivo. *Proceedings of the National Academy of Sciences*, 98, 6009-6014.
- SHIRAKI, N., SHIRAKI, Y., TSUYAMA, T., OBATA, F., MIURA, M., NAGAE, G., ABURATANI, H., KUME, K., ENDO, F. & KUME, S. 2014. Methionine Metabolism Regulates Maintenance and Differentiation of Human Pluripotent Stem Cells. *Cell Metabolism*, 19, 780-794.
- SIDDAPPA, R., LICHT, R., VAN BLITTERSWIJK, C. & DE BOER, J. 2007. Donor variation and loss of multipotency during in vitro expansion of human mesenchymal stem cells for bone tissue engineering. *Journal of Orthopaedic Research*, 25, 1029-1041.
- SIMMONS, P. & TOROK-STORB, B. 1991. Identification of stromal cell precursors in human bone marrow by a novel monoclonal antibody, STRO-1. *Blood*, 78, 55-62.
- SIMS, J. R., KARP, S. & INGBER, D. E. 1992. Altering the cellular mechanical force balance results in integrated changes in cell, cytoskeletal and nuclear shape. *Journal of Cell Science*, 103, 1215-1222.
- SJÖSTRÖM, T., DALBY, M. J., HART, A., TARE, R., OREFFO, R. O. C. & SU, B. 2009. Fabrication of pillar-like titania nanostructures on titanium and their interactions with human skeletal stem cells. *Acta Biomaterialia*, 5, 1433-1441.
- SJÖSTRÖM, T., MCNAMARA, L. E., MEEK, R. M. D., DALBY, M. J. & SU, B. 2013. 2D and 3D Nanopatterning of Titanium for Enhancing Osteoinduction of Stem Cells at Implant Surfaces. *Advanced Healthcare Materials*, 2, 1285-1293.
- SMITH, A. N., MUFFLEY, L. A., BELL, A. N., NUMHOM, S. & HOCKING, A. M. 2012. Unsaturated fatty acids induce mesenchymal stem cells to increase secretion of angiogenic mediators. *Journal of Cellular Physiology*, 227, 3225-3233.
- SONG, L. & TUAN, R. S. 2004. Transdifferentiation potential of human mesenchymal stem cells derived from bone marrow. *The FASEB Journal*.
- SONG, L., WEBB, N. E., SONG, Y. & TUAN, R. S. 2006. Identification and functional analysis of candidate genes regulating mesenchymal stem cell self-renewal and multipotency. *Stem Cell*, 24, 1707-1718.
- SONG, X., ZHU, C.-H., DOAN, C. & XIE, T. 2002. Germline Stem Cells Anchored by Adherens Junctions in the Drosophila Ovary Niches. *Science*, 296, 1855-1857.
- STEELE, J. G., JOHNSON, G. & UNDERWOOD, P. A. 1992. Role of serum vitronectin and fibronectin in adhesion of fibroblasts following seeding onto tissue culture polystyrene. *Journal of Biomedical Materials Research*, 26, 861-884.
- STEVENS, M. M. & GEORGE, J. H. 2005. Exploring and engineering the cell surface interface. *Science*, 310, 1135.

- STRECKFUSS-BÖMEKE, K., WOLF, F., AZIZIAN, A., STAUSKE, M., TIBURCY, M., WAGNER, S., HÜBSCHER, D., DRESSEL, R., CHEN, S., JENDE, J., WULF, G., LORENZ, V., SCHÖN, M. P., MAIER, L. S., ZIMMERMANN, W. H., HASENFUSS, G. & GUAN, K. 2013. Comparative study of human-induced pluripotent stem cells derived from bone marrow cells, hair keratinocytes, and skin fibroblasts. *European Heart Journal*, 34, 2618-2629.
- SUN, N., PANETTA, N. J., GUPTA, D. M., WILSON, K. D., LEE, A., JIA, F., HU, S., CHERRY, A. M., ROBBINS, R. C., LONGAKER, M. T. & WU, J. C. 2009. Feeder-free derivation of induced pluripotent stem cells from adult human adipose stem cells. *Proceedings of the National Academy of Sciences*, 106, 15720-15725.
- SUN, Y., CHEN, C. S. & FU, J. 2012. Forcing Stem Cells to Behave: A Biophysical Perspective of the Cellular Microenvironment. *Annual review of biophysics*, 41, 519-542.
- TAKAHASHI, K., TANABE, K., OHNUKI, M., NARITA, M., ICHISAKA, T., TOMODA, K. & YAMANAKA, S. 2007. Induction of Pluripotent Stem Cells from Adult Human Fibroblasts by Defined Factors. *Cell*, 131, 861-872.
- TAKAHASHI, K. & YAMANAKA, S. 2006. Induction of Pluripotent Stem Cells from Mouse Embryonic and Adult Fibroblast Cultures by Defined Factors. *Cell*, 126, 663-676.
- TANG, D., MEHTA, D. & GUNST, S. J. 1999. Mechanosensitive tyrosine phosphorylation of paxillin and focal adhesion kinase in tracheal smooth muscle. *American Journal of Physiology - Cell Physiology*, 276, C250-C258.
- TAUTENHAHN, R., PATTI, G. J., RINEHART, D. & SIUZDAK, G. 2012. XCMS Online: A Web-Based Platform to Process Untargeted Metabolomic Data. *Analytical Chemistry*, 84, 5035-5039.
- TEO, B. K. K., WONG, S. T., LIM, C. K., KUNG, T. Y. S., YAP, C. H., RAMAGOPAL, Y., ROMER, L. H. & YIM, E. K. F. 2013. Nanotopography Modulates Mechanotransduction of Stem Cells and Induces Differentiation through Focal Adhesion Kinase. *ACS Nano*, 7, 4785-4798.
- TESIO, M. & TRUMPP, A. 2011. Breaking the Cell Cycle of HSCs by p57 and Friends. *Cell Stem Cell*, 9, 187-192.
- THOMSON, J. A., ITSKOVITZ-ELDOR, J., SHAPIRO, S. S., WAKNITZ, M. A., SWIERGIEL, J. J., MARSHALL, V. S. & JONES, J. M. 1998. Embryonic Stem Cell Lines Derived from Human Blastocysts. *Science*, 282, 1145-1147.
- THORESEN, T., LENZ, M. & GARDEL, MARGARET L. 2011. Reconstitution of Contractile Actomyosin Bundles. *Biophysical Journal*, 100, 2698-2705.
- TOMÉ, M., LINDSAY, S. L., RIDDELL, J. S. & BARNETT, S. C. 2009. Identification of Nonepithelial Multipotent Cells in the Embryonic Olfactory Mucosa. *Stem Cells*, 27, 2196-2208.
- TORTOLANI, P., JOHNSTON, J., BACON, C., MCVICAR, D., SHIMOSAKA, A., LINNEKIN, D., LONGO, D. & O'SHEA, J. 1995. Thrombopoietin induces tyrosine phosphorylation and activation of the Janus kinase, JAK2. *Blood* 85, 3444-3451.
- TRIFFITT, J. T. & OREFFO, R. O. C. 1998. Osteoblast lineage. In: ZAIDI, M. (ed.) *Advances in organ biology: molecular and cellular biology of bone*. Greenwich: JAI Press, Inc.
- TSAI, C.-C., YEW, T.-L., YANG, D.-C., HUANG, W.-H. & HUNG, S.-C. 2012. Benefits of hypoxic culture on bone marrow multipotent stromal cells. *American Journal of Blood Research*, 2, 148-159.

- TSIMBOURI, P., GADEGAARD, N., BURGESS, K., WHITE, K., REYNOLDS, P., HERZYK, P., OREFFO, R. & DALBY, M. J. 2014. Nanotopographical Effects on Mesenchymal Stem Cell Morphology and Phenotype. *Journal of Cellular Biochemistry*, 115, 380-390.
- TSIMBOURI, P. M., MCMURRAY, R., J., BURGESS, K., V., ALAKPA, E., V., REYNOLDS, P. M., MURAWSKI, K., KINGHAM, E., OREFFO, R. O. C., GADEGAARD, N. & DALBY, M. J. 2012. Using nanotopography and metabolomics to identify biochemical effectors of multipotency. *ACS Nano*, 6, 10239-10249.
- ULUDAĞ, H. 2014. Grand Challenges in Biomaterials. *Frontiers in Bioengineering and Biotechnology*, 2, 43.
- VADLAMUDI, R. K., LI, F., ADAM, L., NGUYEN, D., OHTA, Y., STOSSEL, T. P. & KUMAR, R. 2002. Filamin is essential in actin cytoskeletal assembly mediated by p21-activated kinase 1. *Nat Cell Biol*, 4, 681-690.
- VAN HORN, R. D., CHU, S., FAN, L., YIN, T., DU, J., BECKMANN, R., MADER, M., ZHU, G., TOTH, J., BLANCHARD, K. & YE, X. S. 2010. Cdk1 Activity Is Required for Mitotic Activation of Aurora A during G2/M Transition of Human Cells. *Journal of Biological Chemistry*, 285, 21849-21857.
- VAN KOOTEN, T. G., SPIJKER, H. T. & BUSSCHER, H. J. 2004. Plasma-treated polystyrene surfaces: model surfaces for studying cell-biomaterial interactions. *Biomaterials*, 25, 1735-1747.
- VANDERSLICE, P., BIEDIGER, R. J., WOODSIDE, D. G., BERENS, K. L., HOLLAND, G. W. & DIXON, R. A. F. 2004. Development of cell adhesion molecule antagonists as therapeutics for asthma and COPD. *Pulmonary Pharmacology & Therapeutics*, 17, 1-10.
- VERMEULEN, K., VAN BOCKSTAELE, D. R. & BERNEMAN, Z. N. 2003. The cell cycle: a review of regulation, deregulation and therapeutic targets in cancer. *Cell Proliferation*, 36, 131-149.
- VIATOUR, P. 2012. Bridges between Cell Cycle Regulation and Self-Renewal Maintenance. *Genes & Cancer*, 3, 670-677.
- WALENDA, T., BORK, S., HORN, P., WEIN, F., SAFFRICH, R., DIEHLMANN, A., ECKSTEIN, V., HO, A. D. & WAGNER, W. 2010. Co-culture with mesenchymal stromal cells increases proliferation and maintenance of haematopoietic progenitor cells. *Journal of Cellular and Molecular Medicine*, 14, 337-350.
- WALKER, J. L., FOURNIER, A. K. & ASSOIAN, R. K. 2005. Regulation of growth factor signaling and cell cycle progression by cell adhesion and adhesion-dependent changes in cellular tension. *Cytokine & Growth Factor Reviews*, 16, 395-405.
- WALL, I., DONOS, N., CARLQVIST, K., JONES, F. & BRETT, P. 2009. Modified titanium surfaces promote accelerated osteogenic differentiation of mesenchymal stromal cells *in vitro*. *Bone*, 45, 17-26.
- WANG, H.-B., DEMBO, M., HANKS, S. K. & WANG, Y.-L. 2001. Focal adhesion kinase is involved in mechanosensing during fibroblast migration. *Proceedings of the National Academy of Sciences*, 98, 11295-11300.
- WANG, N. & INGBER, D. E. 1995. Probing transmembrane mechanical coupling and cytomechanics using magnetic twisting cytometry. *Biochemistry and Cell Biology*, 73, 327-335.
- WANG, N., TYTELL, J. D. & INGBER, D. E. 2009. Mechanotransduction at a distance: mechanically coupling the extracellular matrix with the nucleus. *Nature Reviews Molecular Cell Biology*, 10, 75-82.

- WATSON, A. R., PITCHFORD, S. C., REYNOLDS, L. E., DIREKZE, N., BRITTAN, M., ALISON, M. R., RANKIN, S., WRIGHT, N. A. & HODIVALA-DILKE, K. M. 2010. Deficiency of bone marrow $\beta 3$ -integrin enhances non-functional neovascularization. *The Journal of Pathology*, 220, 435-445.
- WEBER, K. & GROESCHEL-STEWART, U. 1974. Antibody to Myosin: The Specific Visualization of Myosin-Containing Filaments in Nonmuscle Cells. *Proceedings of the National Academy of Sciences of the United States of America*, 71, 4561-4564.
- WEISS, P. 1945. Experiments on cell and axon orientation in vitro: The role of colloidal exudates in tissue organization. *Journal of Experimental Zoology*, 100, 353-386.
- WELSH, C. F., ROOVERS, K., VILLANUEVA, J., LIU, Y., SCHWARTZ, M. A. & ASSOIAN, R. K. 2001. Timing of cyclin D1 expression within G1 phase is controlled by Rho. *Nat Cell Biol*, 3, 950-957.
- WERT, G. D. & MUMMERY, C. 2003. Human embryonic stem cells: research, ethics and policy. *Human Reproduction*, 18, 672-682.
- WILKINSON, C. D. W., RIEHLE, M., WOOD, M., GALLAGHER, J. & CURTIS, A. S. G. 2002. The use of materials patterned on a nano- and micro-metric scale in cellular engineering. *Materials Science and Engineering: C*, 19, 263-269.
- WILLIAMS, D. F. 2008. On the mechanisms of biocompatibility. *Biomaterials*, 29, 2941-2953.
- WILLIAMS, D. F. 2009. On the nature of biomaterials. *Biomaterials*, 30, 5897-5909.
- WILLIAMS, R. L., HILTON, D. J., PEASE, S., WILLSON, T. A., STEWART, C. L., GEARING, D. P., WAGNER, E. F., METCALF, D., NICOLA, N. A. & GOUGH, N. M. 1988. Myeloid leukaemia inhibitory factor maintains the developmental potential of embryonic stem cells. *Nature*, 336, 684-687.
- WILSON, A., LAURENTI, E., OSER, G., VAN DER WATH, R. C., BLANCO-BOSE, W., JAWORSKI, M., OFFNER, S., DUNANT, C. F., ESHKIND, L., BOCKAMP, E., LIÓ, P., MACDONALD, H. R. & TRUMPP, A. 2008. Hematopoietic Stem Cells Reversibly Switch from Dormancy to Self-Renewal during Homeostasis and Repair. *Cell*, 135, 1118-1129.
- WISE, J. K., YARIN, A. L., MEGARIDIS, C. M. & CHO, M. 2008. Chondrogenic Differentiation of Human Mesenchymal Stem Cells on Oriented Nanofibrous Scaffolds: Engineering the Superficial Zone of Articular Cartilage. *Tissue Engineering Part A*, 15, 913-921.
- WOODS, A., COUCHMAN, J. R., JOHANSSON, S. & HÖÖK, M. 1986. Adhesion and cytoskeletal organisation of fibroblasts in response to fibronectin fragments. *The EMBO Journal*, 5, 665-670.
- WOZNIAK, M. A., MODZELEWSKA, K., KWONG, L. & KEELY, P. J. 2004. Focal adhesion regulation of cell behavior. *Biochimica et Biophysica Acta (BBA) - Molecular Cell Research*, 1692, 103-119.
- WU, L., LEIJTEN, J. C. H., GEORGI, N., POST, J. N., VAN BLITTERSWIJK, C. A. & KAPERIEN, M. 2011. Trophic Effects of Mesenchymal Stem Cells Increase Chondrocyte Proliferation and Matrix Formation. *Tissue Engineering Part A*, 17, 1425-1436.
- XIONG, J.-P., STEHLE, T., DIEFENBACH, B., ZHANG, R., DUNKER, R., SCOTT, D. L., JOACHIMIAK, A., GOODMAN, S. L. & ARNAOUT, M. A. 2001. Crystal Structure of the Extracellular Segment of Integrin $\alpha V\beta 3$. *Science*, 294, 339-345.

- XIONG, J.-P., STEHLE, T., ZHANG, R., JOACHIMIAK, A., FRECH, M., GOODMAN, S. L. & ARNAOUT, M. A. 2002. Crystal Structure of the Extracellular Segment of Integrin α V β 3 in Complex with an Arg-Gly-Asp Ligand. *Science*, 296, 151-155.
- XUE, R., LI, J. Y.-S., YEH, Y., YANG, L. & CHIEN, S. 2013. Effects of matrix elasticity and cell density on human mesenchymal stem cells differentiation. *Journal of Orthopaedic Research*, 31, 1360-1365.
- YADLAPALLI, S. & YAMASHITA, Y. M. 2012. Spindle positioning in the stem cell niche. *Wiley Interdisciplinary Reviews: Developmental Biology*, 1, 215-230.
- YAMAMOTO, T., EBISUYA, M., ASHIDA, F., OKAMOTO, K., YONEHARA, S. & NISHIDA, E. 2006. Continuous ERK Activation Downregulates Antiproliferative Genes throughout G1 Phase to Allow Cell-Cycle Progression. *Current Biology*, 16, 1171-1182.
- YAMANAKA, S. 2009. A Fresh Look at iPS Cells. *Cell*, 137, 13-17.
- YANES, O., CLARK, J., WONG, D. M., PATTI, G. J., SÁNCHEZ-RUIZ, A., BENTON, H. P., TRAUGER, S. A., DESPONTS, C., DING, S. & SIUZDAK, G. 2010. Metabolic oxidation regulates embryonic stem cell differentiation. *Nature Chemical Biology*, 6, 411-417.
- YAO, S., CHEN, S., CLARK, J., HAO, E., BEATTIE, G. M., HAYEK, A. & DING, S. 2006. Long-term self-renewal and directed differentiation of human embryonic stem cells in chemically defined conditions. *Proceedings of the National Academy of Sciences*, 103, 6907-6912.
- YIM, E. K. F., DARLING, E. M., KULANGARA, K., GUILAK, F. & LEONG, K. W. 2010. Nanotopography-induced changes in focal adhesions, cytoskeletal organization, and mechanical properties of human mesenchymal stem cells. *Biomaterials*, 31, 1299-1306.
- YIM, E. K. F., PANG, S. W. & LEONG, K. W. 2007. Synthetic nanostructures inducing differentiation of human mesenchymal stem cells into neuronal lineage. *Experimental Cell Research*, 313, 1820-1829.
- YIN, T. & LI, L. 2006. The stem cell niches in bone. *Journal of Clinical Investigation*, 116, 1195-1201.
- YOO, S.-W., CHANG, D.-Y., LEE, H.-S., KIM, G.-H., PARK, J.-S., RYU, B.-Y., JOE, E.-H., LEE, Y.-D., KIM, S.-S. & SUH-KIM, H. 2013. Immune following suppression mesenchymal stem cell transplantation in the ischemic brain is mediated by TGF- β . *Neurobiology of Disease*, 58, 249-257.
- YOSHIHARA, H., ARAI, F., HOSOKAWA, K., HAGIWARA, T., TAKUBO, K., NAKAMURA, Y., GOMEI, Y., IWASAKI, H., MATSUOKA, S., MIYAMOTO, K., MIYAZAKI, H., TAKAHASHI, T. & SUDA, T. 2007. Thrombopoietin/MPL Signaling Regulates Hematopoietic Stem Cell Quiescence and Interaction with the Osteoblastic Niche. *Cell Stem Cell*, 1, 685-697.
- YUSUF, RUSHDIA Z. & SCADDEN, DAVID T. 2012. Fate through Fat: Lipid Metabolism Determines Stem Cell Division Outcome. *Cell Metabolism*, 16, 411-413.
- ZAIDEL-BAR, R., COHEN, M., ADDADI, L. & GEIGER, B. 2004. Hierarchical assembly of cell-matrix adhesion complexes. *Biochemical Society Transactions*, 32, 416-420.
- ZAIDEL-BAR, R., ITZKOVITZ, S., MA'AYAN, A., IYENGAR, R. & GEIGER, B. 2007. Functional atlas of the integrin adhesome. *Nature cell biology*, 9, 858-867.
- ZAMIR, E. & GEIGER, B. 2001. Molecular complexity and dynamics of cell-matrix adhesions. *Journal of Cell Science*, 114, 3583-3590.

- ZAYZAFON, M. 2006. Calcium/calmodulin signaling controls osteoblast growth and differentiation. *Journal of Cellular Biochemistry*, 97, 56-70.
- ZHANG, W., ZHU, C., YE, D., XU, L., ZHANG, X., WU, Q., ZHANG, X., KAPLAN, D. L. & JIANG, X. 2014. Porous Silk Scaffolds for Delivery of Growth Factors and Stem Cells to Enhance Bone Regeneration. *PLoS ONE*, 9, e102371.
- ZHANG, Z., MORLA, A., VUORI, K., BAUER, J., JULIANO, R. & RUOSLAHTI, E. 1993. The alpha v beta 1 integrin functions as a fibronectin receptor but does not support fibronectin matrix assembly and cell migration on fibronectin. *The Journal of Cell Biology*, 122, 235-242.
- ZHAO, F. 2013. Manipulating Mesenchymal Stem Cells for Vascular Tissue Engineering. *JSM Biotechnology & Biomedical Engineering*, 1, 1012.
- ZOU, P., YOSHIHARA, H., HOSOKAWA, K., TAI, I., SHINMYOZU, K., TSUKAHARA, F., MARU, Y., NAKAYAMA, K., NAKAYAMA, KEIICHI I. & SUDA, T. 2011. p57Kip2 and p27Kip1 Cooperate to Maintain Hematopoietic Stem Cell Quiescence through Interactions with Hsc70. *Cell Stem Cell*, 9, 247-261.
- ZOUANI, O. F., CHANSEAU, C., BROUILLAUD, B., BAREILLE, R., DELIANE, F., FOULC, M.-P., MEHDI, A. & DURRIEU, M.-C. 2012. Altered nanofeature size dictates stem cell differentiation. *Journal of Cell Science*, 125, 1217-1224.
- ZUK, P. A., ZHU, M., MIZUNO, H., HUANG, J., FUTRELL, J. W., KATZ, A. J., BENHAIM, P., LORENZ, H. P. & HEDRICK, M. H. 2001. Multilineage Cells from Human Adipose Tissue: Implications for Cell-Based Therapies *Tissue Engineering*, 7, 211-228.